SITE RESPONSE EFFECT AND MICROZONATION OF ALMALQA AREA, NW OF RIYADH CITY

Submitted to : **Wilbur Smith Associates**

Prepared By : Prof. Abdullah M. Al-Amri, KSU
Eng. Mostafa Homaidah, KACST
Eng. Ahmad R. Khalil, KSU

SSC – Technical Report (6)

Sep. 25, 2007

SITE RESPONSE EFFECT AND MICROZONATION OF ALMALQA AREA, NW OF RIYADH CITY

Table of Content

Summary

Modern societies and economics depend upon engineered infrastructures supplying externally supplies such as power for their continued successful operation. The supplies and services enable development and growth to proceed and progress. The administration and distribution of the supplies and services are the means by which society operates on a daily basis, and without which the infrastructures of the region would be adversely affected, economically, socially, and politically. In the foreseeable future, there will be rapid growth of industrial development, increased population, and urban expansion. Experience has demonstrated that natural disaster, and earthquakes in particular have tended to become increasingly destructive since these affect a larger concentration of national properties and population, thus, generating calamitous incidents.

The impact of an earthquake is not limited to direct losses, such as the loss of life, loss of structures, and business interruptions. Earthquakes also cause indirect losses by producing supply shortages and demand reductions in various economic sectors. In a city with a vibrant economy like Riyadh, a large earthquake can cause an economic downturn lasting for a long period of time.

We bring to this project the state of art knowledge in the filed of seismic hazard assessment. Similar projects have been implemented elsewhere in Saudi Arabia. This proposal presents the methodology and the work plan to asses the seismic hazard in Almalqa area, NW of Riyadh city. Riyadh is the commercial and financial capital of Saudi Arabia. With an economic growth rate, it is one of the fastest growing cities in the Middle East. The ongoing construction projects in NW Riyadh are valued. Although there is no known seismic source directly under Riyadh, there are numerous sources nearby that can cause damaging seismic shaking in Riyadh.

Although they are not very close, a large earthquake can cause major damage to structures in Riyadh. While the high-frequency components of seismic waves attenuate rapidly with distance, the Low-frequency components can travel very far without much attenuation. The low-frequency waves also tend to have very long durations. These are the waves that would be most critical for Riyadh, because they can cause resonant vibrations in tall, flexible structures since these structures will all have very low natural frequencies. Long-period, long-duration shaking created by distant earthquakes cause tall buildings undergo a large number of stress reversals, resulting in strength deteriorations in concrete elements and fatigue failures in steel connections.

Geologic Setting

Arabian Platform

The platform consists of the Paleozoic and Mesozoic sedimentary rocks that unconformably overlays the shield and dip very gently and uniformly to the E-NE towards the Arabian Gulf (Powers et al., 1966). The accumulated sediments in the Arabian platform represent the southeastern part of the vast Middle east basin that extend eastward into Iran, westward into the eastern Mediterranean and northward into Jordan, Iraq and Syria.

The Arabian shield isolated the Arabian platform from the north African Tethys and played an active paleogeographic role through gentle subsidence of its northern and eastern sectors during the Phanerozoic, allowing almost 5000 m of continental and marine sediments deposited over the platform. This accumulation of sediments represents several cycles from the Cambrian onward, now forms a homocline dipping very gently away from the Arabian shield (Fig. 1).

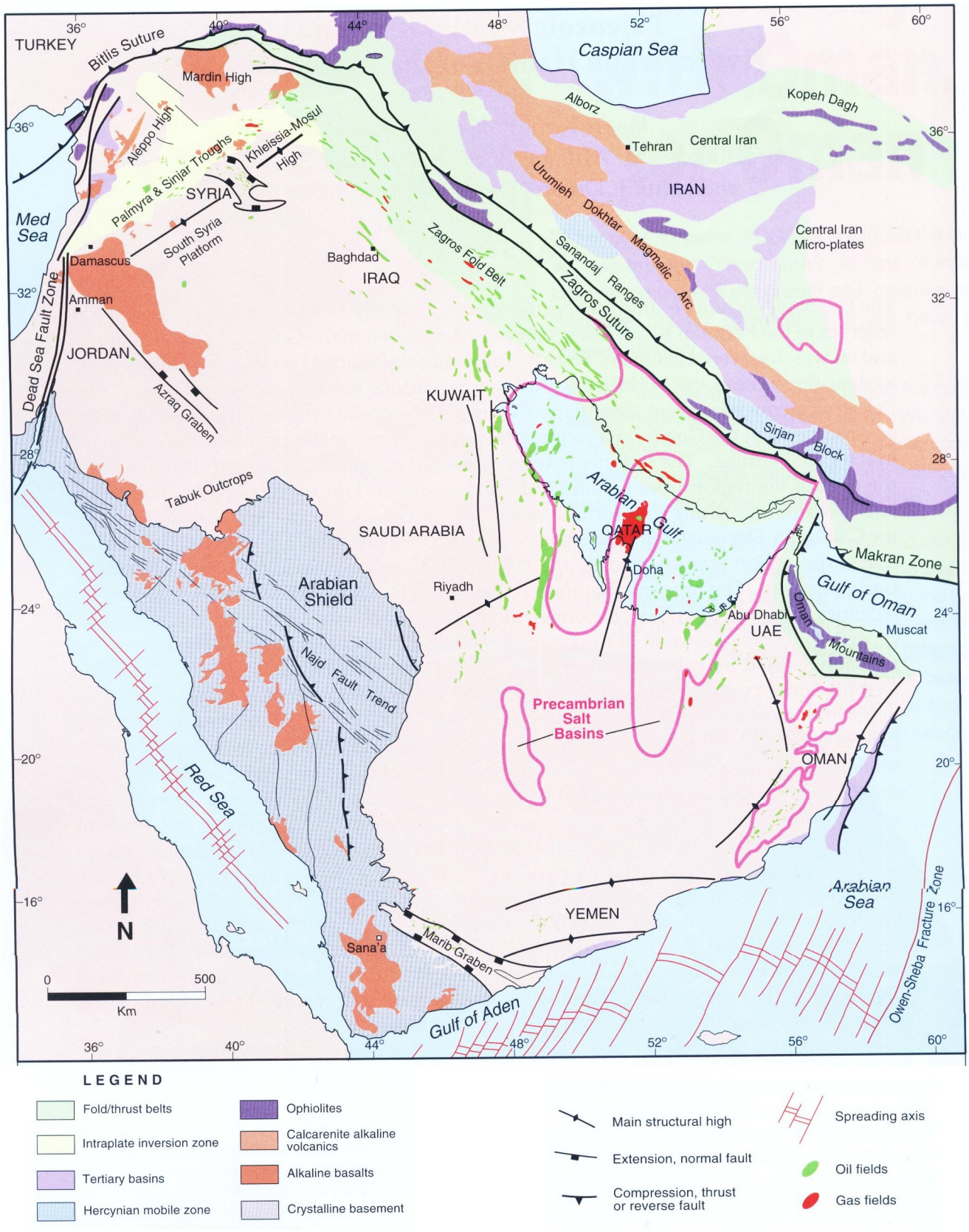

Fig. 1: Location and major tectonic elements of the Arabian plate and Iran. The Makran and Zagros separate the Arabian plate from the microplates of interior Iran.

Several structural provinces can be identified within the Arabian platform : 1) An interior homocline in the form of a belt, about 400 km wide, in which the sedimentary rocks dip very gently away from the shield outcrops. 2) An interior platform, up to 400 km wide, within which the sedimentary rocks continue to dip regionally away from the shield at low angles. 3) Intra-shelf depressions, found mainly around the interior homocline and interior platform (Fig. 2).

Unfortunately, no locally recorded earthquake data have been used to determine the crustal characteristics of the Arabian platform. The regularly spaced north trending Summan platform, Khurais-Burgan and En Nala-Ghawar anticlines, and Qatar arch in the eastern part of the Arabian plate appear to have formed during the Precambrian Amar Collision about 640-620 million years ago (Ma). This collision occurred along the north trending Amar suture that bisects the Arabian peninsula at about 45 degrees east longitude when the Rayn microplate in the east was fused to the western part of the Arabian craton (Al-Husseini 2000 ; Looseveld et al 1996). The great anticlines are bounded by the northeast trending Wadi Batin fault and northwest trending Abu Jifan fault that converge on the Amar suture. The anticlines intersected deformed metasediments that are dated as syn-collisional. The Amar collision was followed by a widespread extensional collapse of the Arabian-Nubian shield between about 620-530 Ma. The extensional collapse culminated in the regional development of the extensive Najd fault and its complimentary rift basins, Zagros suture, the northeast trending Oman salt basins, Dibba fault, and the Sinai triple junction.

The Sinai triple junction is composed of the Najd fault system, the Egypt rift, the Jordan valley, and Derik rift. During the final extensional stage about 530-570 Ma, the northwest trending Najd fault system dislocated the Arabian shield left-laterally by about 250-300 kilometers. This dislocation appears to compliment the northeast oriented intra-continental rifts in Oman, Zagros mountain, and the Arabian gulf. These rift basins accumulated thick sequences of clastic and carbonate rocks and salt such as the Ara group in Oman, Hormuz

series in the Arabian gulf and Zagros mountain (Ziegler 2001). During the extensional collapse, the north trending anticlines probably remained elevated as elongated horst bounded by normal faults. The intervening subsiding grabens accumulated syn-rift sediments including the Hormuz salt, and form an inter-fingering pattern between the great north trending anti-clines.

The striking geometric pattern appears to have formed in two tectonic stages. The Precambtian Amar collision between about 640-620 Ma, followed by the development of the Najd rift system between about 570-530 Ma.

In Oman, during the intra-extensional tectonics (rift cycle 1), a series of north-south to northeast –southwest trending basement highs may have developed from north to south. These are the Ghudun-Khasfah high, the Anzaus-Rudhwan Ridge and the Makarem-Mabrouk

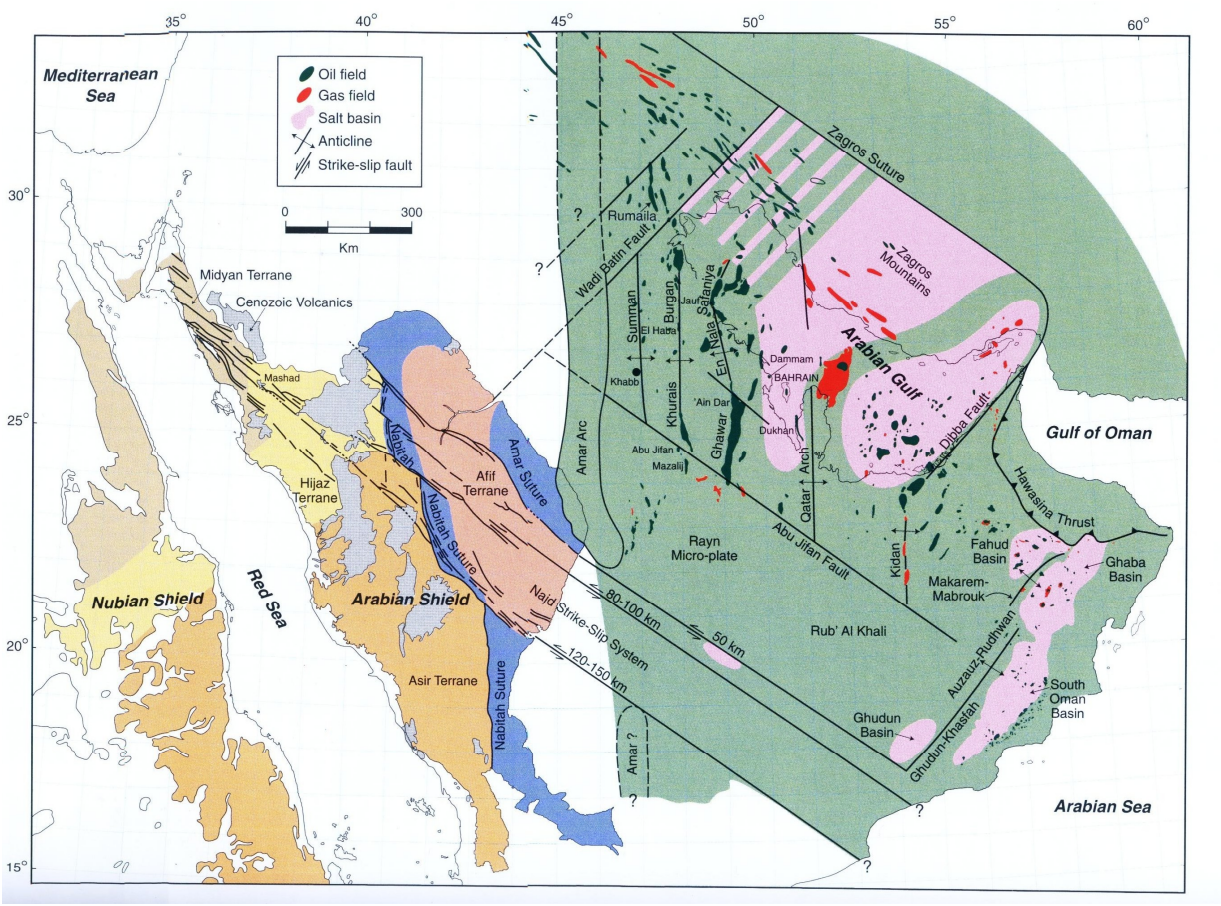

Fig. 2 : The terranes, and Amar Arc of the Rayn micro-plate. The Rayn micro-plate (Green) forms the eastern part of the Arabian Plate (Al-Husseini, 2000).

high, separating different basin segments. The event is also associated with igneous activity which is the formation of the Oman mountains and is followed by a thermal subsidence phase. During this cycle, there may have been widespread rifting of the Abu Mahara group (During the Cambrian to mid-Carboniferous (Rift Cycle 2), the Abu Mahara rift configuration was reactivated. The re-activated eastern angle low-angle bounding fault of the Ghudun-Khasfah high becomes the western margin of the asymmetrical South Oman basin. In the north, the Ghaba salt basin develops as a narrower, deeper and asymmetrical feature with some asymmetry reversals. The South Oman and Ghaba salt basins are related to the Najd event of rifting and wrenching dated at between 600-540 Ma (Looseveld et al.,1996). Around 110 Ma, the Atlantic ocean started to open, leading to the closure of the Neo-Tethys between the Afro-

Arabian and Eurasian plates. A northeasterly dipping intra-oceanic subduction zone developed, accompanied by back-arc spreading. At approximately 93 Ma, this subduction complex collided with the continental crust of Oman. Uplift and partial erosion of the Natih formation and the development of a major hard ground signaled the onset of this event. The initial onset has been described as a mobile or stationary fore-bulge that preceded down-warping of the foreland ahead of the advancing thrust front. During this phase, the Hawasina and Samail Nappes are emplaced, the region south of the nappes are downwarped with local footwall uplift, the Aruma foredeep develops, a dextral transtension along the Fahud fault zone, and a sinistral transtension along the Maradi fault zone occur. In the Eocene-Pliocene second Alpine phase, folding commences in the Oman mountains and shortening overprints extension in the area around Natih, Fahud, and the northern Maradi fault zone (Noweir & Asharhan 2000). The Salakh arch develops, reverse faulting occur in foredeep, the northern portion of the Maradi fault zone is inverted in dextral transpression, and the Fahud main fault is re-activated with a small sinistral component.

At the Cretaceous-Tertiary boundary, intra-oceanic north-over-south thrusting between the lower and upper nappes of Masirah island occurred, immediately followed in the Paleocene by the oblique obduction of the Masirah complex onto the Arabian continent (Peters et al 1995). Along the east coast of Oman, largely offshore under Masirah bay and Sawqrah bay, a narrow, gently folded foreland basin, the Masirah trough, developed. The western margin is bounded by normal faults reactivating Mesozoic rift related faults. On its eastern margin, a wedge of ophiolitic and probably continental slope sediments is largely underthrusted below the eastern and uplifted part of this foredeep basin.

SEISMIC SOURCES

The Arabian Peninsula presents several interesting seismological problems. On the west, rifling in the Red Sea has split a large Precambrian Shield. Active rifling is responsible for the geometry of the plate margins in the west, and southwest. To the south, similar rifling running in a more east-west direction through the Gulf of Aden has separated the Arabian Peninsula from Africa. In the northwest, the Gulf of Aqabah forms the southernmost continuation of the Dead Sea transform. The northern and northeastern boundaries of the Arabian Plate are areas of continental collision, with the Arabian Plate colliding with the Persian Plate.

Earthquake hazard depends not only on the seismicity of a region, but also on population density and economic development. Even though seismicity remains constant, both population and economic development are increasing rapidly. Identifying sources of vulnerability and taking steps to mitigate the consequences of future earthquake disaster are the most essential elements of disaster preparedness. Because the existing facilities represent the main earthquake risk, research and performance evaluation have much desire to be done in this critical area.

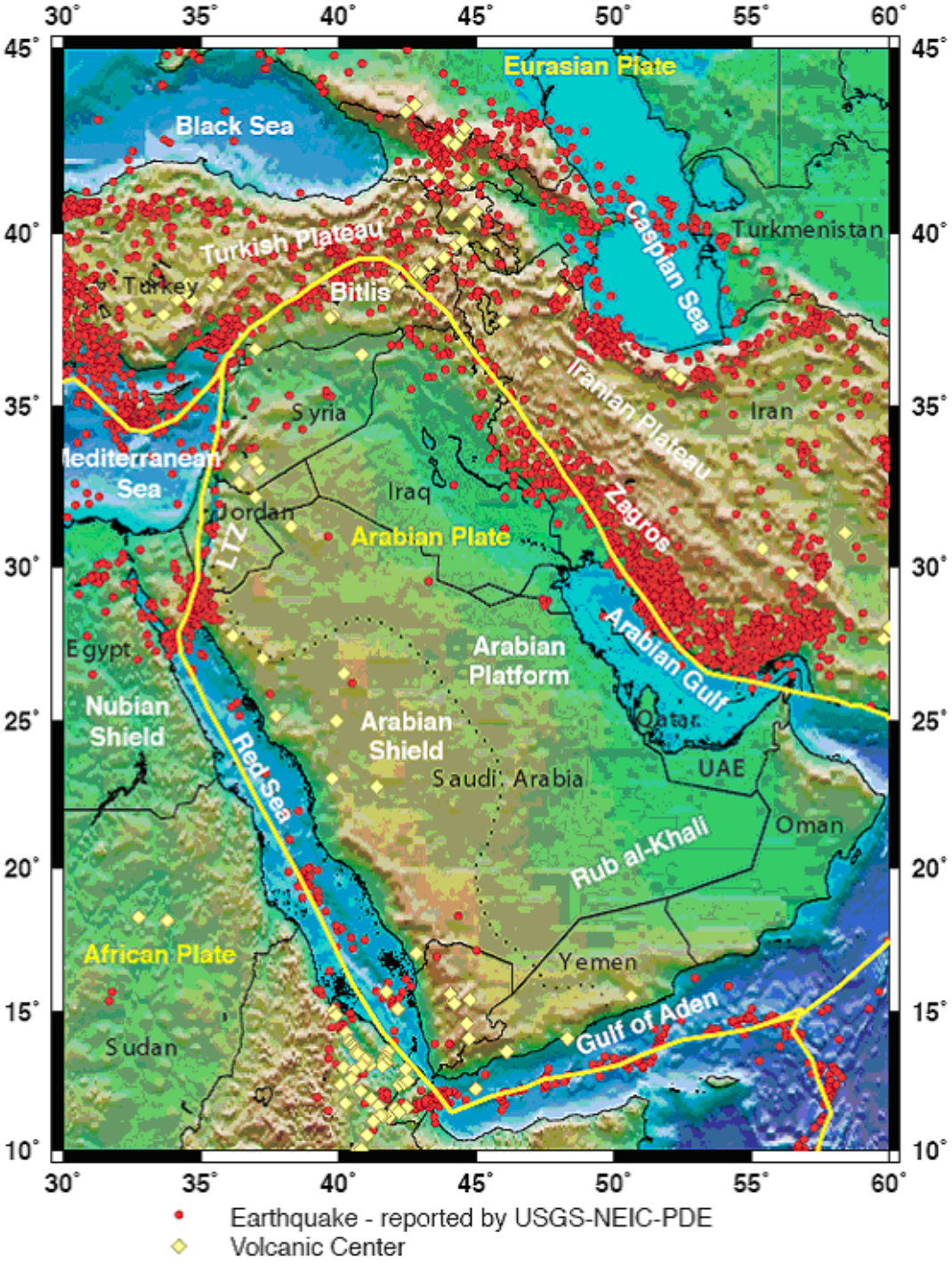

Figure 2.1 . Map of the Arabian Peninsula and surrounding regions. Major geographic and tectonic features are indicated. Plate boundaries are indicated by yellow lines. Earthquakes and volcanic centers : shown as red circles and yellow diamond, respectively.

In order to reduce earthquake hazards in a rational way, it is necessary to have a clear understanding of the phenomena associated with earthquakes and their adverse effects. The key element in coping with earthquake hazard is the ability to assess seismic hazard. To make rational decisions in coping with earthquakes, it is necessary to know the answers to some questions related to:

- **Sources of destructive earthquakes**
- **Locations of earthquake occurrences**
- **Frequency of various size of earthquakes**
- **Nature of the severe ground motion near the source and its attenuation with distance**
- **Influence of local geology and site condition on the severity of ground shaking**
- **Types of earthquake hazards**
- **Main characteristics that define the damage potential of earthquake shaking**

The characterization of the seismogenic source zones is composed of two parts. These are the brief discussions covering the possible association of each source zone to the tectonic and seismicity model of the areas contained in each source zone. The other part is a logic tree diagram for graphical description of the physical and seismicity parameters involved in seismotectonic correlation.

Two methods of approach were employed in the study. These are seismicity and fractures. Under the seismicity approach, the set of seismic data in each source zone was utilized to plot the magnitude-frequency relation, and for the estimation of the linear seismic slip and seismic moment release rates. From the frequency graphs, the respective seismicity parameters were determined for correlation to tectonic structures and probable earthquake source mechanisms. Under the second approach, the tectonic structures contained in each source zones were examined based on existing geological / tectonic maps for identification and association to the types of earthquake source mechanisms, and to the seismicity of the source area. Combination of the two approaches lead to the preliminary framework of a seismotectonic model for each seismogenic source zone.

From the findings, there were at most two types of sources for the tectonic model. These are the fault and area source. Under the fault source are the transcurrent and normal faults and their respective variations. Under the area source are the seismic events not directly associated to known presence of fractures or are off located, and or the sudden or randomly distributed dislocations of the ground within the source zones. Presumably, the causes of these seismic

events under the area source are due to lateral and vertical structural discontinuities, or connected to some anomalous behavior of geophysical phenomena, and or undetected fractures.

For earthquake source mechanisms, there are also at most two types. These are the extrusion and transcursion mechanisms. The zones of extrusion are the seats of volcanic activity and high heat flow. Seismological and other geophysical data suggest that ridges and their continental extension are characterized by rifting, spreading, and other aspects of extensional tectonics.

Zone 16 (Central Arabian Graben Zone)

Zone 16 is roughly composed of the central Arabian graben and trough system; Wadi Batin and Abu Jifan fault; Summan platform, Khurais- Burgan and En Nala-Ghawar anticlines, Qatar Arch, and the Kuwait complex structures ranging from megascale, mesoscale, and microscale. The approximately 560 km compound graben system defines an arc concave to the northeast. It comprises six (6) major grabens and three (3) large synclinal troughs, together with subsidiary grabens and troughs. The major grabens are Majma, Al Barrah, Qaradan, Durma, Awsat, and Nisah. The Durma, Awsat, and Nisah lie entirely within the present region, which also includes 4 km of the eastern end of the Qaradan graben. The Majma, Awsat and Nisah grabens are compound structures. The Majma graben comprises many offset segments, whereas, the Awsat and Nisah grabens each consists of two overlapping segments. The three (3) large troughs are Buayja, Mughrah, and Sahba. Mughrah trough and the Maraghah monocline defined as separate structures.

Graben boundaries are defined high-angle normal faults commonly cutting the steep limbs of associated inward-facing monoclinal flexure zones. Trough margins are defined by inward-facing monoclinal flexures locally accompanied by subsidiary normal faults. Many grabens die out laterally through monoclinal flexures of decreasing amplitudes.

On the basis of stratigraphic and facies relationships, Powers et al., (1966) proposed that

faulting on the central Arabian graben and trough system began in the Late-Cretaceous time and may have continued until the Eocene. The grabens developed between Late Cretaceous and the Late Quaternary, most movement being Paleogene age but succeeded by subsidiary Neogene and Quaternary movements.

Three (3) west-facing escarpments arranged in concentric arcs concave to the west dominate the topography. The western and highest escarpment, Jabal Tuwayq, is a double scarp. The western end is capped by the Tuwayq Mountain Limestone and the eastern end is capped by the Jubaila Limestone. The eastern end is the Jubayl escarpment capped of the Sulaiy Formation. The Durma basin lies west of the Tuwayq escarpment and the Kharj basin is situated between the Tuwayq and Al Jubayl escarpments.

The approximately 140 km Majma graben complex comprises many overlapping faults and en-echelon grabens replacing one another. The first is to the west and then to the east as the structure is traced from south to north (Powers et al 1966).The southern segment trends 340 degrees, while the northern segment trends 356 degrees. Displacement on their boundary faults range from 150-200 m. From south to north , the graben complex cuts outcrops from the Dhruma formation to the Aruma formation. The 23 km Al Barrah graben trends 305 degrees. Displacements on its boundary faults are estimated to range from 200 – 300 m (Powers et al 1966). The graben is expressed by a relatively low dissected ridge that mainly exposes the Tuwayq Mountain limestone. The approximate length of the Durma-Nisah segment of the central Arabian graben system is 150 km and its width is about 25 km. The Nisah, Awsat, Durma, and Qaradan grabens are arranged en echelon. The Awsat and Nisah grabens are compound, each comprises two overlapping segment, the sense of overlap being the opposite of that displayed by the four grabens. Fault zones along graben margins commonly comprise a principal boundary fault, subsidiary antithetic or synthetic normal faults, and minor antithetic or synthetic extension faults, that is, small faults that result in layer-parallel elongation (Norris 1958).

The Qaradan graben is at least 12 km long and an average of 2.5 km width. The graben trends 310 degrees and its displacement on its boundary faults exceeds 400 m in the northeast. According to Powers et al (1966), the Qaradan graben is separated from the Durma graben by transverse fault striking 290 degrees. The exposed length of the Durma graben is about 63 km. Its width is from 1-1.5 km. It trends 295 degrees. Displacements on the boundary faults increases progressively westward. A few meters at the eastern end of the graben to about 100 m near longitude 46 degrees 27 minute east, 330 m near longitude 46 degrees and 17 minutes east, and about 400 m at the western end of the graben. The Awsat graben can be traced for about 90 km. It comprises two segments each 1-2 km wide. Powers et al (1966) recorded an overlap of about 7 km, while present mapping shows the overlap of the graben boundary faults is about 25 km. The eastern segment lies north of the western segment Displacement on the high angle normal boundary faults are about 20-30 m close to the extreme western end of the structure, 200 m near (46 degrees, 8 minutes east), 300 m in the central section (46 degrees, 33 minutes east), and decline to about 50 m at the eastern end.

The Nisah graben is about 95 km in length and comprises two segments overlapping around 4 km along a common boundary fault near 46 degrees, 36 minutes east. The 1.5-2.5 km wide western sement trends 290 degrees at it western end and 280 degrees at its eastern end. The eastern segment which is 2.5-3.5 km wide trends 275 degrees. The Buayja trough is approximately 40 km in length. In the west, it is about 1 km wide and broadens to about 3 km in the east. Along most of its length, the trough forms a shallow topographic depression crossed by transverse wadis. The Mughrah trough is about 40 km long to the east from 47 degrees and 19 minutes east. It has a gentler fold than the Buayja trough. The structural homolog of the Nisah graben east of longitude 47 degrees and 10 minutes east is the Sahba trough. It has a broad structural and topographic depression of about 8 km wide. According to Brown (1972), it is possible that this structure extends further east up to the Arabian Gulf.

Seismicity of the area has been studied mainly on the data from the Seismic Studies Center

(SSC) of King Saud University, the Bahrain Seismic Network (BSN), the Qatar Seismic Network (QSN), the Kuwait National Seismic Network (KNSN), and Ambraseys (1988) compilation. Historical data indicates that an earthquake of magnitude 5.8 - 6.0 was reported to have occurred in 1832 near the Al-Ghawar reservoir and Qatar arch. Instrumental data show that the Al-Ghawar area and its vicinity has experienced 86 earthquakes (2.5<Md<5.4) from 1965-1998. Most of these seismic events are located south to southeast of the Ghawar reservoir and the rest on the west of Qatar peninsula. Clusters of seismic events were also to occur in the Qassim area. Range of magnitude of these events is from 3 to 3.8. Instrumental seismicity indicates that an observed maximum magnitude of 5.3 has occurred in the vicinity of the central anticlines of the Arabian platform in June 1, 2002.

The seismicity of Kuwait reveals two main cluster of events. The first is around the Minagish-Umm Gudair oil field zone, and the second is around the Raudhatain-Sabriya oil field. The spatial correlation of earthquakes and oil fields suggest that the seismic events have been induced by oil production. The historical seismicity in this area indicates a magnitude 5.5 occurring north of Kuwait in Sept. 9, 1903.

The historical data for this zone shows insufficiency for the determination of seismicity parameters, while from the instrumental data the values of the seismicity parameters are as follows: a = 3.54; b = -0.64; and Mmax = 5.4

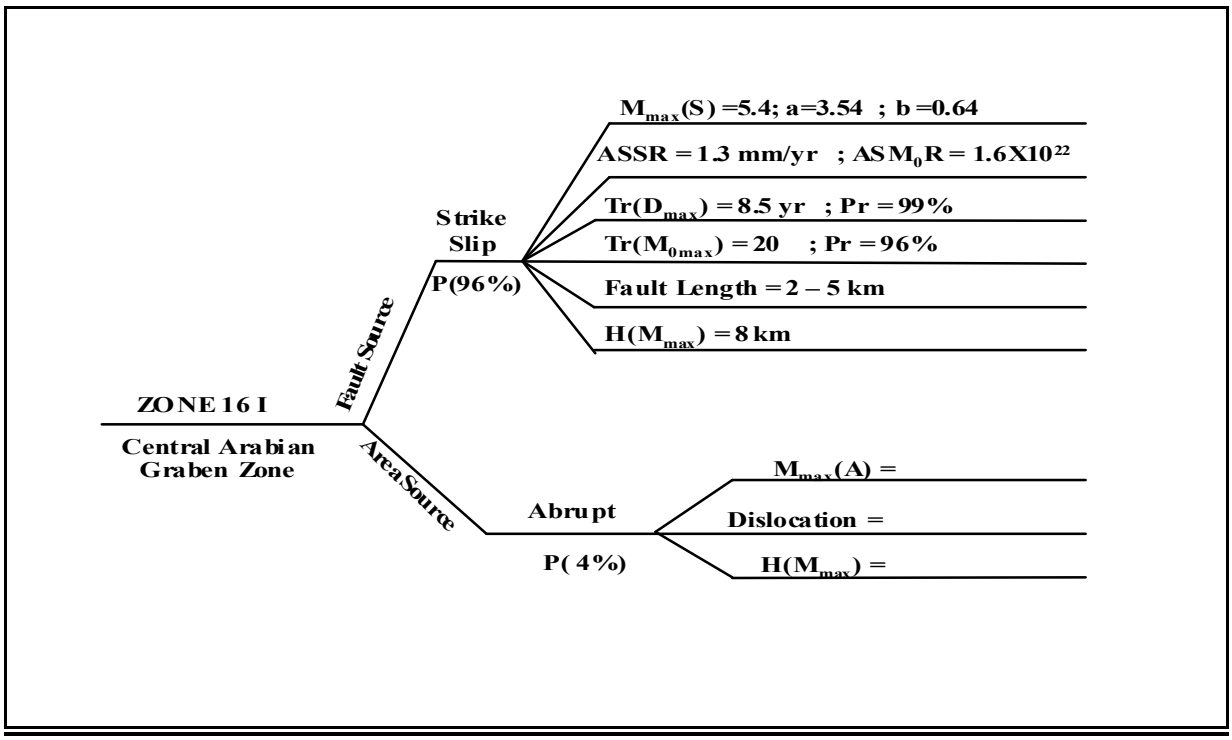
ZONE 16 I
Central Arabian Graben Zone
Fault Source
Area Source
Strike Slip
P(96%)
Abrupt
P(4%)
M_{max}(S) =5.4; a=3.54 ; b =0.64
ASSR = 1.3 mm/yr ; ASM_0R = 1.6X10^{22}
Tr(D_{max}) = 8.5 yr ; Pr = 99%
Tr(M_{0max}) = 20 ; Pr = 96%
Fault Length = 2 – 5 km
H(M_{max}) = 8 km
M_{max}(A) =
Dislocation =
H(M_{max}) =

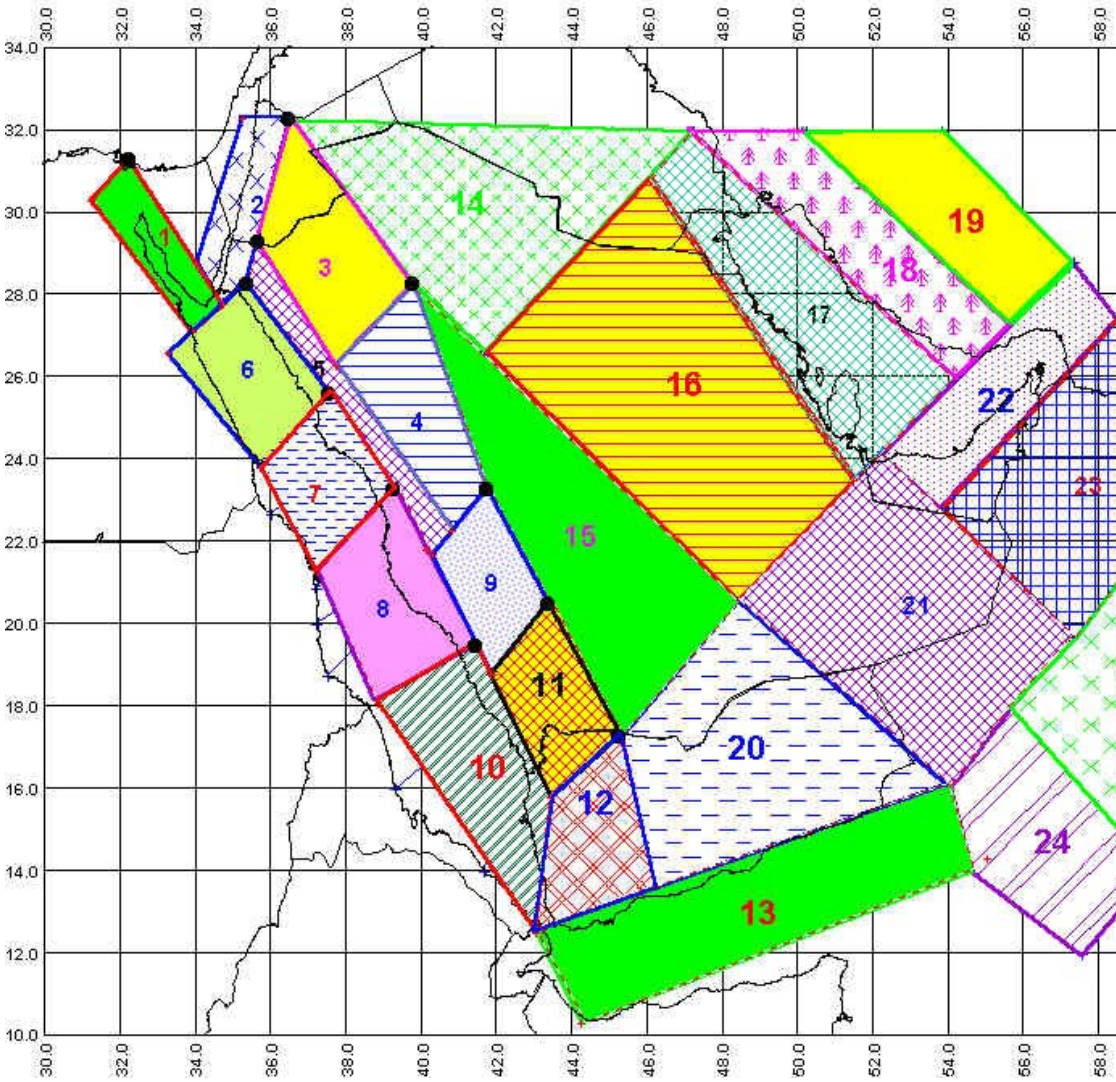

Fig. 3 Seismic zones of the Arabian Peninsula

Methodology

There are three major components of seismic hazard assessment and risk mitigation: (1) assessment of seismic hazard, (2) assessment of seismic risk and losses, and (3) development of loss reduction strategies. Assessment of seismic hazard involves determining the expected level of shaking by accounting for seismic sources in the region, past history of earthquakes, and local soil characteristics. Assessment of seismic losses is accomplished by incorporating structural inventory and the associated fragility relationships (i.e., ground shaking versus level of damage curves) into seismic hazard. Loss reduction strategies include retrofit, demolition, land use planning, monitoring systems, training, and education. Ultimate products of a seismic hazard study are a series of digital GIS maps (i.e., seismic hazard maps, site amplification maps, microzonation maps, structural inventory maps, structural damage maps, and loss estimation maps), and a software package to manipulate and modify the maps to assess seismic hazard and risk. Figure 4 gives a flow chart, which summarizes the steps in seismic hazard assessment and risk reduction. Seismic hazard assessment and risk mitigation includes (3) components:

1. Probabilistic seismic hazard maps
2. Deterministic seismic hazard maps
3. Site amplification and microzonation maps

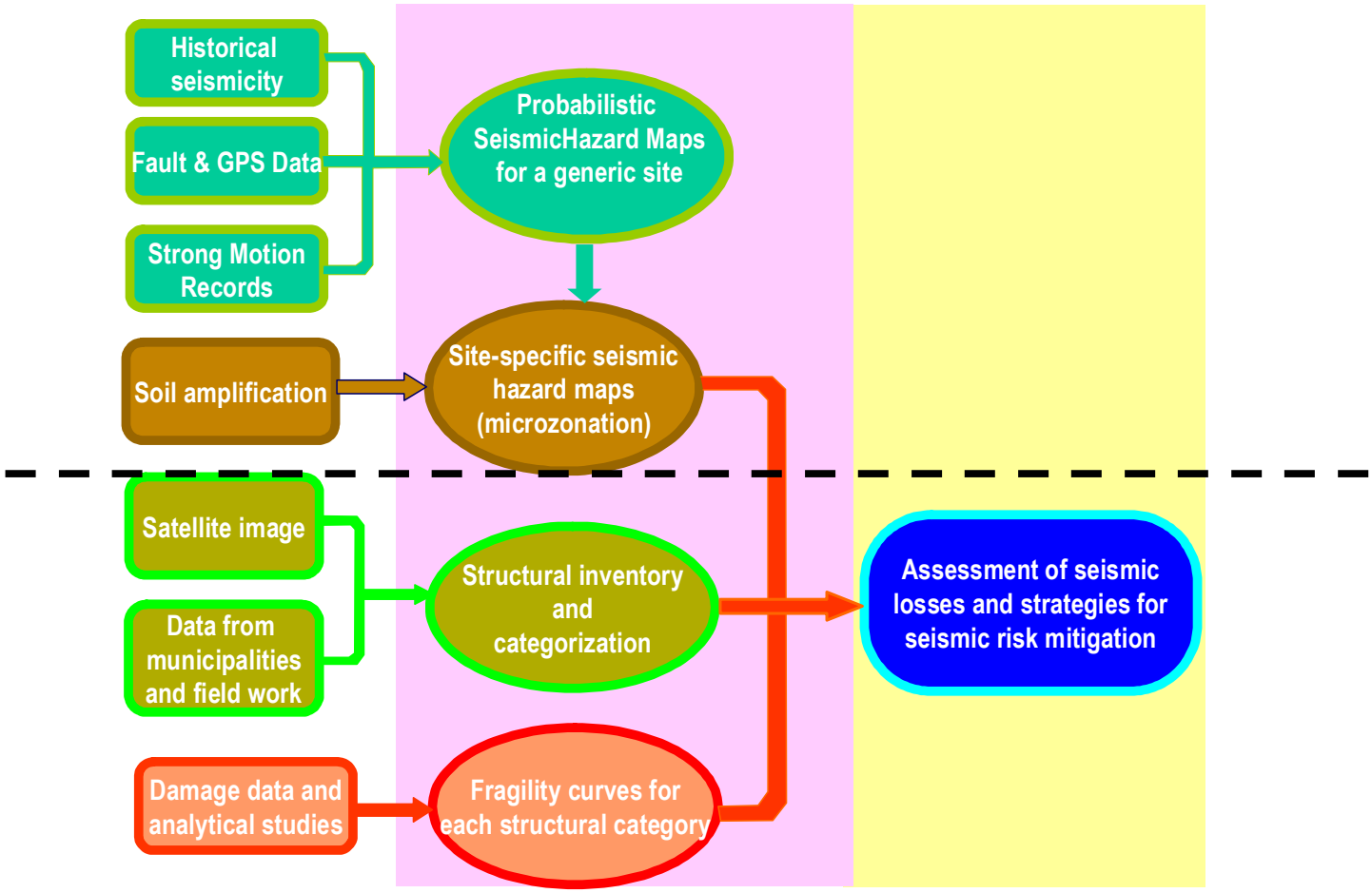

FIGURE 4- Components of seismic hazard assessment and risk reduction.

Assessment of Seismic Hazard

Assessment of seismic hazard involves development of tools and techniques to predict the intensity of ground shaking for likely earthquakes in the region. In the proposed study an accurate probabilistic seismic hazard maps, were developed for Riyadh using the USGS (United States Geological Survey) methodology, which is used to develop official seismic hazard maps for the United States. The detail is presented below.

The probabilistic assessment of seismic hazard involves calculation of the expected value of ground shaking for a specified probability of exceedance within a specified time period (e.g., peak ground acceleration that has a 10-perecent probability of being exceeded within the next 50 years). Figure 5 presents schematically the steps of probabilistic hazard assessment. To calculate seismic hazard, we will utilize the methodology recently developed by the USGS (Frankel, et al., 1996). This methodology has been reviewed extensively by the scientific and the users communities in several workshops convened by the USGS, the Building Seismic Safety Council, and the Applied Technology Council in the United States. The seismic hazard and design maps that resulted from this methodology have now officially been published by FEMA as National Earthquake Hazard Reduction Program Recommended Provisions for Seismic Regulations for New Buildings in the United States (FEMA, 1997). The USGS methodology for the probabilistic assessment of seismic hazard includes the following steps:

1. Produce comprehensive earthquake catalogue with uniform magnitude scale.
2. Produce database of active faults with slip rates, estimated recurrence times, and estimated maximum magnitudes.
3. Assess appropriate attenuation relations for ground motions as a function
4. Integrate (1)-(3) into probabilistic calculation of seismic hazard curves with uncertainties.

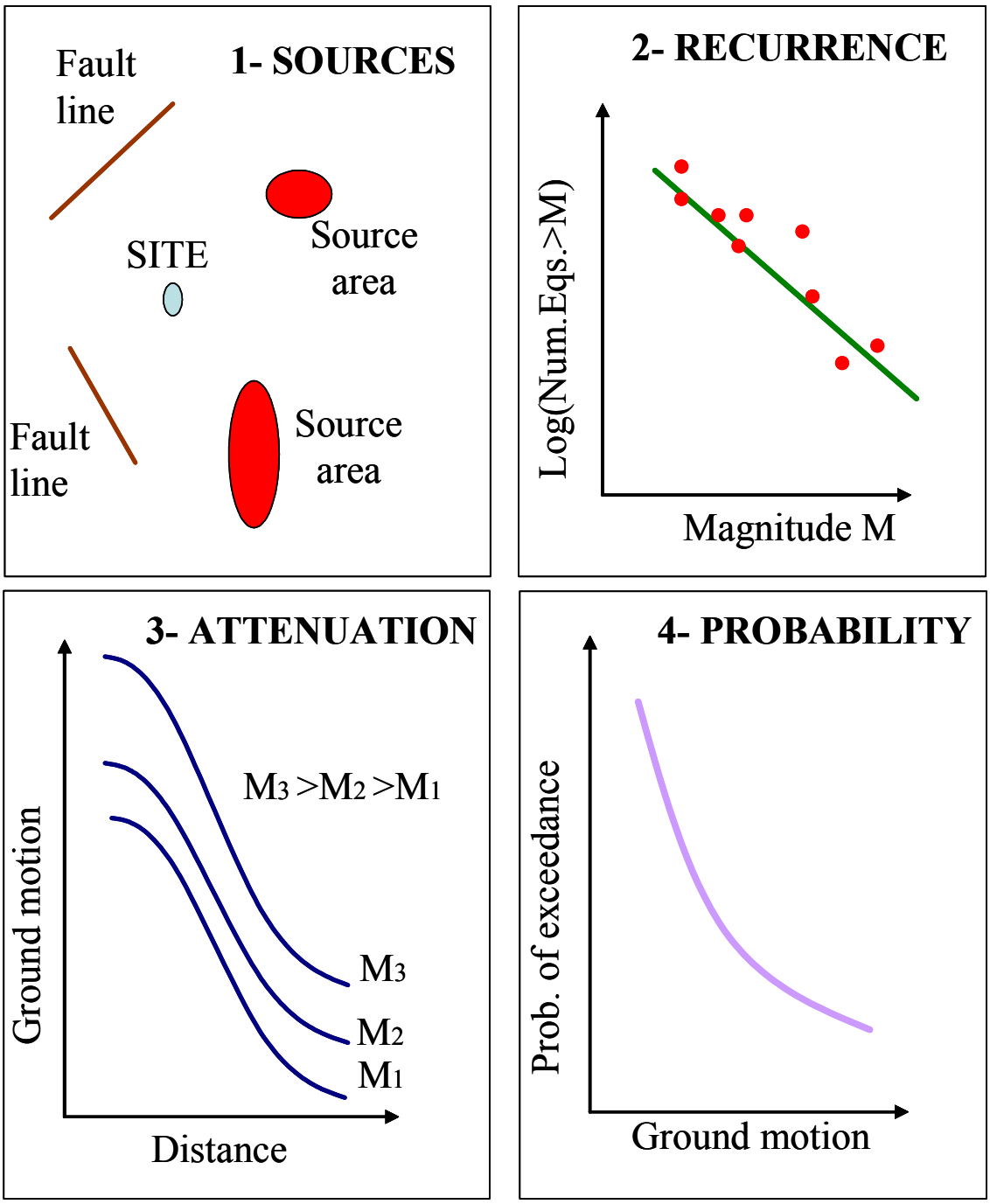

FIGURE 5- Steps of probabilistic seismic hazard analysis for a given site: (1) definition of earthquake sources, (2) earthquake recurrence characteristics for each source, (3) attenuation of ground motions with magnitude and distance, and (4) ground motions for specified probability of exceedance levels (calculated by summing probabilities over all the sources, magnitudes, and distances).

The calculations give the numerical values of various ground motion parameters (e.g., peak acceleration, peak velocity, root-mean-square acceleration, response spectra, spectral intensity, etc.) for any given probability of exceedance or return period. The products from this task will be a set of probabilistic seismic hazard maps showing peak ground accelerations and pseudo-acceleration response spectra at 0.2, 1.0, 2.0, and 4.0-sec. periods for 10% probability in 50 years, and 2% probability in 50 years. The maps will be presented in a digital format compatible with commonly used GIS software packages.

Site Amplification and Microzonation

The term "site amplification" refers to the increase in the amplitudes of seismic waves as they propagate through the soft geologic layers near the surface of the earth. Site amplification is a critical factor influencing the damage in structures during earthquakes. Soft soil layers can cause five to ten fold increase in the amplitudes of seismic waves.

The probabilistic and deterministic seismic hazard maps, discussed above, are developed for a generic soil type. To determine the actual ground shaking at a specific location, the shaking values given in seismic hazard maps should be multiplied with the local site amplification factors. The resulting maps are known as Microzonation Maps. These are the maps that are used to design and evaluate structures because they represent the actual ground shaking in that location. The most accurate way to determine site amplification factors is to use field measurements.

We determined site amplification factors by recording ambient ground noise with portable instruments. In an urban area like Riyadh, there are a lot of sources that generate ground vibrations, such as the wind-induced motions of tall buildings that are transmitted to ground through their foundations, vibrations induced by machinery and moving vehicles on ground surface, and microtremors. Figure 6 shows a schematic of such excitation sources. If the objective were to locate earthquake sources, such noise would be detrimental, because it interferes with waves generated by the earthquake. That is why seismologists do not want to locate their instruments in urban areas. However, when the objective is to determine site amplification factors,

such noise are very useful because they incorporate a lot of information on the characteristics of sub-surface soil layers. It can be shown that by proper analysis we can extract site amplification factors from ambient ground vibrations (Safak, 2005; Safak, 2006).

For Riyadh, we deployed 4 sets of portable broadband seismic recorders with built-in three-component sensors for two weeks, record ground noise continuously. The results presented in the form of a site amplification values for Riyadh, and charts for microzonation.

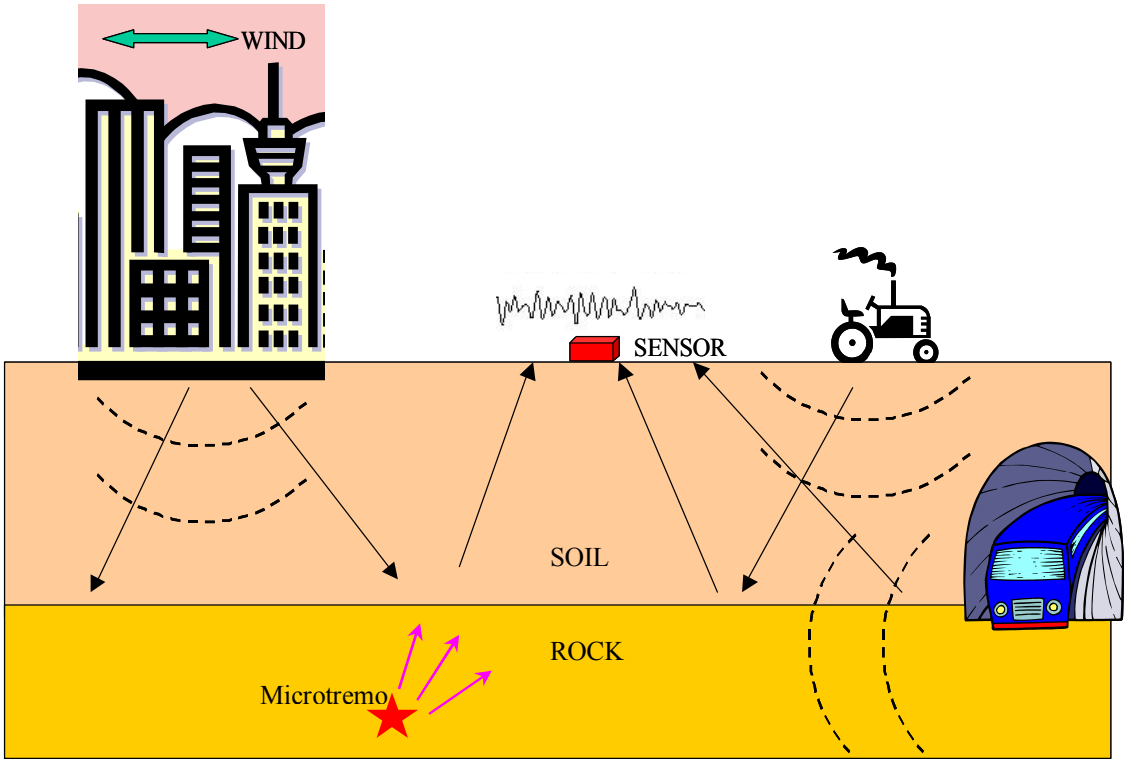

FIGURE 6. Sources for ambient ground vibrations.

Data Collection and Analysis

1- **Data Collection :** Data collection was achieved by the following steps:-

1-A- Station Site Selection

Reference to the site map, we decided to employ four seismic stations at the locations shown in Fig. x1. The location of the each station was determined based on three factors. First, the nature of each site to be suitable for equipment installation to get best results. Second, the information of WilburSmith's representative **Eng. Ma'an Abu Olba** that the most important buildings will be at the center area of the site. Third, our experience about the geological nature of the area.

From fig. x1, it is clear that station No. 1 and No. 2 are near the center of the whole area and stations No. 3 and 4 are near to the main road to detect the maximum noise of the main road.

Note, the primary overall site map is shown in index1, Fig. Inx1, in addition to four other detailed map for each station.

Fig. x1 : Location of seismic stations

Table 1x shows the location of each site station.

Station name	Latitude (N)	Longitude (E)	Elevaion (m)
STA1	24.8497	46.5324	747.7
STA2	24.8401	46.5342	742.0
STA3	24.8466	46.5468	700.1
STA4	24.8577	46.5421	725.3
RYDS	24.7200	46.6400	

RYDS station is a permanent station owned by KACST (King Abdulaziz City for Science and Technology) seismic network and its waveform information is used as additional information source for the site analysis.

1-B- Station design and preparation:

1-B-1- Seismic Station Design:

Generally, each seismic station consists of main devices. These devices are seismometer, digitizer, external storage, power supply and accurate timing source. In this project, we used two types of seismometer namely, the SS-1 short period (velocity) seismometer and in the same time the Episensor ES-T (acceleration) seismometer. The data from the seismometer is digitized by a 6 channels digitizer called "Quanterra Q-330". The External storage device is called "Quanterra Packet Baler" model PB14F, with a capacity of 40 GB of continues waveform data. For the power supply, we use non-liquid battery 92 Amps. Finally, the Timing source is the Trimble GPS which is compatible with the recording system.

Design consideration for seismometers :

Site response requires the measure of the velocity and acceleration of the earth at the specified region. Therefore, we used two types of seismometers, first is the SS-1 Ranger and the second sensor type is Episensor ES-T Seismometer.

The SS-1 seismometer is a short period seismometer with a "moving coil" style (velocity) transducer and it is chosen for the following reasons:-

a- The SS-1 is widely recognized as an excellent short-period field seismometer.
b- The SS-1 is frequently used as a sensor for ambient vibration measurements of buildings, bridges, foundations and offshore platforms.
c- The SS-1 is frequently used as a sensor for ambient vibration measurements of buildings, bridges, foundations and offshore platforms.

The complete features of the SS-1 seismometer is listed in Appendix II. Figure 2x, shows the SS-1 ranger seismometer .

Figure 2x. The SS-1 seismometer (vertical and horizontal components)

The second seismometer is the low noise seismometer Episensor ES-T, which is acceleration seismometer with a bandwidth starts from almost DC to 200 Hz. It ‘s dynamic range is 155 dB. Figure 3x shows the Episensor ES-T seismometer and its complete features is listed in Appendix II.

Figure 3x. The low noise Episensor ES-T

Design consideration for digitizer unit :

The digitizer used is the 6 channel digitizer Quanterra Q-330. The dynamic range of the Q-330 digitizer is 132-135dB, so it is very accurate to digitize the seismic signals (noise or natural earthquakes or explosions) and accurate enough to express any tiny information of the original waveform.

Since the period of recording is designed to be at least one week, so the internal buffer of the Q-330 which is 8 Mb RAM is not enough and an external storage device must be used. The internal buffer is used only to save waveforms till it transfer it to the external storage which saves the power consumption during field operations.

Figure 4x shows the Quanterra Q-330 model.

Figure 4x. The Quanterra Q-330 digitizer.

The Quanterra Q-330 digitizer features is listed in the Appendix II .

Design consideration for the external storage unit :

The external storage device "Quanterra Packet Baler" model PB14F with a capacity of 40 GB of continues waveform data is found to be enough for at least one month of continues recording. Figure 5x shows the Baler storage unit. Simple calculations, based on the sampling rates, was done to determine the data size to be stored every week and therefore the number of site trips to collect the data recorded and prepare the disk to store new data. In fact 2-3 weeks needs no trips except these trips for ensuring the data collection, battery status, security and other testing operation purposes. Using Laptop portable computer with a special software to explore the data collected in the field and ensure the data quality and time gaps. These field trips were every 2 days of the total recording period.

Figure 5x. The Quanterra Packet Baler model PB14F.

The features of the Quanterra Packet Baler is given in appendix II.

Design consideration for the power supply unit :

Since the Quanterra Q-330 digitizer is a low power consumption unit and the only the external storage Baler unit is consuming power during the data transfer from the digitizer which takes about 20 minutes every 6 hours of recording time, so the non-liquid battery 92 Amps is sufficient for the needed power especially with a check and testing field trips every two days. Accordingly, there was no need for solar cell to recharge the batteries during night times.

1-B-2- Seismic Station preparation:

Each seismic station should be assembled and each unit should be connected as the system design at the lab before moving to the field. Configuration of the Quanterra Packet Baler is a must to determine the communication protocols between the digitizer Q-330 and the external storage Baler to ensure automatic transfer of the data at the field. Figure 6x shows a general view of the Digitizer Q-330 and the external storage Baler while configuration using special software on Laptop computer at the lab. Note the Trimble GPS antenna is connected to the digitizer Q-330 and lay out of the window to get the satellite timing signals. Later during data collection, the same laptop computer, with the configuration files, is used at all the field trips to check the data and all other tests at the field.

Figure 5x, shows a general view of the Digitizer Q-330 and the external storage Baler while configuration at the lab. After configuration and testing all units then the system is disassembled again and packetized to be moved to the field sites.

Data retrieve and analysis:

At the end of the data collection period, all seismic stations are disassembled from the sites and moved back to the lab. The Baler of each station contains the data colleted by its station. The configuration file on the standard PC laptop contains all information about each station. Using the PC Browser to collect the data from each station. All files are in the miniSEED format. A special database containing the stations information (locations, sensor types, …) was built on the Sun Ultra 45 computer to be able to organize the wave forms of the continues recording. The analysis of data was done using special software called Antelope Real Time System (ARTS) which is designed manipulate the environmental monitoring information. In our case, Antelope is used on the off line mode.

Using Antelope software version 4.8 .

All the data collected were scanned to find out earthquake events or explosions and background noise. We found x explosions originally located south Riyadh. From each explosion we get the waveform windows for the ranger and the episensor as shown in fig 6x. Then using the Antelope software to find out the displacement amplitude with respect to the frequency. As shown from the figure 7x.

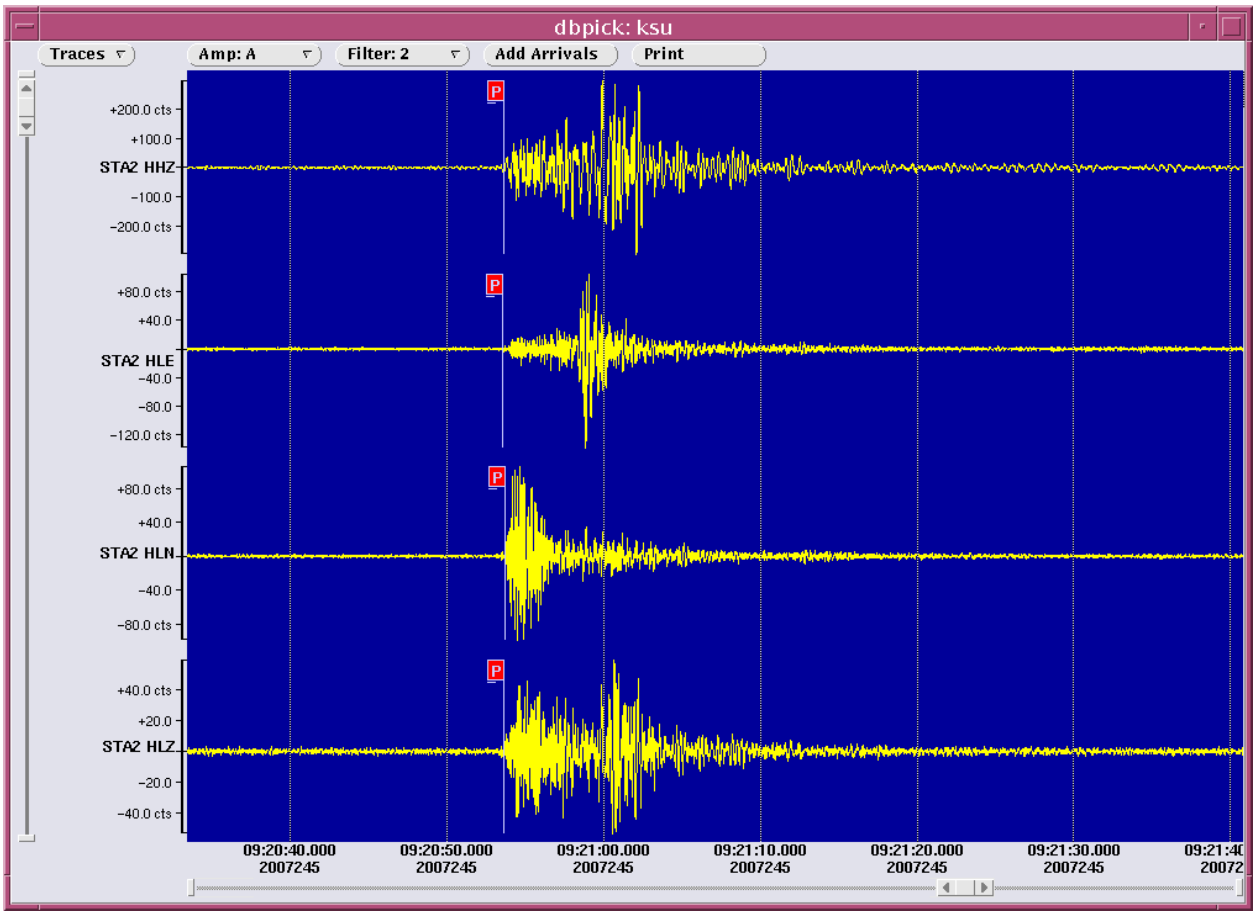

Figure 6x, explosion on 10 of Sept., 2007 at 09:20 minutes, originally located at south Riyadh

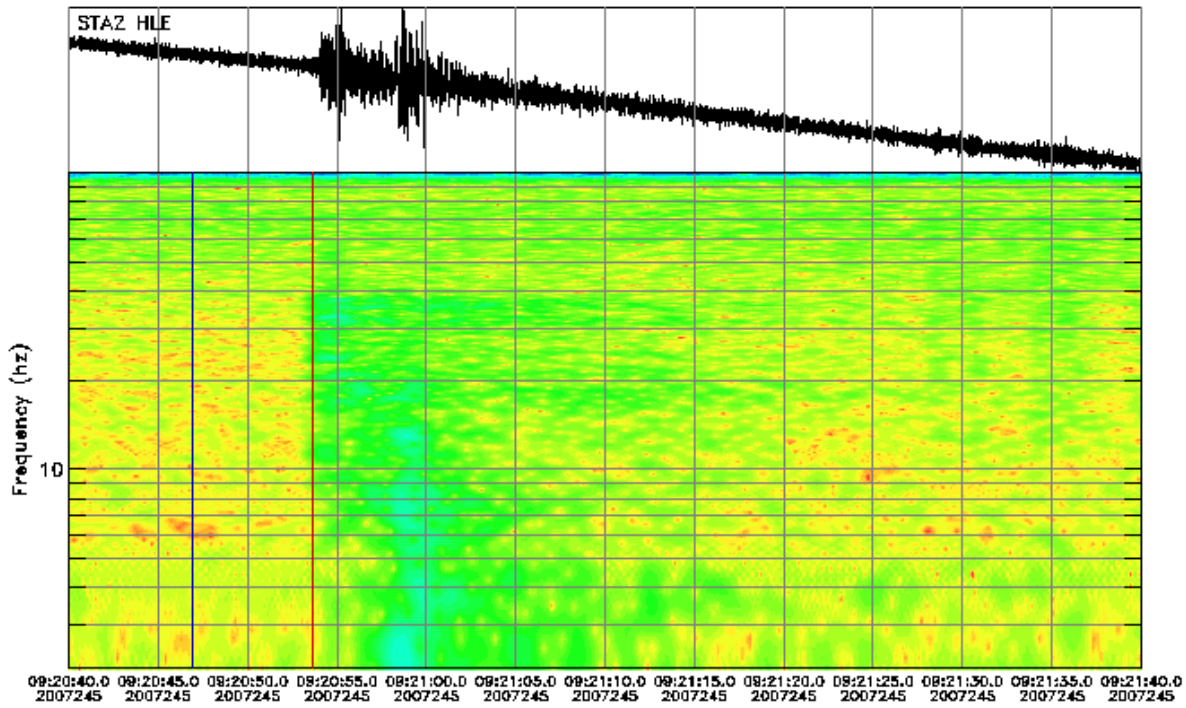

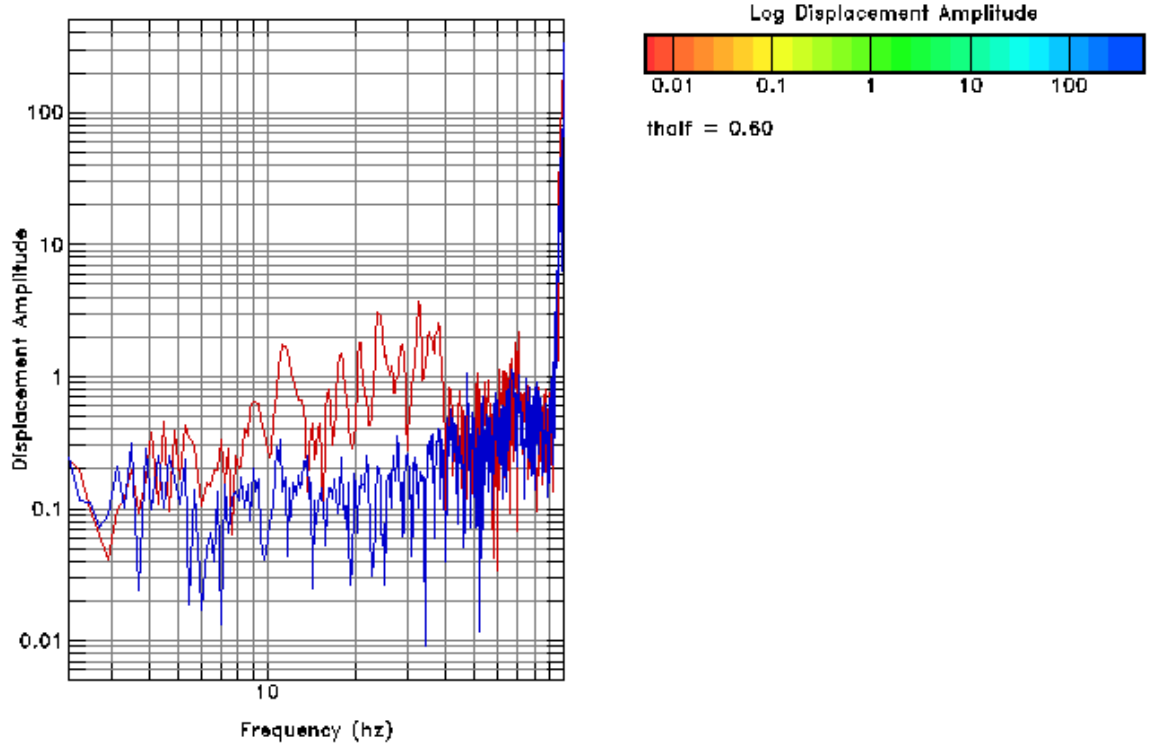

Instrument Correction: Episensor 200 Hz 10 Volt FS 2g/Quanterra 330 Linea

RESULTS

During the data collection period, we detect one earthquake from Iran and six explosions as follows:

- Iran Earthquake on 31/8/2007 (243) at 05:26
- Explosion on 1/9/2007 (244) at 07:10
- Explosion on 2/9/2007 (245) at 07:25
- Explosion on 2/9/2007 (245) at 09:20
- Explosion on 3/9/2007 (246) at 07:14
- Explosion on 4/9/2007 (247) at 07:11
- Explosion on 5/9/2007 (248) at 07:10

We used two methods to analyze the data using different programs. The results from both methods are given below and finally are confirming each other.

The first method is to select the Maximum Displacement Amplitude for the reasonable frequency for each component and or each station, then get the amplification factor by dividing the two horizontal components by the vertical one and get the average of the two ratios. As follows :

The total results collected from the site can be summarized as shown in the following table:

Event Date & Time	Name & component	Max.Displacement Amplitude	Ratio To HLZ
31/8/2007 (243) 05:26 (Iran)	Sta1 HLE (acceleration)	1.8 at freq. 2.8 Hz	0.72
31/8/2007 (243) 05:26 (Iran)	Sta2 HLE (acceleration)	1 at freq. 2.8 Hz	0.56
31/8/2007 (243) 05:26 (Iran)	Sta3 HLE (acceleration)	Not Clear	
31/8/2007 (243) 05:26 (Iran)	Sta4 HLE (acceleration)	2.01 at freq. 3 Hz	0.87
31/8/2007 (243) 05:26 (Iran)	Sta1 HLN (acceleration)	1.9 at freq. 2.9 Hz	0.76
31/8/2007 (243) 05:26 (Iran)	Sta3 HLN (acceleration)	0.9 at freq. 3.2 Hz	0.45
31/8/2007 (243) 05:26 (Iran)	Sta4 HLN (acceleration)	1.1 at freq. 4 Hz	0.48
31/8/2007 (243) 05:26 (Iran)	Sta1 HLZ (acceleration)	2.5 at freq. 2.8 Hz	

31/8/2007 (243) 05:26 (Iran)			Sta2 (acceleration)	HLZ	1.8 at freq. 2.8 Hz	
31/8/2007 (243) 05:26 (Iran)			Sta3 (acceleration)	HLZ	2 at freq. 3 Hz	
31/8/2007 (243) 05:26 (Iran)			Sta4 (acceleration)	HLZ	2.3 at freq. 3 Hz	
1/9/2007 (explo.)	(244)	07:10	Sta1 (acceleration)	HLZ	0.85 at freq. 6 Hz	
1/9/2007 (explo.)	(244)	07:10	Sta2 (acceleration)	HLZ	0.8 at req. 7 Hz	
1/9/2007 (explo.)	(244)	07:10	Sta1 (acceleration)	HLN	0.9 at freq. 5.5 Hz	1.06
1/9/2007 (explo.)	(244)	07:10	Sta2 (acceleration)	HLN	0.8 at freq. 6 Hz	1.0
1/9/2007 (explo.)	(244)	07:10	Sta1 (acceleration)	HLE	1 at freq. 8 Hz	1.18
1/9/2007 (explo.)	(244)	07:10	Sta2 (acceleration)	HLE	1 at freq. 6Hz	1.25
2/9/2007 (explo.)	(245)	07:25	Sta2 (acceleration)	HLZ	0.7 at freq. 3.5 Hz	
2/9/2007 (explo.)	(245)	07:25	Sta3 (acceleration)	HLZ	0.6 at freq. 3.5 Hz	
2/9/2007 (explo.)	(245)	07:25	Sta4 (acceleration)	HLZ	0.3 at freq. 2.9 Hz	
2/9/2007 (explo.)	(245)	07:25	Sta2 (acceleration)	HLE	0.8 at freq. 2.8 Hz	1.143
2/9/2007 (explo.)	(245)	07:25	Sta3 (acceleration)	HLE	0.85 at freq. 2.9 Hz	1.42
2/9/2007 (explo.)	(245)	07:25	Sta4 (acceleration)	HLE	0.3 at freq. 2.9 Hz	1.0
2/9/2007 (explo.)	(245)	07:25	Sta2 (acceleration)	HLN	1.0 at freq. 2.9 Hz	1.43
2/9/2007 (explo.)	(245)	07:25	Sta3 (acceleration)	HLN	1.8 at freq. 3 Hz	3
2/9/2007 (explo.)	(245)	07:25	Sta4 (acceleration)	HLN	0.38 at freq. 3.8Hz	1.27
2/9/2007 (explo.)	(245)	09:20	Sta2 (acceleration)	HLZ	2 at freq. 4 Hz	
2/9/2007 (explo.)	(245)	09:20	Sta3 (acceleration)	HLZ	3.2 at freq. 4 Hz	

2/9/2007 (explo.)	(245)	09:20	Sta4 (acceleration)	HLZ	2 at freq. 4 Hz	
2/9/2007 (explo.)	(245)	09:20	Sta2 (acceleration)	HLE	0.48 at freq. 4.5 Hz	
2/9/2007 (explo.)	(245)	09:20	Sta3 (acceleration)	HLE	3.3 at freq. 3.5 Hz	1.03
2/9/2007 (explo.)	(245)	09:20	Sta4 (acceleration)	HLE	0.33 at freq. 3.8Hz	
2/9/2007 (explo.)	(245)	09:20	Sta2 (acceleration)	HLN	5.8 at freq. 3.8 Hz	2.9
2/9/2007 (explo.)	(245)	09:20	Sta3 (acceleration)	HLN	4 at freq. 4 Hz	1.25
2/9/2007 (explo.)	(245)	09:20	Sta4 (acceleration)	HLN	1.7 at freq. 4 Hz	0.85
3/9/2007 (explo.)	(246)	07:14	Sta2 (acceleration)	HLZ	0.47 at freq. 2.5 Hz	
3/9/2007 (explo.)	(246)	07:14	Sta3 (acceleration)	HLZ	0.7 at freq. 3 Hz	
3/9/2007 (explo.)	(246)	07:14	Sta4 (acceleration)	HLZ	0.6 at freq. 2.5 Hz	
3/9/2007 (explo.)	(246)	07:14	Sta2 (acceleration)	HLN	0.7 at freq. 2.5 Hz	1.49
3/9/2007 (explo.)	(246)	07:14	Sta3 (acceleration)	HLN	1.8 at freq. 2.5 Hz	2.57
3/9/2007 (explo.)	(246)	07:14	Sta4 (acceleration)	HLN	1 at freq. 2.8 Hz	1.67
3/9/2007 (explo.)	(246)	07:14	Sta2 (acceleration)	HLE	1 at freq. 2.5 Hz	2.12
3/9/2007 (explo.)	(246)	07:14	Sta3 (acceleration)	HLE	1.1 at freq. 2.5Hz	1.57
3/9/2007 (explo.)	(246)	07:14	Sta4 (acceleration)	HLE	0.5 at freq. 2.5Hz	0.833
4/9/2007 (explo.)	(247)	07:11	Sta2 (acceleration)	HLZ	0.4 at freq. 2.5 Hz	
4/9/2007 (explo.)	(247)	07:11	Sta3 (acceleration)	HLZ	0.5 at freq. 3 Hz	
4/9/2007 (explo.)	(247)	07:11	Sta4 (acceleration)	HLZ	0.35 at freq. 2.8 Hz	
4/9/2007 (explo.)	(247)	07:11	Sta2 (acceleration)	HLN	0.3 at freq. 3 Hz	0.75

4/9/2007 (explo.)	(247)	07:11	Sta3 (acceleration)	HLN	0.7 at freq. 3 Hz	1.4
4/9/2007 (explo.)	(247)	07:11	Sta4 (acceleration)	HLN	1.1 at freq. 2.8 Hz	3.1
4/9/2007 (explo.)	(247)	07:11	Sta2 (acceleration)	HLE	0.9 at freq. 2.5 Hz	2.25
4/9/2007 (explo.)	(247)	07:11	Sta3 (acceleration)	HLE	1.0 at freq. 2.5 Hz	2.0
4/9/2007 (explo.)	(247)	07:11	Sta4 (acceleration)	HLE	0.38 at freq. 3Hz	1.1
5/9/2007 (explo.)	(248)	07:10	Sta2 (acceleration)	HLZ	0.5 at freq. 3 Hz	
5/9/2007 (explo.)	(248)	07:10	Sta3 (acceleration)	HLZ	0.85 at freq. 3.1 Hz	
5/9/2007 (explo.)	(248)	07:10	Sta4 (acceleration)	HLZ	0.6 at freq. 2.5 Hz	
5/9/2007 (explo.)	(248)	07:10	Sta2 (acceleration)	HLN	1.85 at freq. 2.8 Hz	3.7
5/9/2007 (explo.)	(248)	07:10	Sta3 (acceleration)	HLN	2.1 at req. 2.5 Hz	2.47
5/9/2007 (explo.)	(248)	07:10	Sta4 (acceleration)	HLN	1.2 at freq. 2.5 Hz	2
5/9/2007 (explo.)	(248)	07:10	Sta2 (acceleration)	HLE	1.1 at freq. 2.8Hz	2.2
5/9/2007 (explo.)	(248)	07:10	Sta3 (acceleration)	HLE	2.0 at freq. 2.8 Hz	2.36
5/9/2007 (explo.)	(248)	07:10	Sta4 (acceleration)	HLE	1.4 at freq. 2.5 Hz	2.33

Notes:

1- The Maximum displacement amplitude is in Nanometers.

2-The figures related to the shaded rows for south Riyadh explosion dated 2/9/2007 (245) at 09:20 will be included in the report in the same sequence of the rows, other figures related to the rest of events and explosions will be given in Appendix III.

The last step is to get the ratio of the two horizontal components to the vertical component, we got the following amplification factor for each site as follows

Station	Latitude	Longitude	Frequency Hz	Amplification Factor
STA1	24.8497	46.5324	4.3	0.875
STA2	24.8401	46.5342	2.84	2.0
STA3	24.8466	46.5468	2.85	2
STA4	24.8577	46.5421	2.98	1.57

The above results means that the average frequency is 3.2425 Hz (i.e. 3.2 Hz) and the corresponding amplification factor is 1.61125 (1.6 g) of the earth acceleration (g).

The second method using other analysis programs .

In this method, we plot the acceleration versus time for the event, and select the time window of the signal starting from its P-wave as shown in yellow rectangle of figure xx0. The signal in this range will be analyzed.

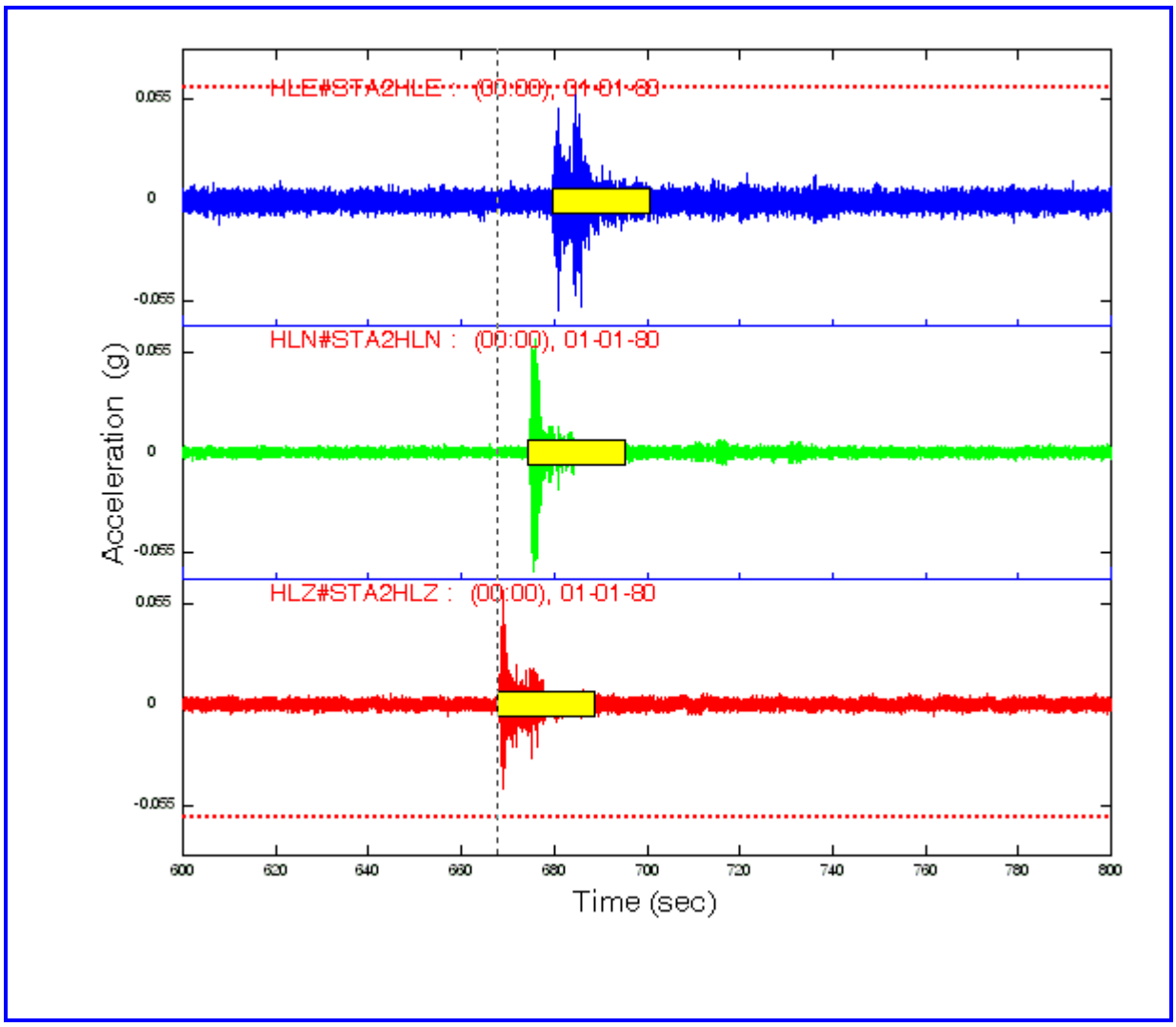

figure xx0 shows the wave form of the event and the selected time windows.

The spectral amplitude (g) versus frequency is plotted for the three acceleration components as shown in the following figure xx1. Note the frequency when the vertical component goes down from its peak (at frequencies 1.65 and at 3.356 Hz) relative to the other two horizontal components HLE and HLN.

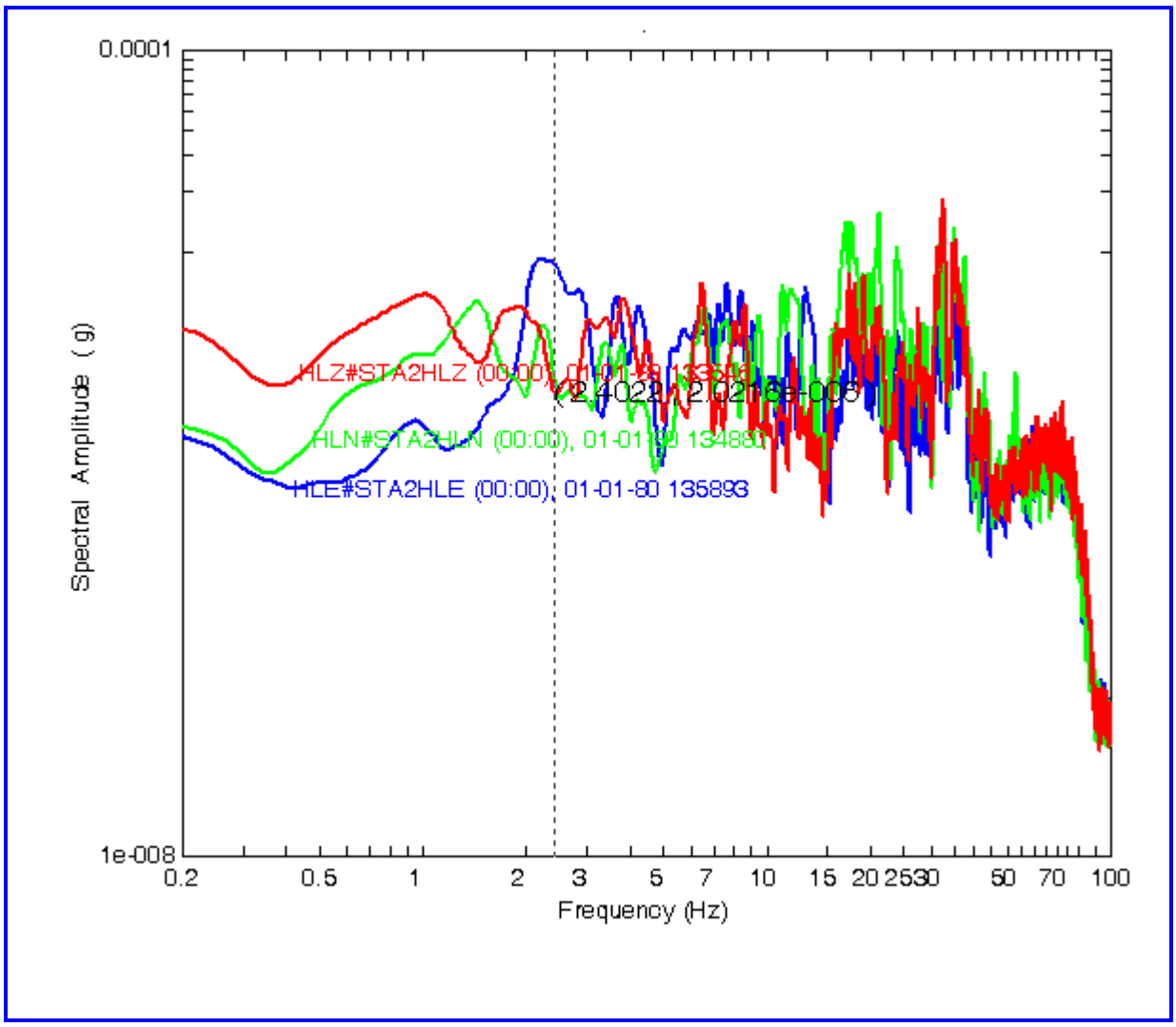

Figure xx1, shows the spectral amplitude (g) VS. frequency (Hz).

Then dividing the spectrum of the two horizontal component by the vertical component (Blue is the East-West component HLE divided by the vertical component HLZ and the Green is the North-South component HLN divided by the vertical component HLZ) as shown in figure xx2.

Then concluding the average of the two spectrum ratios to get the Black Curve from which the amplification factor can be concluded.

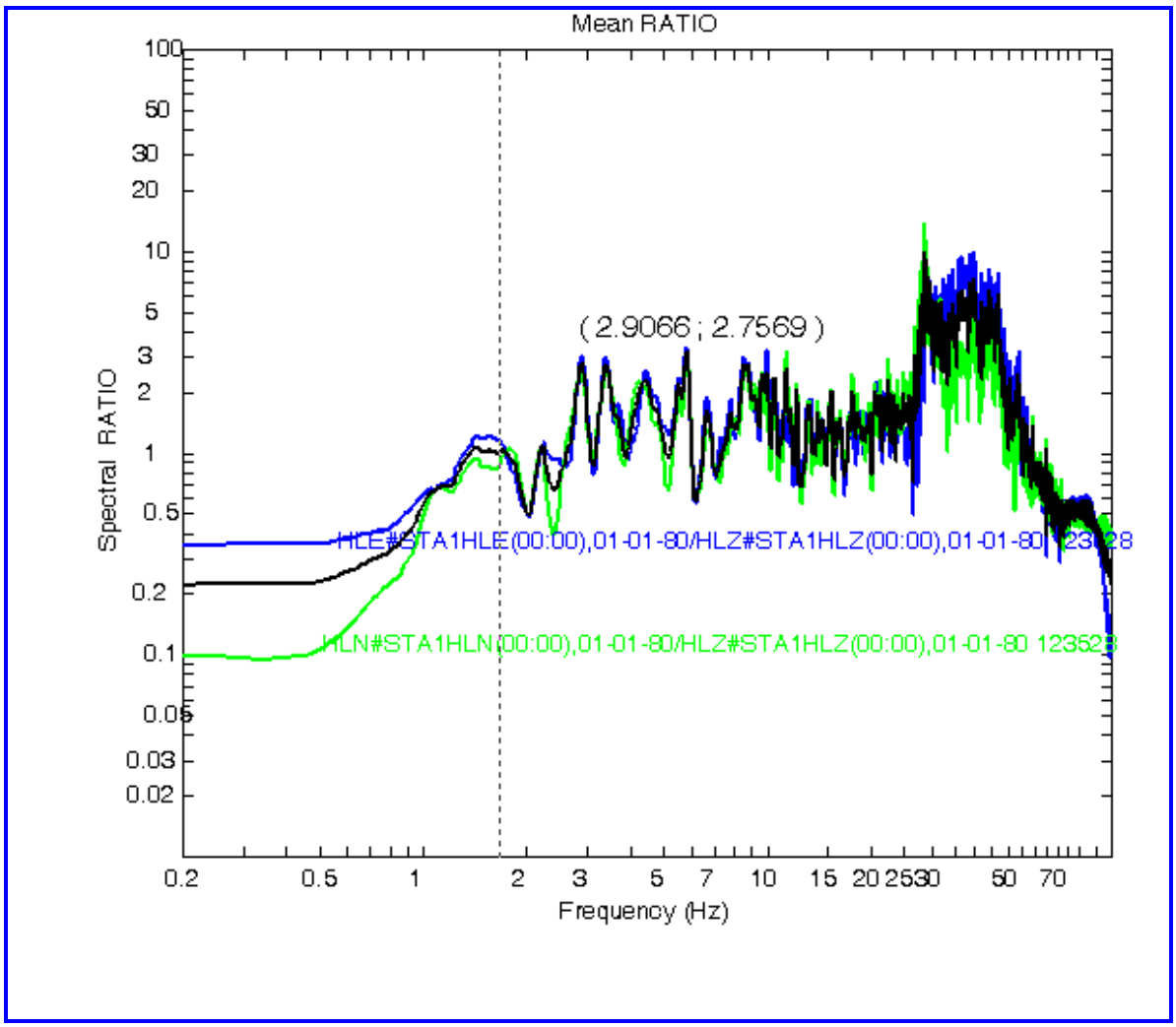

Fig. xx2 shows the spectral ratio of the HLE and HLN component relative to HLZ component. The Black curve is the average of the amplification factor spectrum.

The following amplification factor for each site can be concluded as follows

Station	Latitude	Longitude	Frequency Hz	Amplification Factor
STA1	24.8497	46.5324	**1.73**	**1.25**
STA1			**2.9066**	**2.7569**
STA2	24.8401	46.5342	**1.7**	**1.25**
STA2			**2.4**	**2.55**
STA3	24.8466	46.5468	**1.6545**	**1.9**
STA3	24.8466	46.5468	**3.5**	**2.3**
STA3	24.8466	46.5468	**10.2**	**4**
STA4	24.8577	46.5421	**1.7**	**1.23**
STA4			**2.7**	**2.2**
STA4			**7.12**	**6.87**

Note that:

The curves used for the analysis are given at appendix III.

The above results means that the average frequency is 2.6 Hz and the corresponding amplification factor is about 1.99 of the earth acceleration (g).

Conclusions

We can conclude that there are 3 zones of different frequencies and different amplification factors of the earth acceleration in gravity values (g) . These zones are as follows :

- Up to 1.7 Hz which is related to deep seismic events, the amplification factor is 1.23 of the earth acceleration (g).
- From 1.7 Hz to 3.5 Hz , the amplification factor is 2.75 % of (g).
- From 3.5 Hz to 10 Hz , the amplification factor is 6.87 % of (g).

Generally, the amplification values indicate that the upper layers and site response are strong enough to resist moderate earthquakes of magnitudes 5. Low-velocity sedimentary structures trap and amplify seismic waves. Near-surface (< 50 m) velocities most strongly control ground motions amplitudes. Attenuation will dissipate high frequency motions, however, low frequency motions may persist to affect large buildings and structures. Long-period, long-duration shaking created by distant earthquakes cause tall buildings undergo a large number of stress reversals, resulting in strength deteriorations in concrete elements and fatigue failures in steel connections. Long-period response should be of concern for large structures. Site response estimates for One-story buildings are 10 Hz , 3-4 story buildings are 2 Hz, Tall buildings 0.5 – 1.0 Hz and 0.17 Hz for High-rise buildings.

The explosion dated 2/9/2007 (245) at 09:20 waveform and analysis graphs are as follows:

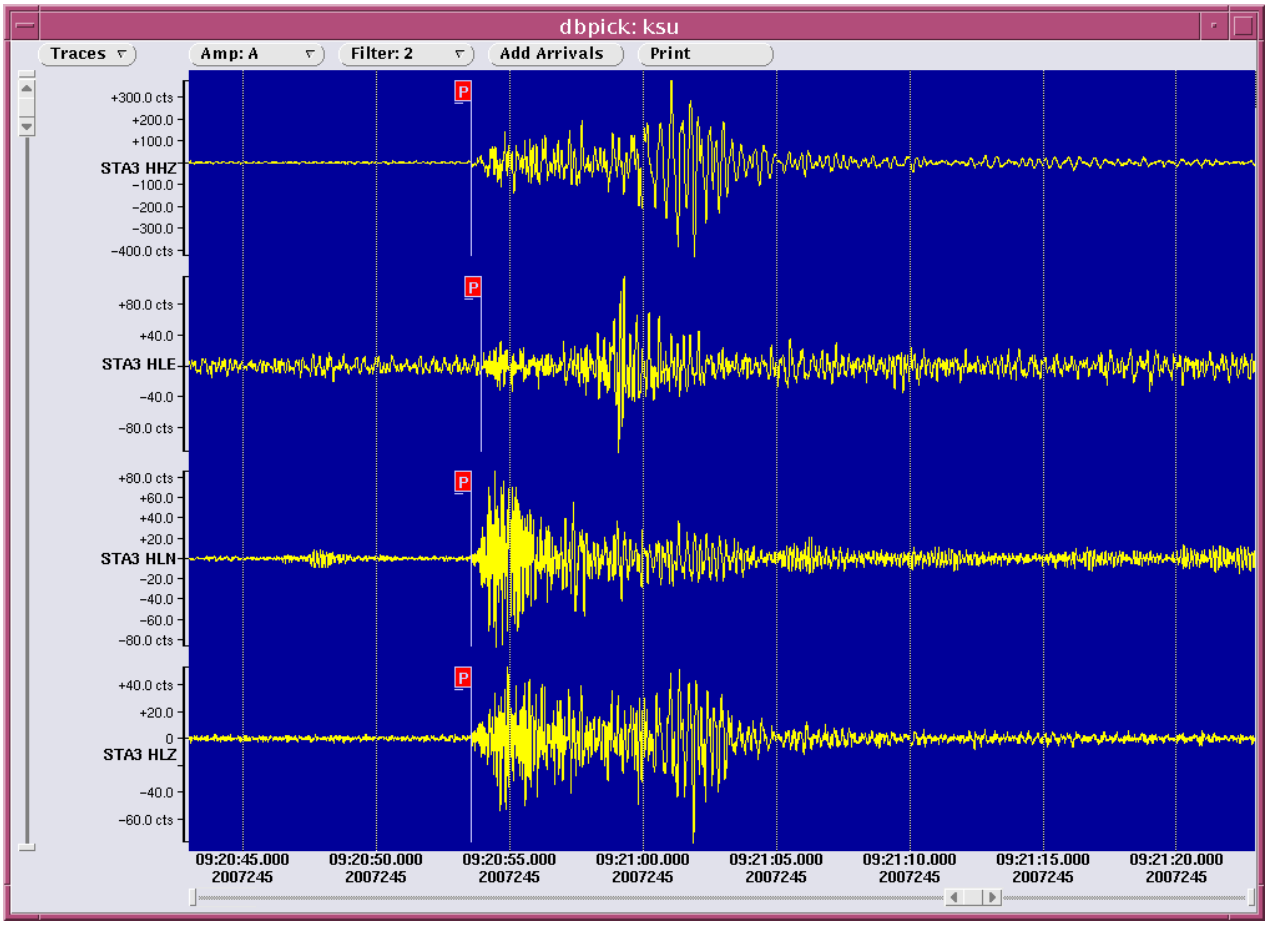

Fig. xx shows the wave form of explosion dated 2/9/2007 at 9:20 am for station No. 3 the velocity component HHZ and the 3 acceleration component HLE, HLN, and HLZ. (waveform shown from Antelope program).

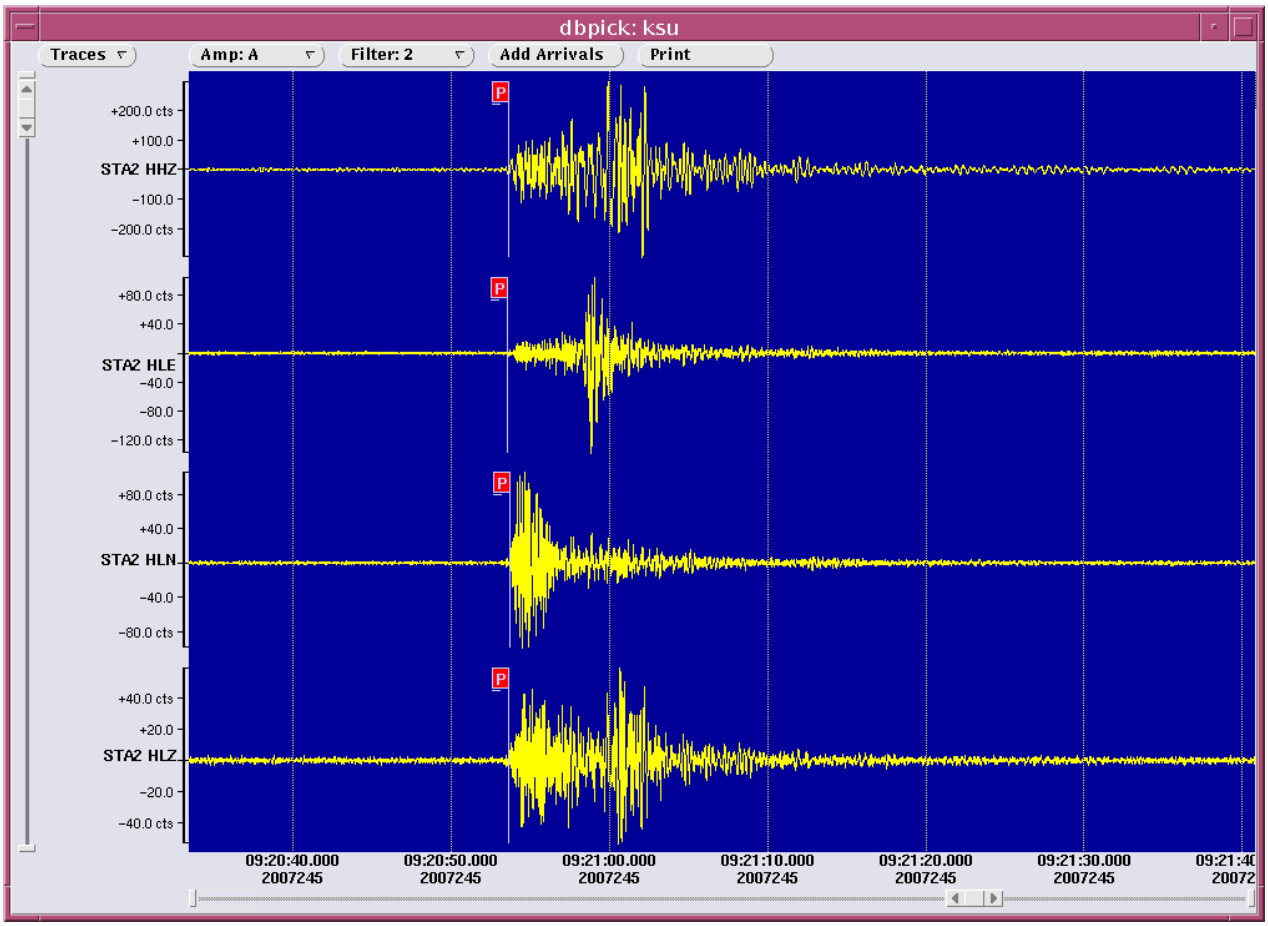

Fig. xx shows the wave form of explosion dated 2/9/2007 at 9:20 am for station No. 2, the velocity component HHZ and the 3 acceleration component HLE, HLN, and HLZ. (waveform shown from Antelope program).

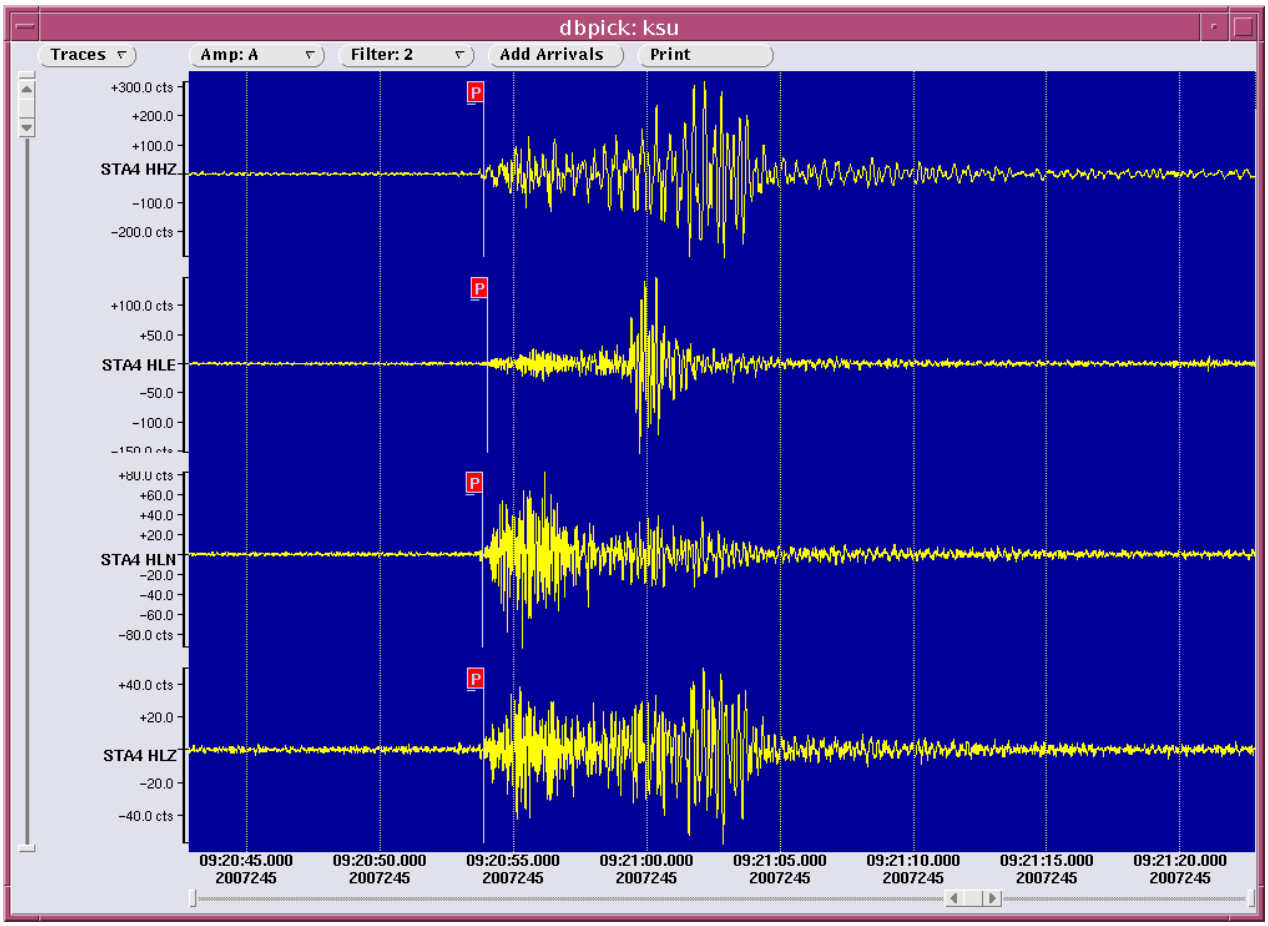

Fig. xx shows the wave form of explosion dated 2/9/2007 at 9:20 am for station No.4, the velocity component HHZ and the 3 acceleration component HLE, HLN, and HLZ. (waveform shown from Antelope program).

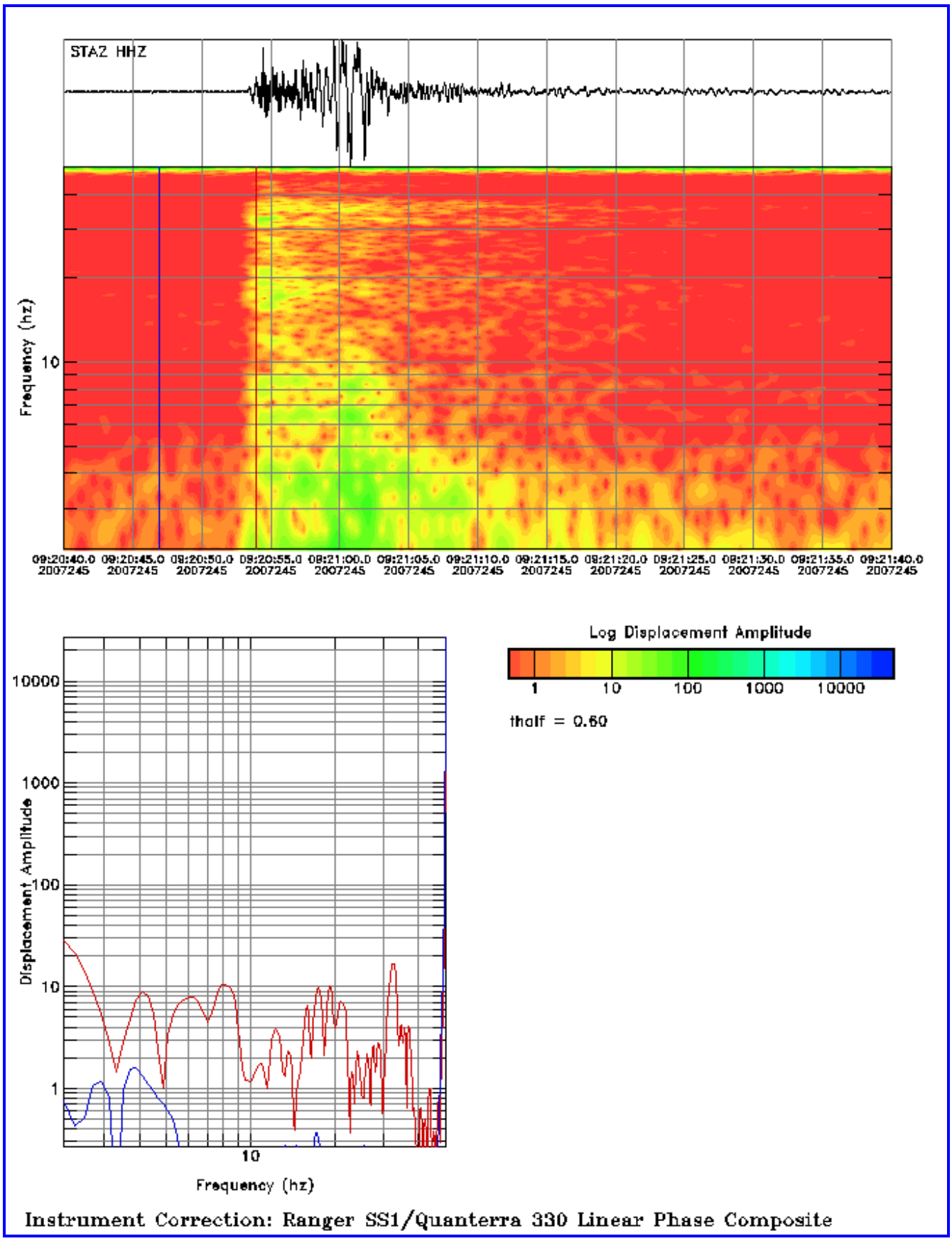

Fig. xx shows the signal (Red) and noise (blue) of the SS! Ranger (Velocity) for station No. 2 , event dated 2/9/2007 at 9:20 am (HHZ component).

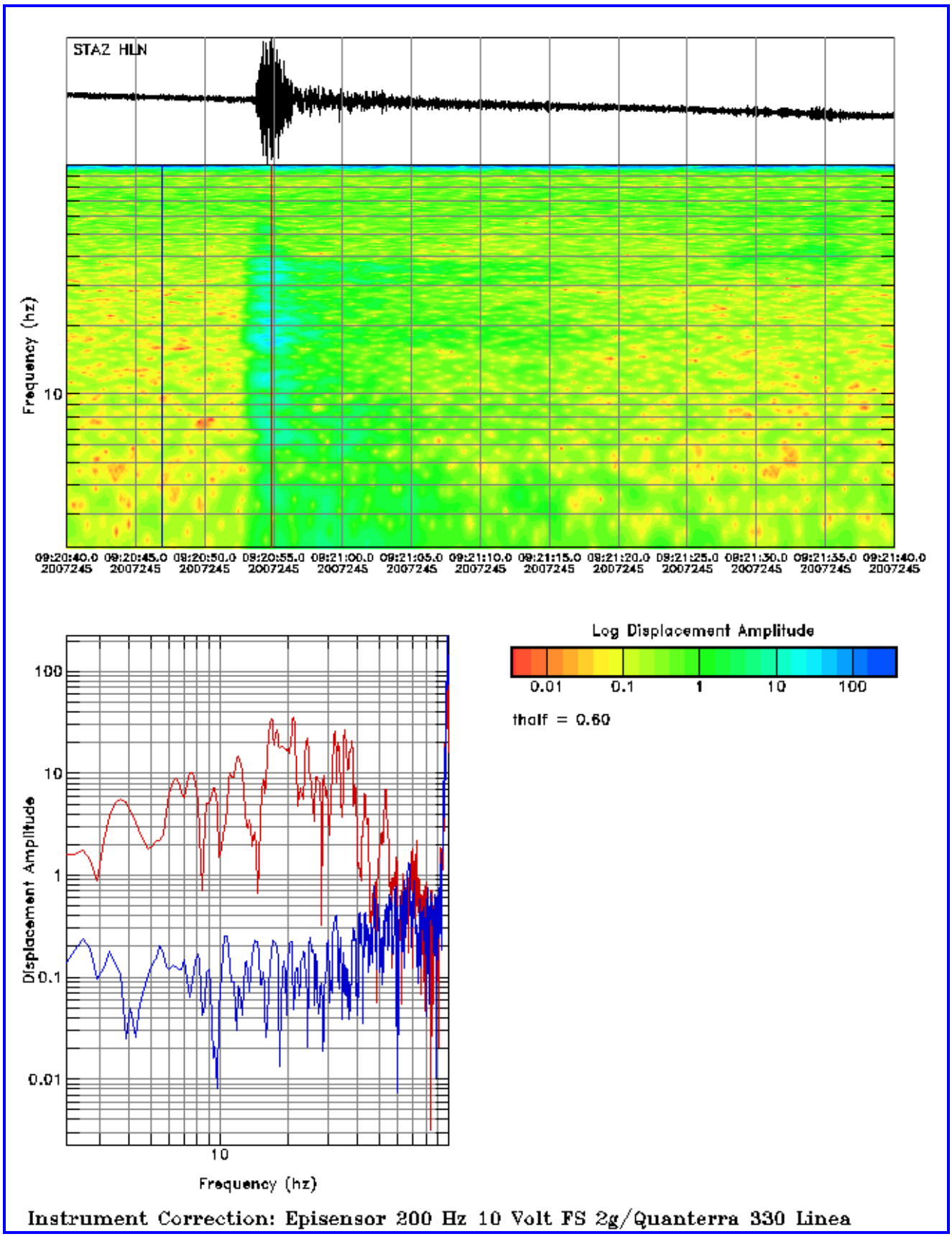

Fig. xx shows the signal (Red) and noise (blue) of the Episensor (acceleration) for station No. 2 , event dated 2/9/2007 at 9:20 am (HLN component).

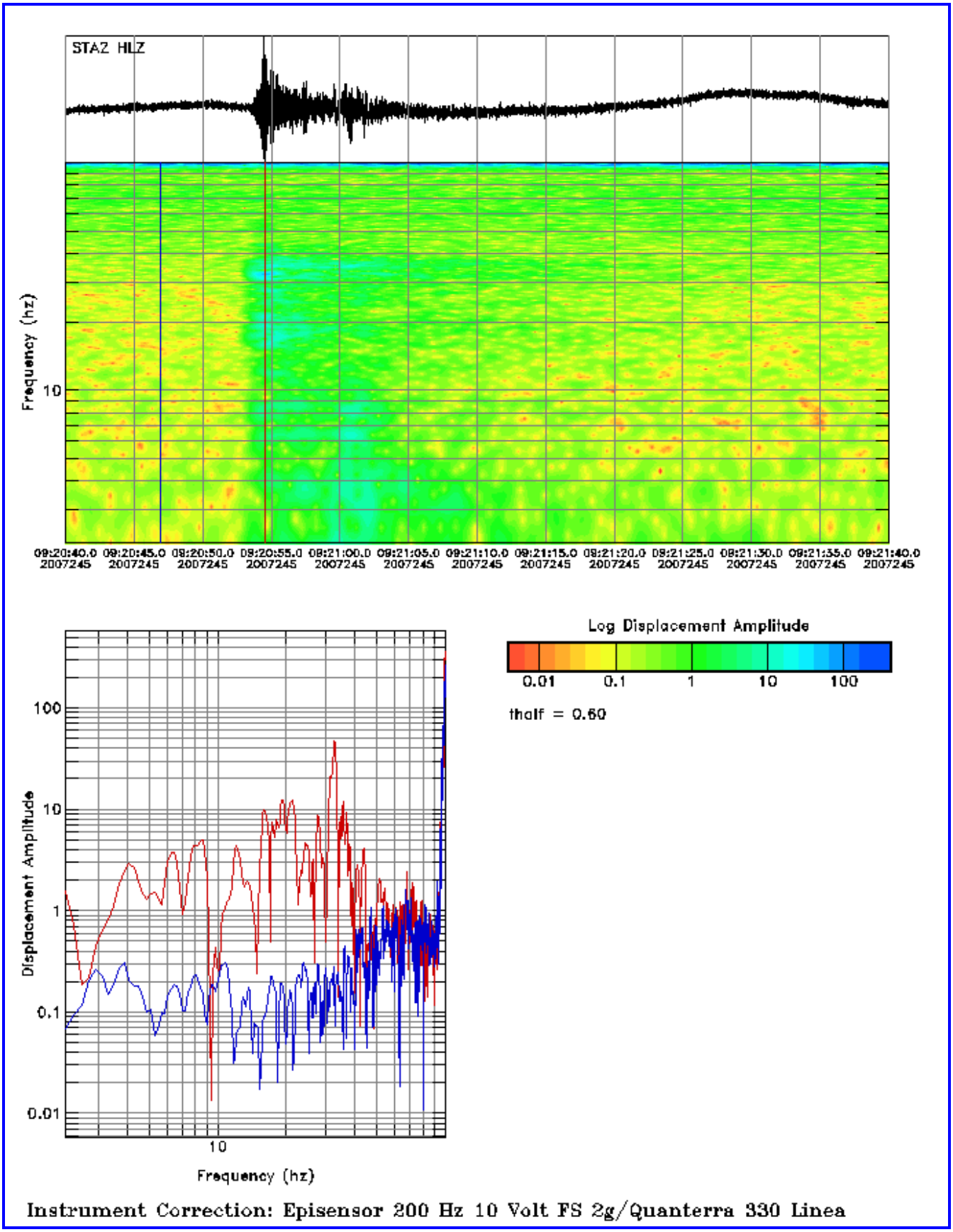

Fig. xx shows the signal (Red) and noise (blue) of the Episensor (acceleration) for station No. 2 , event dated 2/9/2007 at 9:20 am (HLZ component).

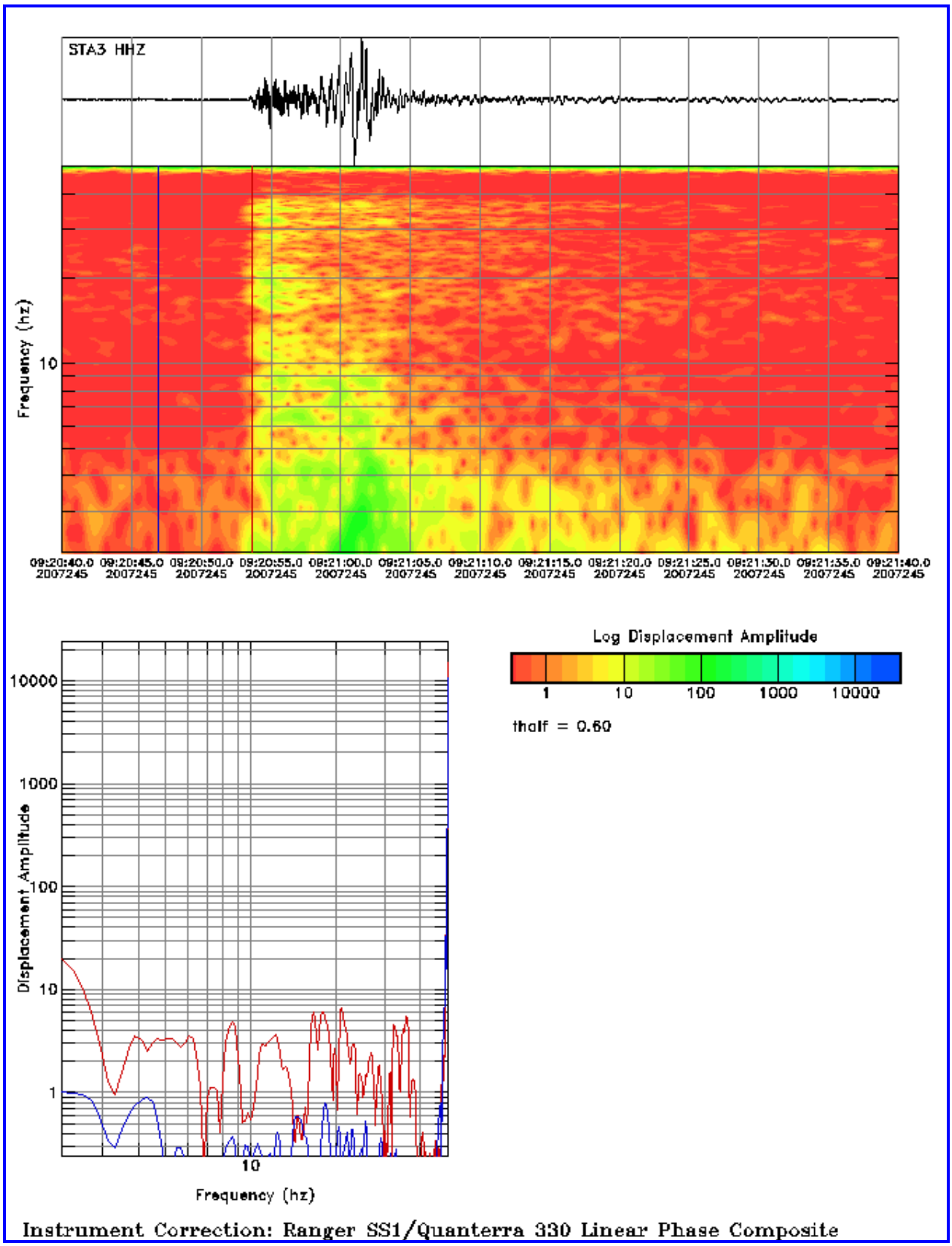

Fig. xx shows the signal (Red) and noise (blue) of the SS! Ranger (Velocity) for station No. 3 , event dated 2/9/2007 at 9:20 am (HHZ component).

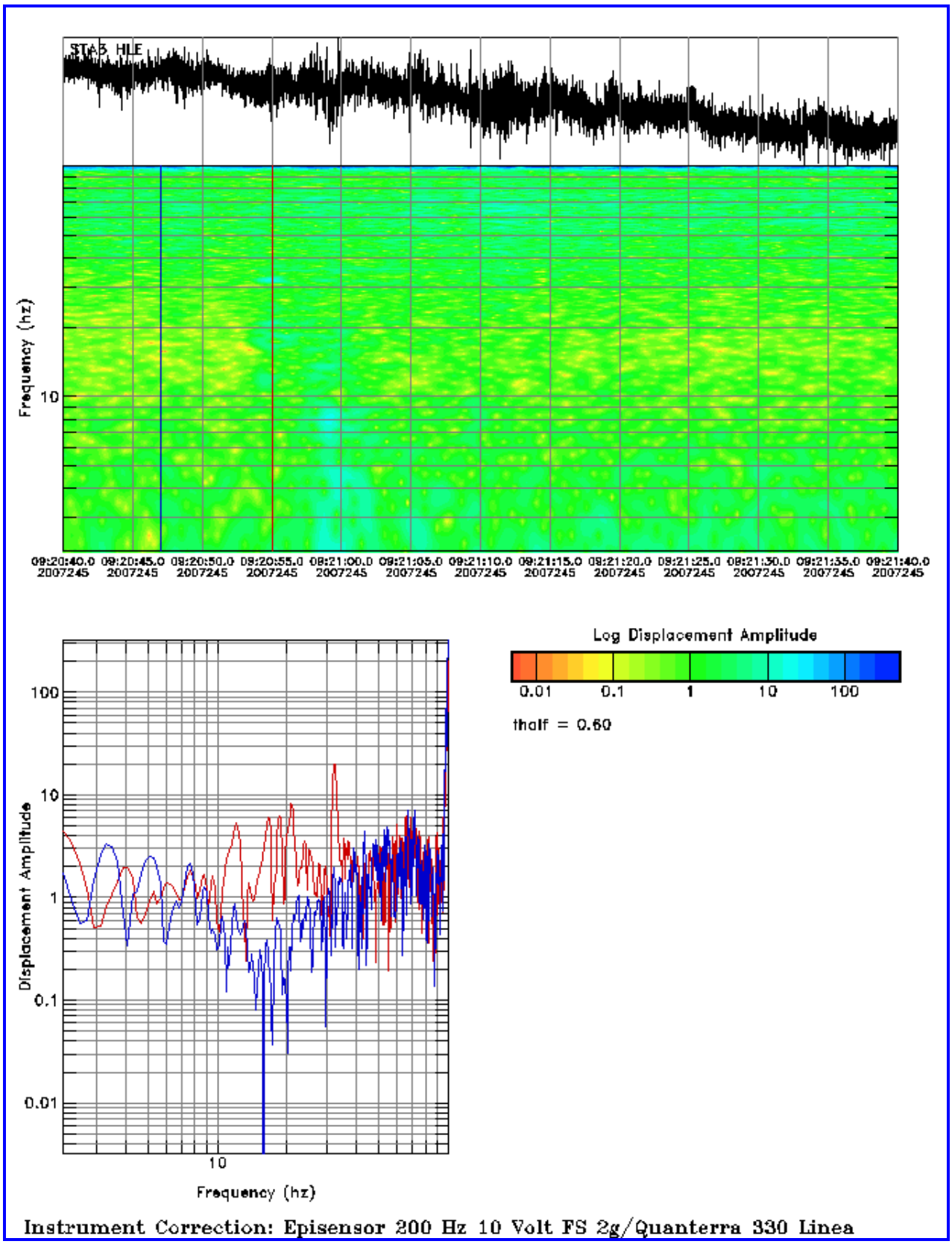

Fig. xx shows the signal (Red) and noise (blue) of the Episensor (acceleration) for station No. 3 , event dated 2/9/2007 at 9:20 am (HLE component).

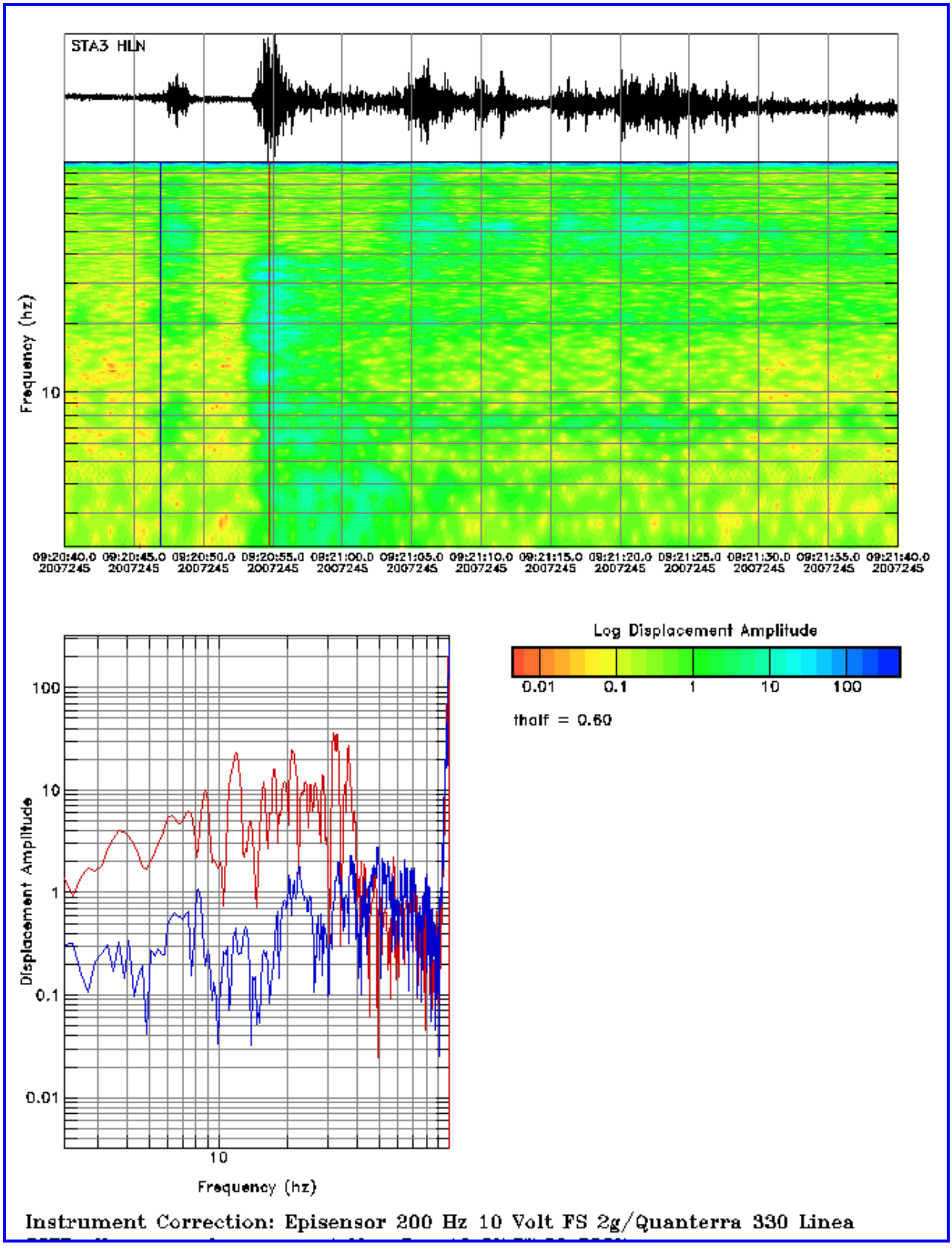
STA3 HLN
Frequency (hz)
10
09:20:40.0 2007245
09:20:45.0 2007245
09:20:50.0 2007245
09:20:55.0 2007245
09:21:00.0 2007245
09:21:05.0 2007245
09:21:10.0 2007245
09:21:15.0 2007245
09:21:20.0 2007245
09:21:25.0 2007245
09:21:30.0 2007245
09:21:35.0 2007245
09:21:40.0 2007245
Log Displacement Amplitude
0.01
0.1
1
10
100
thalf = 0.60
Displacement Amplitude
100
10
1
0.1
0.01
10
Frequency (hz)
Instrument Correction: Episensor 200 Hz 10 Volt FS 2g/Quanterra 330 Linea

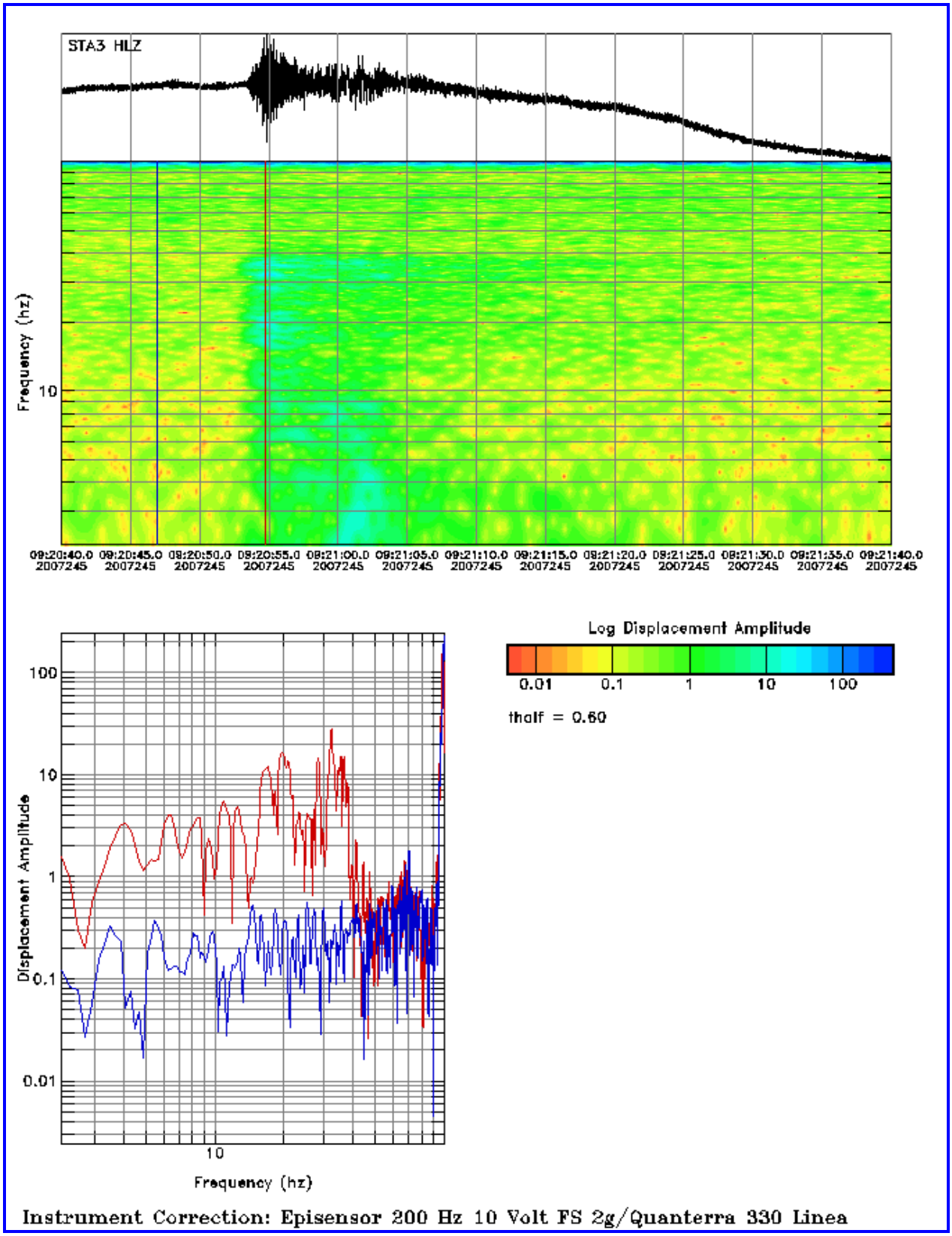
STA3 HLZ
Frequency (hz)
10
09:20:40.0 2007245
09:20:45.0 2007245
09:20:50.0 2007245
09:20:55.0 2007245
09:21:00.0 2007245
09:21:05.0 2007245
09:21:10.0 2007245
09:21:15.0 2007245
09:21:20.0 2007245
09:21:25.0 2007245
09:21:30.0 2007245
09:21:35.0 2007245
09:21:40.0 2007245
Log Displacement Amplitude
0.01
0.1
1
10
100
thalf = 0.60
Displacement Amplitude
100
10
1
0.1
0.01
10
Frequency (hz)
Instrument Correction: Episensor 200 Hz 10 Volt FS 2g/Quanterra 330 Linea

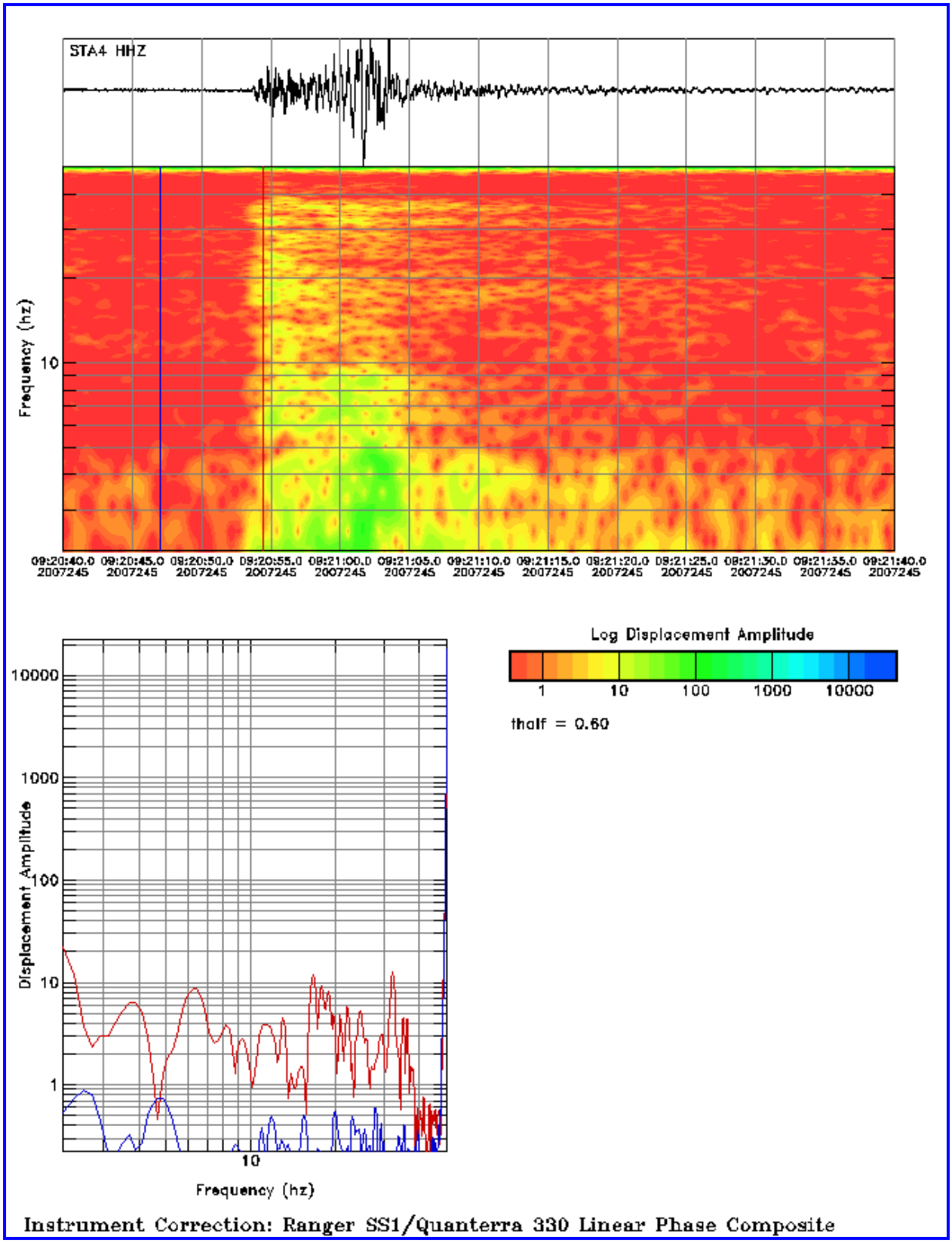
STA4 HHZ
Frequency (hz)
10
09:20:40.0 2007245
09:20:45.0 2007245
09:20:50.0 2007245
09:20:55.0 2007245
09:21:00.0 2007245
09:21:05.0 2007245
09:21:10.0 2007245
09:21:15.0 2007245
09:21:20.0 2007245
09:21:25.0 2007245
09:21:30.0 2007245
09:21:35.0 2007245
09:21:40.0 2007245
Log Displacement Amplitude
1
10
100
1000
10000
thalf = 0.60
10000
1000
100
10
1
Displacement Amplitude
10
Frequency (hz)
Instrument Correction: Ranger SS1/Quanterra 330 Linear Phase Composite

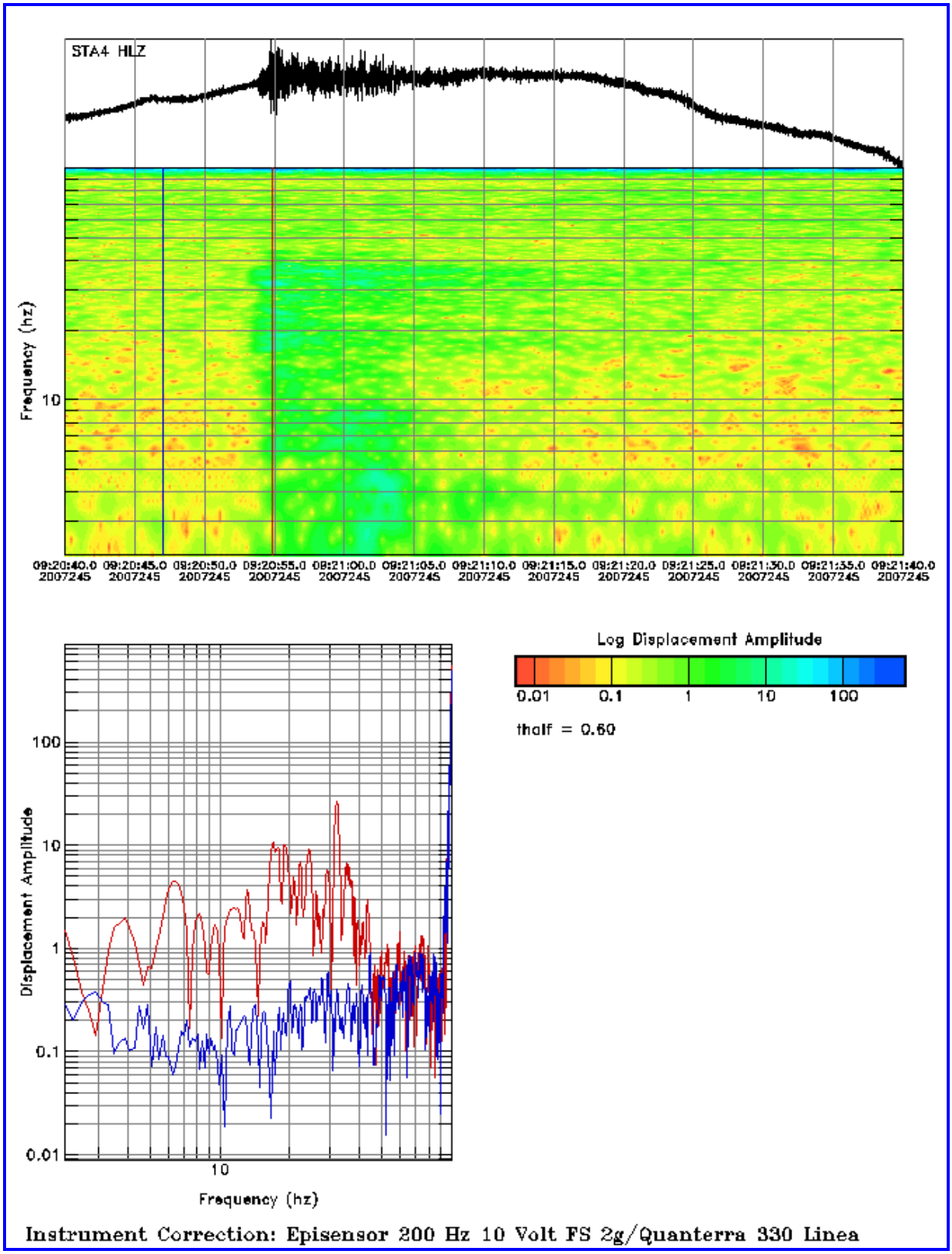
STA4 HLZ
Frequency (hz)
10
09:20:40.0 2007245
09:20:45.0 2007245
09:20:50.0 2007245
09:20:55.0 2007245
09:21:00.0 2007245
09:21:05.0 2007245
09:21:10.0 2007245
09:21:15.0 2007245
09:21:20.0 2007245
09:21:25.0 2007245
09:21:30.0 2007245
09:21:35.0 2007245
09:21:40.0 2007245
Log Displacement Amplitude
0.01
0.1
1
10
100
thalf = 0.60
Displacement Amplitude
100
10
1
0.1
0.01
10
Frequency (hz)
Instrument Correction: Episensor 200 Hz 10 Volt FS 2g/Quanterra 330 Linea

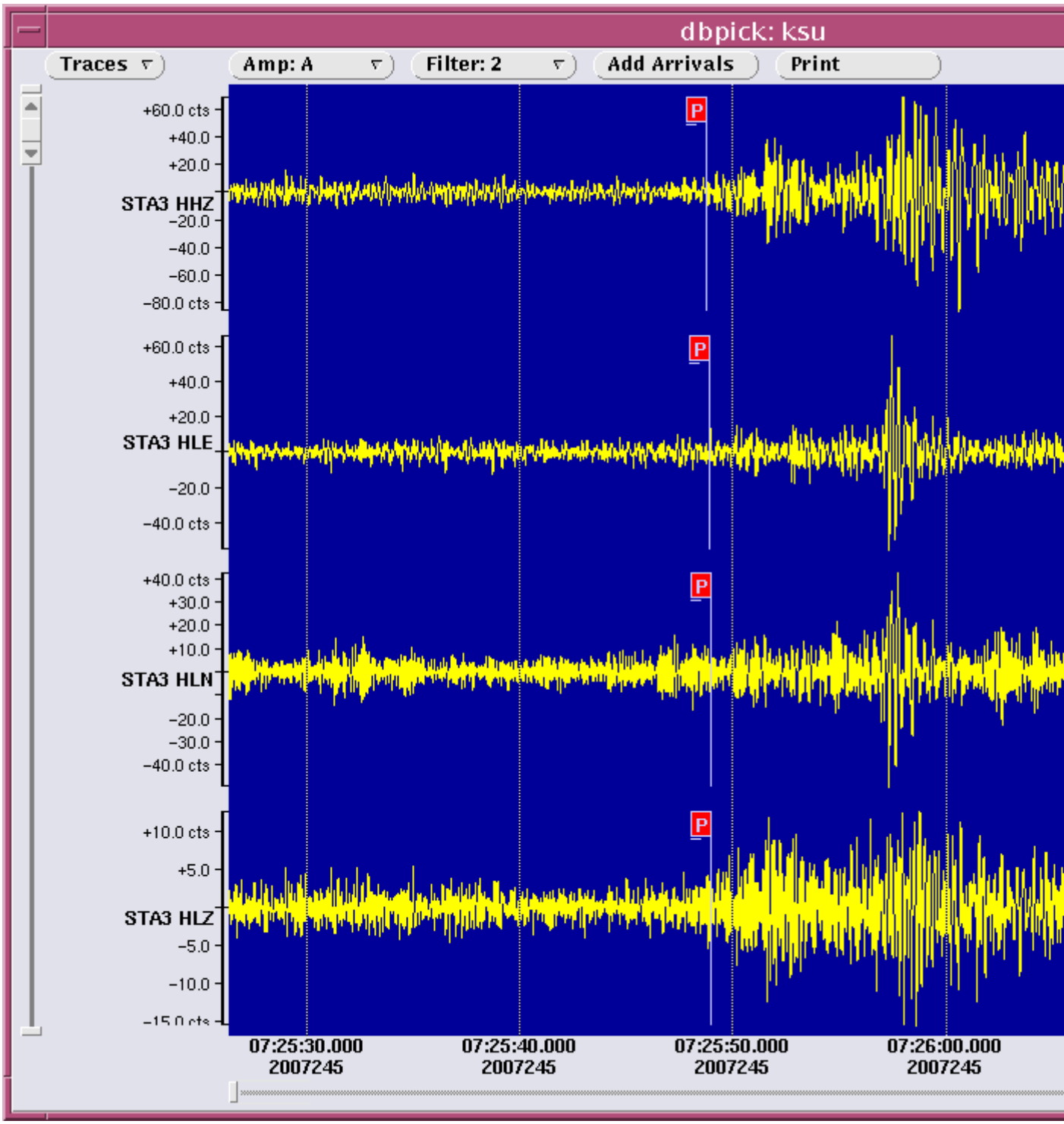
dbpick: ksu
Traces
Amp: A
Filter: 2
Add Arrivals
Print
+60.0 cts
+40.0
+20.0
STA3 HHZ
-20.0
-40.0
-60.0
-80.0 cts
+60.0 cts
+40.0
+20.0
STA3 HLE
-20.0
-40.0 cts
+40.0 cts
+30.0
+20.0
+10.0
STA3 HLN
-20.0
-30.0
-40.0 cts
+10.0 cts
+5.0
STA3 HLZ
-5.0
-10.0
-15.0 cts
P
07:25:30.000
2007245
07:25:40.000
2007245
07:25:50.000
2007245
07:26:00.000
2007245

Appendix I

The primary overall site map is shown in Fig. Inx1.

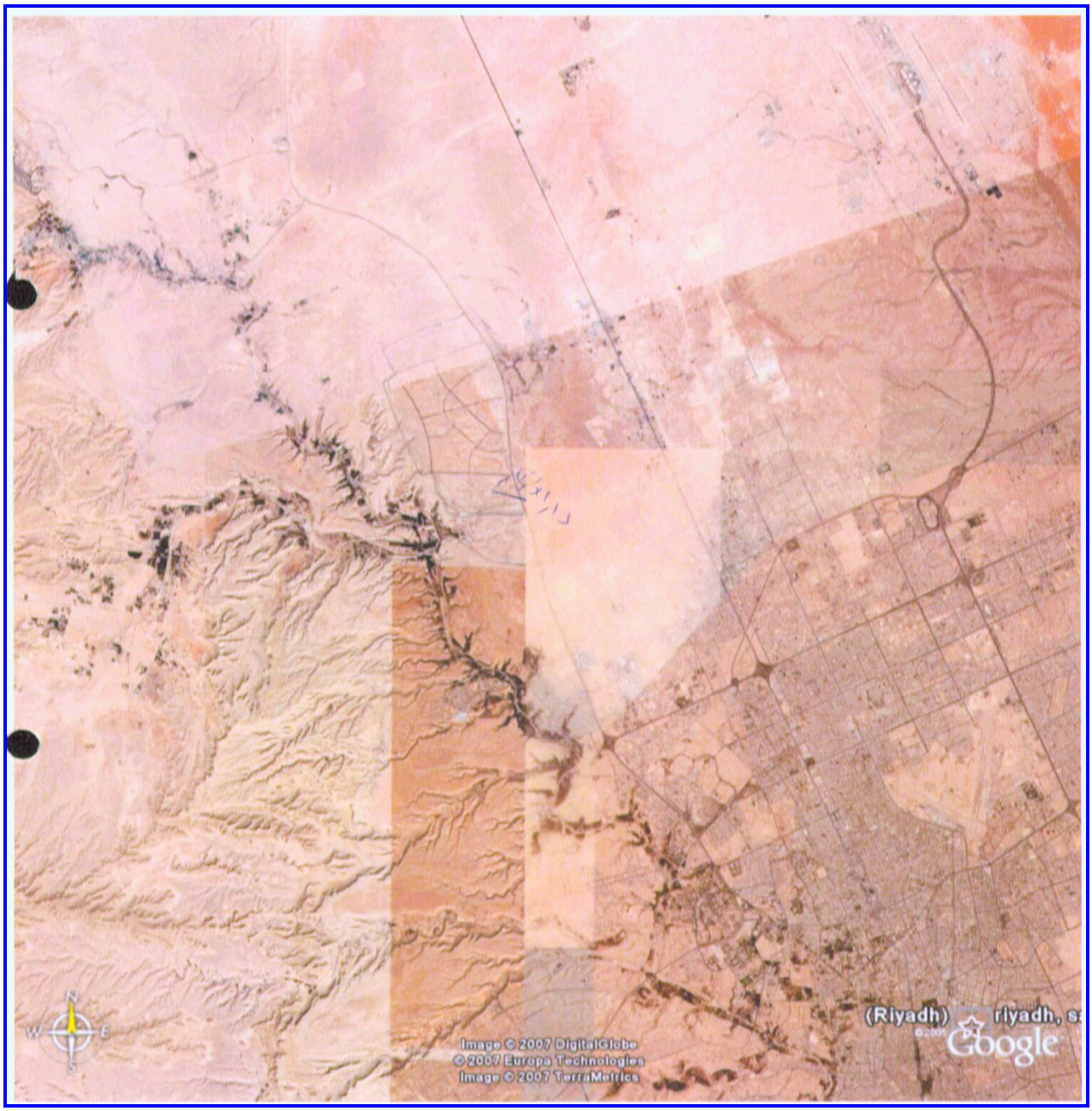

Fig. Inx1 : Primary overall site map

He detailed map for each station are shown in the following figures.

Fig. Inx2 : Detailed map for station No. 1

Fig. Inx2 : Detailed map for station No. 2

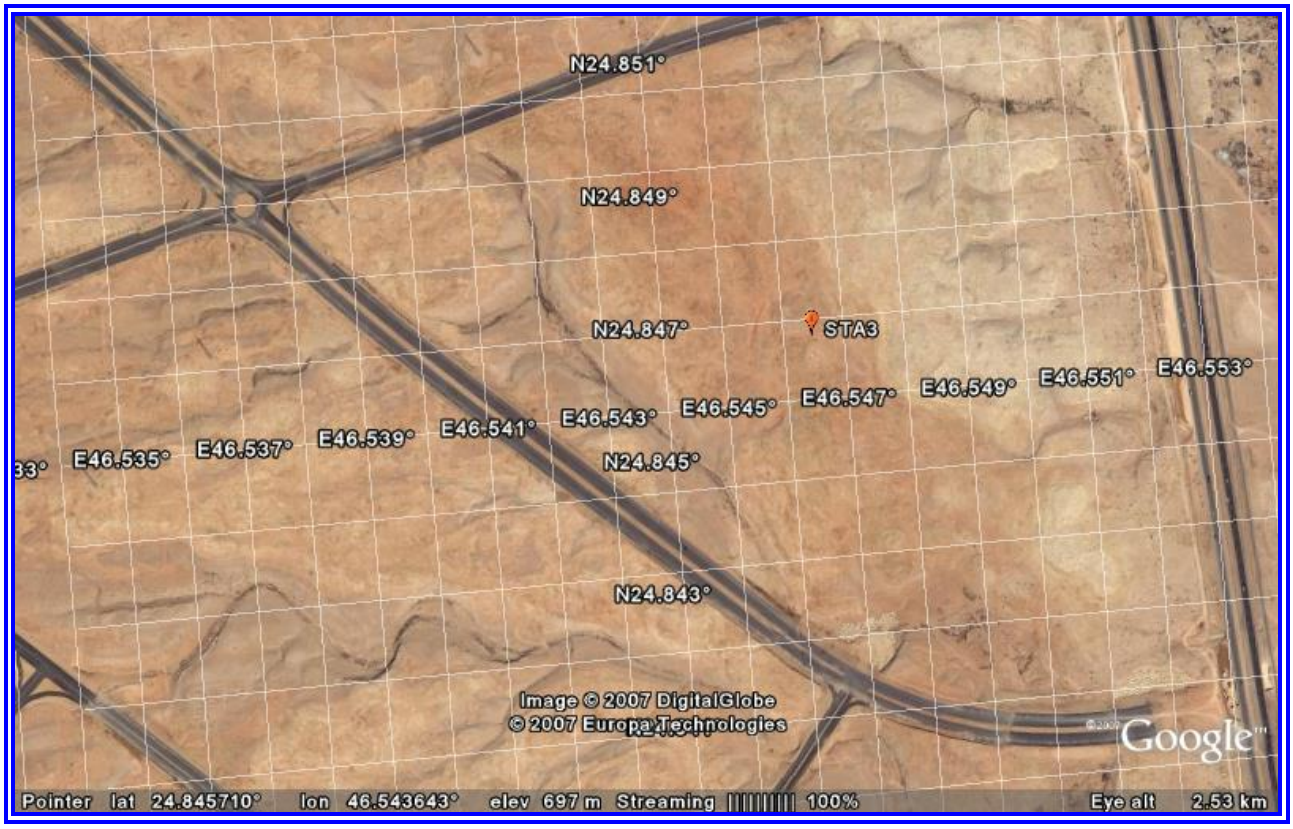

Fig. Inx2 : Detailed map for station No. 3

Fig. Inx5 : Detailed map for station No. 4

Reference to the above four stations maps (figures Inx2, Inx3, Inx4, Inx5) , station one and two are almost at the center of the whole site (where the important building will be) and stations three and four are near to the main road to detect the maximum noise of the road.

Appendix II

Seismometers

1- The SS-1 Ranger Seismometer

The SS-1 Ranger Seismometer, widely recognized as an excellent short-period field seismometer, is the terrestrial version of the "lunar seismometer" designed for the Ranger lunar program. The current SS-1 retains the original features of small size, high sensitivity, adjustable natural period and rugged watertight construction. An important feature of the Ranger is that it can be adapted as either a vertical or horizontal seismometer by simple adjustment of the mass centering spring. The SS-1 is frequently used as a sensor for ambient vibration measurements of buildings, bridges, foundations and offshore platforms.

The SS-1 Ranger Seismometer has been used extensively for years as a field seismometer by major seismological observatories. As a structural dynamics instrument, the SS-1 Ranger pioneered in the determination of multi-modes of vibration under low-level excitation; structures studied under this application have included dams, high-rise buildings and nuclear power plants.

General Description The SS-1 Ranger Seismometer is a "moving coil" style (velocity) transducer. The coil is stationary, however, while the strong permanent magnet serves as the seismic inertial mass. The mass is supported and constrained by annular springs at the top and bottom of the moving magnet.

The basic natural period of 0.35 seconds is extended to 1 second or more by means of small rod magnets which surround the periphery of the mass, interacting with its magnetic field. The separate calibration coil in the base provides a simple and accurate means of field-calibrating the SS-1, using only a known-voltage and a fixed precision resistor. In a vertical position, the unit is 5.5 inches in diameter and 12 inches high, including the inertial mass centering extension. For transportation, a protective clamp for the moving mass is incorporated into the base of the seismometer. Available as options for the SS-1 are adjustable leveling feet and bulls-eye levels.

.

2- ES-T

Episensor

Technical Specifications	
Natural Period:	1 second nominal
Weight of Mass:	1.45 kg
Mass Travel:	+/-1 mm
External Resistance for 70% of critical damping:	Approximately equal to coil resistance
Calibration Coil Resistance:	100 ohm
Calibration Coil Motor Constant:	0.4 newtons per ampere nominal
Transducer Coil Options:	Transducer Coil - 5000 ohms nominal
	Approximate Generator Constant V/(m/s) - 345
	Approximate CDR at 1 second - 6530
Physical Characteristics	
Housing:	Watertight case
Operating Temperature:	-40° to 70° C (-40° to 160 F)
Size:	305 mm x 140 mm diameter (12" x 5.5")
Weight:	5.0 kg (10.9 Ibs)
Ordering Information	
	1. If desired natural period is greater than one second, specify for vertical or horizontal operation.
	2. Specify desired transducer coil resistance, if other than 5000 ohms.
	3. Specify options desired; bulls-eye levels and/or leveling feet.
Key Features	
	Low noise
	Extended bandwidth -- DC to 200 Hz
	User-selectable full-scale range
	Calibration coil (standard)
	Single-end or differential output (user selectable)
	Double-stage transient protection
Specifications	
Dynamic range:	155 dB+
Bandwidth:	DC to 200 Hz
Calibration coil:	Standard
Full-scale range:	User selectable at ± 0.25g, ± 0.5g, ± 1g, ± 2g or ± 4g

Outputs:	User selectable at: ± 2.5V single-ended; ± 10V single-ended;± 5 V differential;± 20 V differential
Zero adjust:	Three user-friendly access holes for simple,safe, efficient adjustment
Linearity:	< 1000 $\mu g/g^2$
Hysteresis:	< 0.1% of full scale
Cross-axis sensitivity:	< 1% (including misalignment)
Zero point thermal drift:	< 500µg/°C (1g sensor)
ESD, RF, EMI protection:	Double stage transient protection withgas arrester elements
Power consumption:	12 mA from +/- 12V (Standard Amp), 35 mA from +/- 12 V (Low Noise Amp), Single supply option available
Physical size:	13.3 cm diameter (cylinder), 6.2 cm high
Mounting:	Single bolt mounting, three adjustable leveling feet and bubble level
Connection:	Single military-style metal connector
Operating Temperature:	-20º to 70ºC (0º to 160ºF)
Housing:	Watertight enclosure

The Quanterra Q-330 Digitizer

Specifications

Specification	Description
Channels	3 or 6-channel
Dynamic Range	132-135 dB wideband RMS typical. Typical band-limited 136 dB
Format	32-bit integer, Level 2 compressed 1-second packets
Input Range	40V P-P at gain=1
Gain	Selectable per channel: 1,30
Filtering	Linear or Minimum Phase FIR.
Sample Rate	200, 100, 50, 40, 20, 10, 1 Other rates available.
Time Base	Precision TCXO, locked to GPS. No adjustment.
DSP/CPU	ADSP-2189M
Telemetry	Full Duplex, efficient positive acknowledge with error control. UDP/IP over serial and Ethernet. Burst or continuous. Operates with major application software.
Temperature	Fully specified -20 to +50C Operative -40 to +70C
Sensor Control	Calibrate step, sine, or random. Recenter, on-command
Operational Data	Temp, DC voltage, GPS status, Sensor boom position (6 chan)
Memory	8Mb RAM standard
Network	IEEE 802 10Base-T Ethernet UDP/IP Protocol Stack
Serial Ports	2 serial telemetry and 1 console ports up to 115kbaud.
Wireless	IrDA interface supported.
Power	<0.6 W avg. 12VDC 3-channel <0.8 W avg. 12VDC 6-channel
Physical	Sealed, Aluminum, 14 X 4 X 6 in., 8 lbs., Rubber endcaps, Externally visible status and fault indicators.

The Quanterra Packet Baler model PB14F

Specifications

Specification	Description
Channels	No limit. Defined by Q330
Capacity	Defined by media. Standard 20Gb. Removable Compact Flash or Microdrive available with smaller capacity
Format	Federation of Digital Seismic Networks MSEED
Retrieval Functions	Data may be recovered by an HTTP time/channel request, or by files containing all available data for selected channels
File sizes	Selectable. 16Mb standard. 4096-byte MSEED standard.
Offload Rate	Up to 400kbyte/s.
Routing and Network Connectors	Baler routes IP packets between its independently addressed serial IP and 10BaseT Ethernet ports.
Serial Configure Mode	ASCII terminal using serial port to select some configuration options Accessed by button press.
Network Configure Mode	Supports simple configuration of a group of Balers over an IP network, including automatic address discovery. Software upgrade via network.
Telemetry from Q330	Full Duplex, efficient positive acknowledge with error control. UDP/IP over serial and Ethernet. Burst or continuous from Q330.
Temperature	Electronics specified -40 to +85C Operating range constrainted by rotating media. CF fully rated.
Operating Modes	Continuous or Power-Cycled (standard). Typical duty cycle < 1%.
Operational Data	Baler monitors its own power consumption
Memory	16Mb RAM standard
Network	IEEE 802 10Base-T Ethernet UDP/IP. TCP/IP Protocol Stack
Serial Ports	1 serial telemetry (up to 115kbaud) and 1 debug port.(19200 baud)
Technology	Industry-standard PC/104
Power	<6 W max. <0.06W typical, including duty cycle
Physical	Desktop: Aluminum, 9 X 6 X 3 in., 3 lbs., Externally visible LED status and fault indicators.

Appendix III

Earthquakes and explosions analysis graphs

- **Iran Earthquake on 31/8/2007 (243) at 05:26**
- **Explosion on 1/9/2007 (244) at 07:10**
- **Explosion on 2/9/2007 (245) at 07:25**
- **Explosion on 2/9/2007 (245) at 09:20**
- **Explosion on 3/9/2007 (246) at 07:14**
- **Explosion on 4/9/2007 (247) at 07:11**
- **Explosion on 5/9/2007 (248) at 07:10**

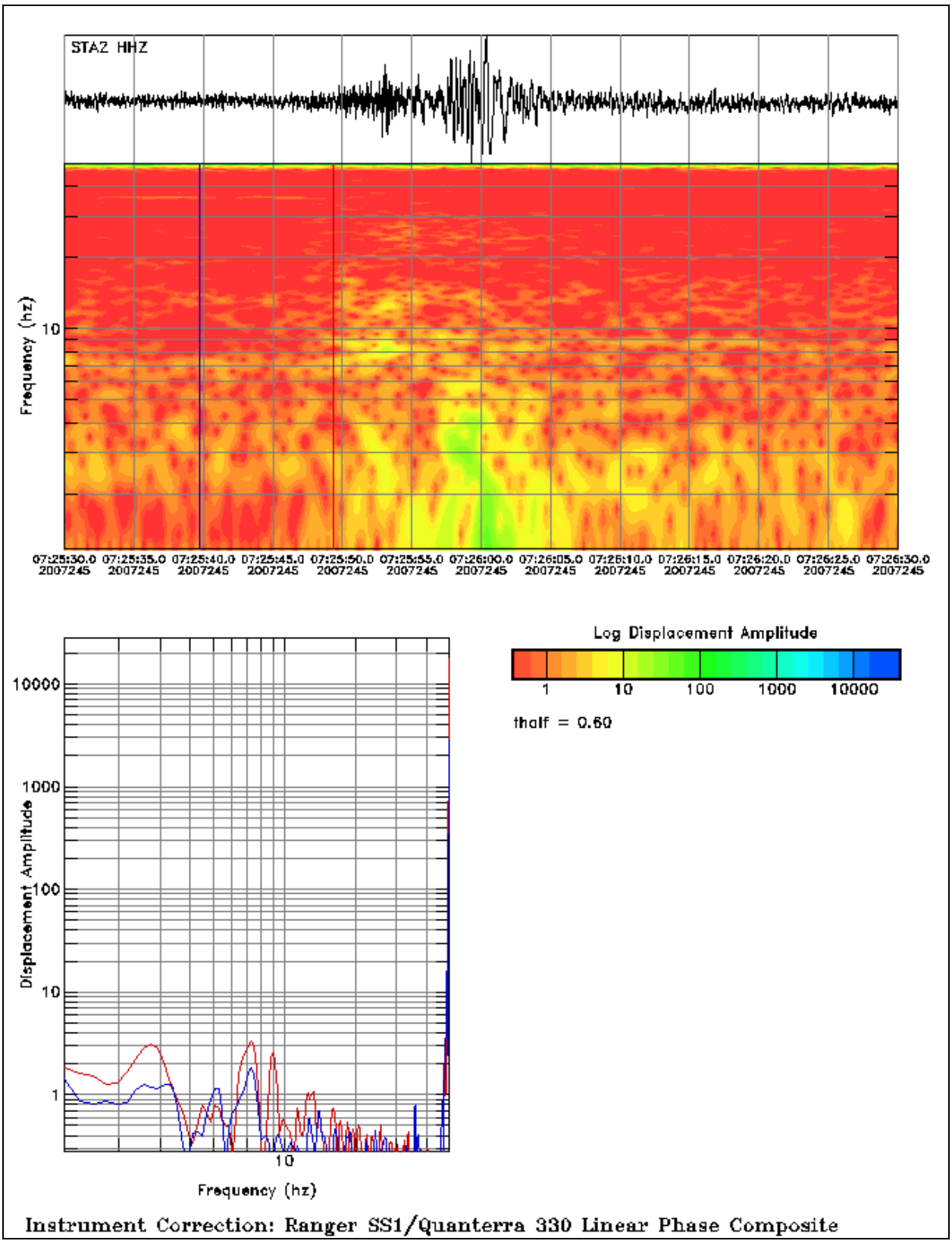
STAZ HHZ
Frequency (hz)
10
07:25:30.0 2007245
07:25:35.0 2007245
07:25:40.0 2007245
07:25:45.0 2007245
07:25:50.0 2007245
07:25:55.0 2007245
07:26:00.0 2007245
07:26:05.0 2007245
07:26:10.0 2007245
07:26:15.0 2007245
07:26:20.0 2007245
07:26:25.0 2007245
07:26:30.0 2007245
Log Displacement Amplitude
1
10
100
1000
10000
thalf = 0.60
10000
1000
100
10
1
Displacement Amplitude
10
Frequency (hz)
Instrument Correction: Ranger SS1/Quanterra 330 Linear Phase Composite

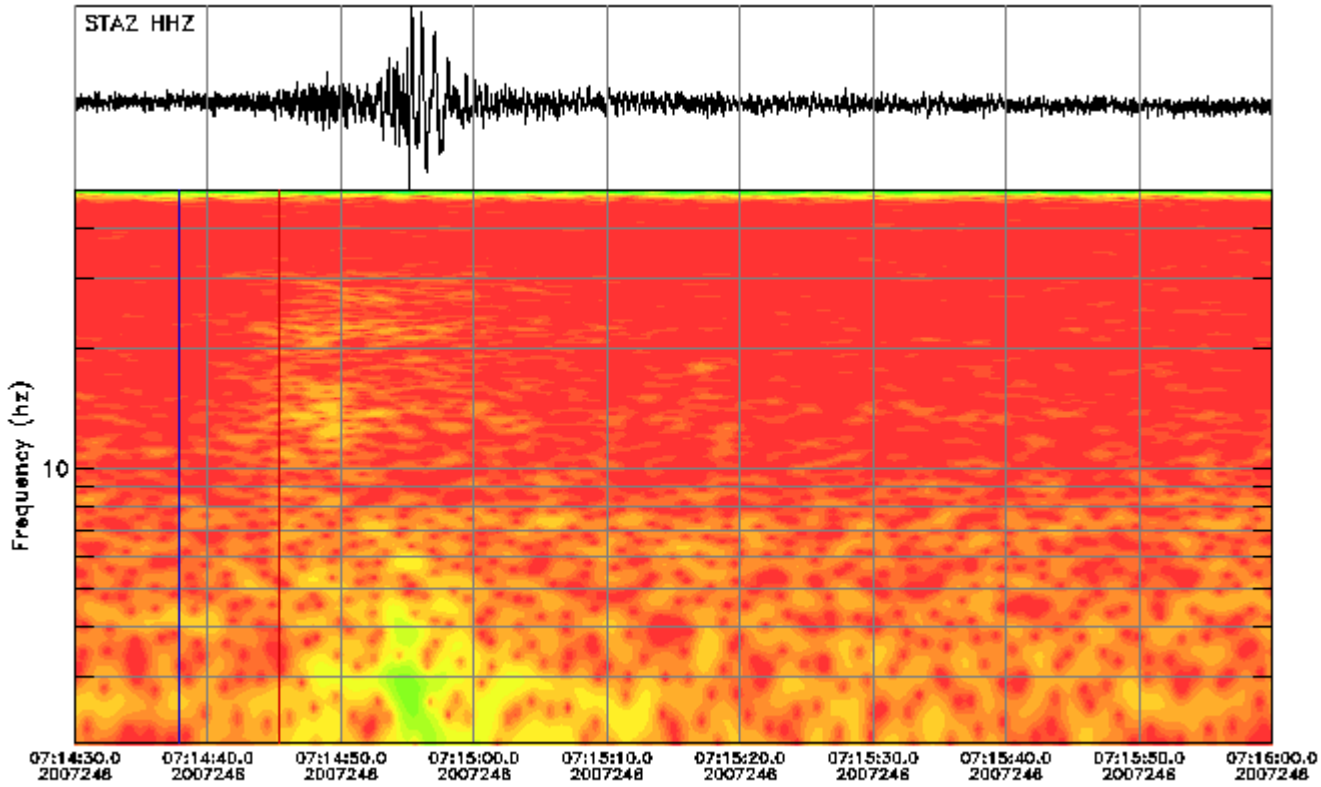

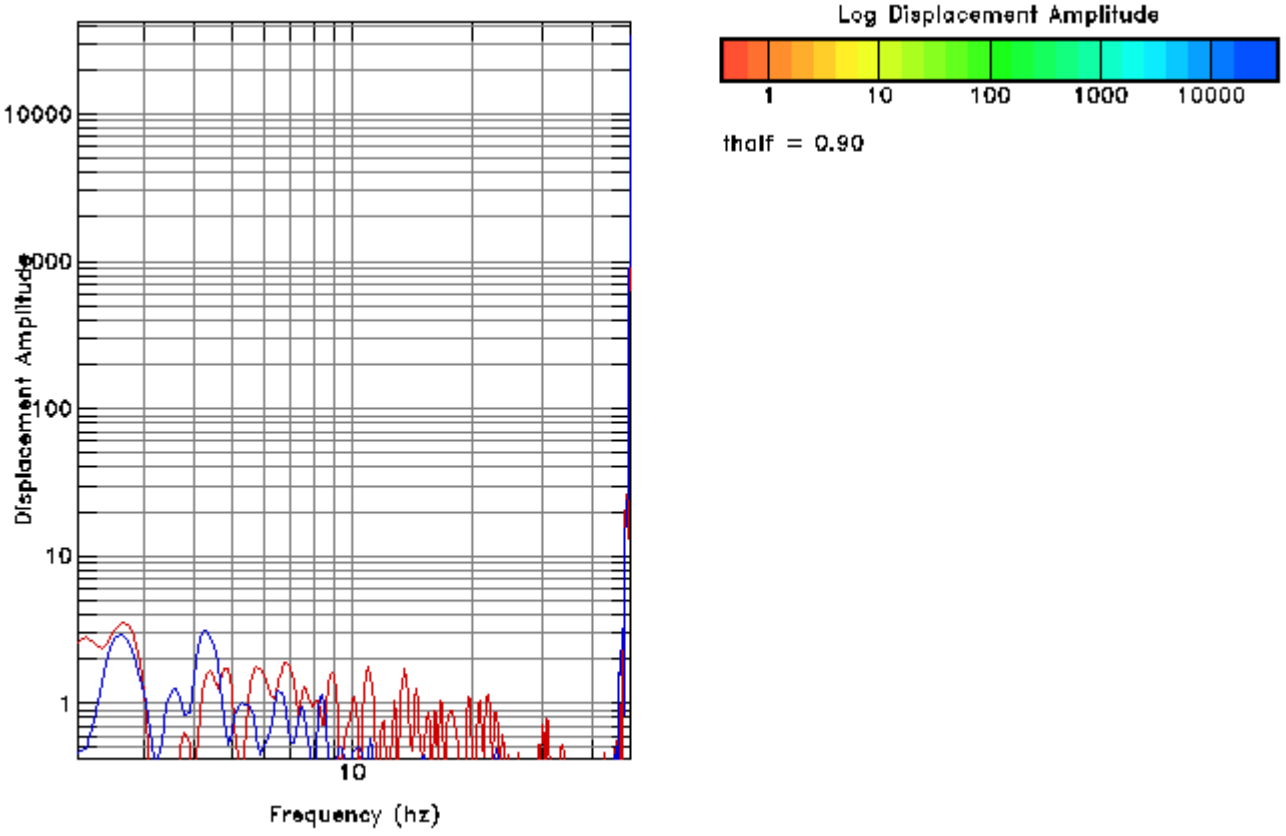

Instrument Correction: Ranger SS1/Quanterra 330 Linear Phase Composite

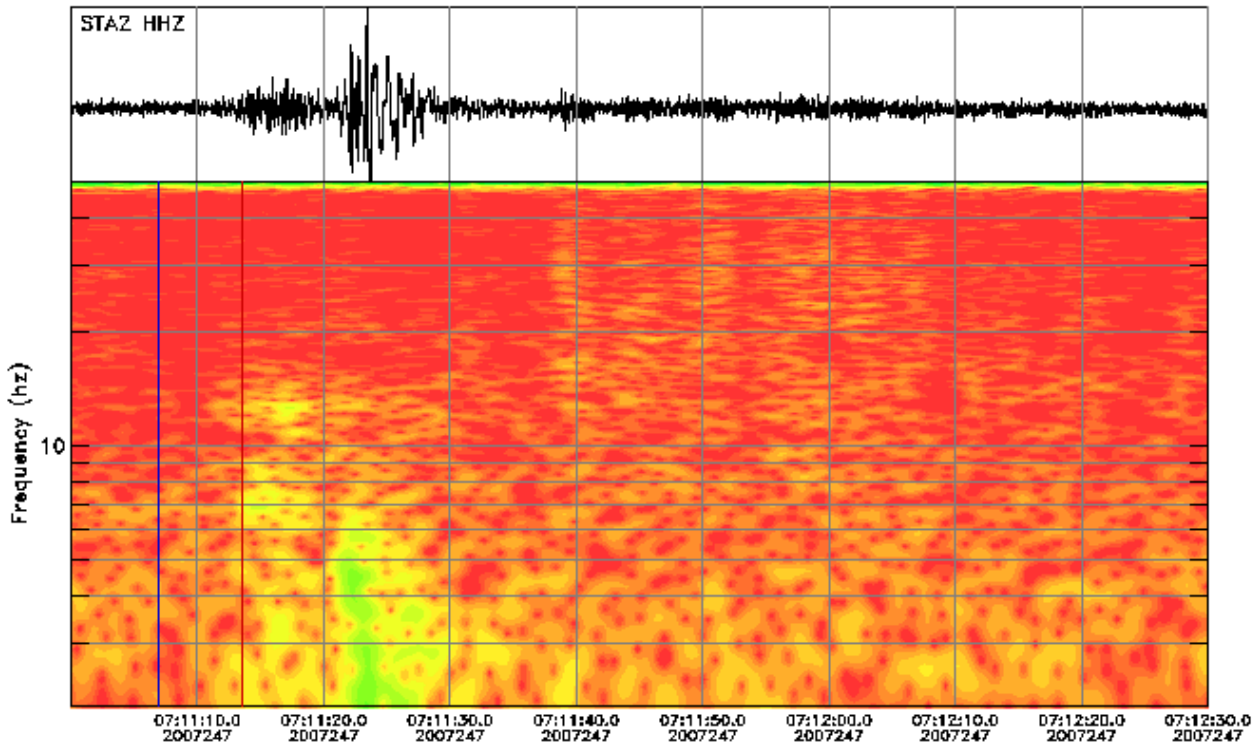

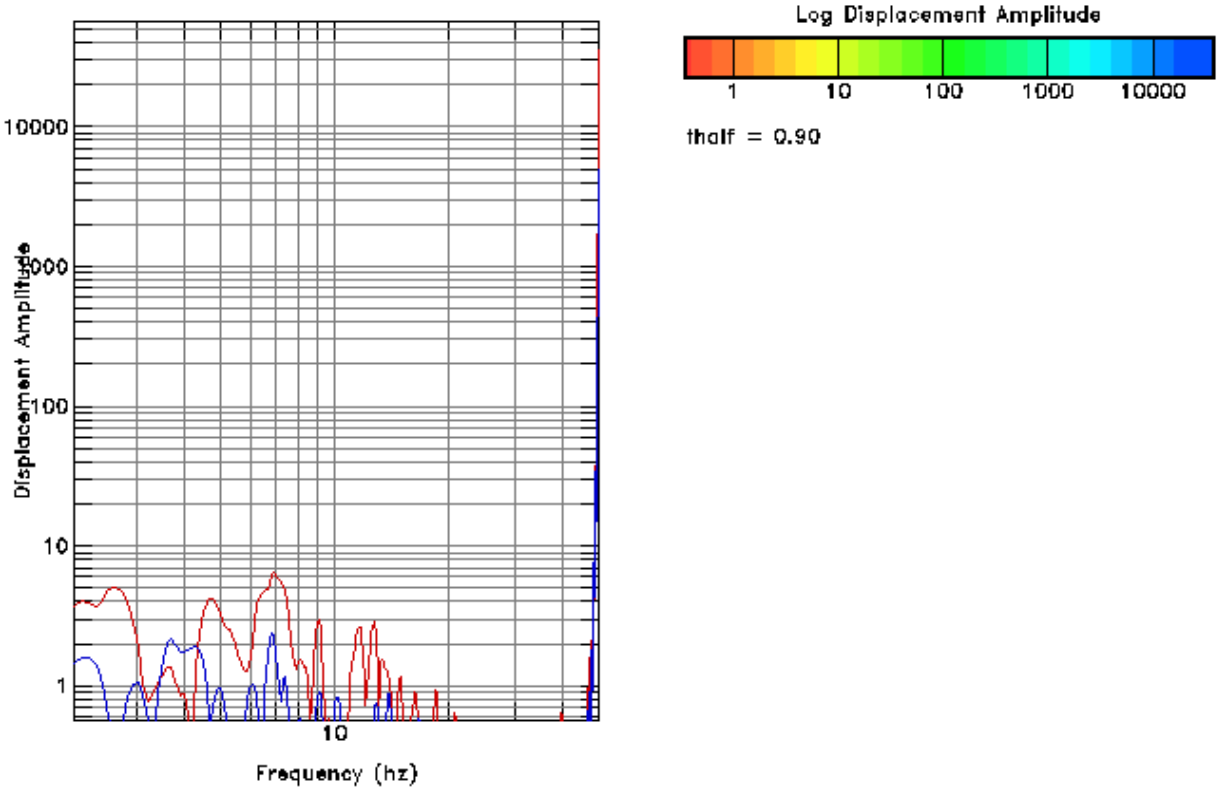

Instrument Correction: Ranger SS1/Quanterra 330 Linear Phase Composite

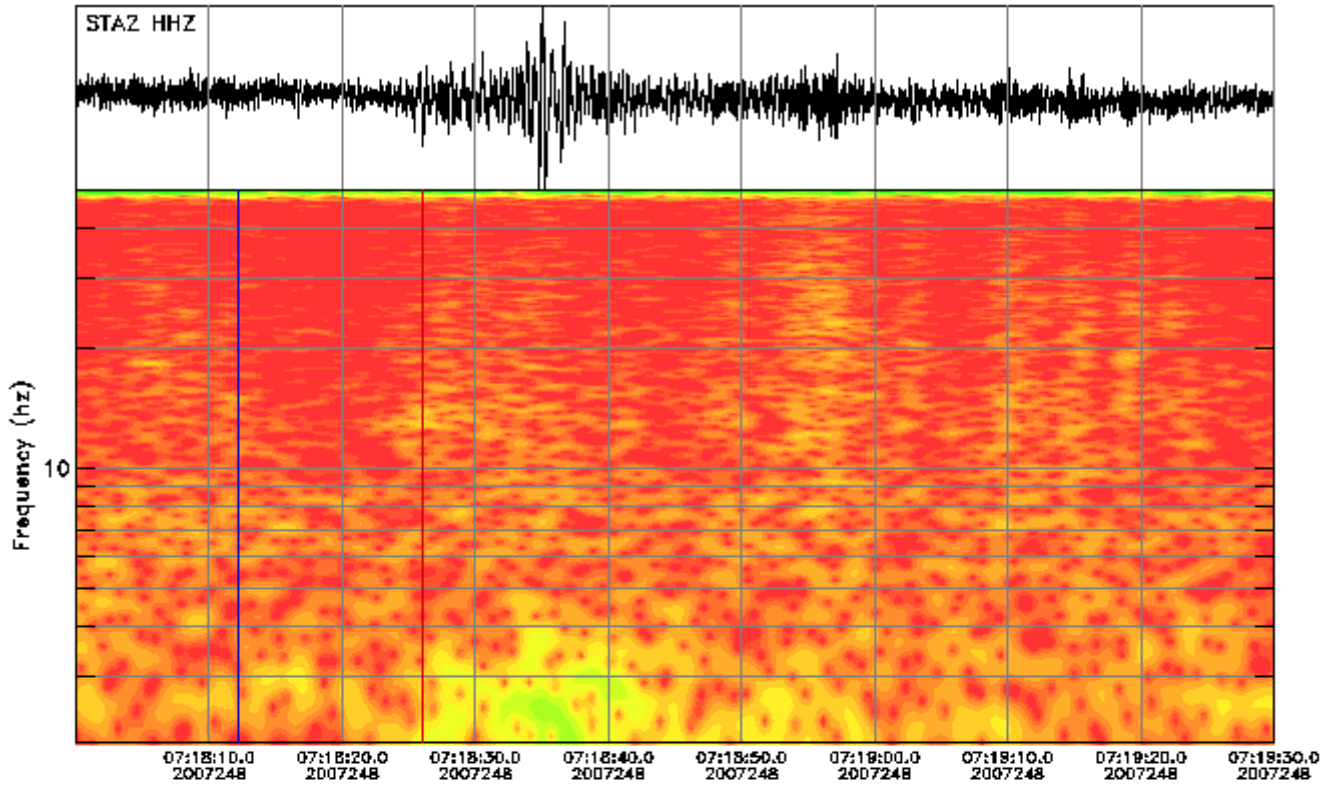

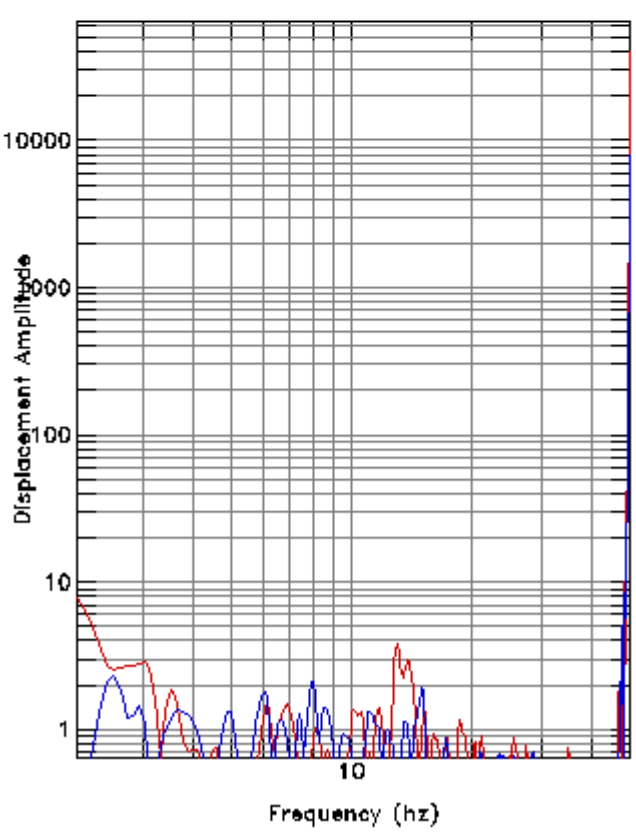

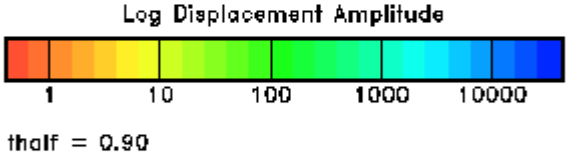

thalf = 0.90

Instrument Correction: Ranger SS1/Quanterra 330 Linear Phase Composite

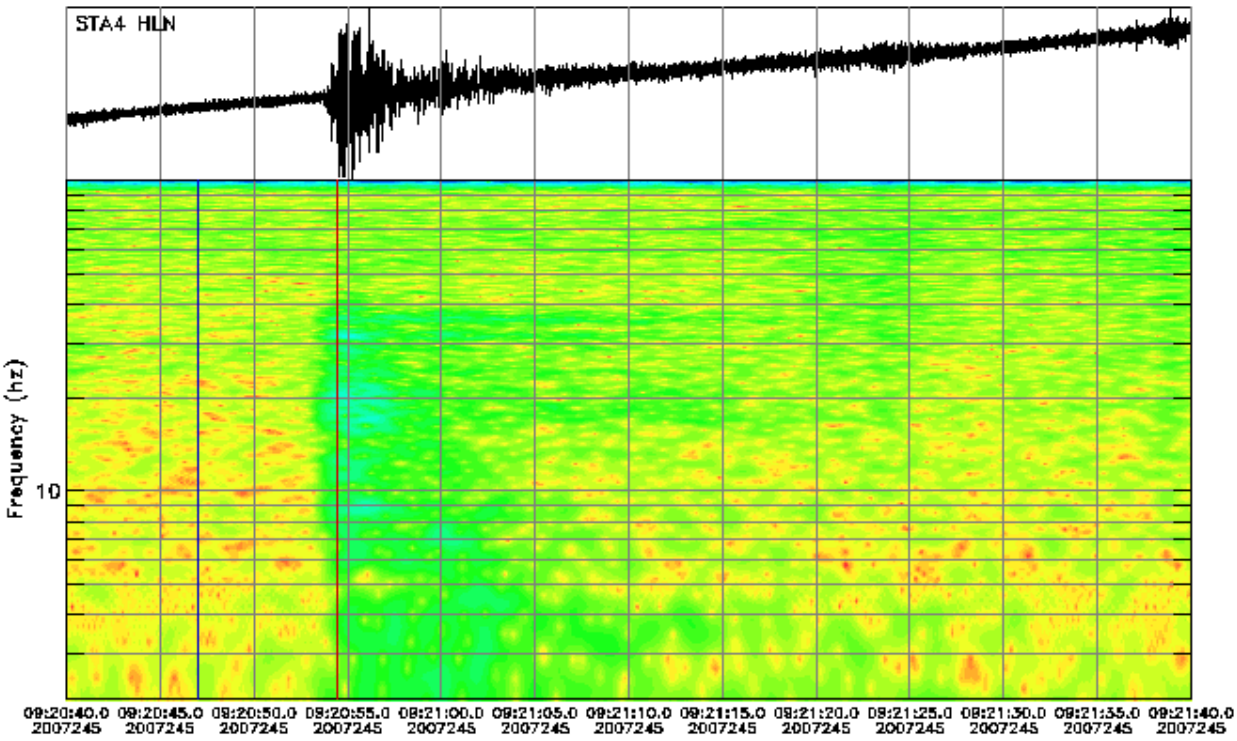

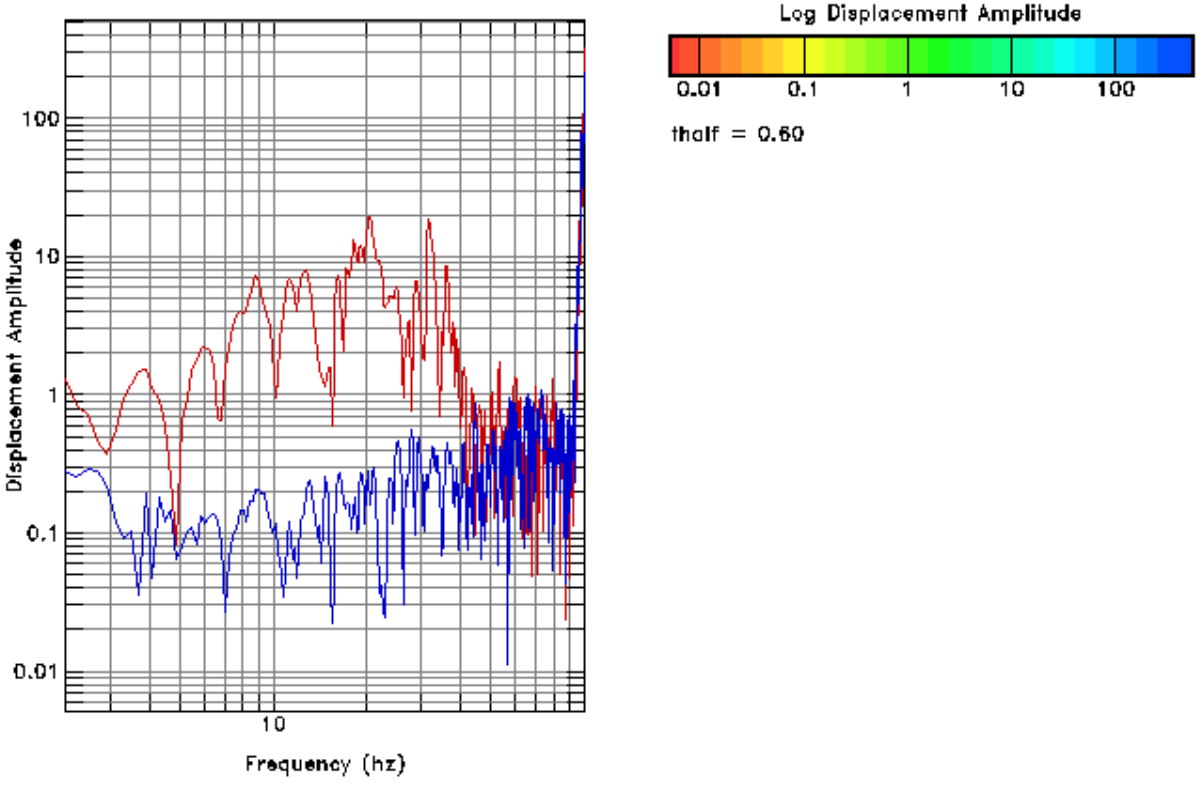

Instrument Correction: Episensor 200 Hz 10 Volt FS 2g/Quanterra 330 Linea

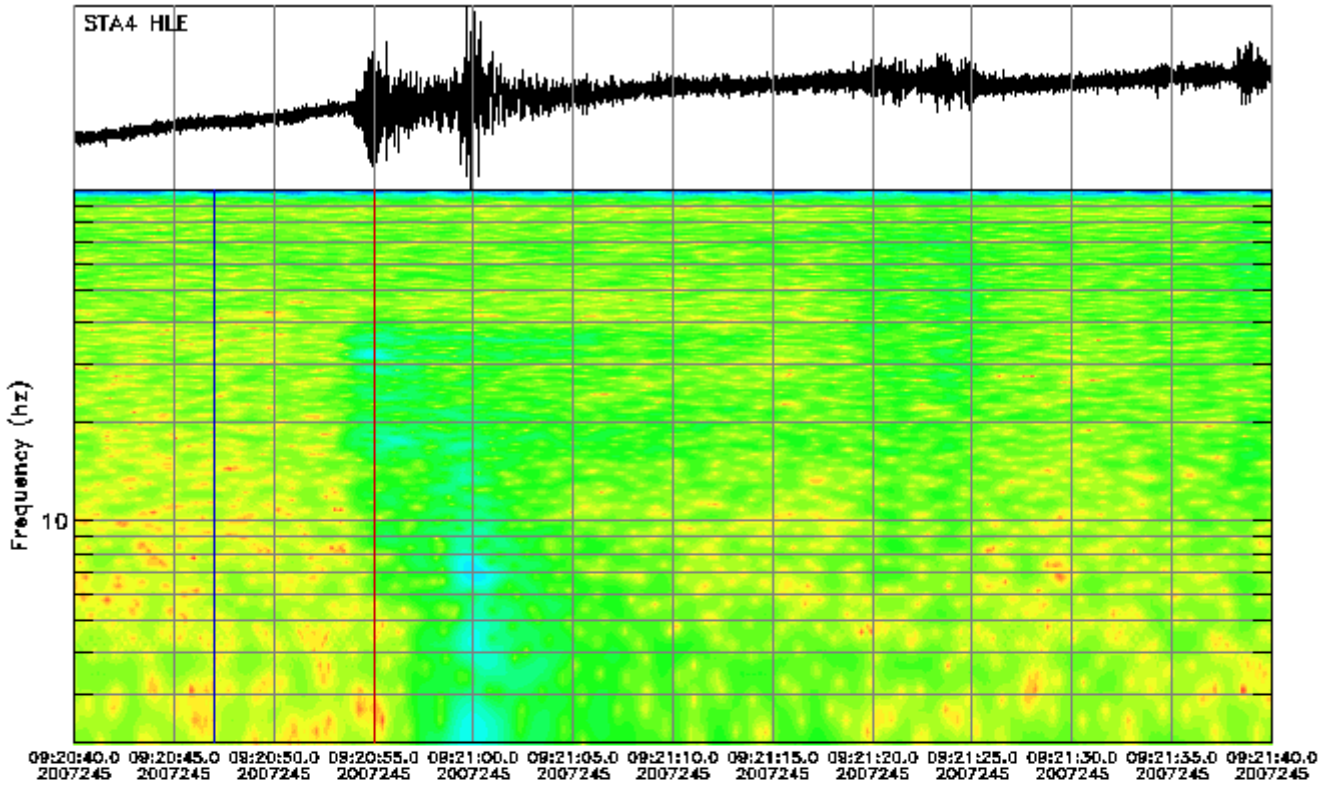

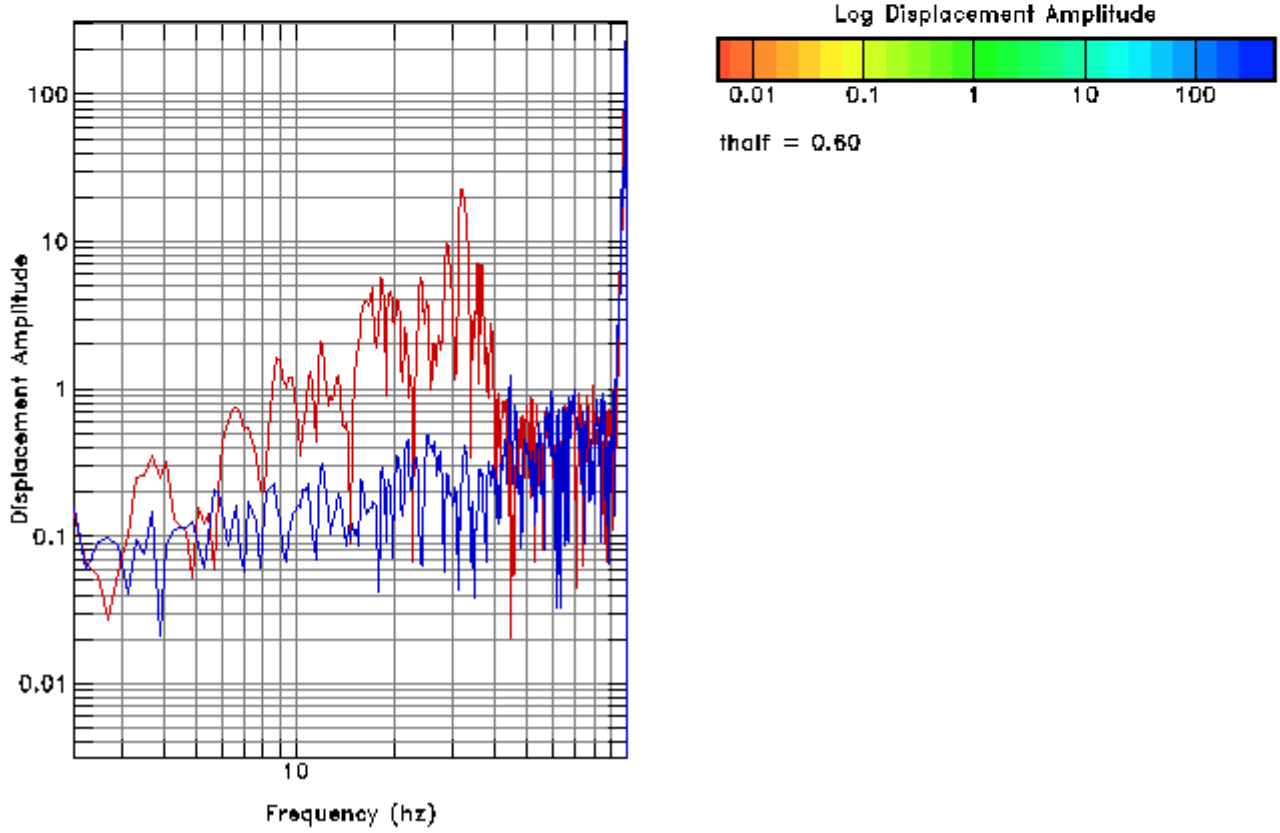

Instrument Correction: Episensor 200 Hz 10 Volt FS 2g/Quanterra 330 Linea

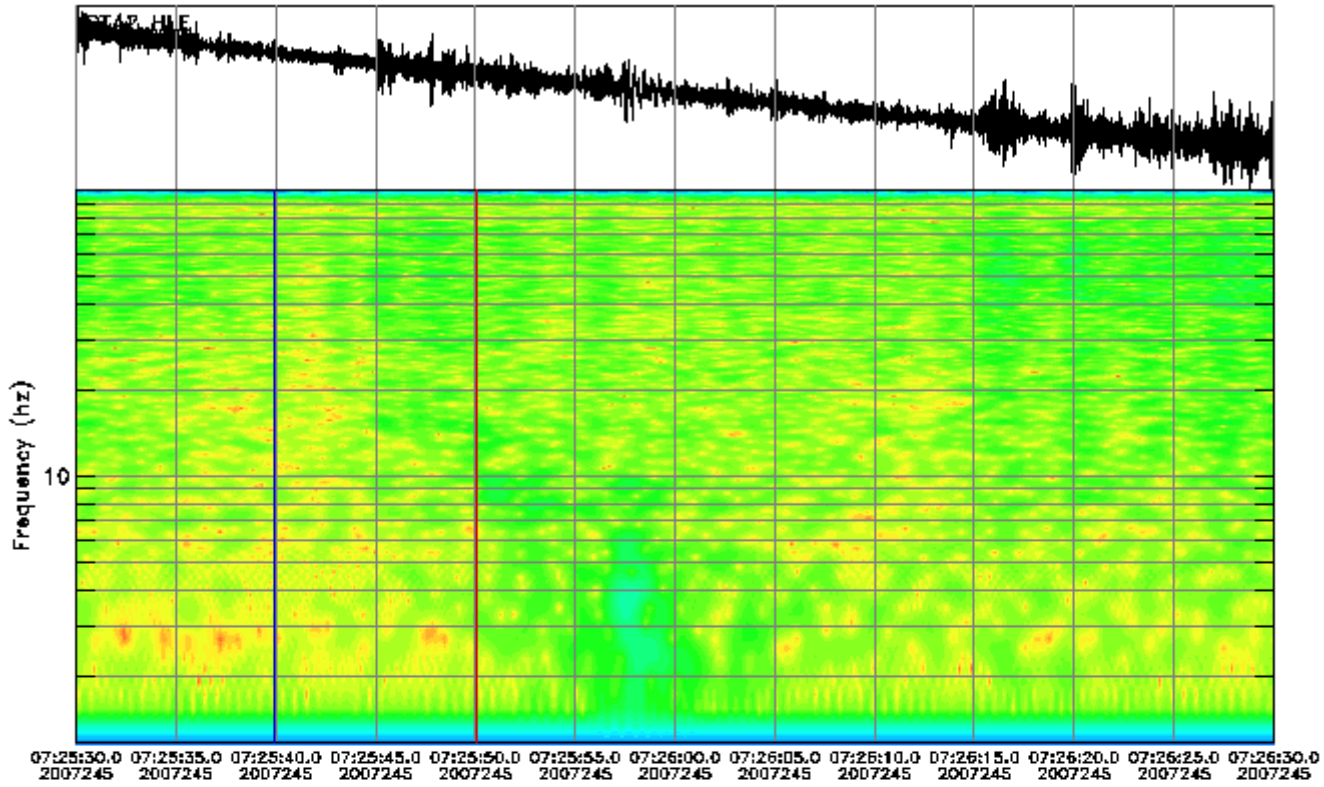

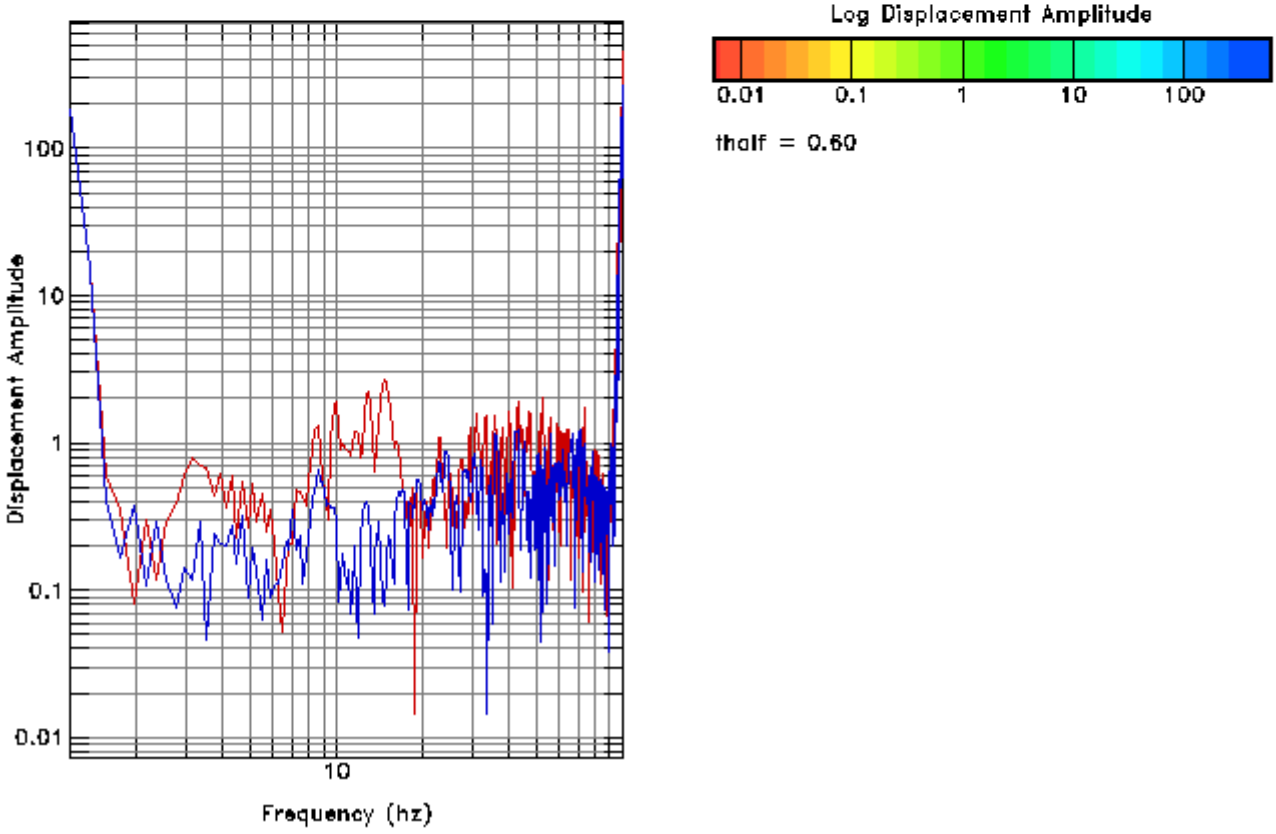

Instrument Correction: Episensor 200 Hz 10 Volt FS 2g/Quanterra 330 Linea

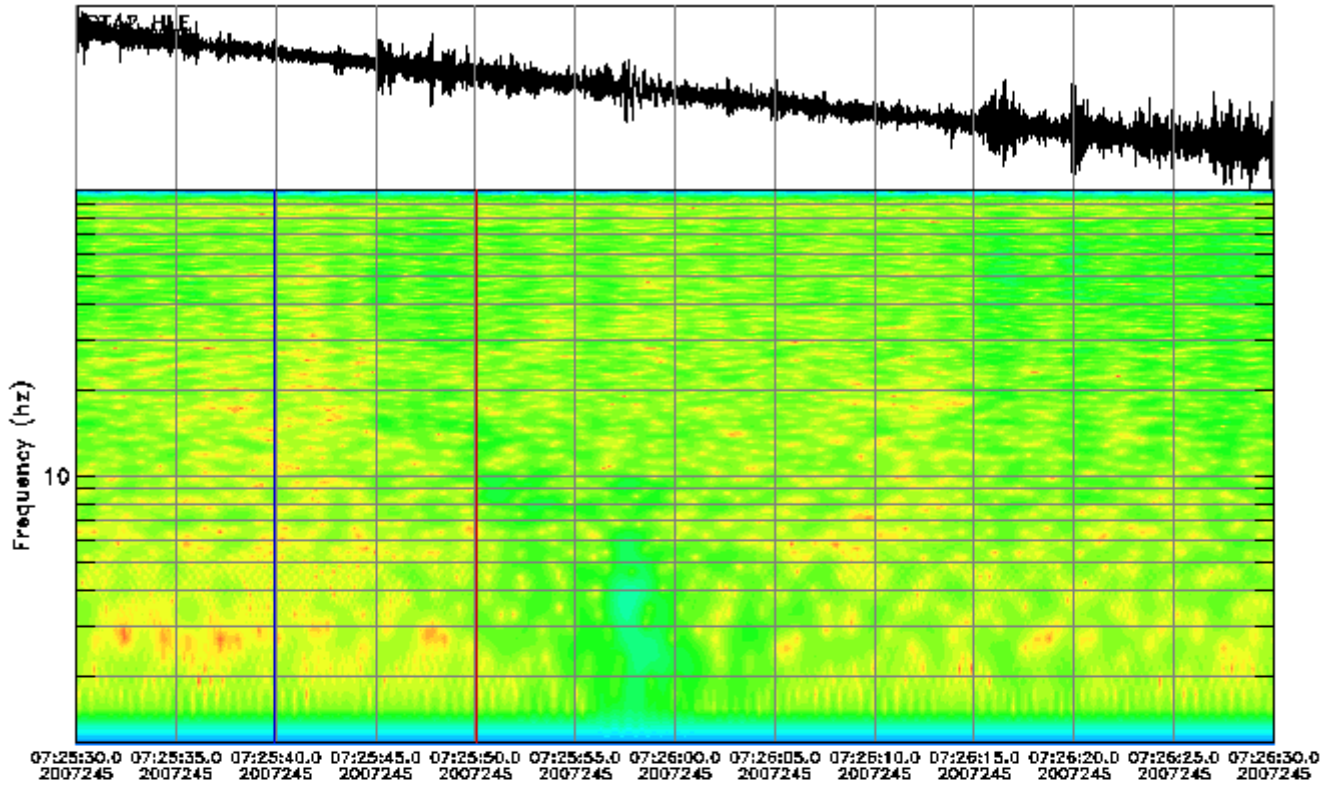

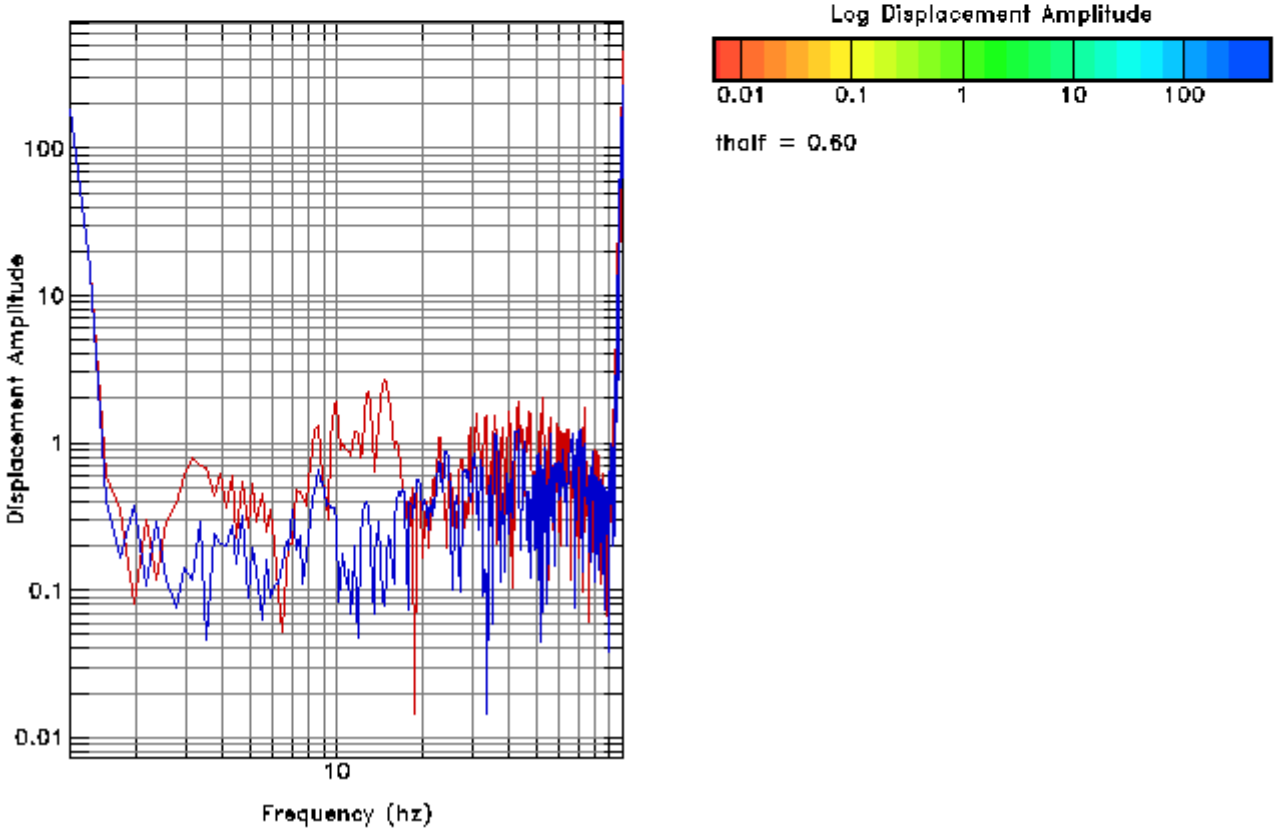

Instrument Correction: Episensor 200 Hz 10 Volt FS 2g/Quanterra 330 Linea

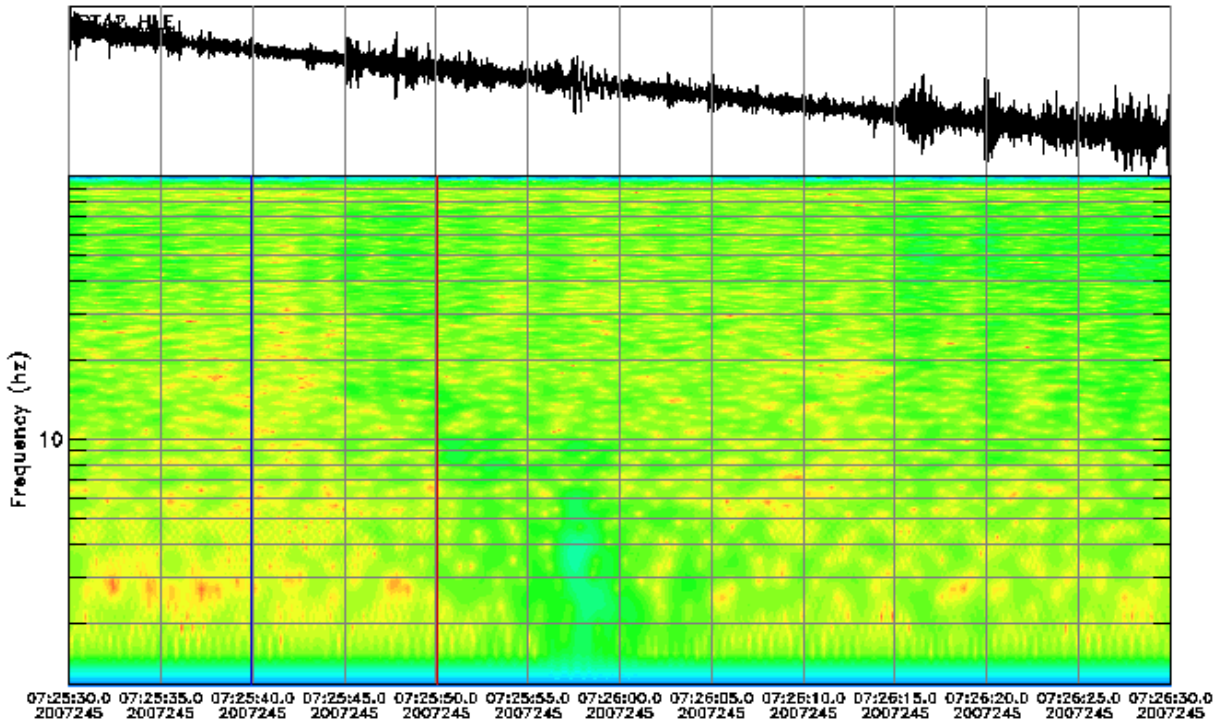

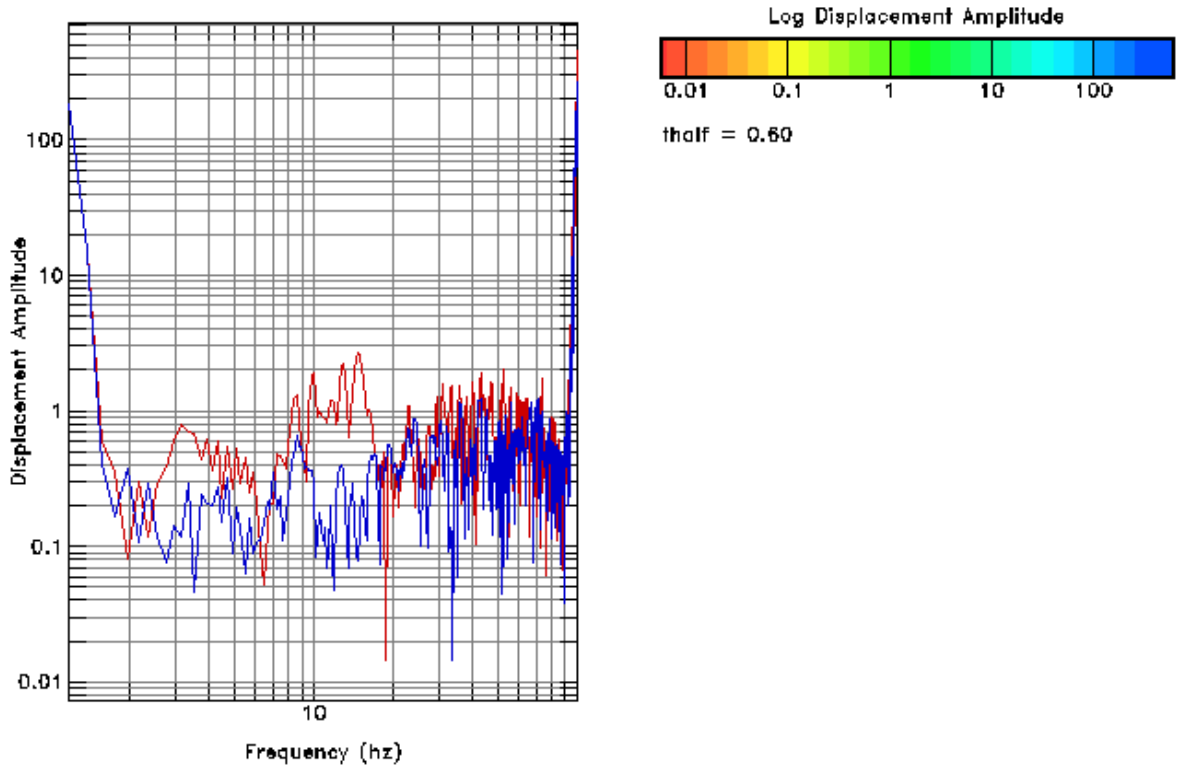

Instrument Correction: Episensor 200 Hz 10 Volt FS 2g/Quanterra 330 Linea

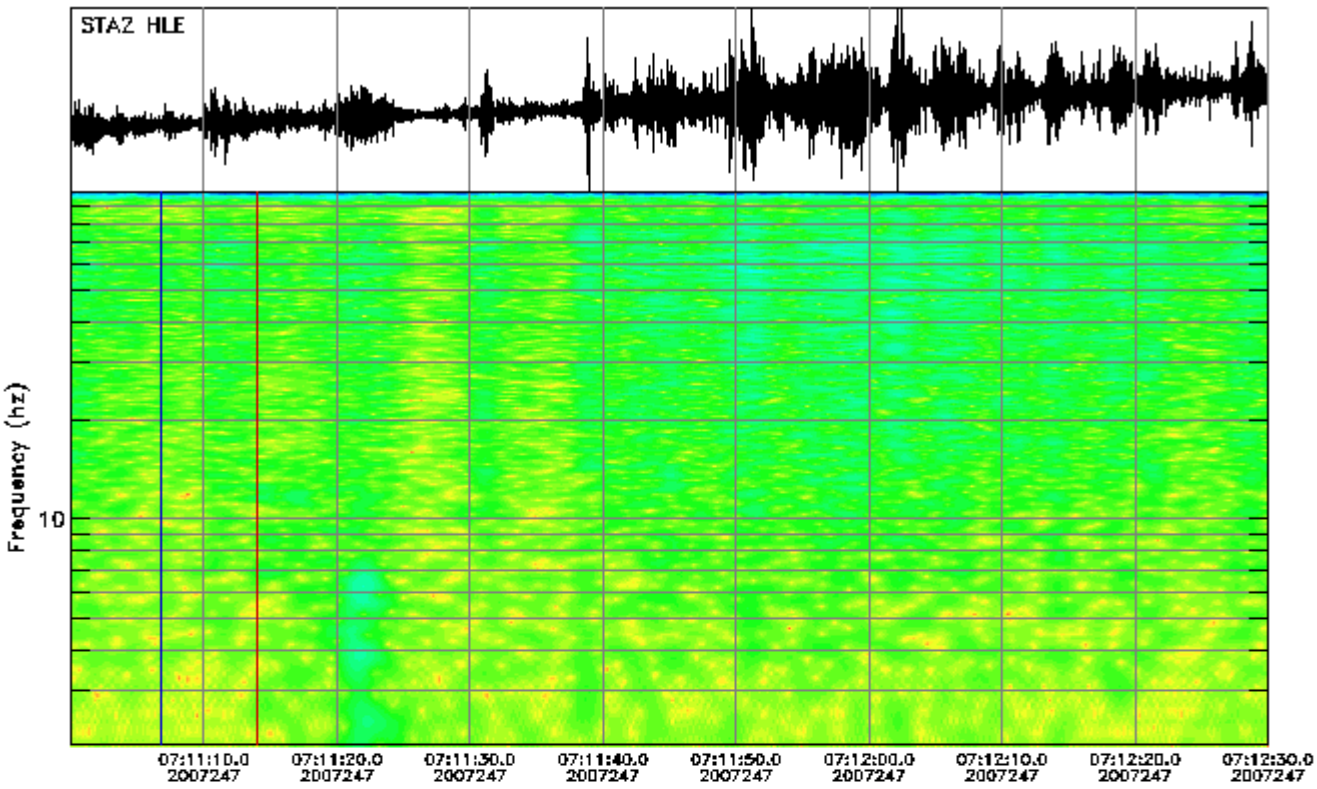

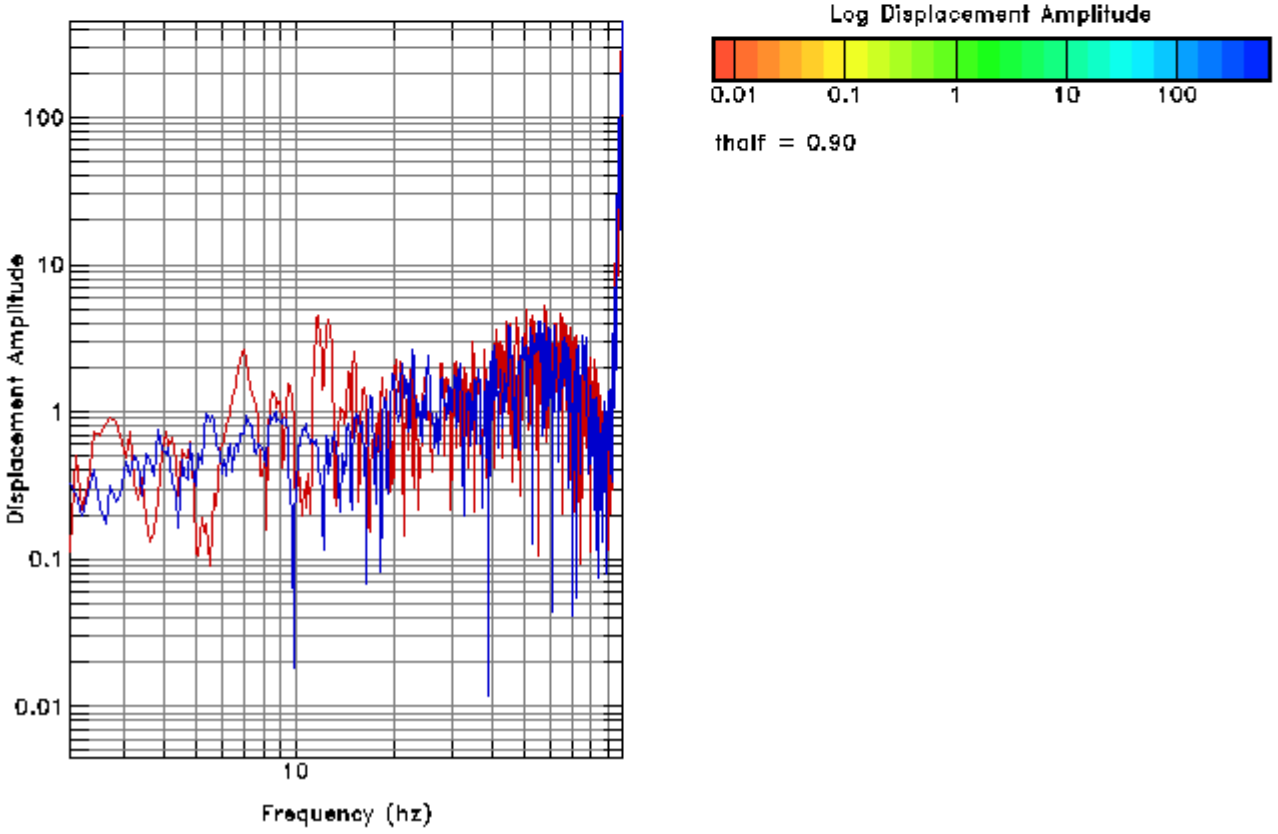

Instrument Correction: Episensor 200 Hz 10 Volt FS 2g/Quanterra 330 Linea

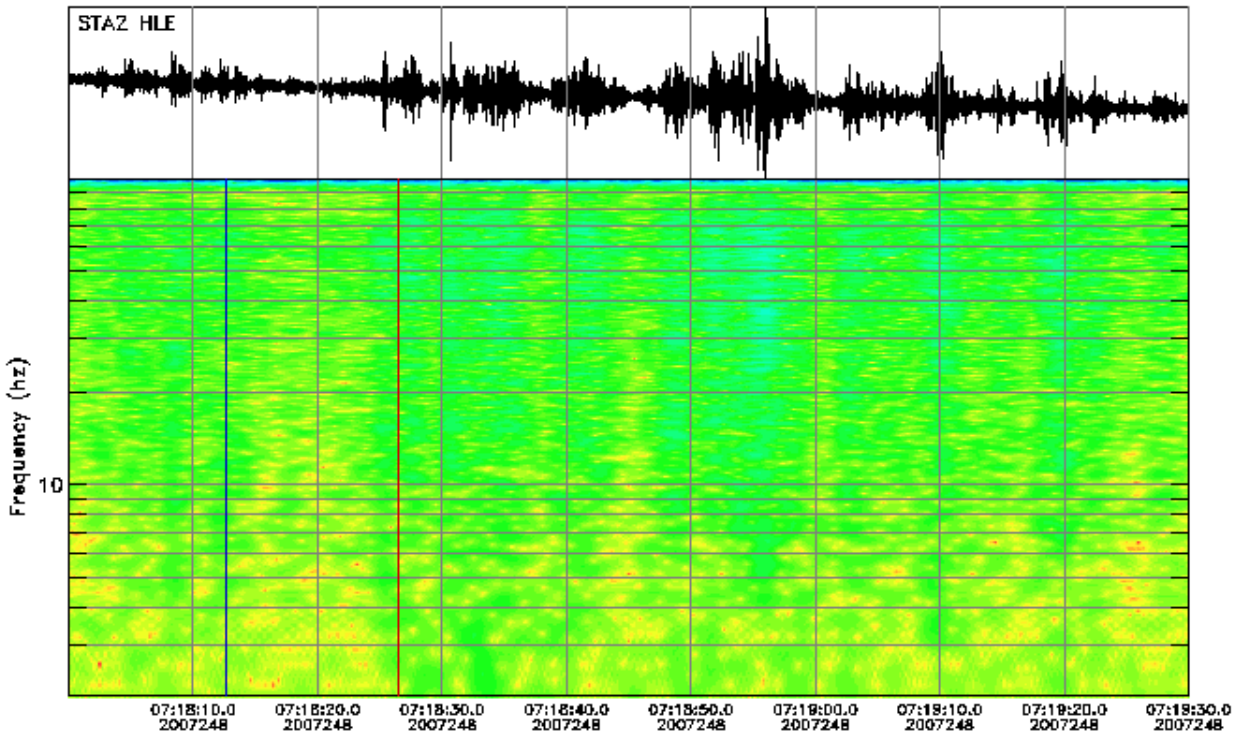

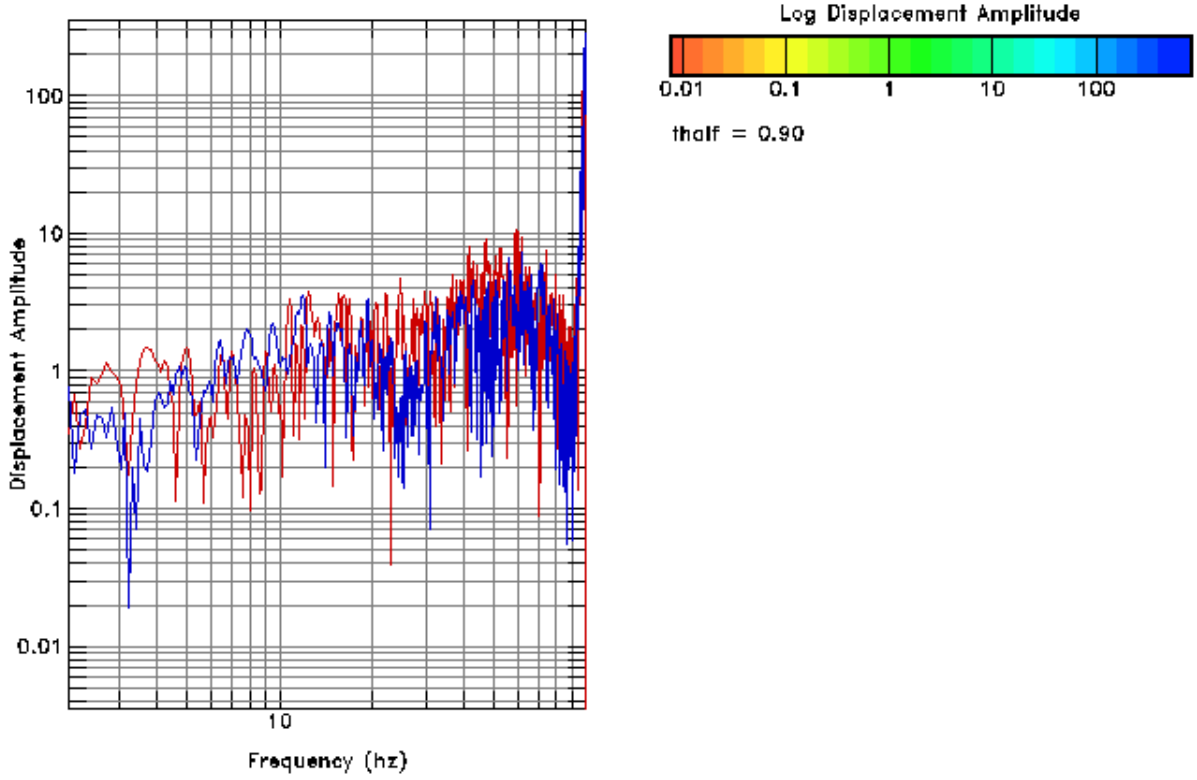

Instrument Correction: Episensor 200 Hz 10 Volt FS 2g/Quanterra 330 Linea

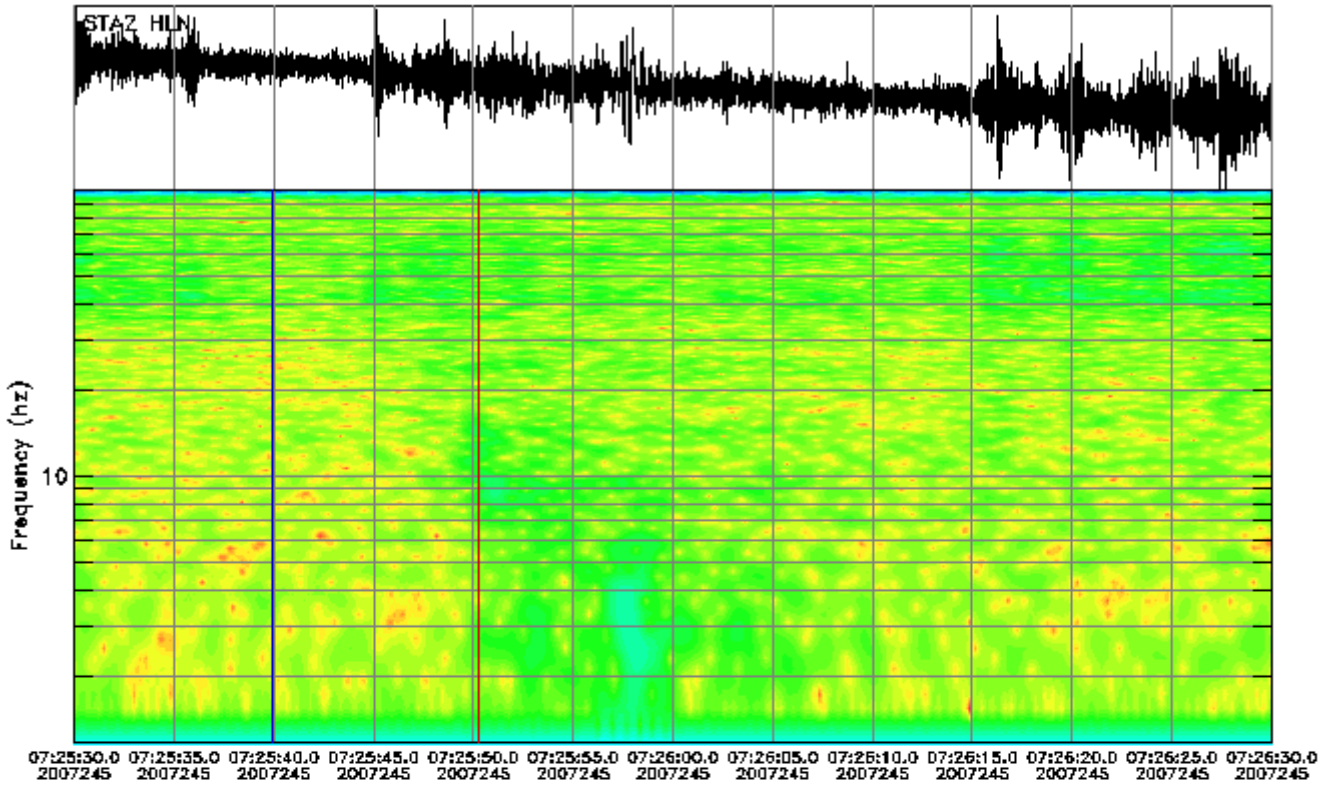

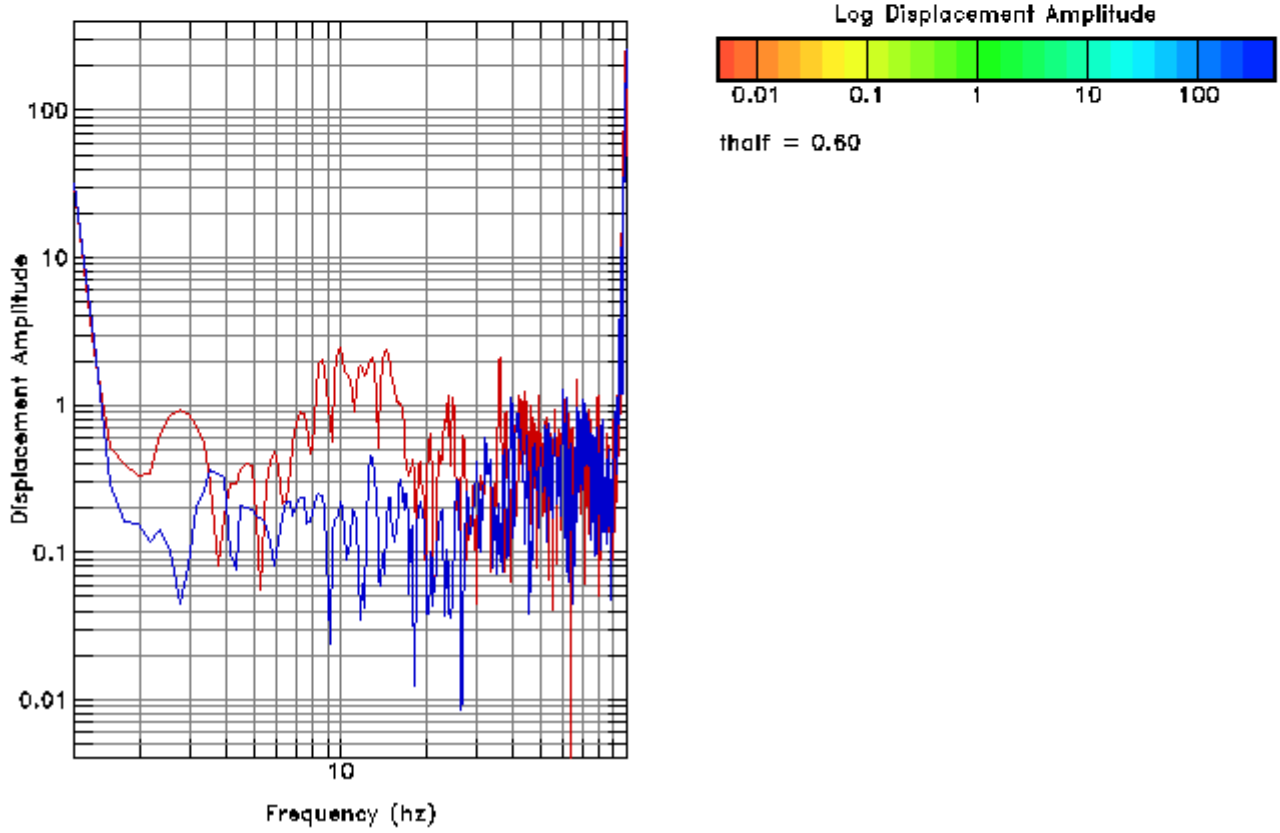

Instrument Correction: Episensor 200 Hz 10 Volt FS 2g/Quanterra 330 Linea

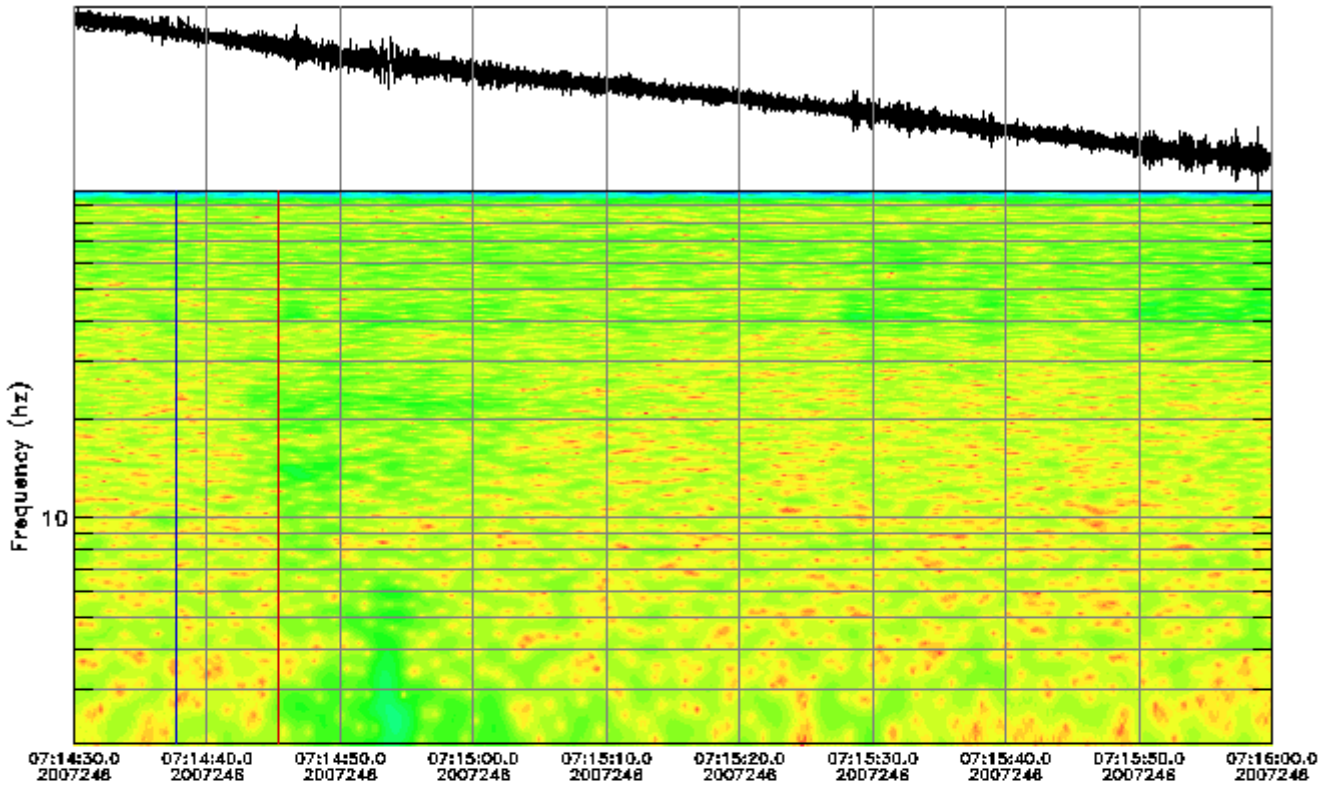

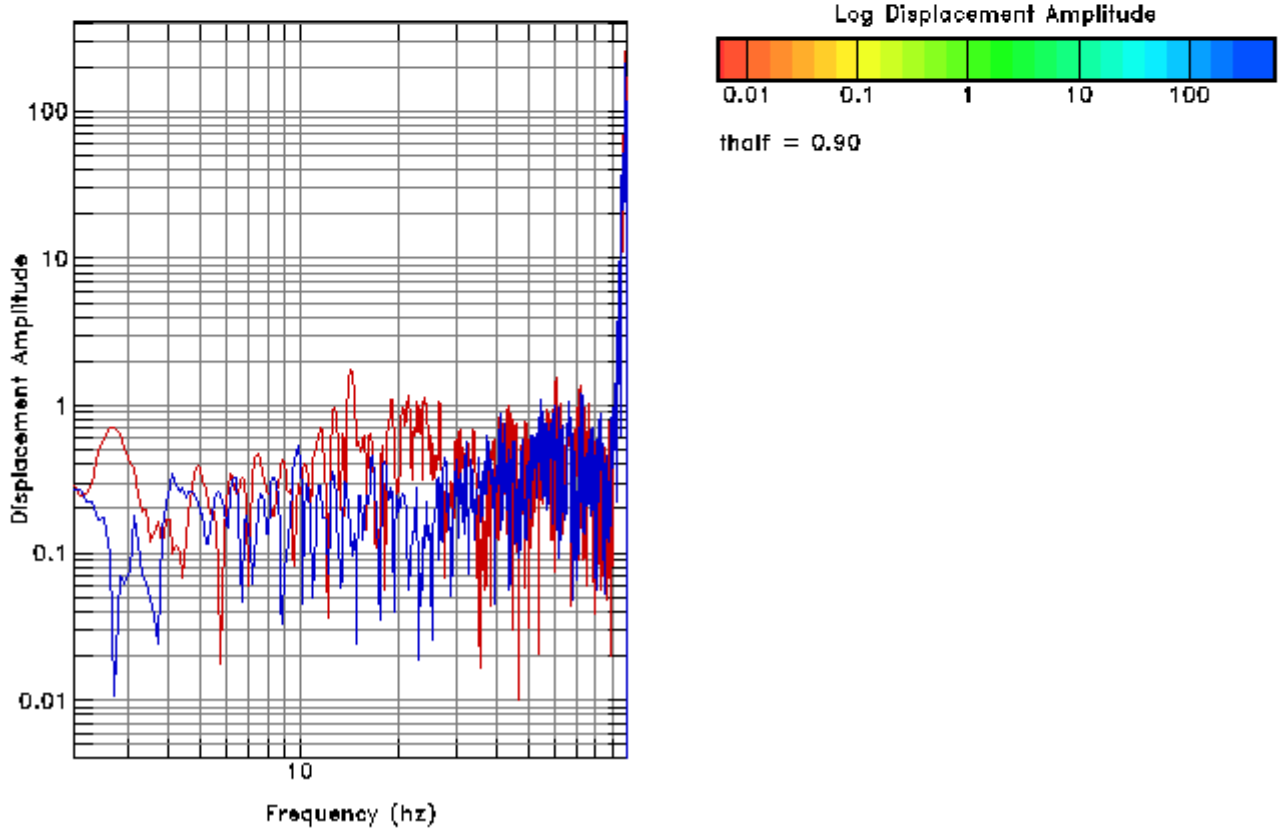

Instrument Correction: Episensor 200 Hz 10 Volt FS 2g/Quanterra 330 Linea

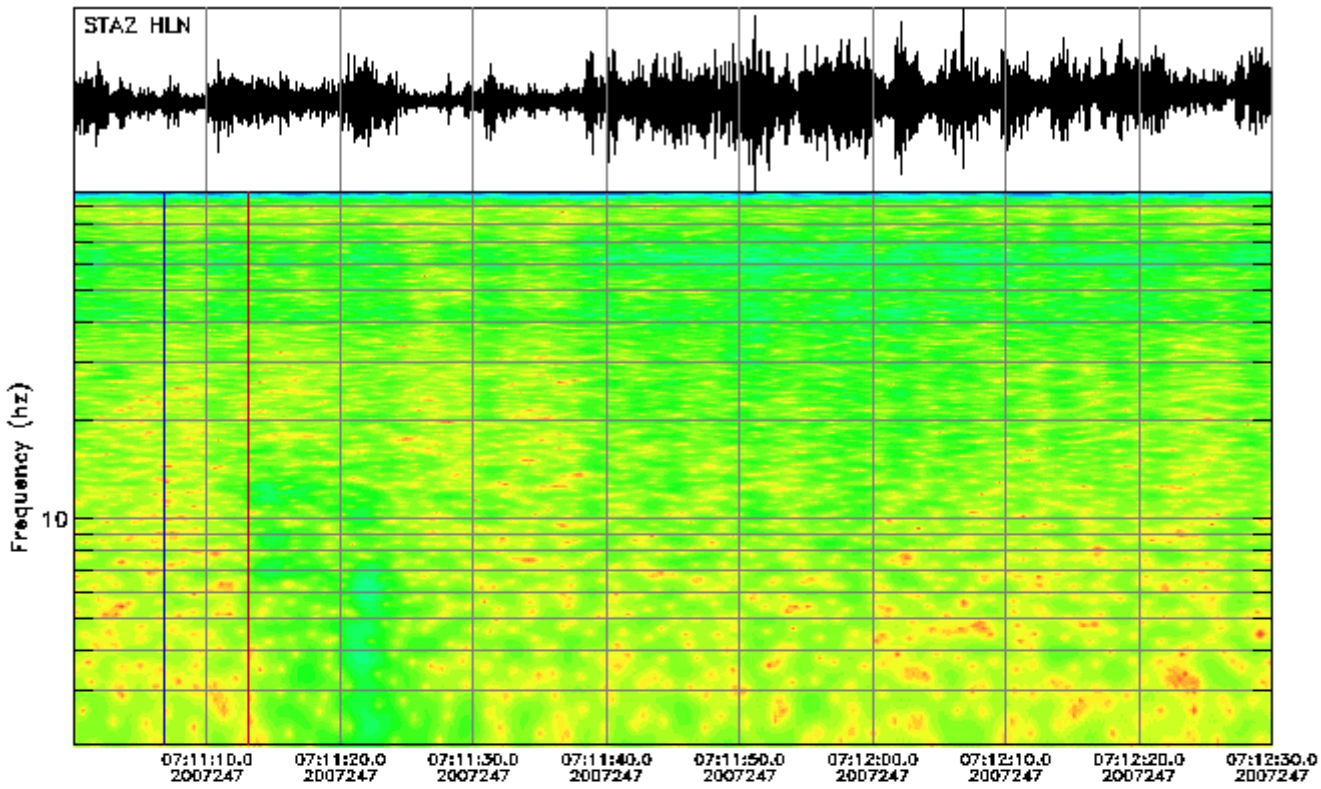

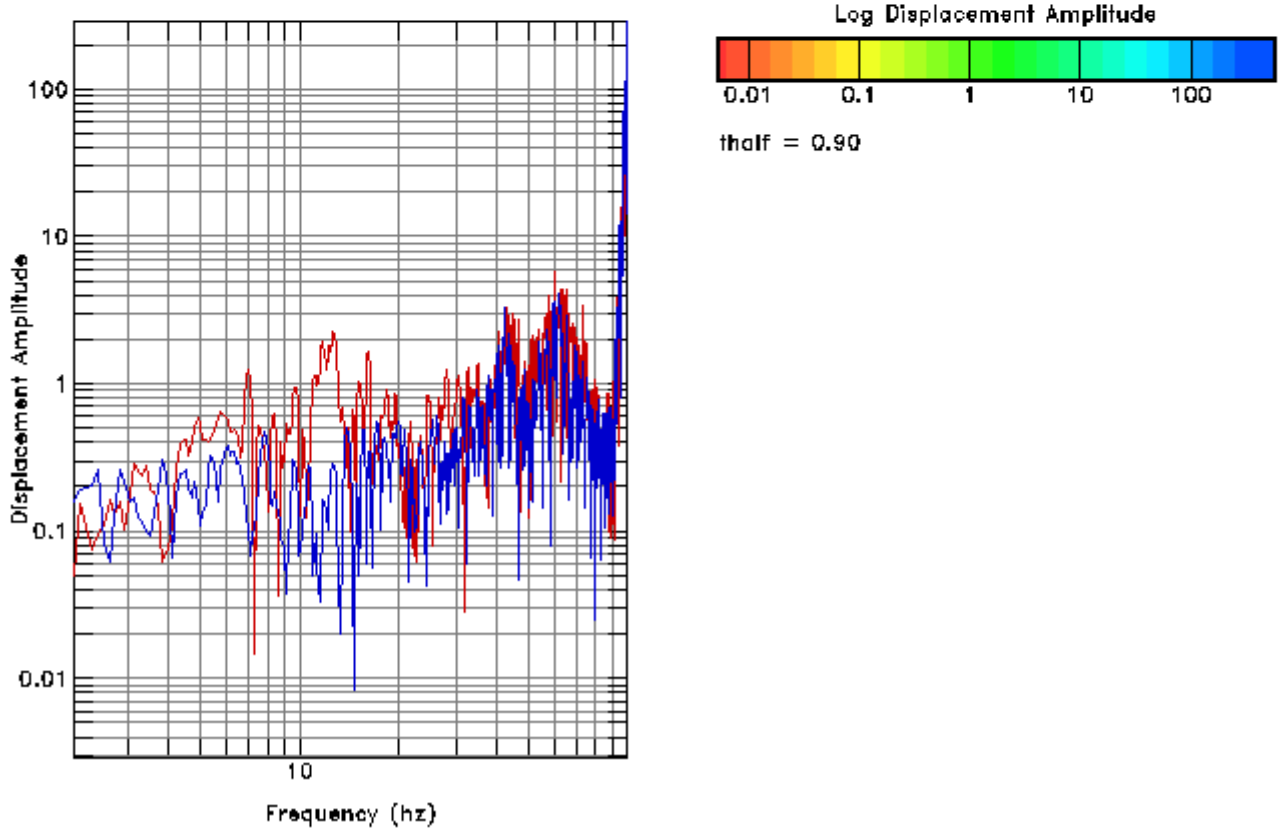

Instrument Correction: Episensor 200 Hz 10 Volt FS 2g/Quanterra 330 Linea

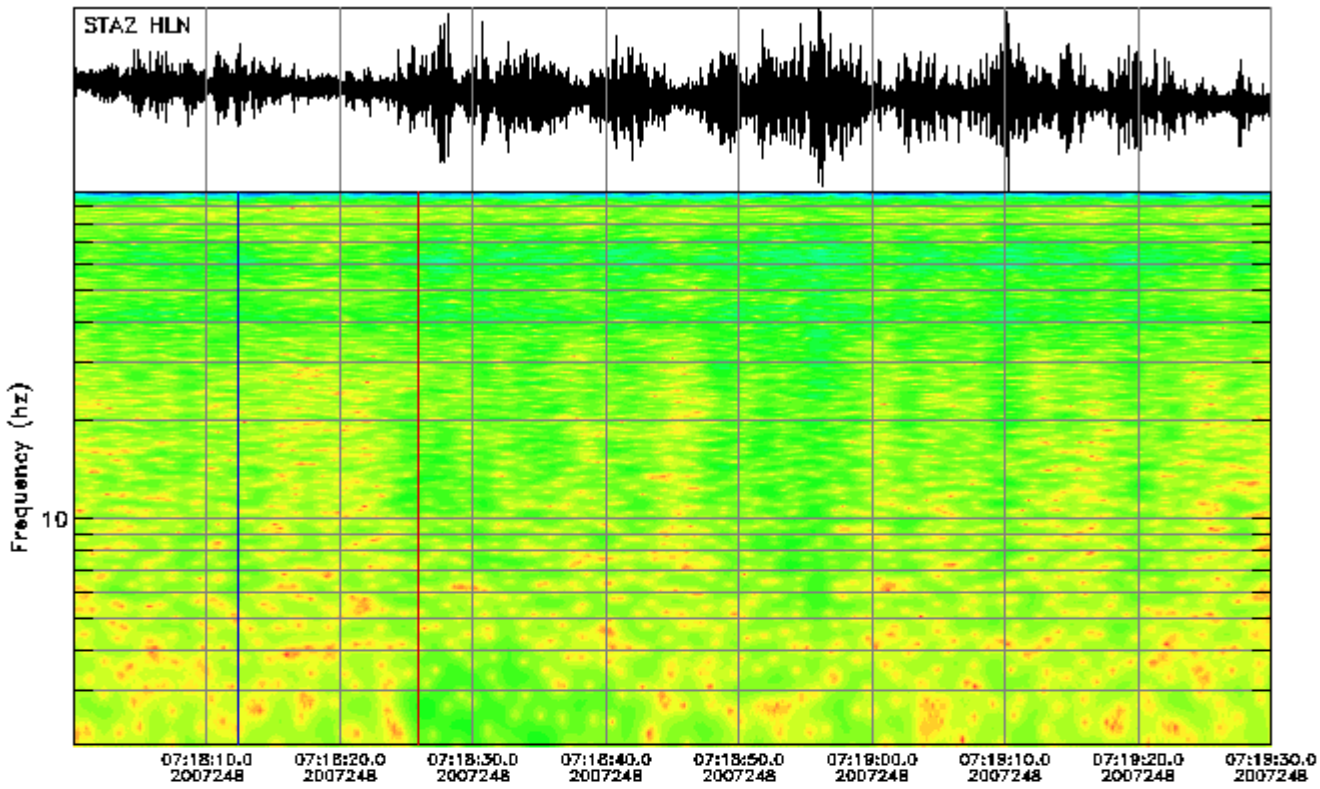

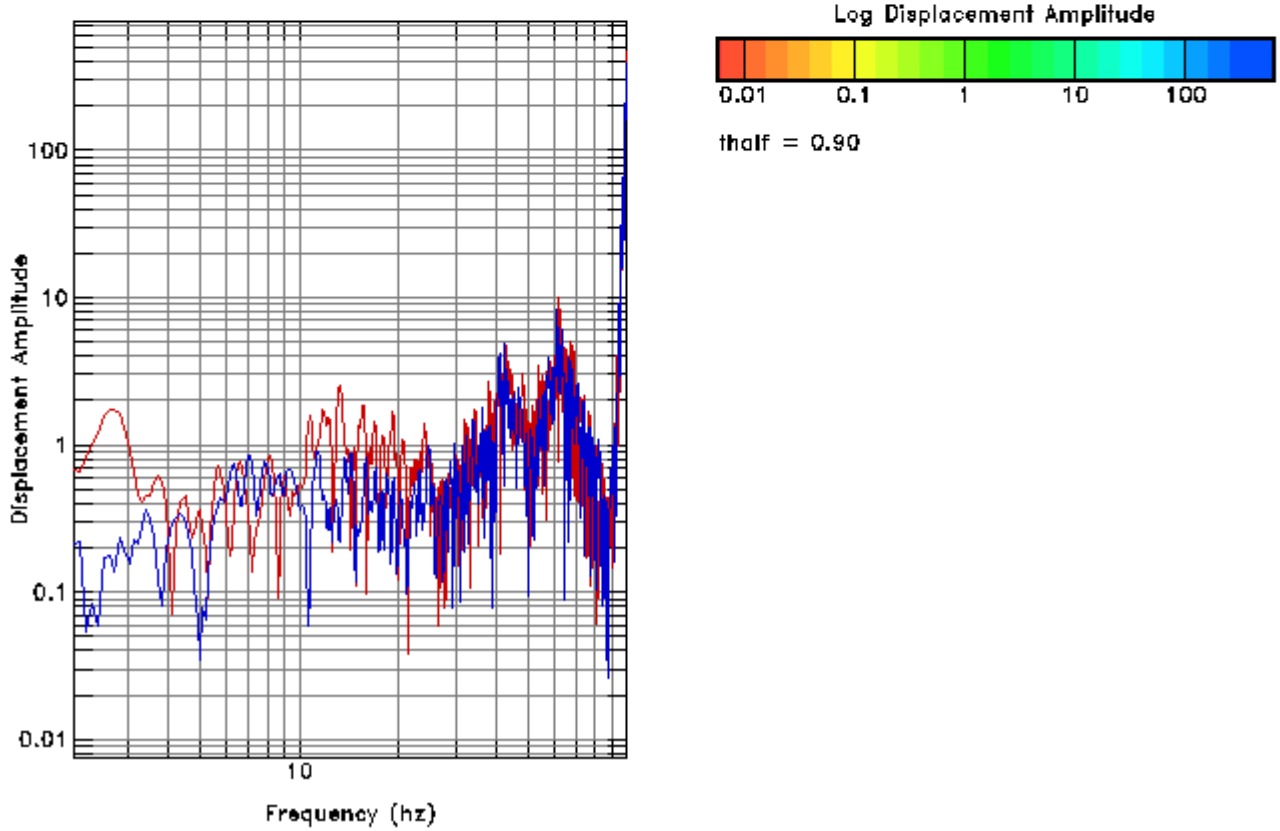

Instrument Correction: Episensor 200 Hz 10 Volt FS 2g/Quanterra 330 Linea

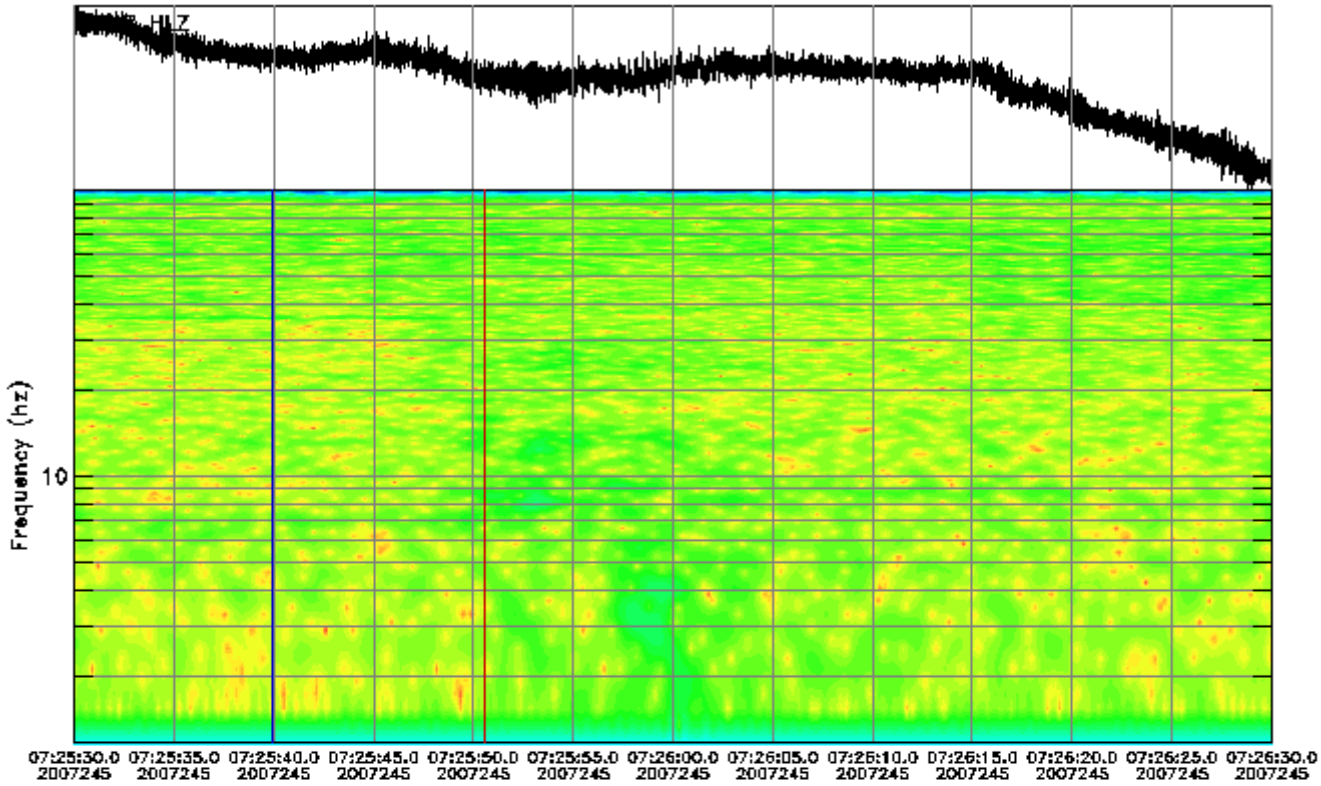

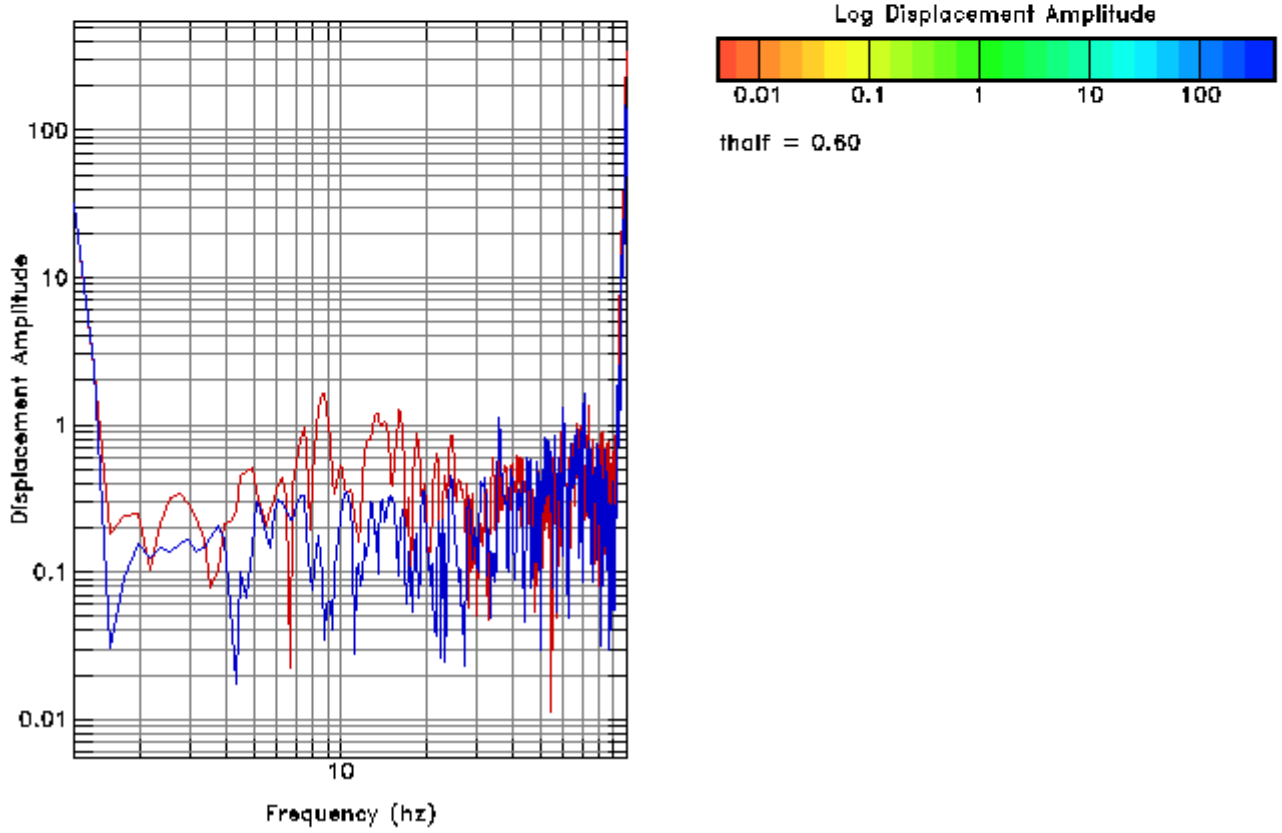

Instrument Correction: Episensor 200 Hz 10 Volt FS 2g/Quanterra 330 Linea

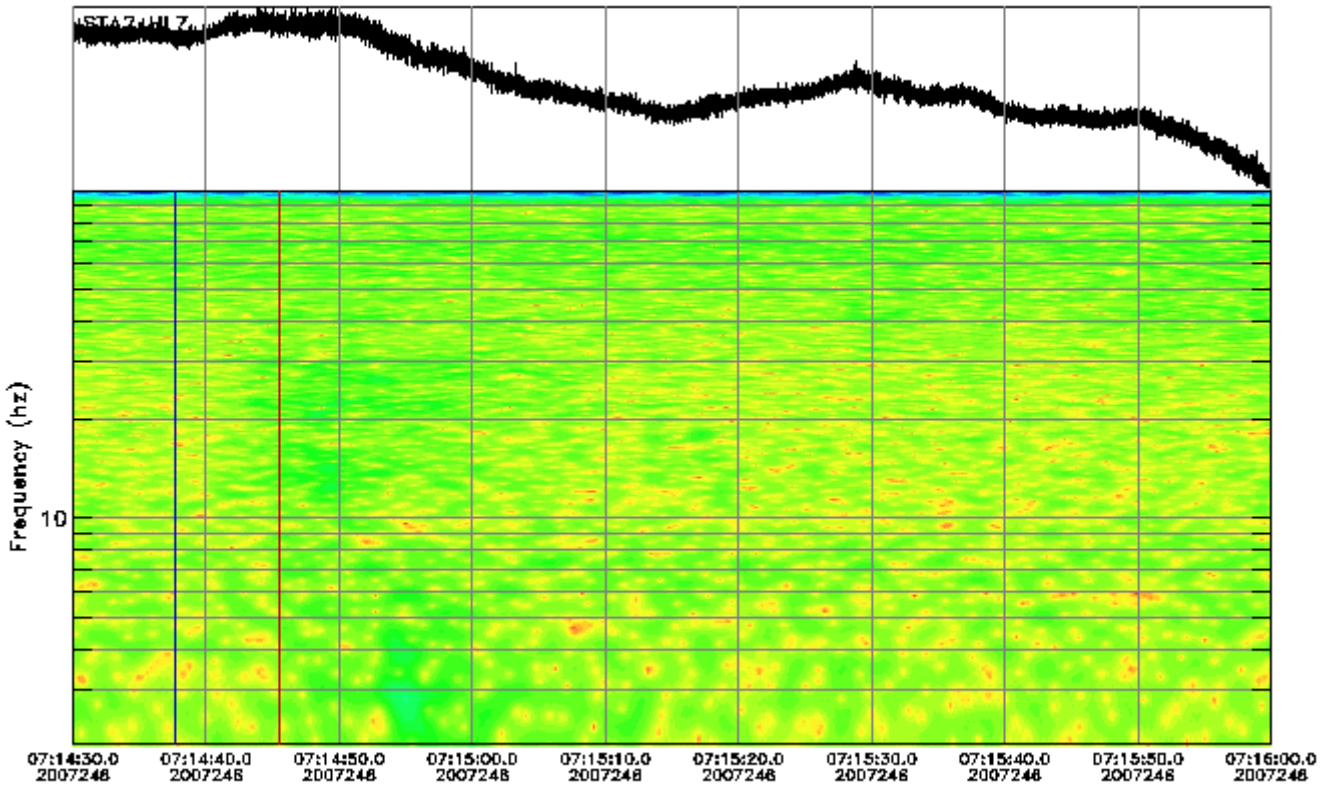

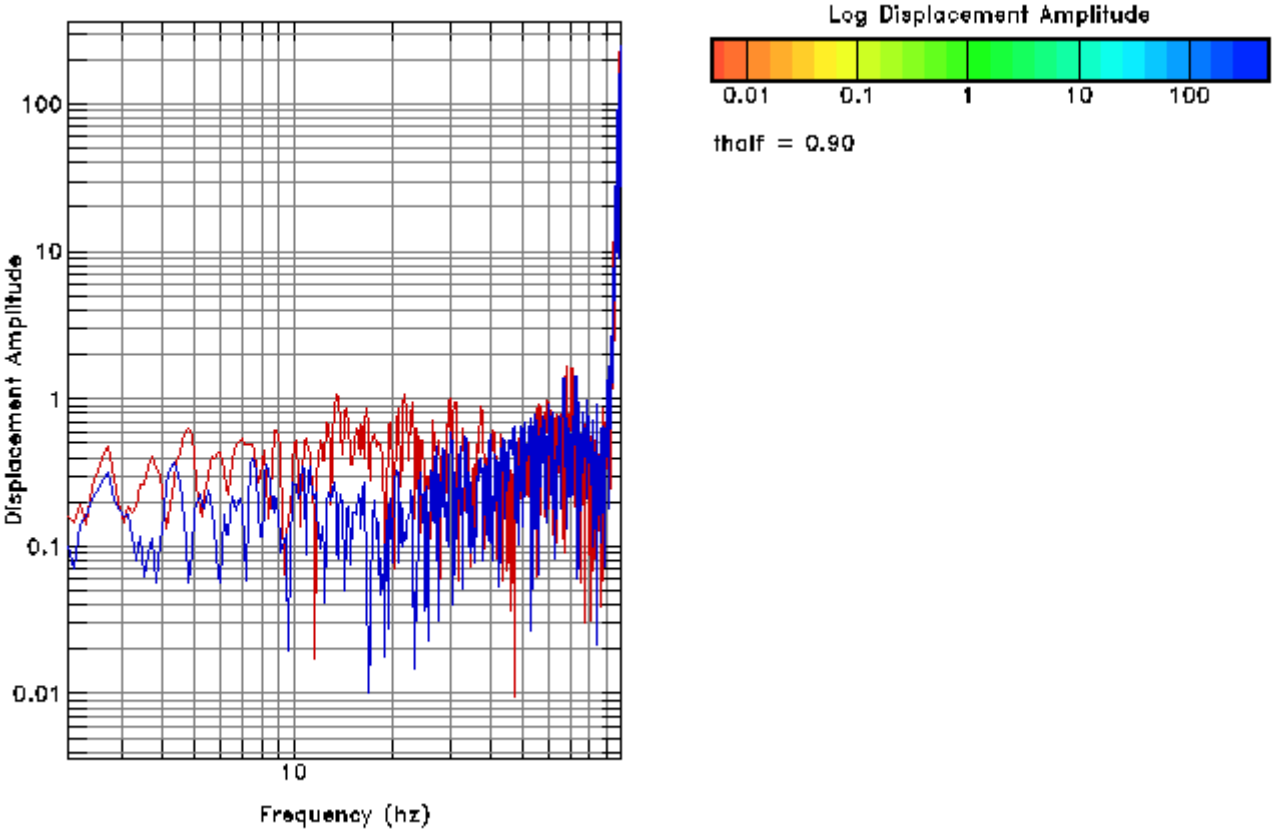

Instrument Correction: Episensor 200 Hz 10 Volt FS 2g/Quanterra 330 Linea

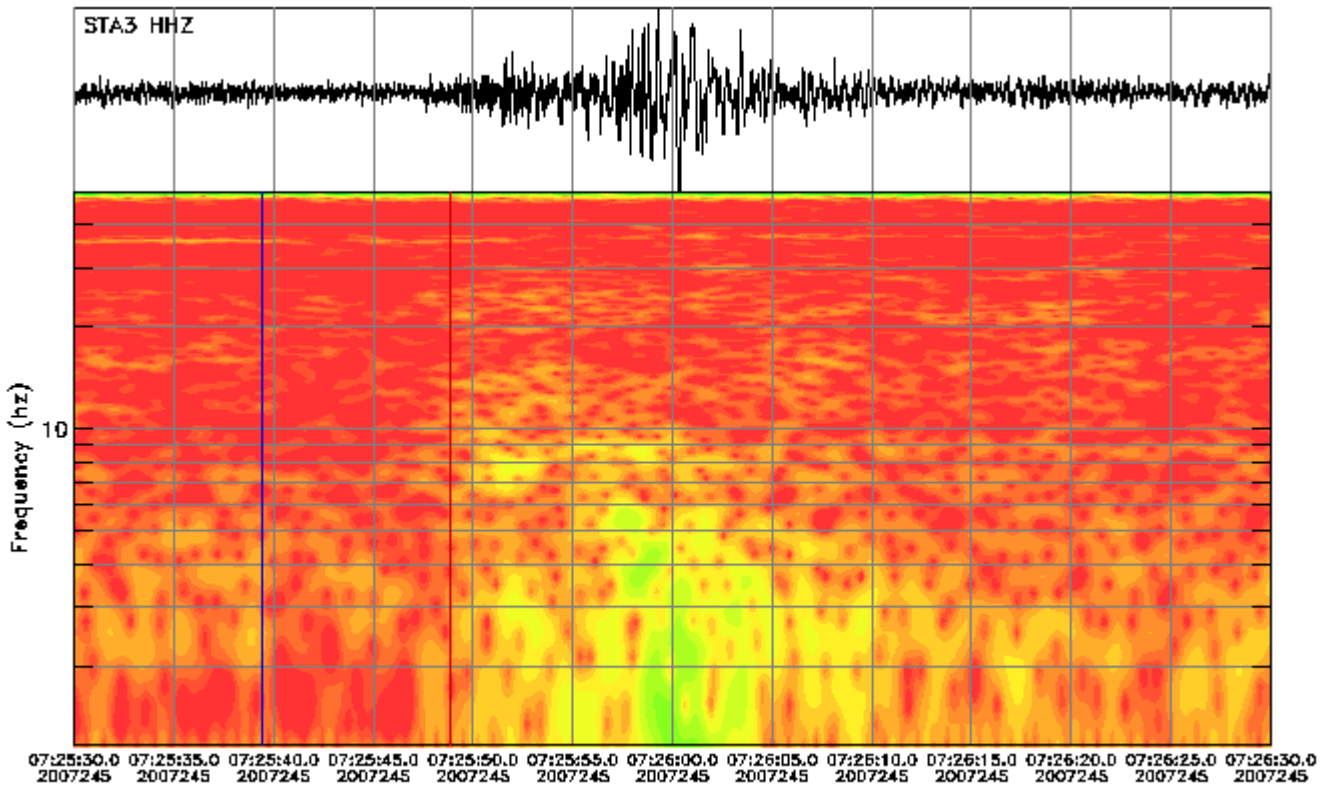

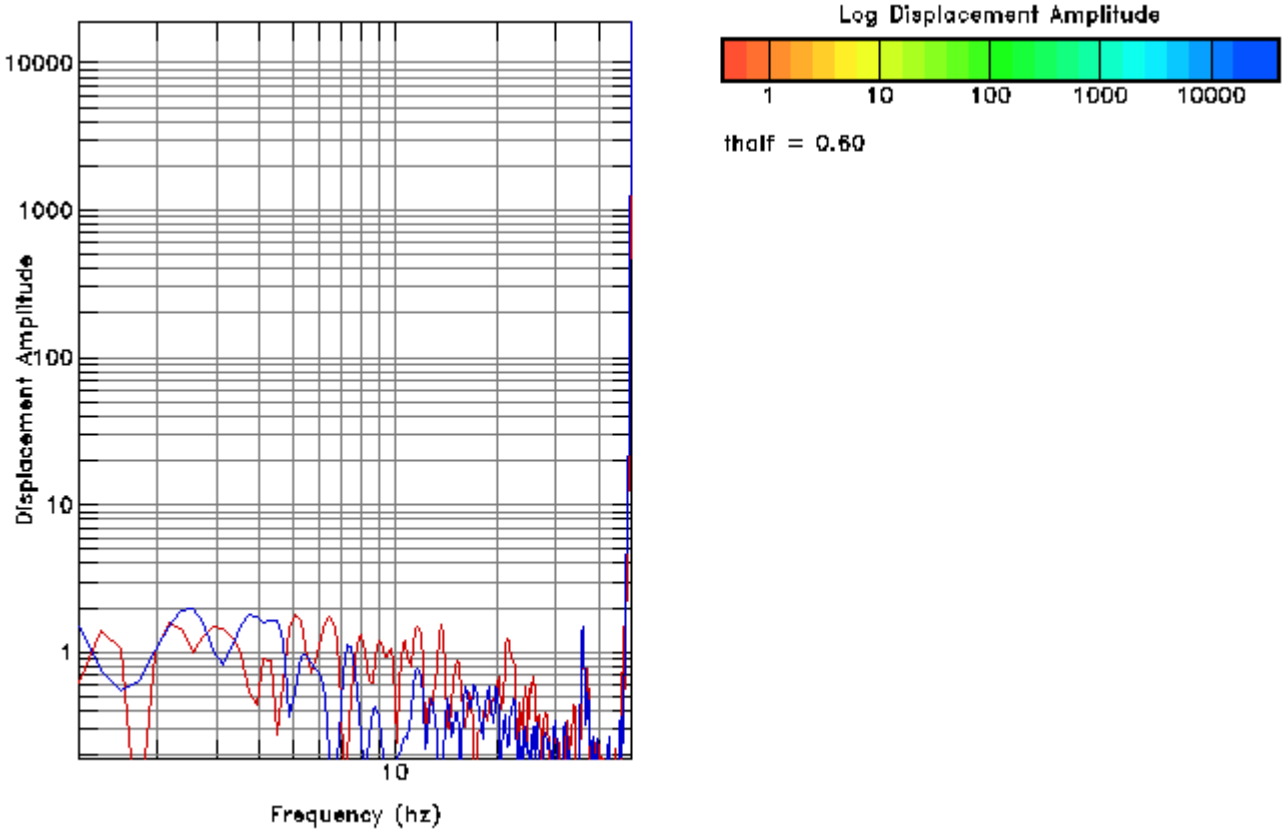

Instrument Correction: Ranger SS1/Quanterra 330 Linear Phase Composite

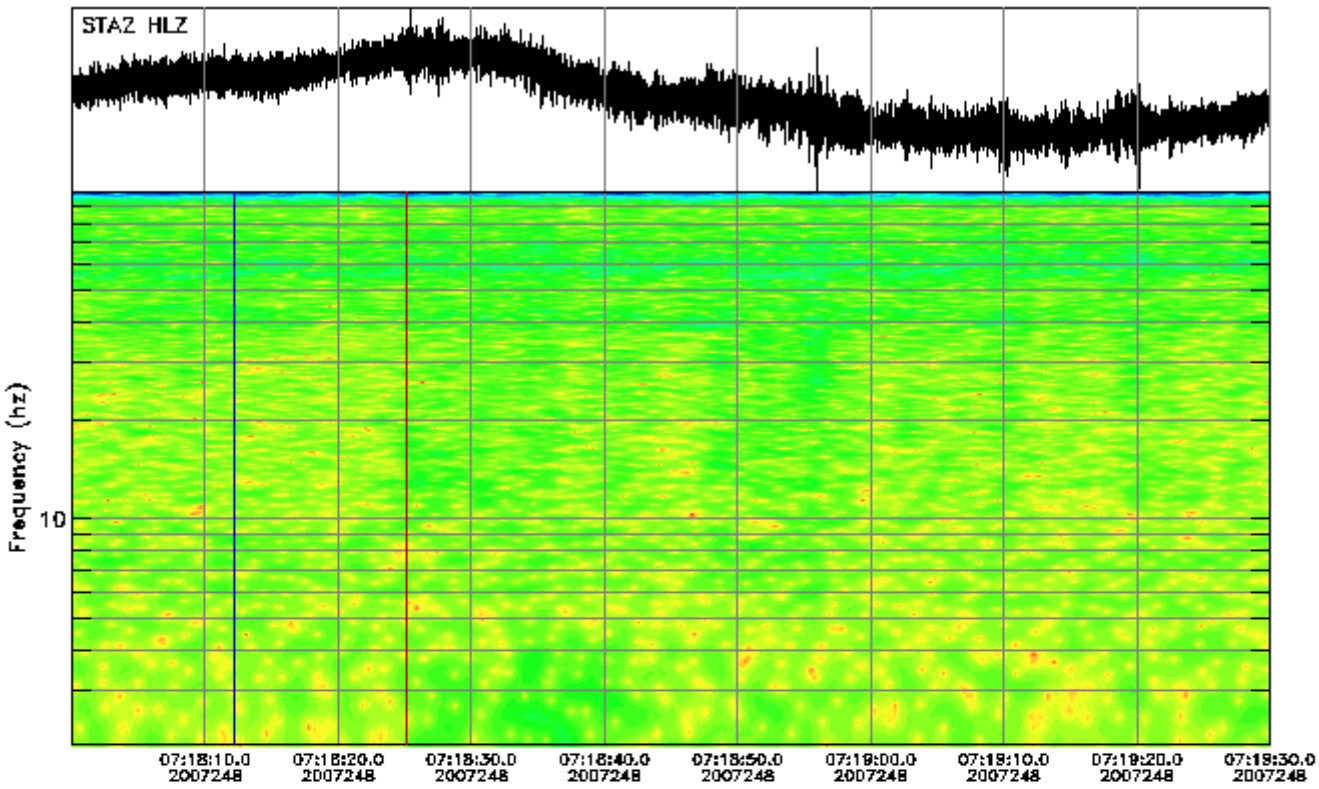

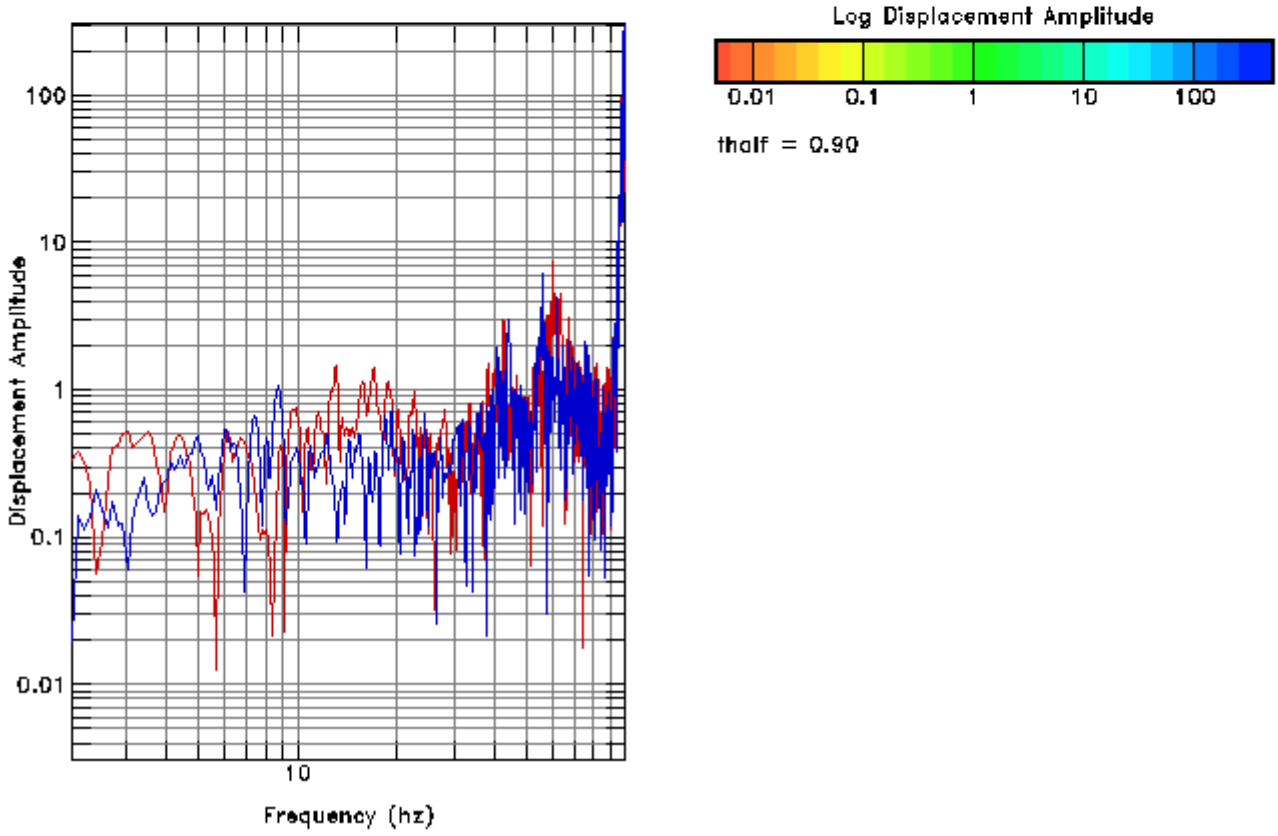

Instrument Correction: Episensor 200 Hz 10 Volt FS 2g/Quanterra 330 Linea

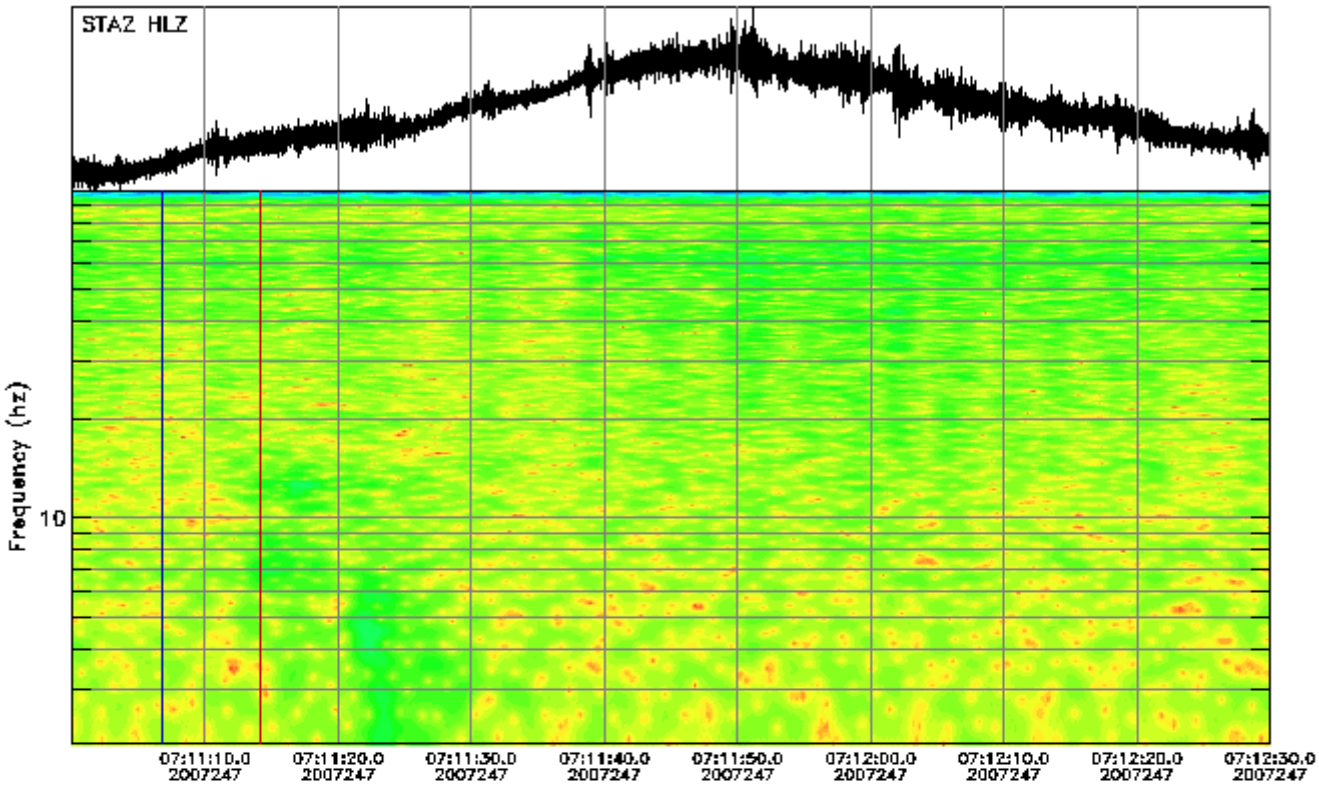

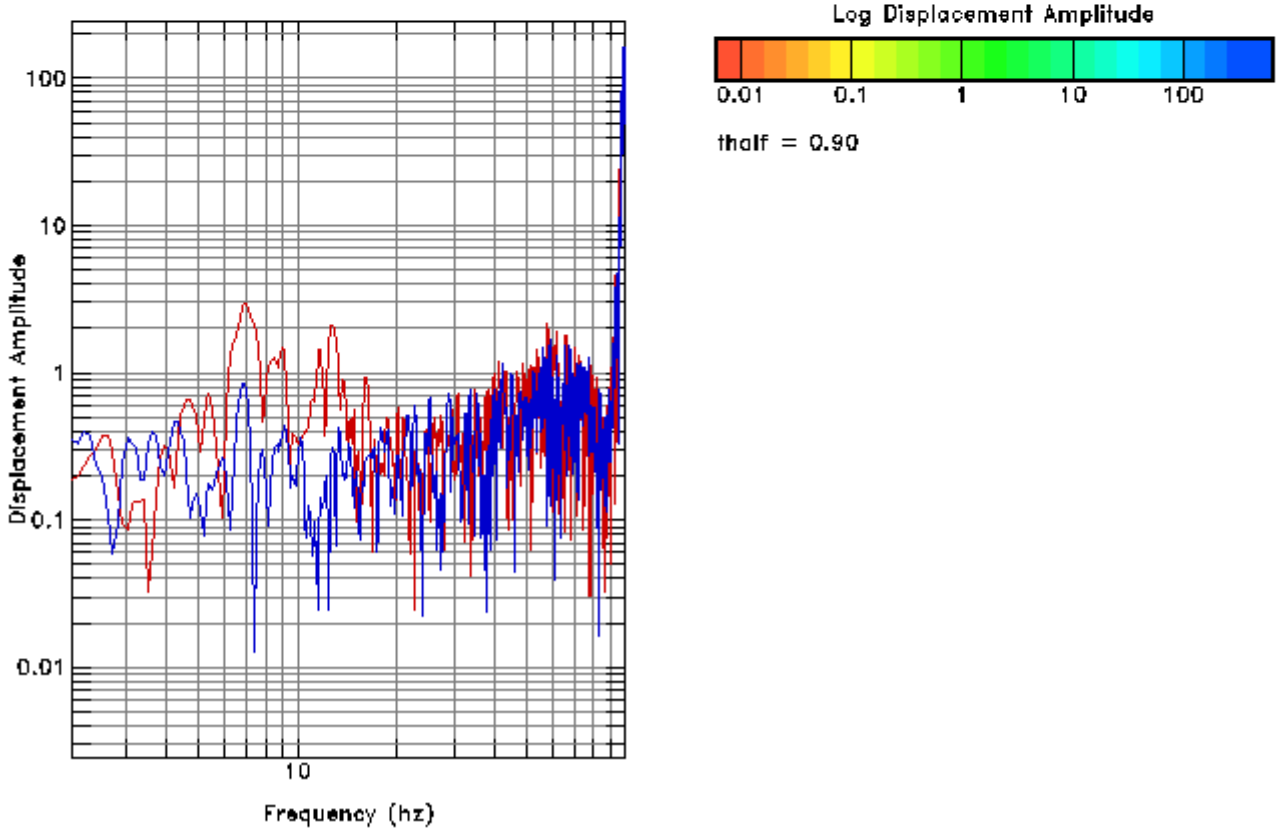

Instrument Correction: Episensor 200 Hz 10 Volt FS 2g/Quanterra 330 Linea

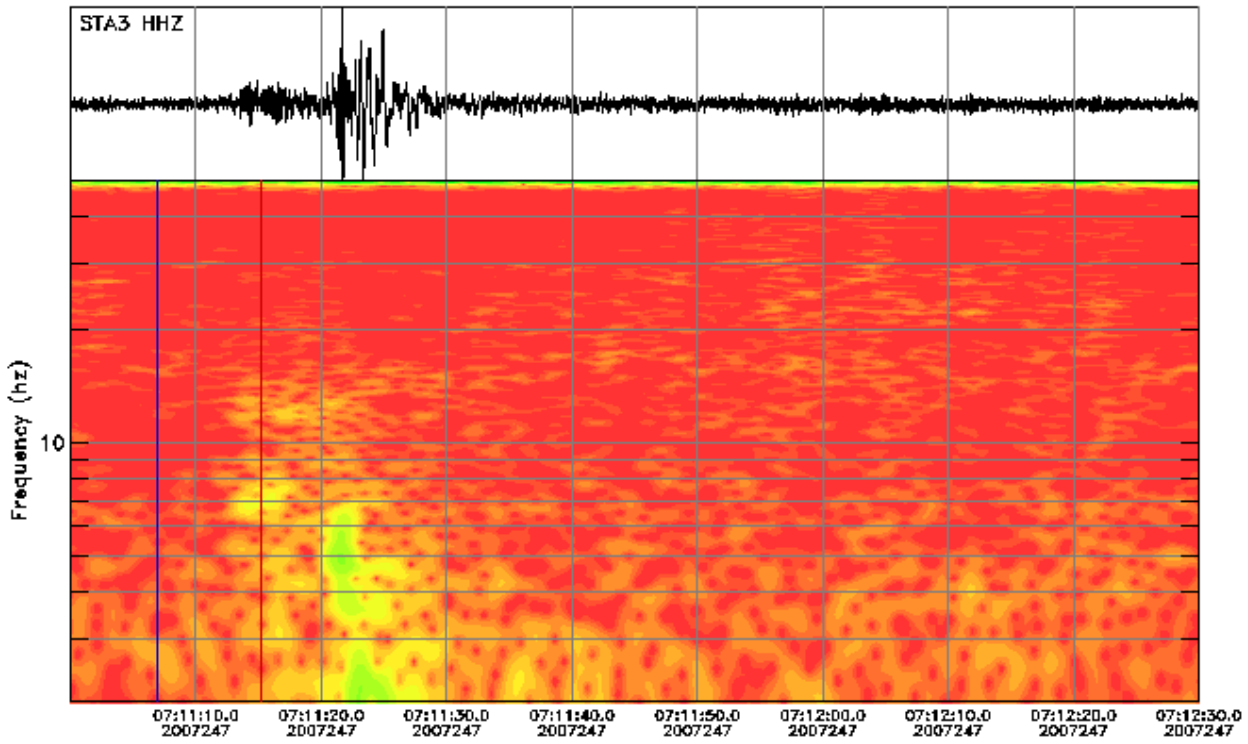

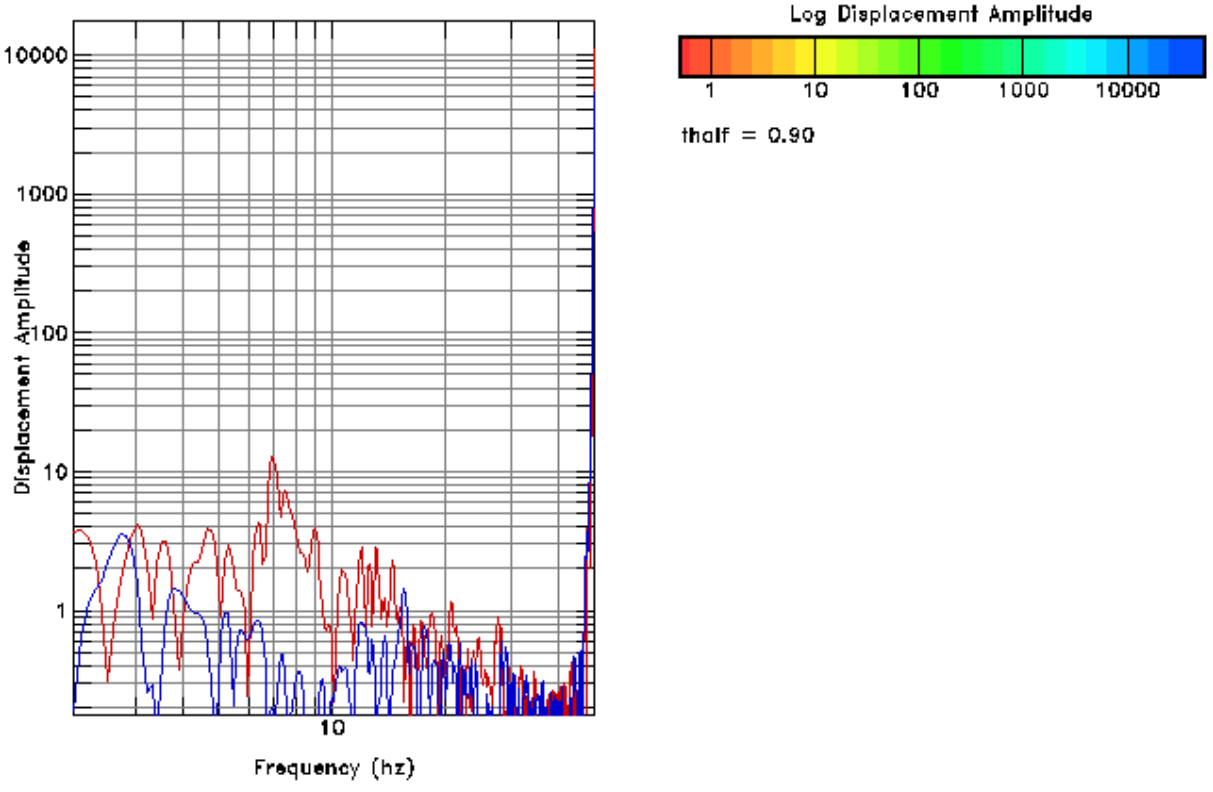

Instrument Correction: Ranger SS1/Quanterra 330 Linear Phase Composite

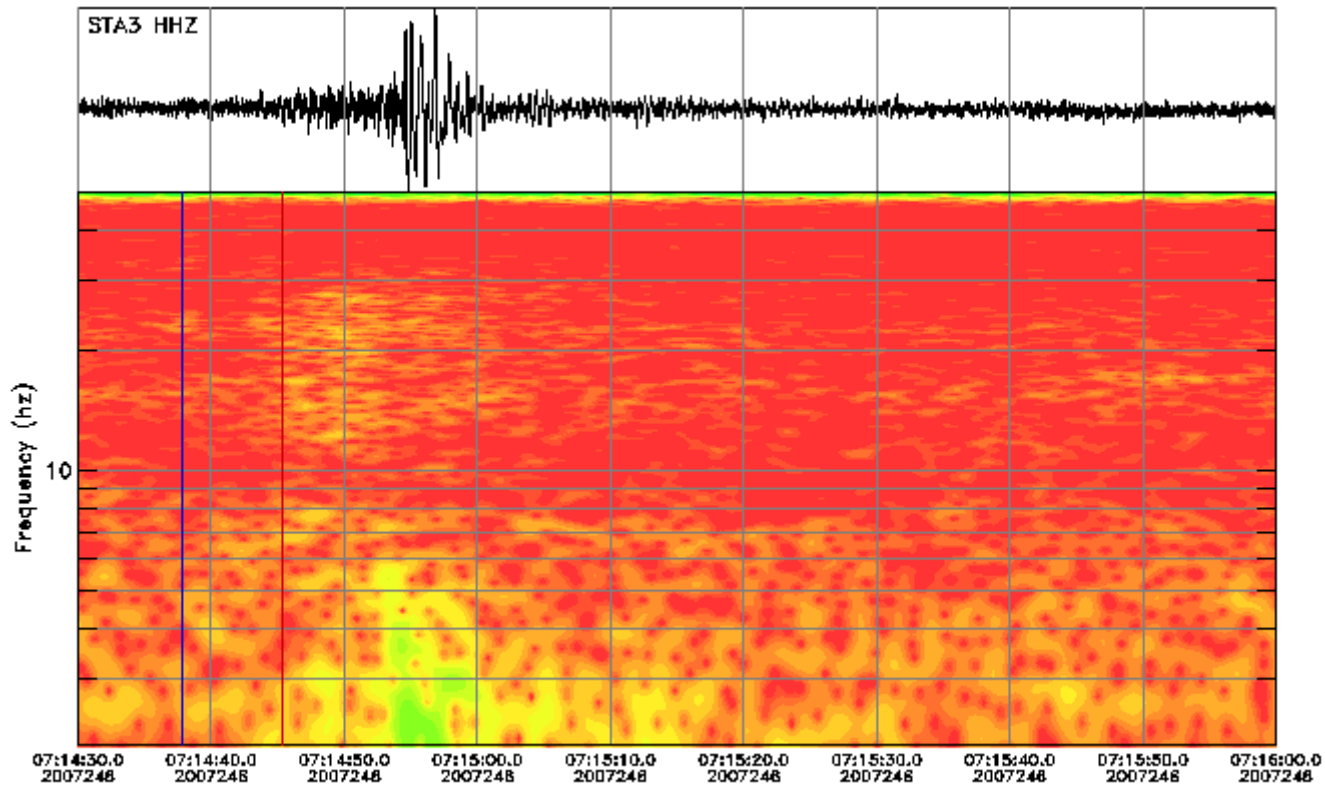

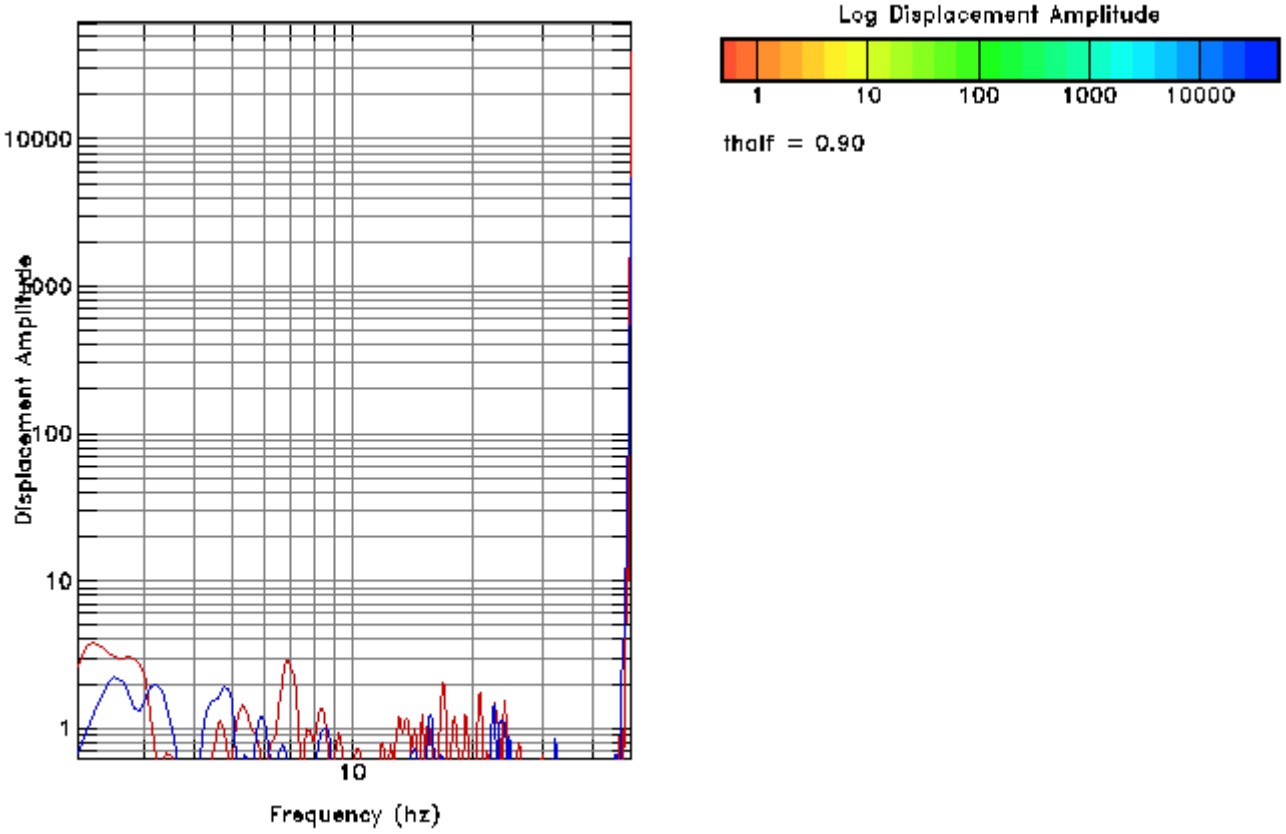

Instrument Correction: Ranger SS1/Quanterra 330 Linear Phase Composite

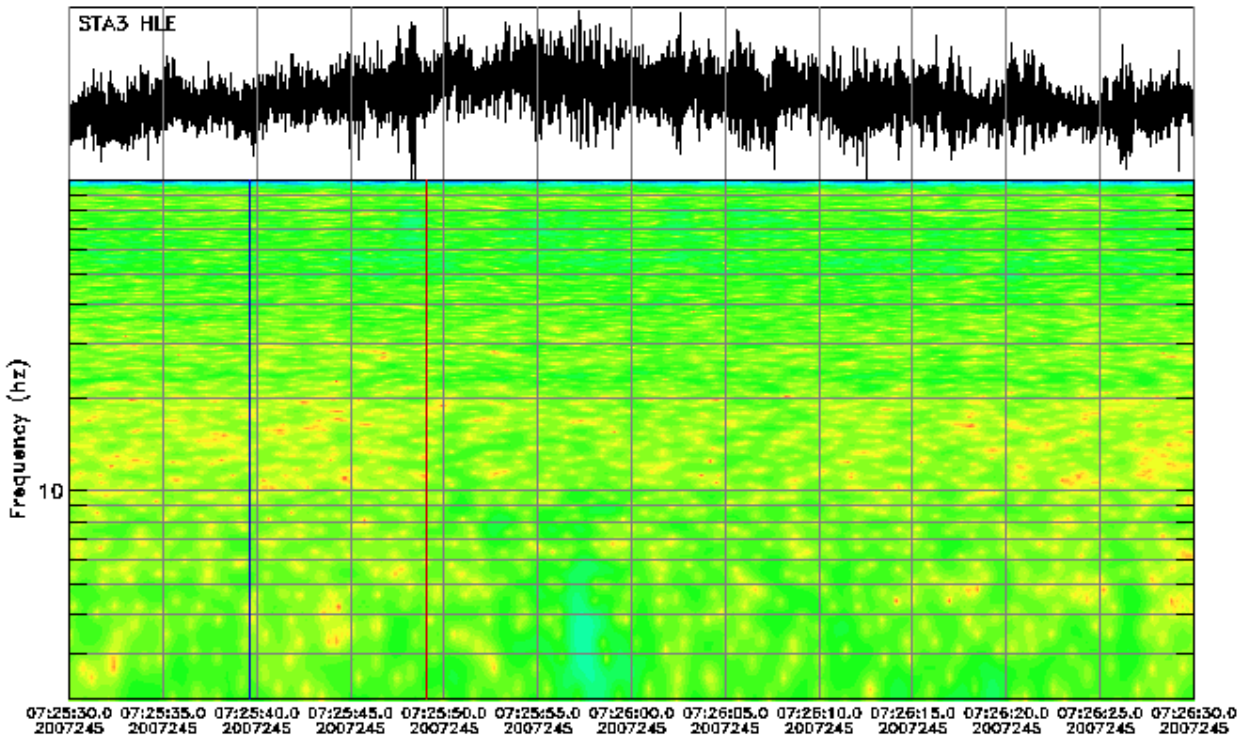

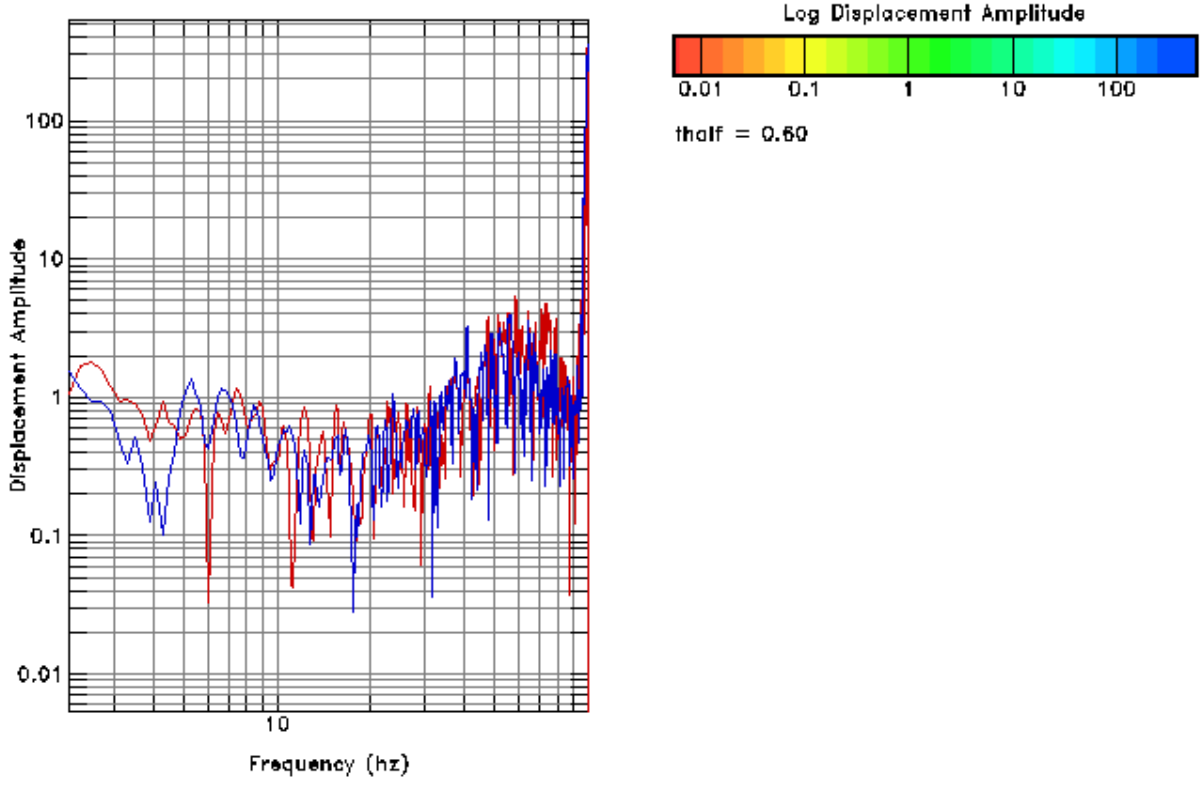

Instrument Correction: Episensor 200 Hz 10 Volt FS 2g/Quanterra 330 Linea

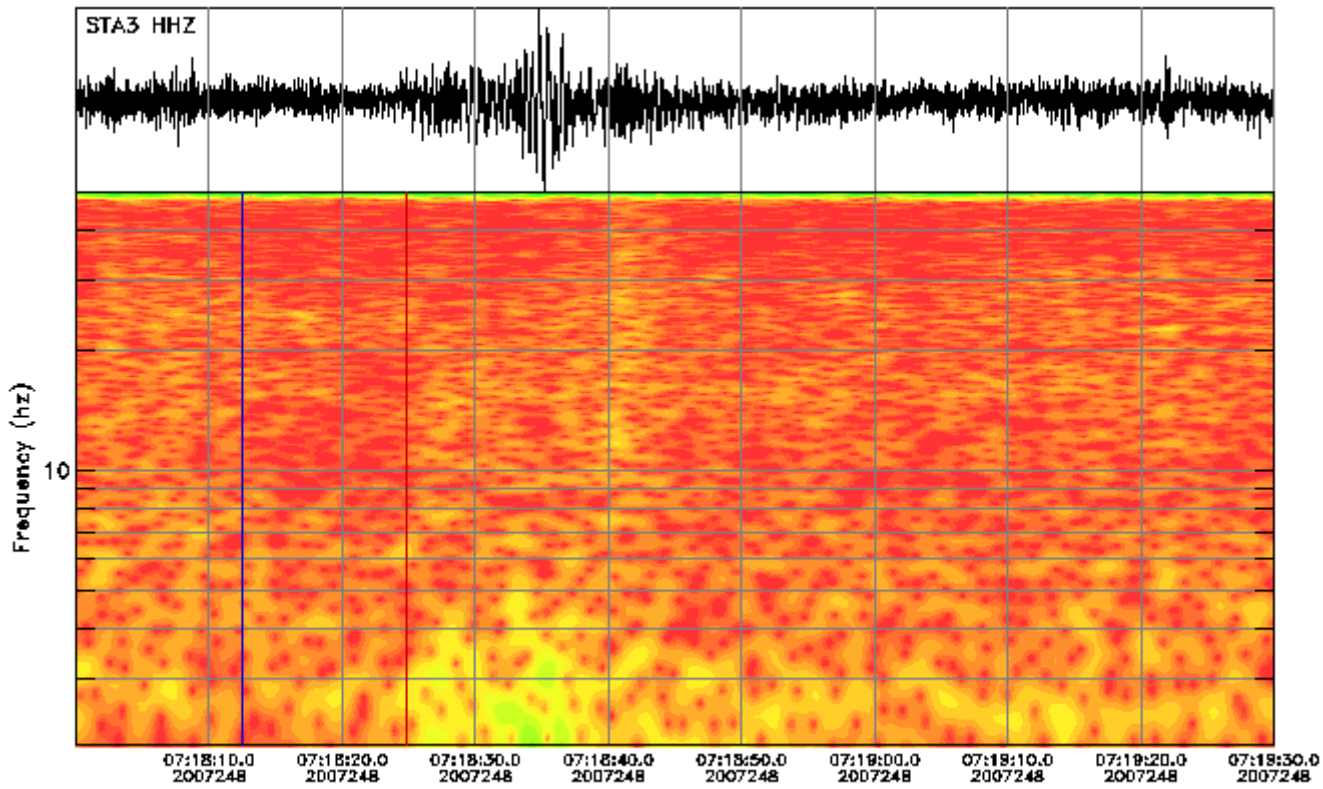

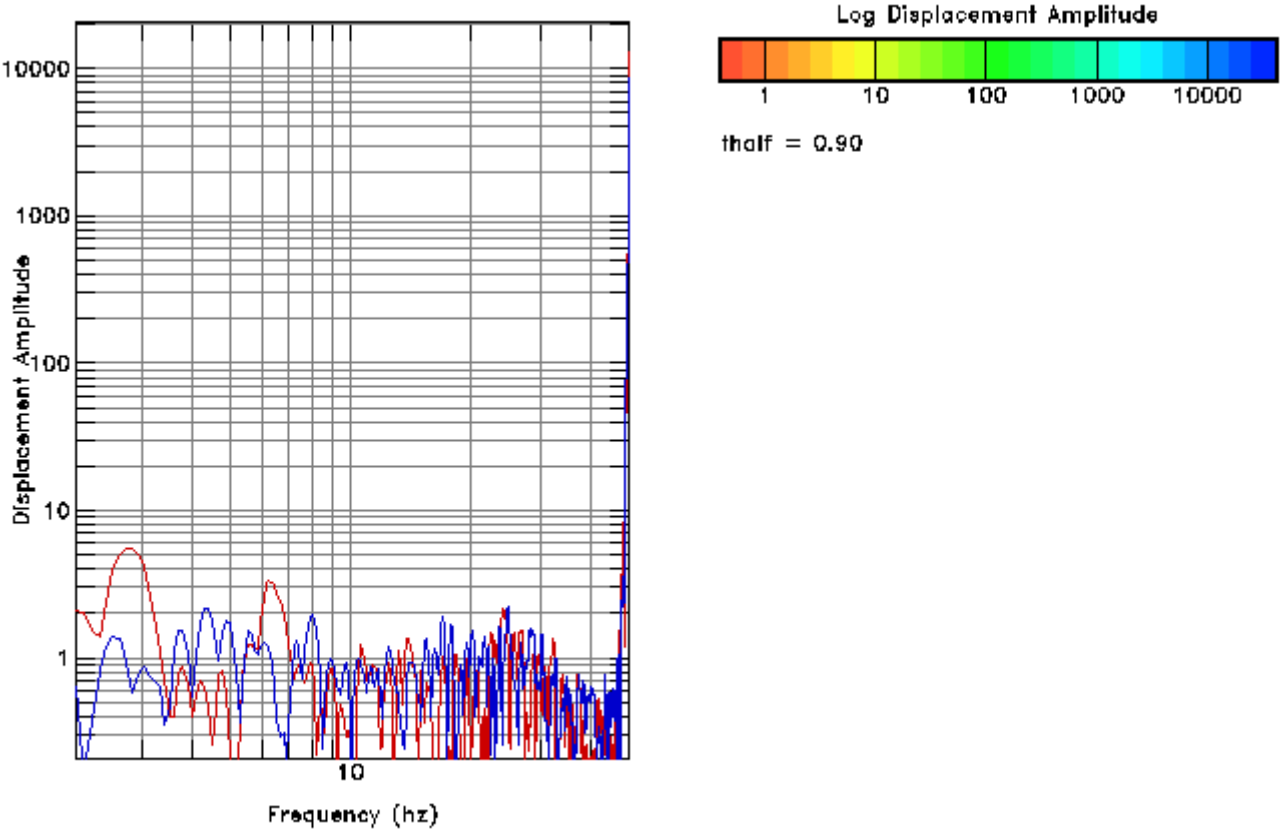

Instrument Correction: Ranger SS1/Quanterra 330 Linear Phase Composite

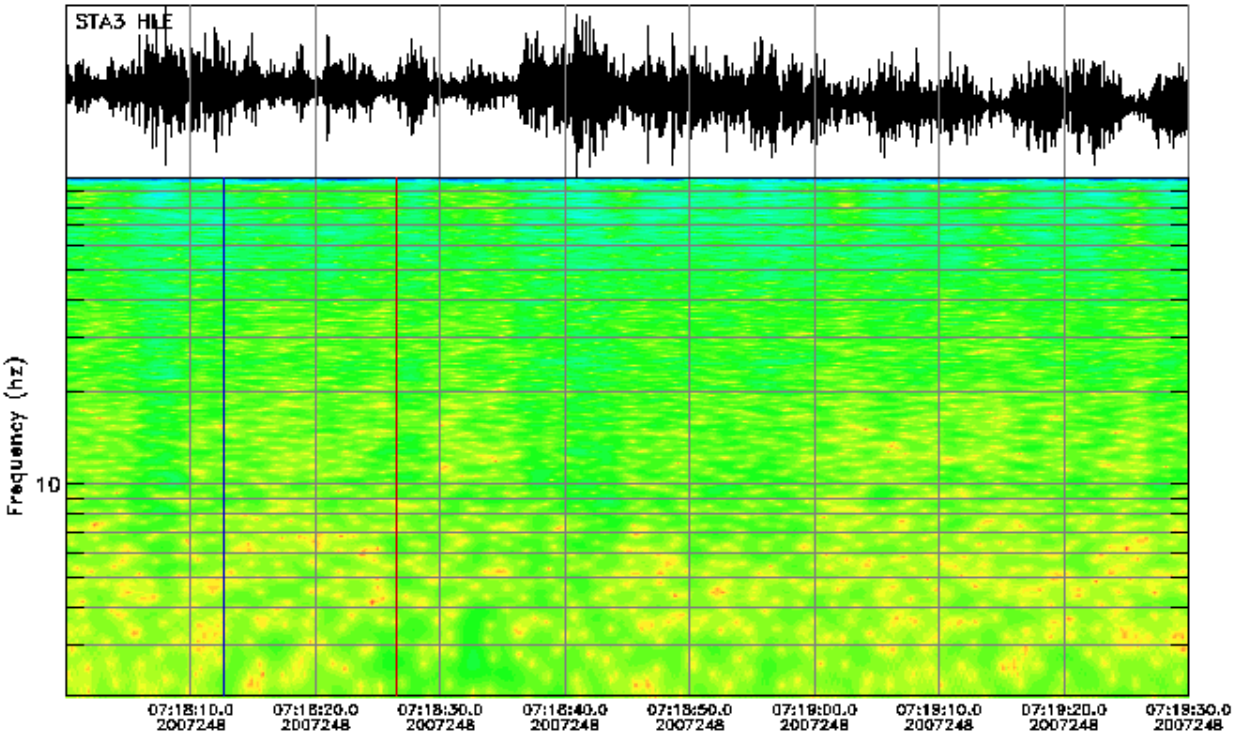

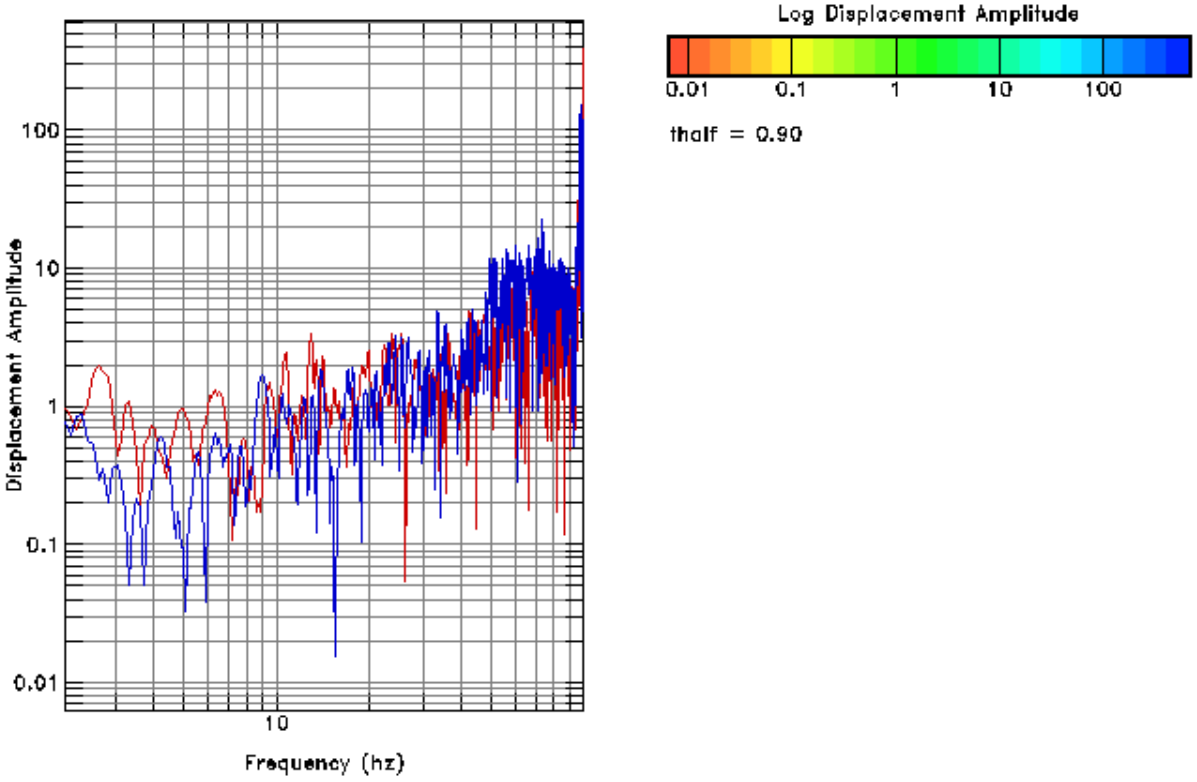

Instrument Correction: Episensor 200 Hz 10 Volt FS 2g/Quanterra 330 Linea

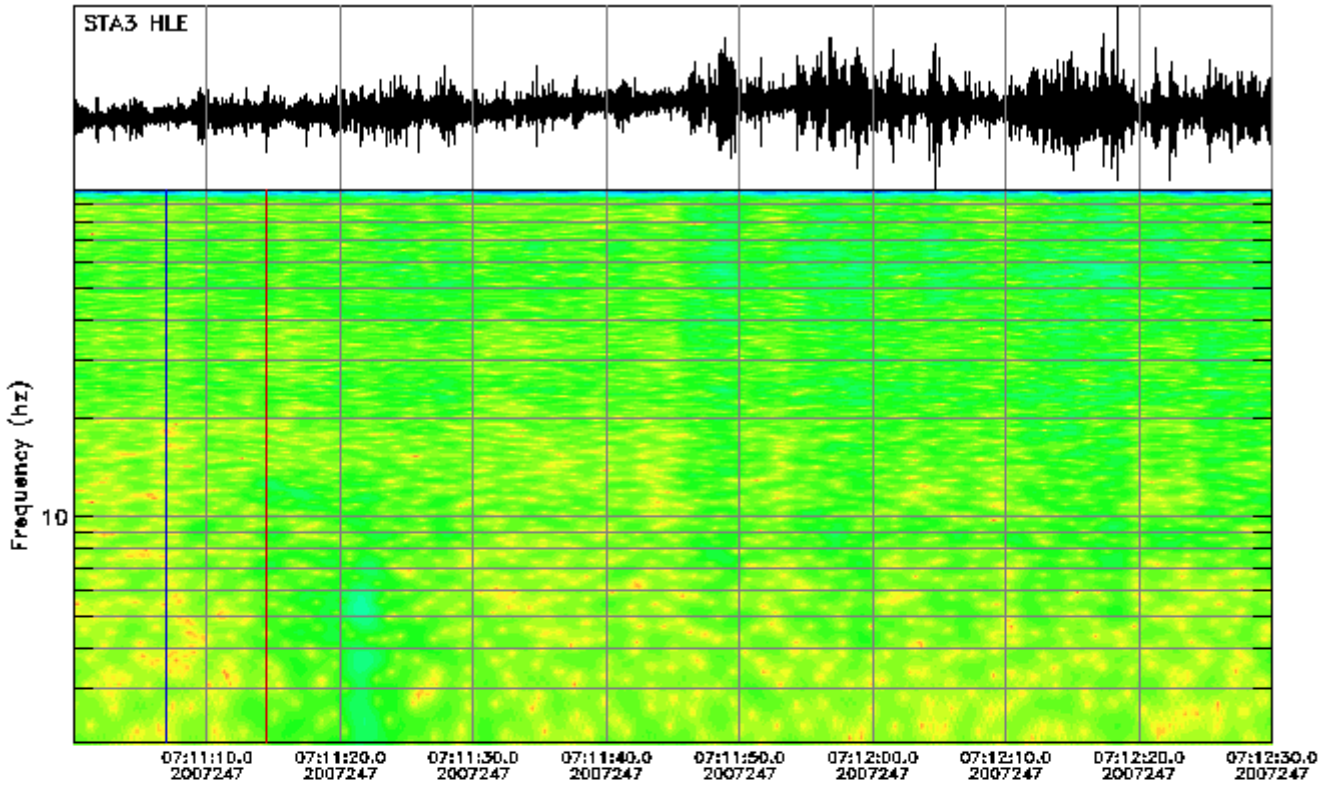

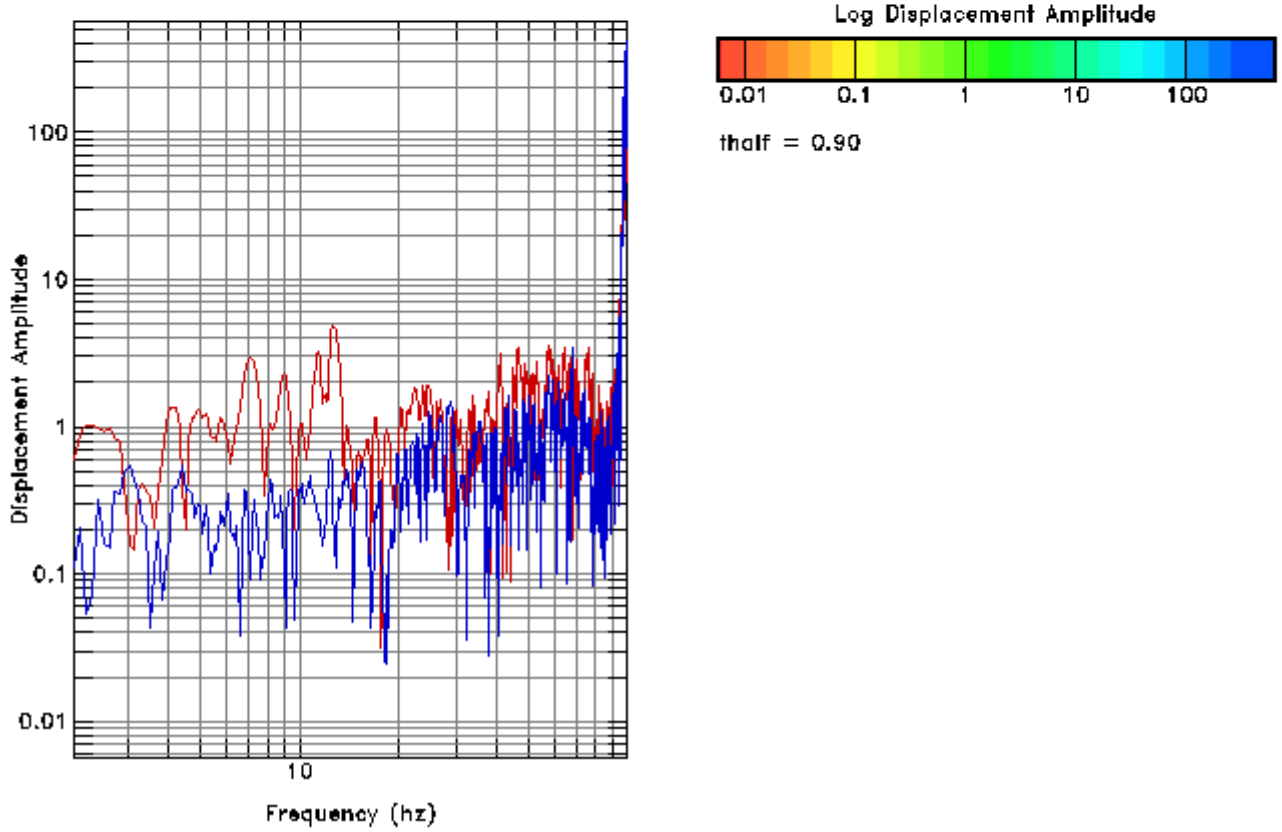

Instrument Correction: Episensor 200 Hz 10 Volt FS 2g/Quanterra 330 Linea

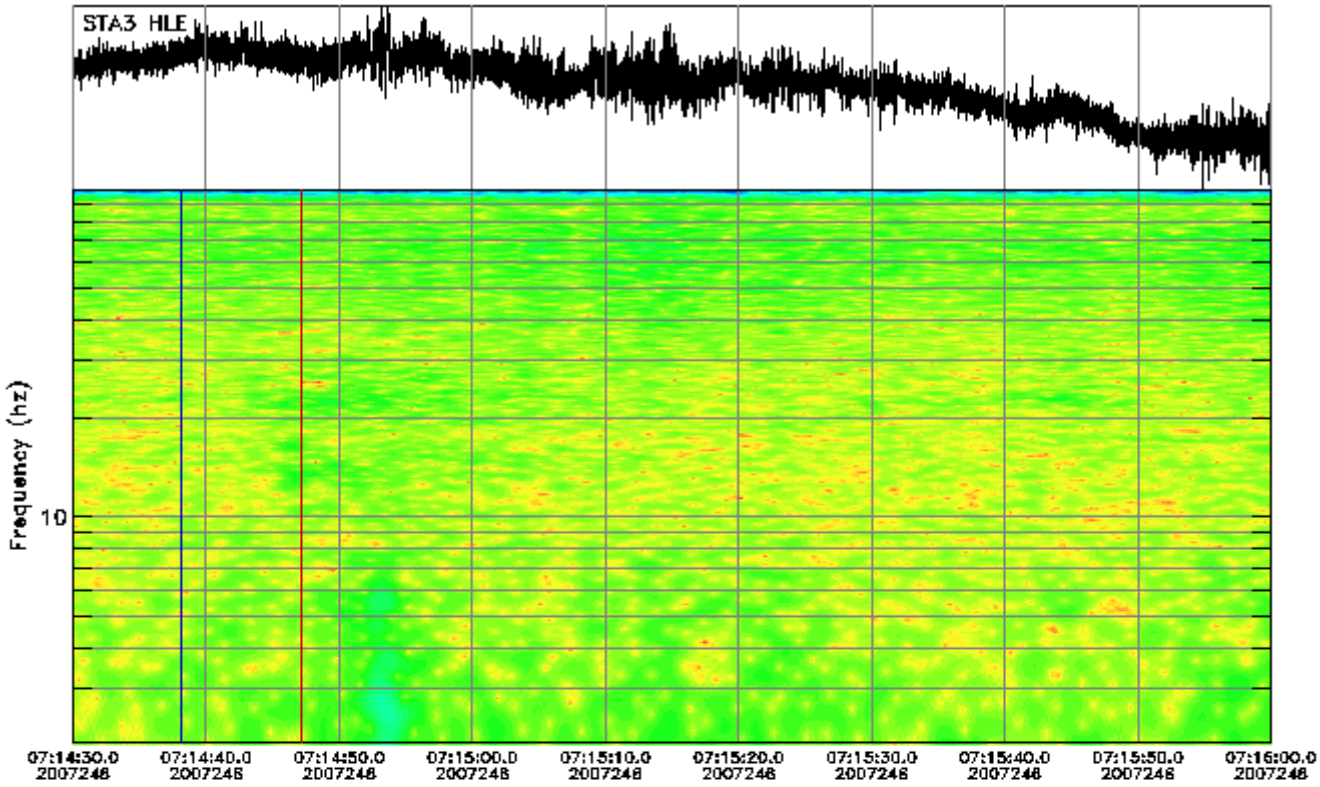

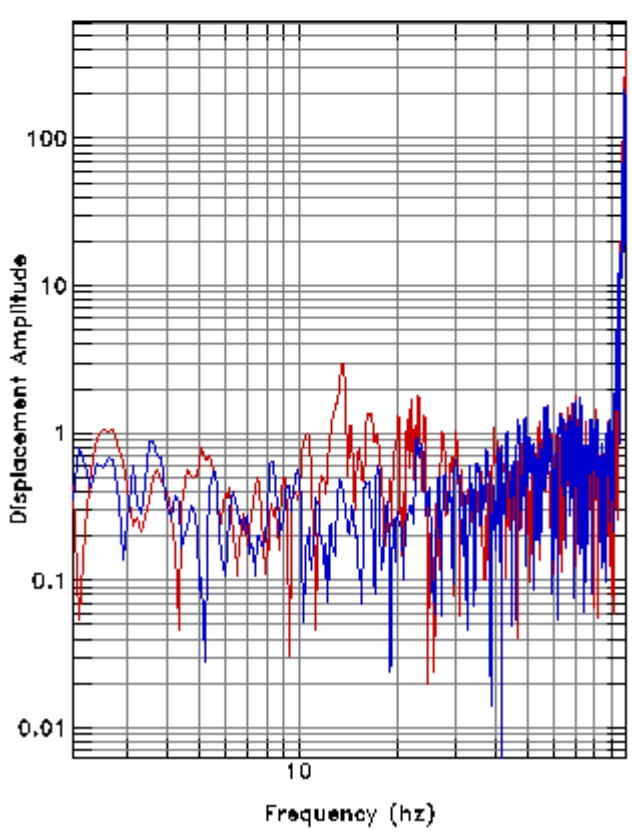

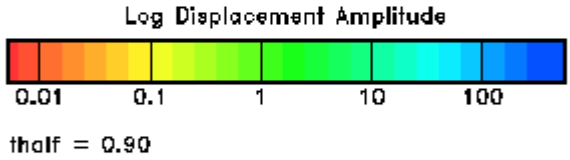

Instrument Correction: Episensor 200 Hz 10 Volt FS 2g/Quanterra 330 Linea

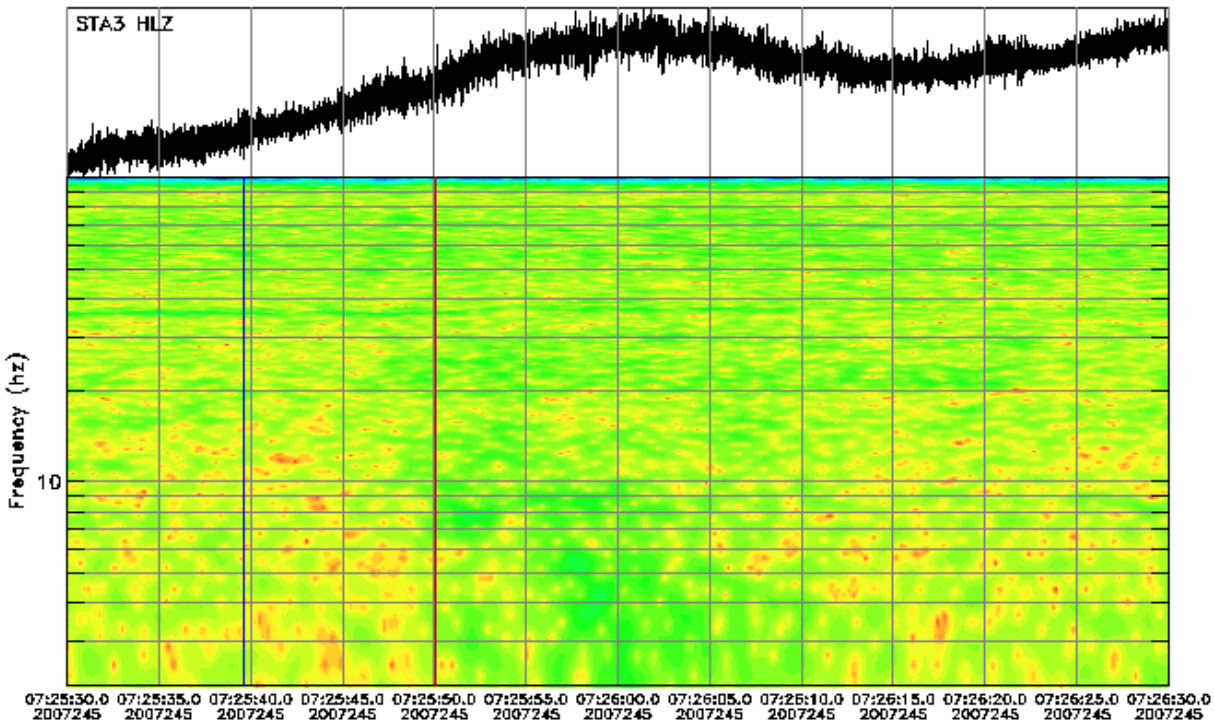

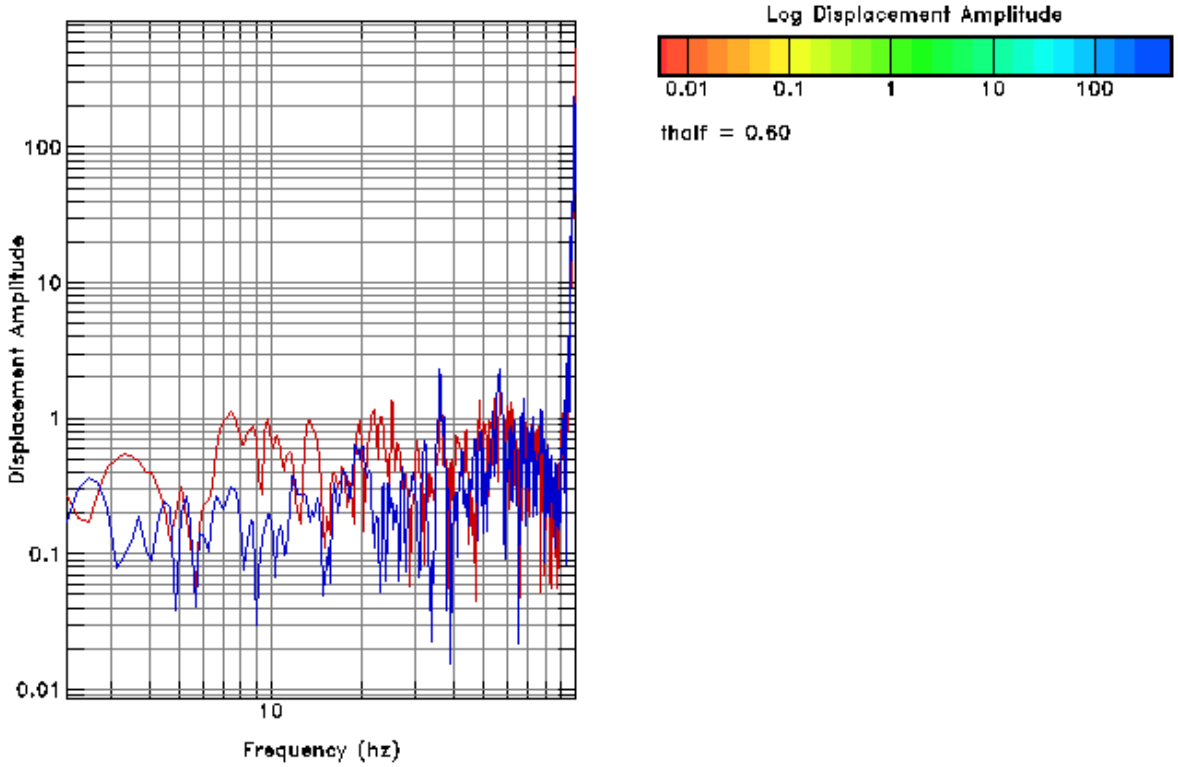

Instrument Correction: Episensor 200 Hz 10 Volt FS 2g/Quanterra 330 Linea

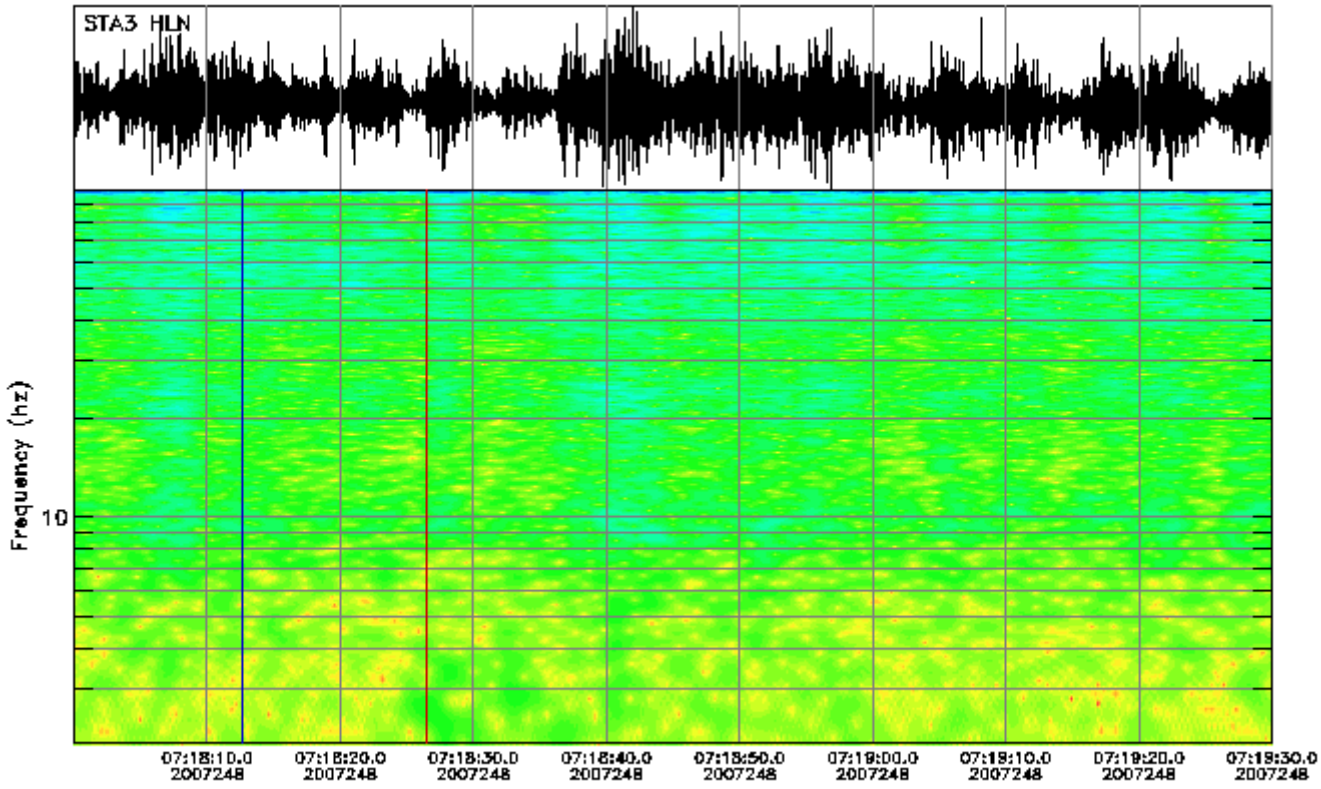

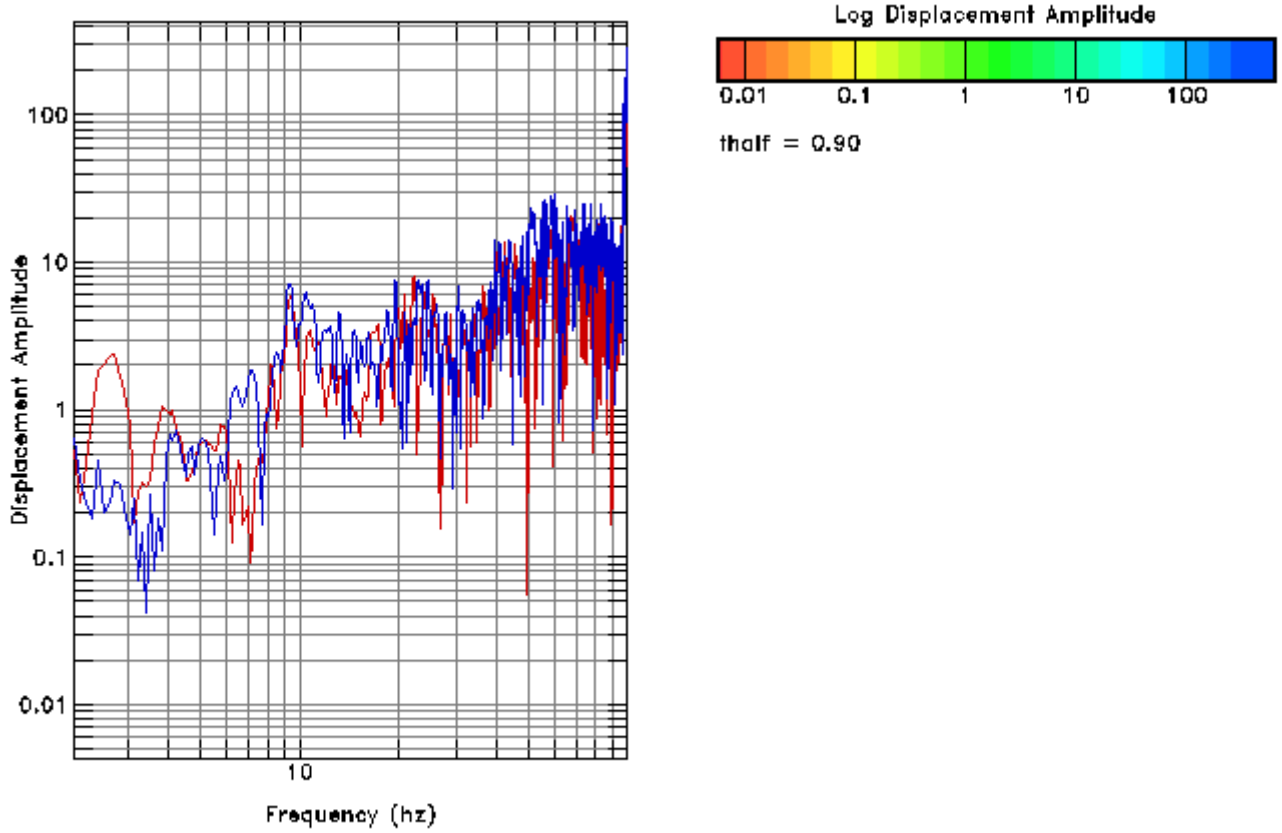

Instrument Correction: Episensor 200 Hz 10 Volt FS 2g/Quanterra 330 Linea

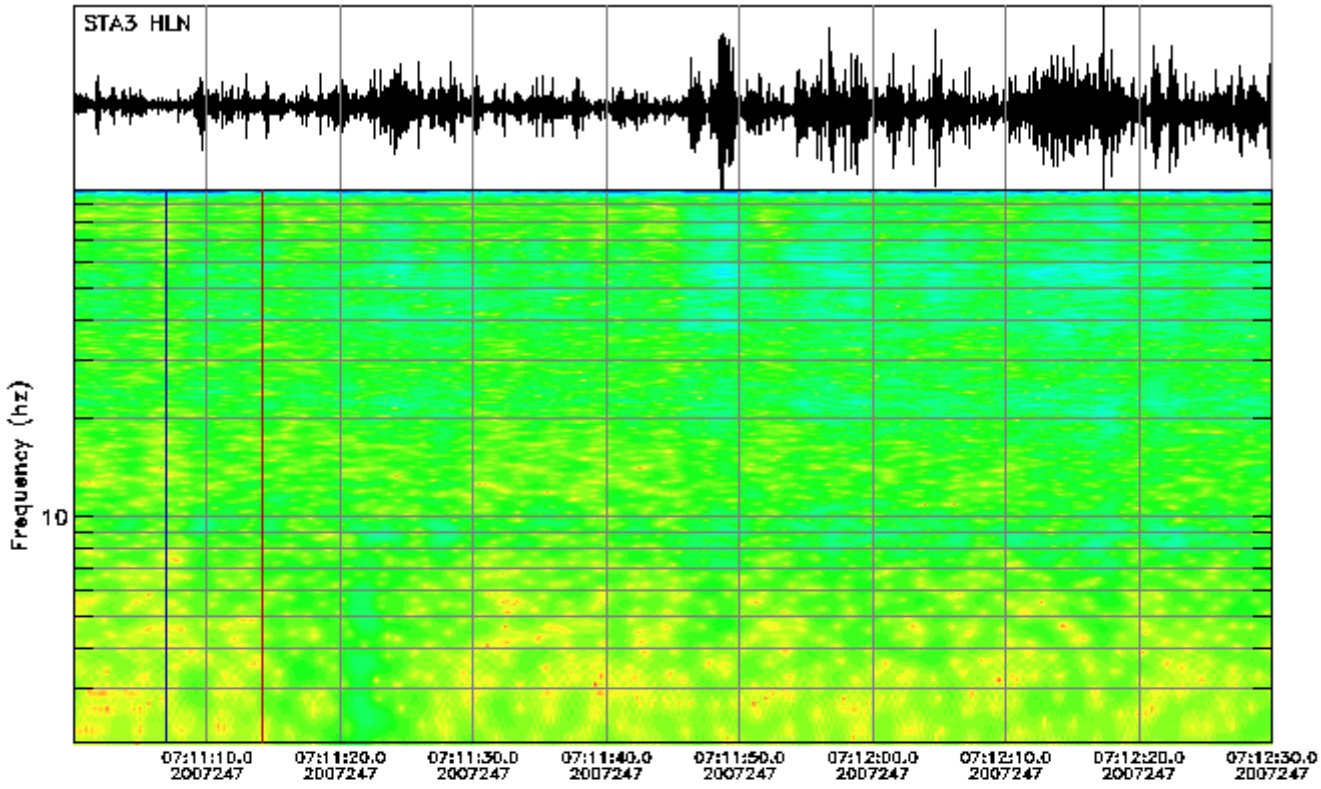

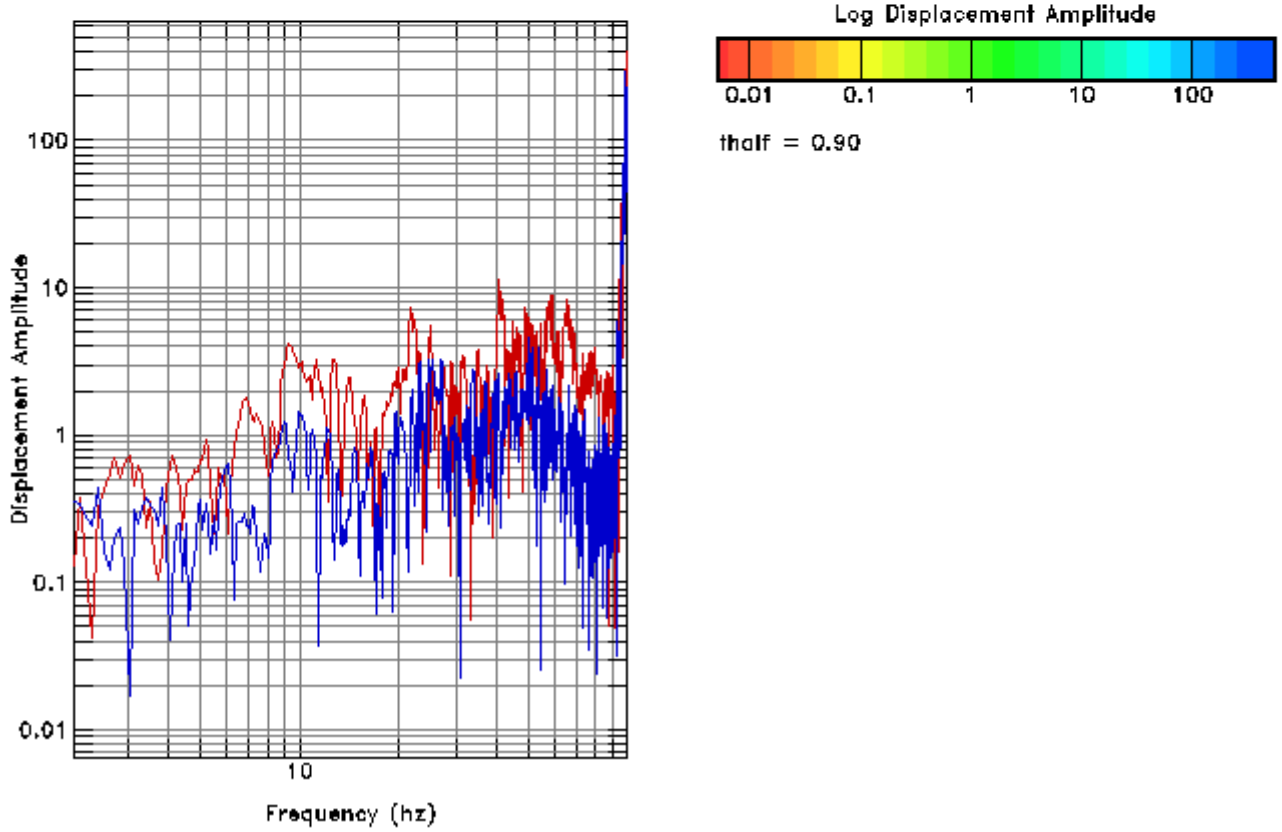

Instrument Correction: Episensor 200 Hz 10 Volt FS 2g/Quanterra 330 Linea

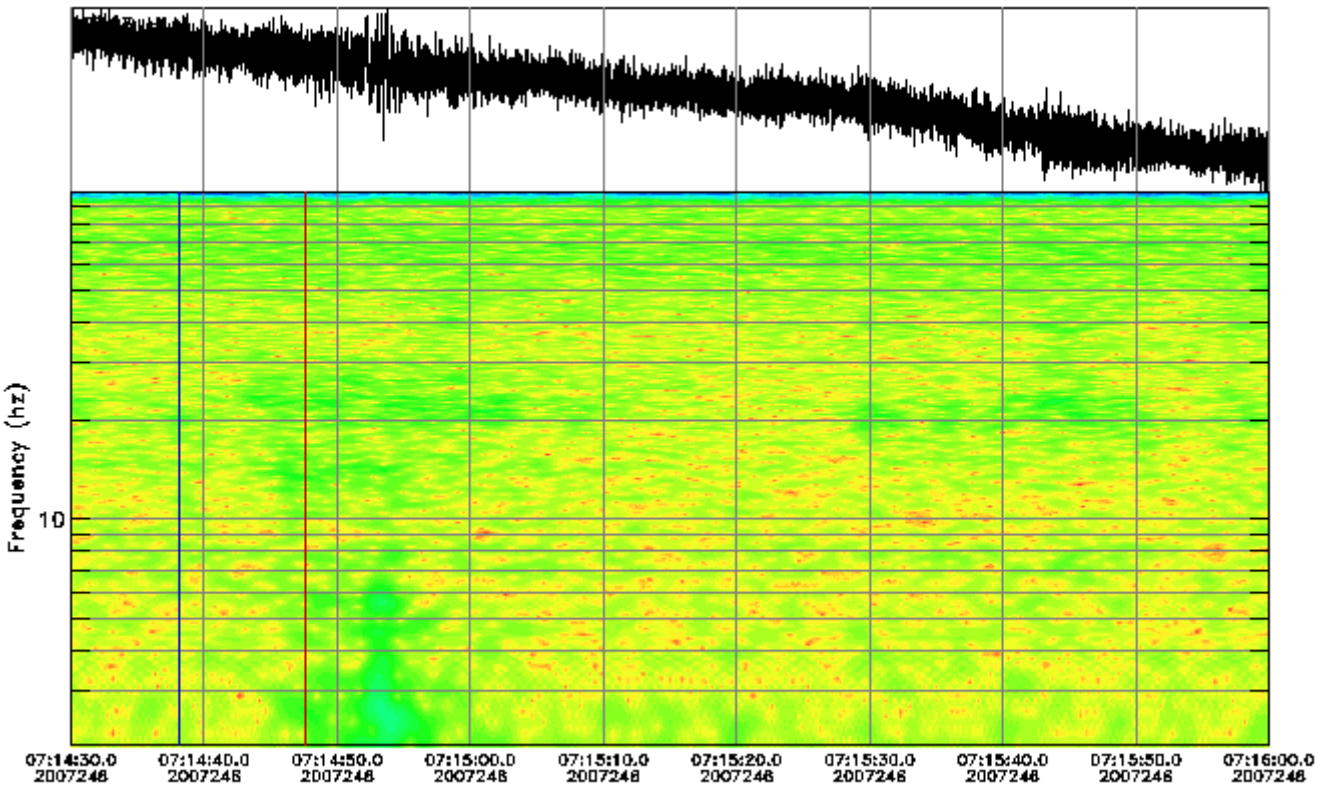

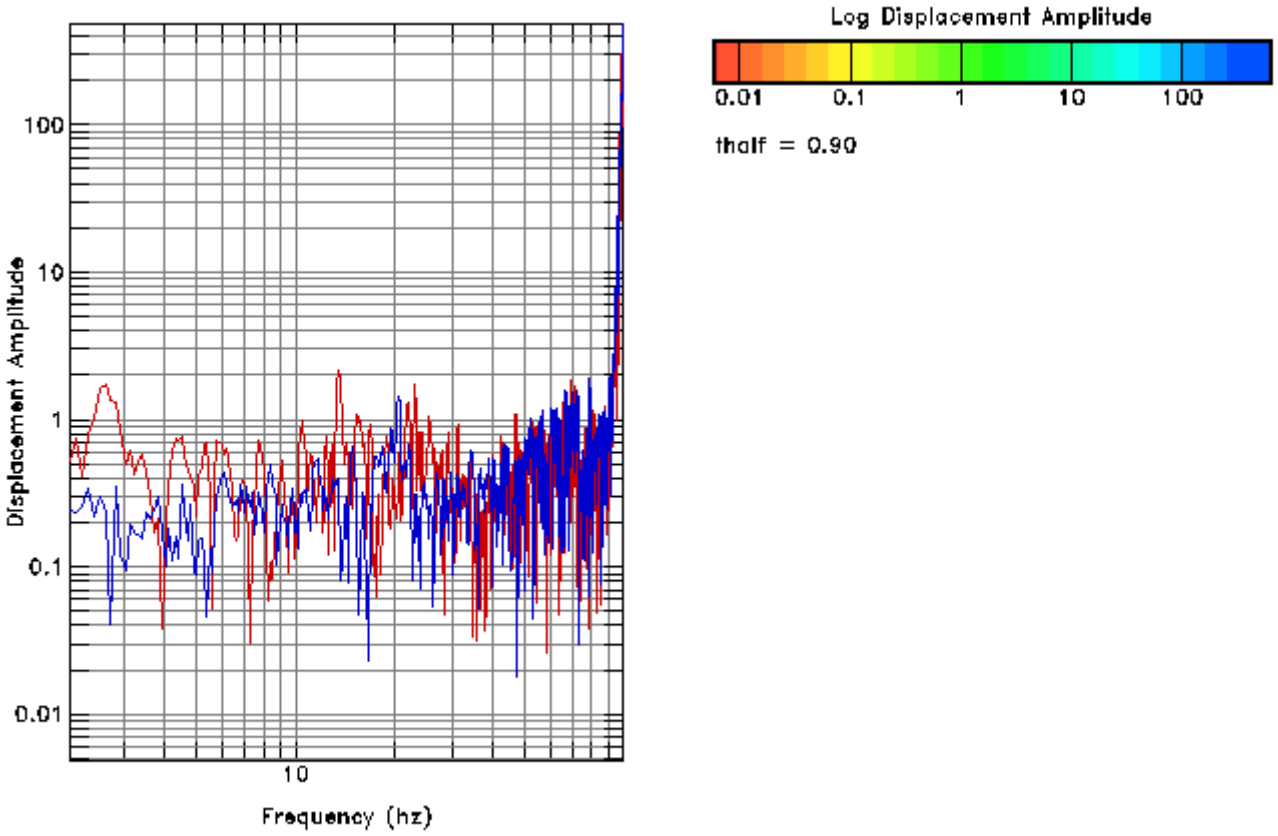

Instrument Correction: Episensor 200 Hz 10 Volt FS 2g/Quanterra 330 Linea

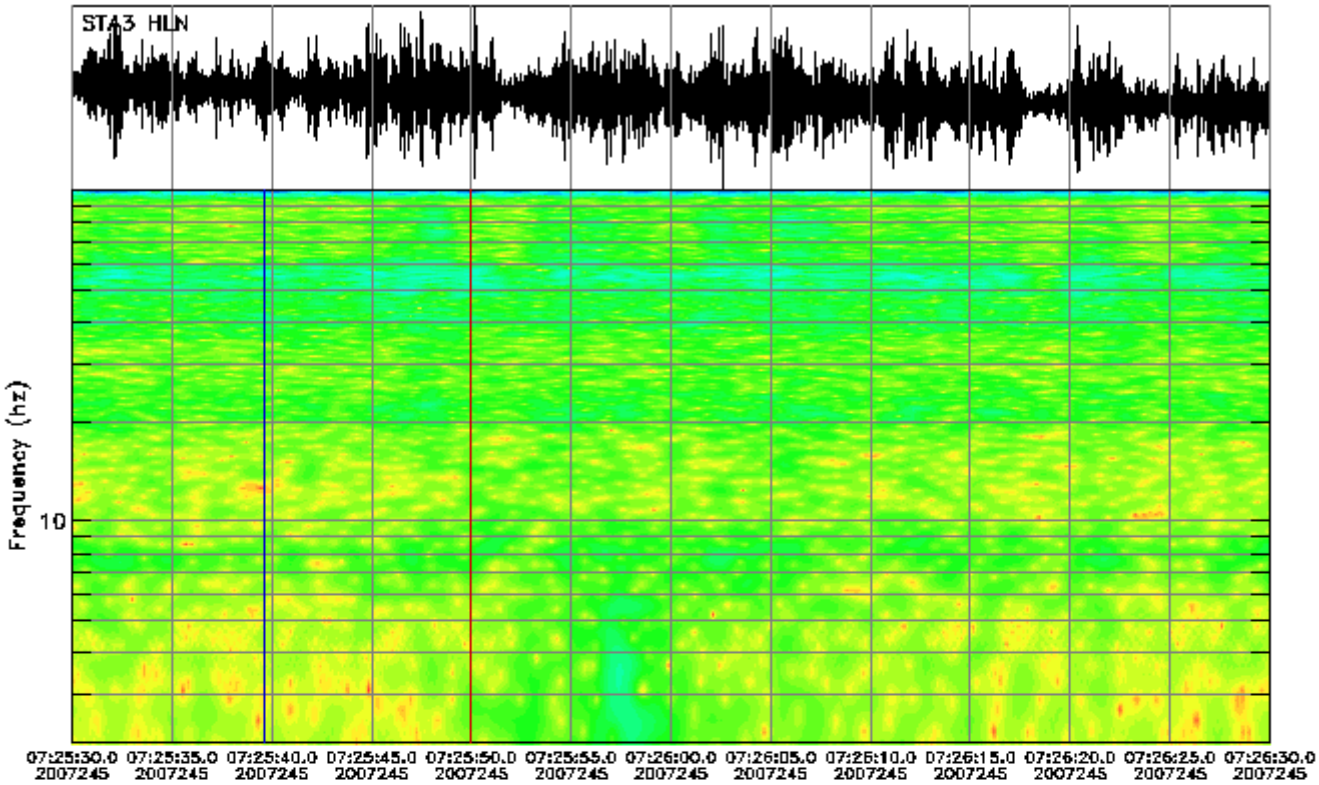

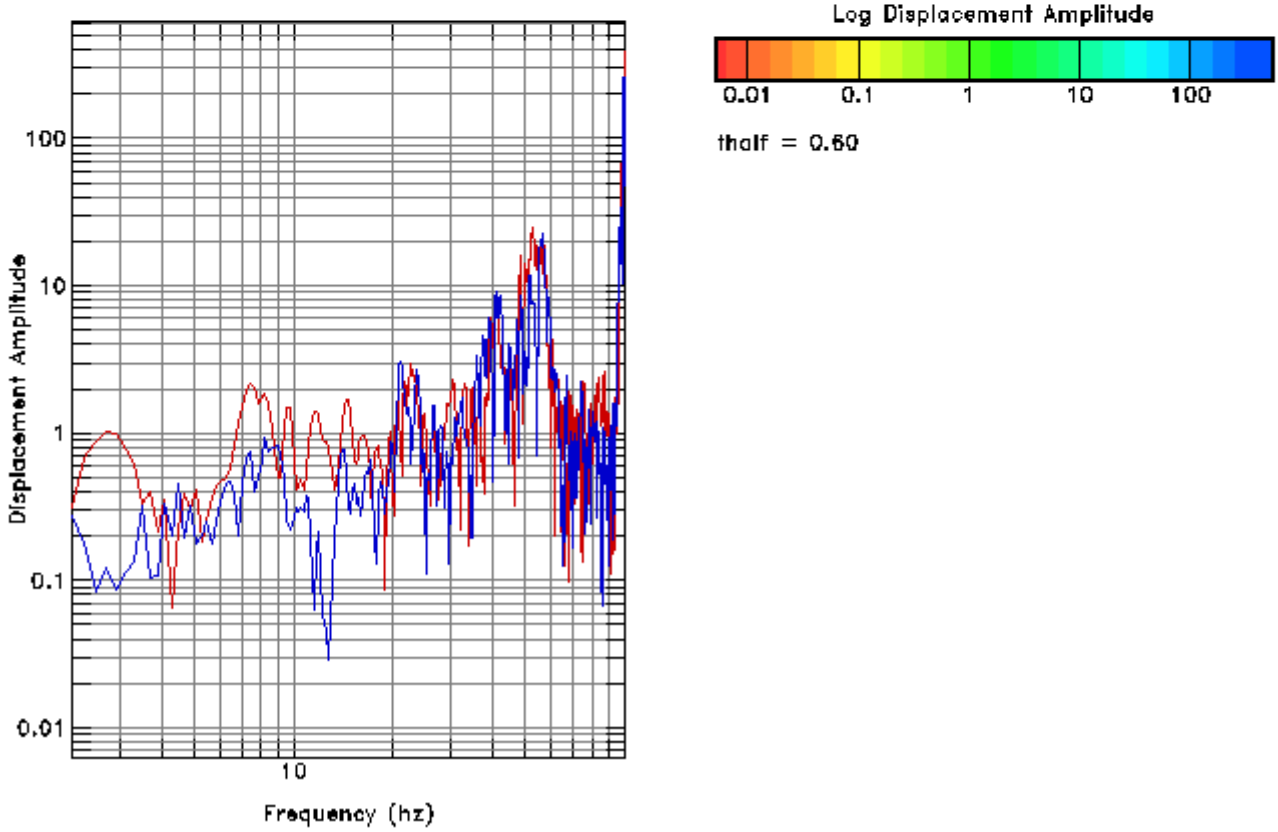

Instrument Correction: Episensor 200 Hz 10 Volt FS 2g/Quanterra 330 Linea

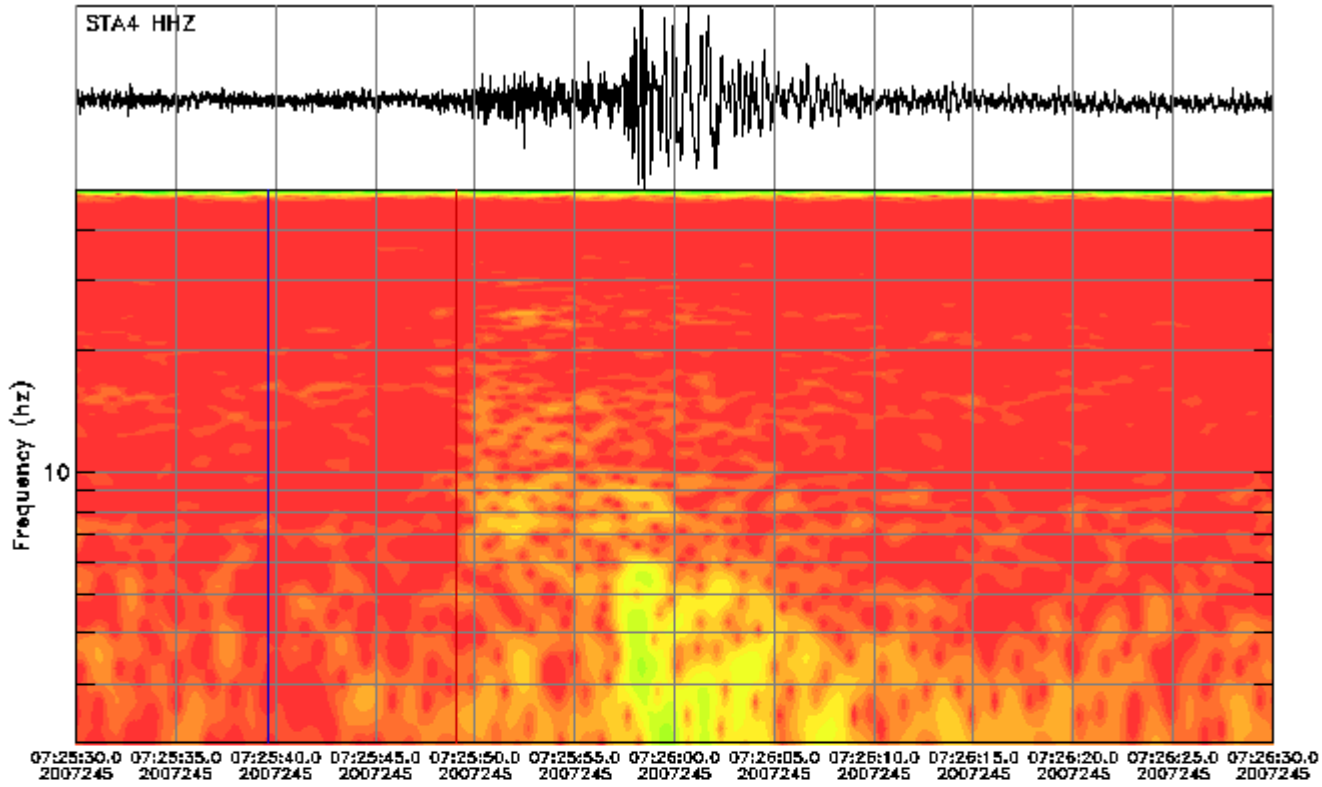

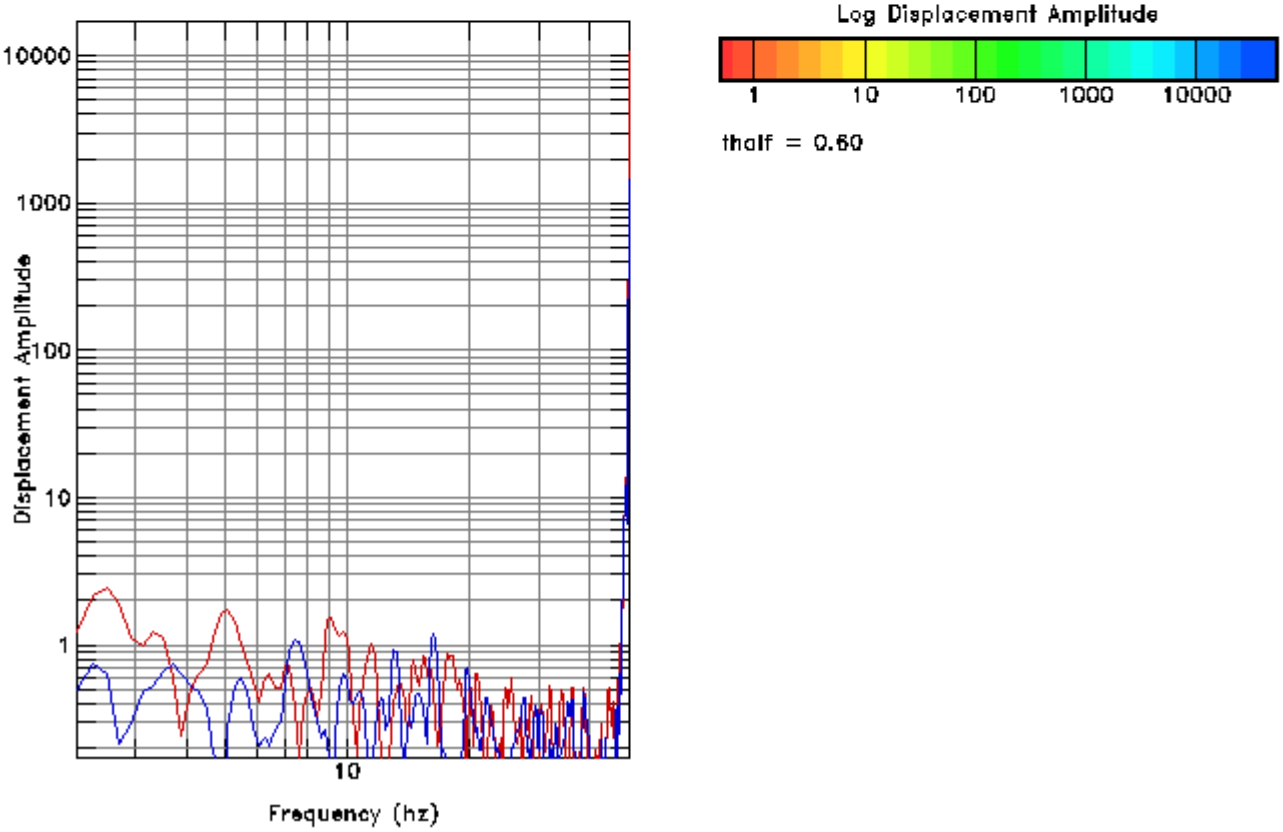

Instrument Correction: Ranger SS1/Quanterra 330 Linear Phase Composite

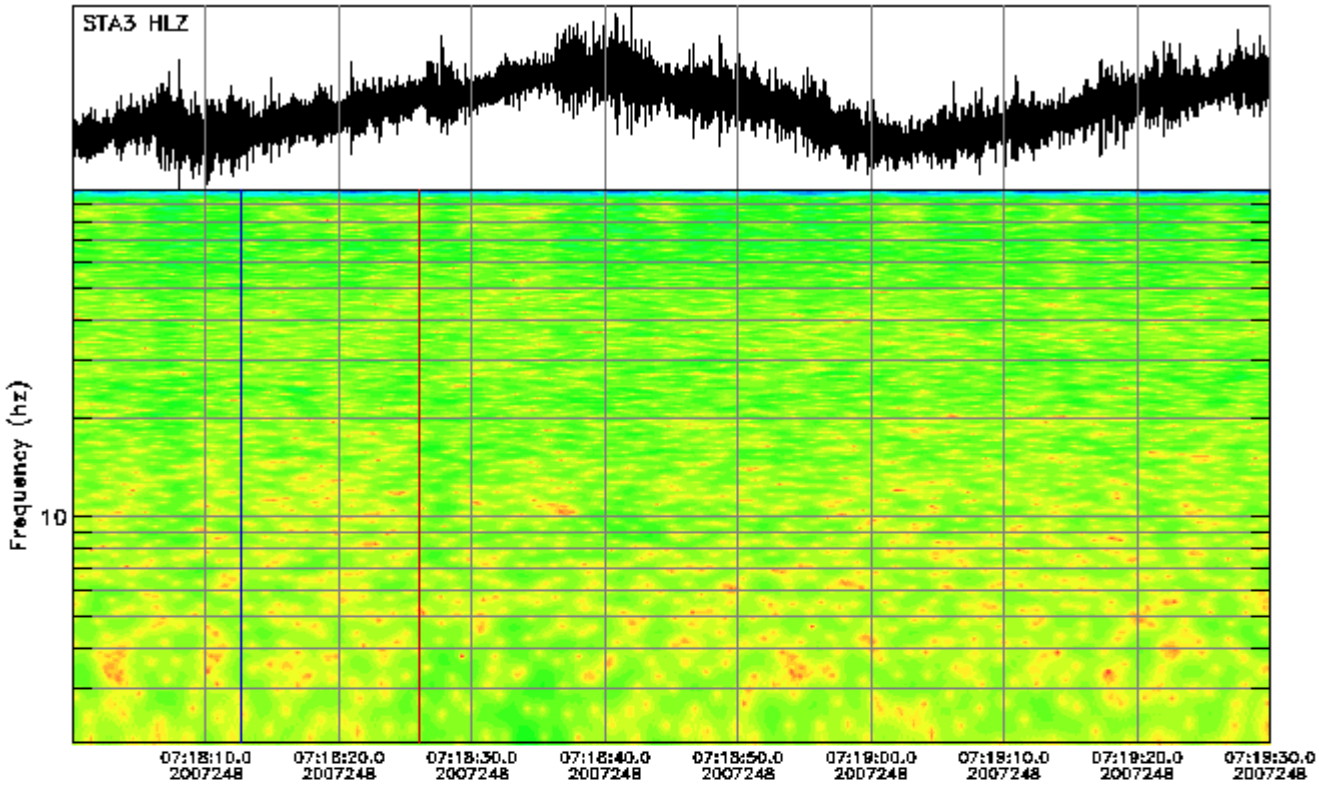

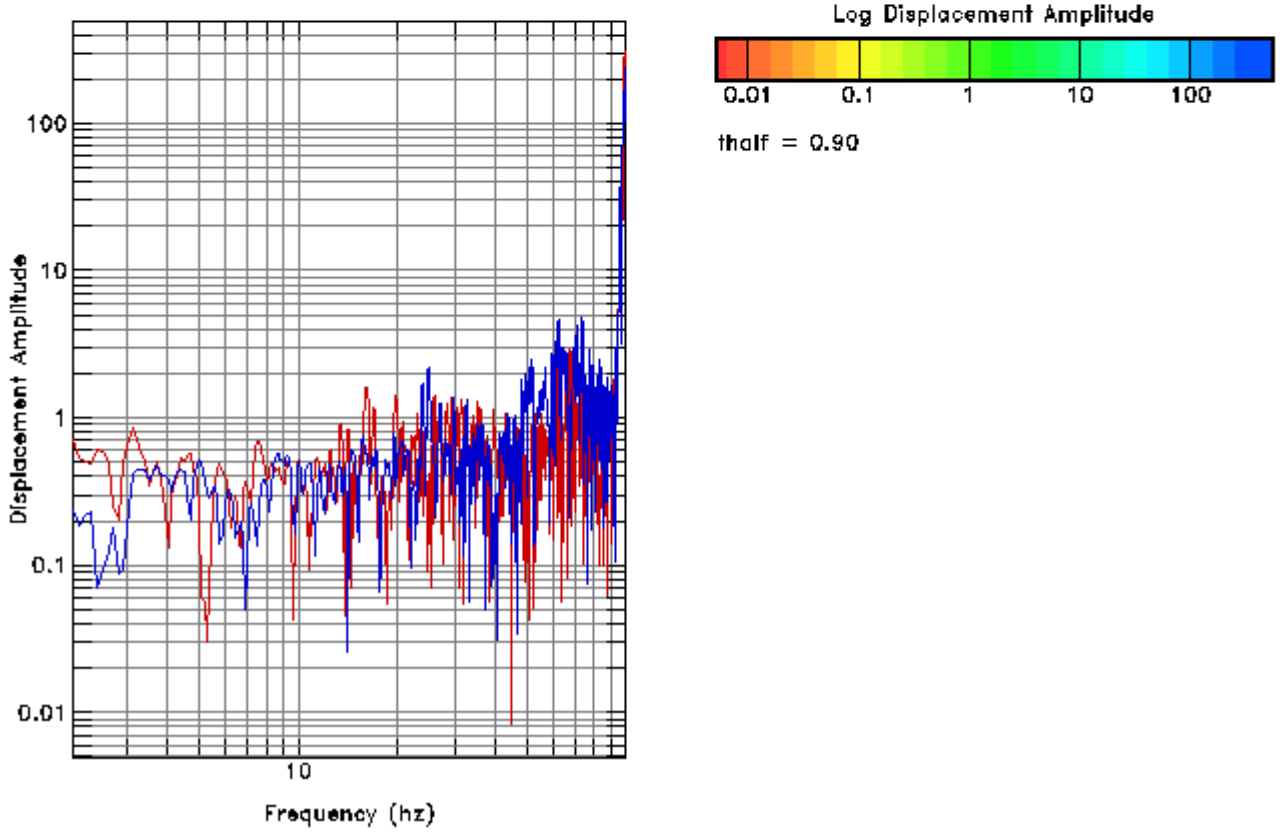

Instrument Correction: Episensor 200 Hz 10 Volt FS 2g/Quanterra 330 Linea

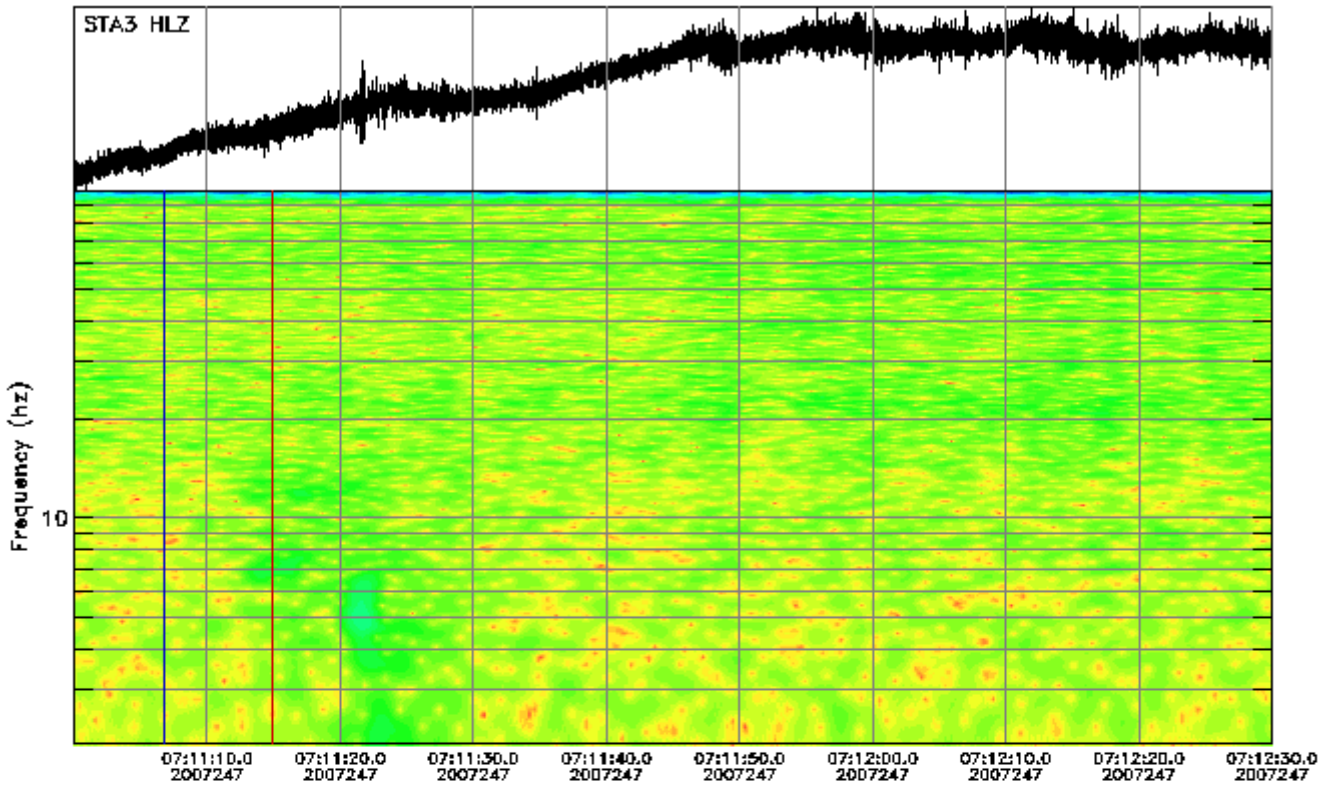

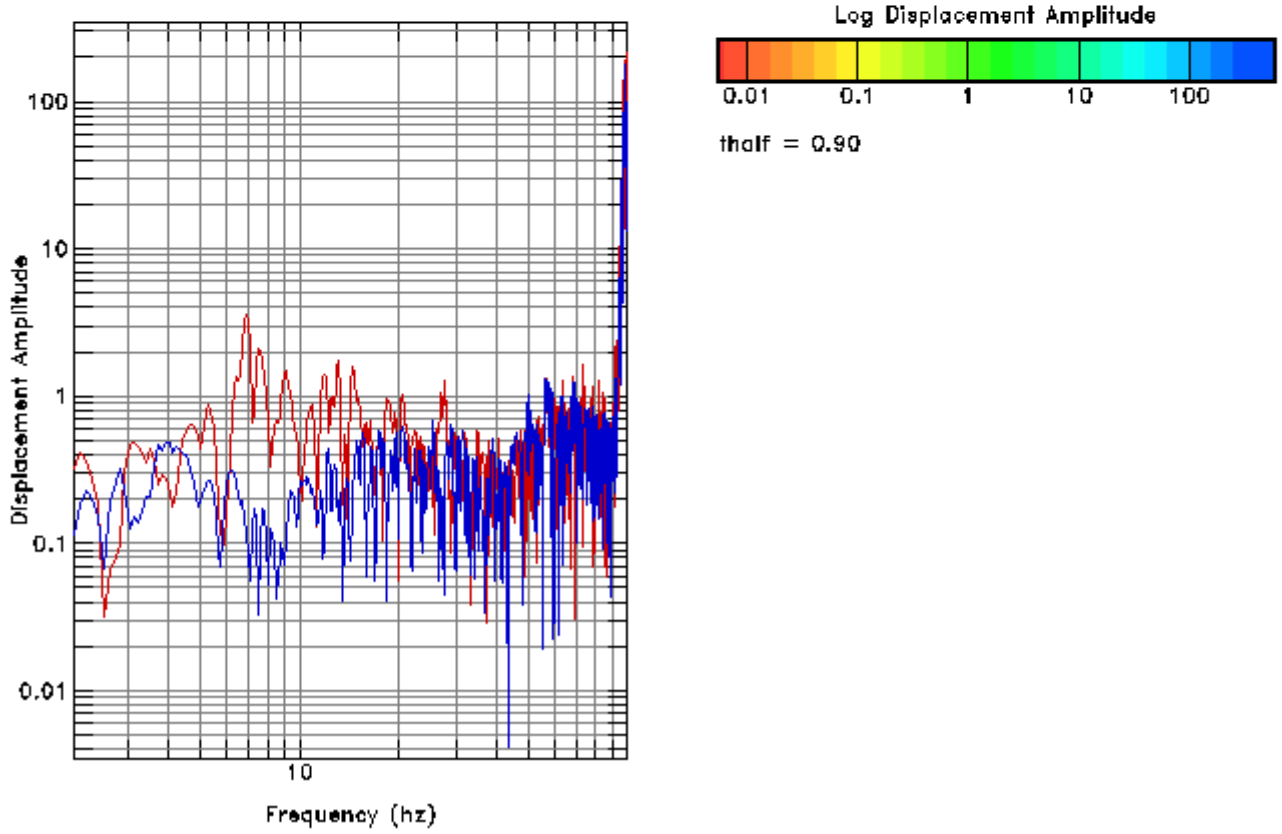

Instrument Correction: Episensor 200 Hz 10 Volt FS 2g/Quanterra 330 Linea

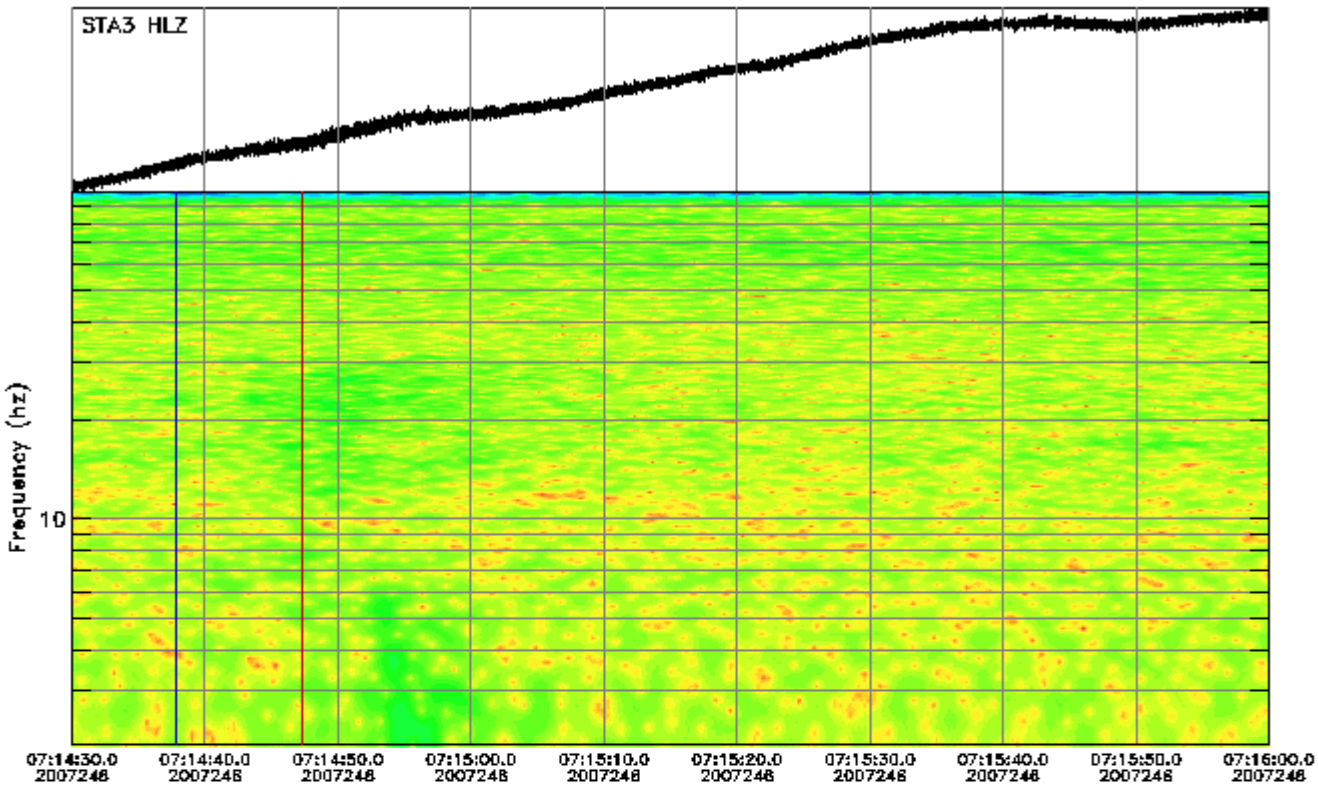

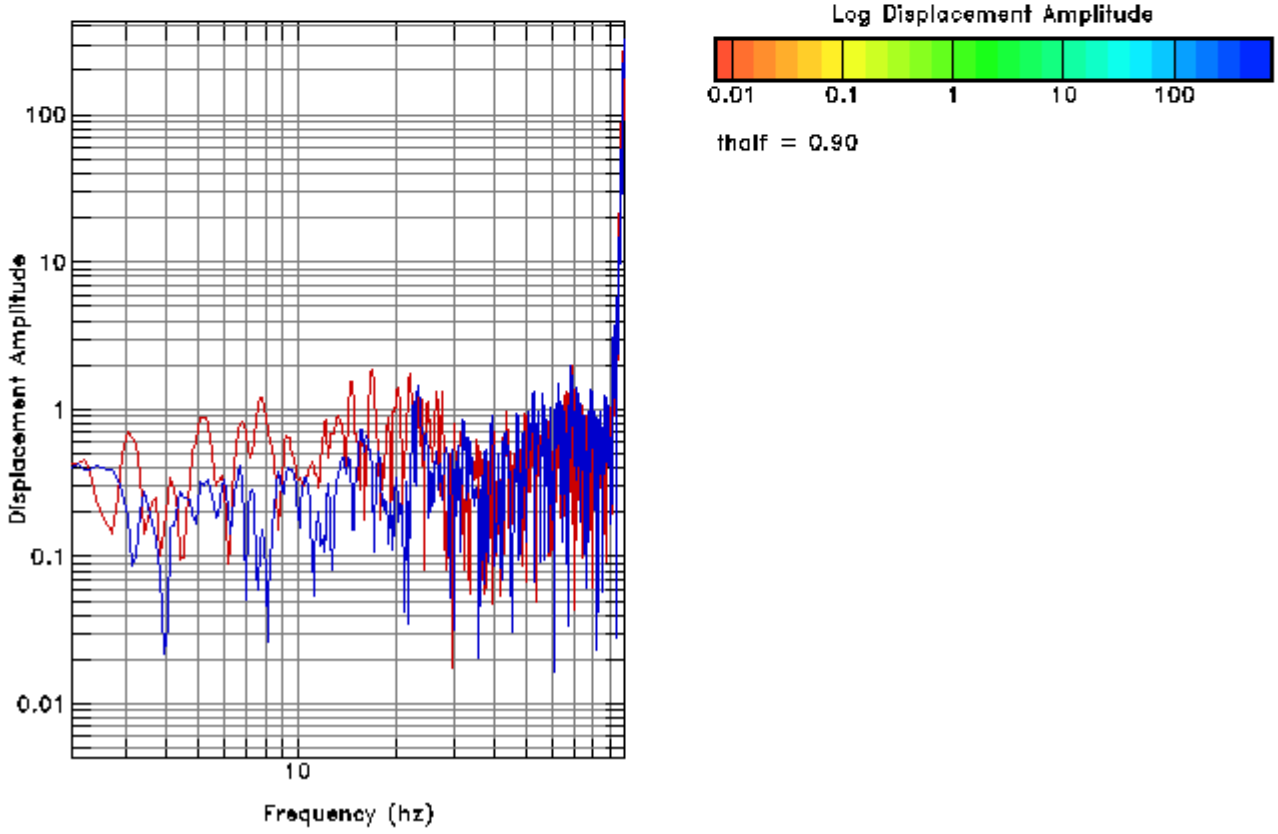

Instrument Correction: Episensor 200 Hz 10 Volt FS 2g/Quanterra 330 Linea

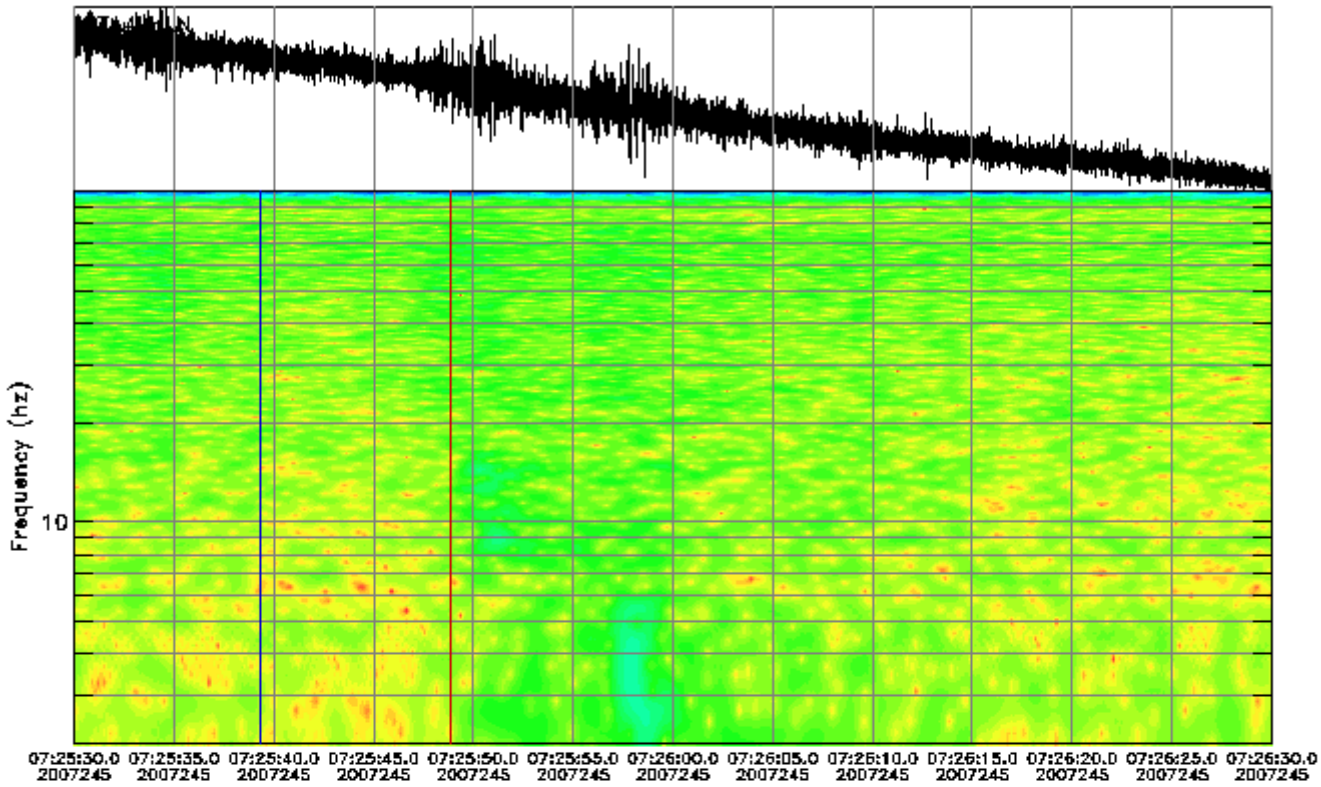

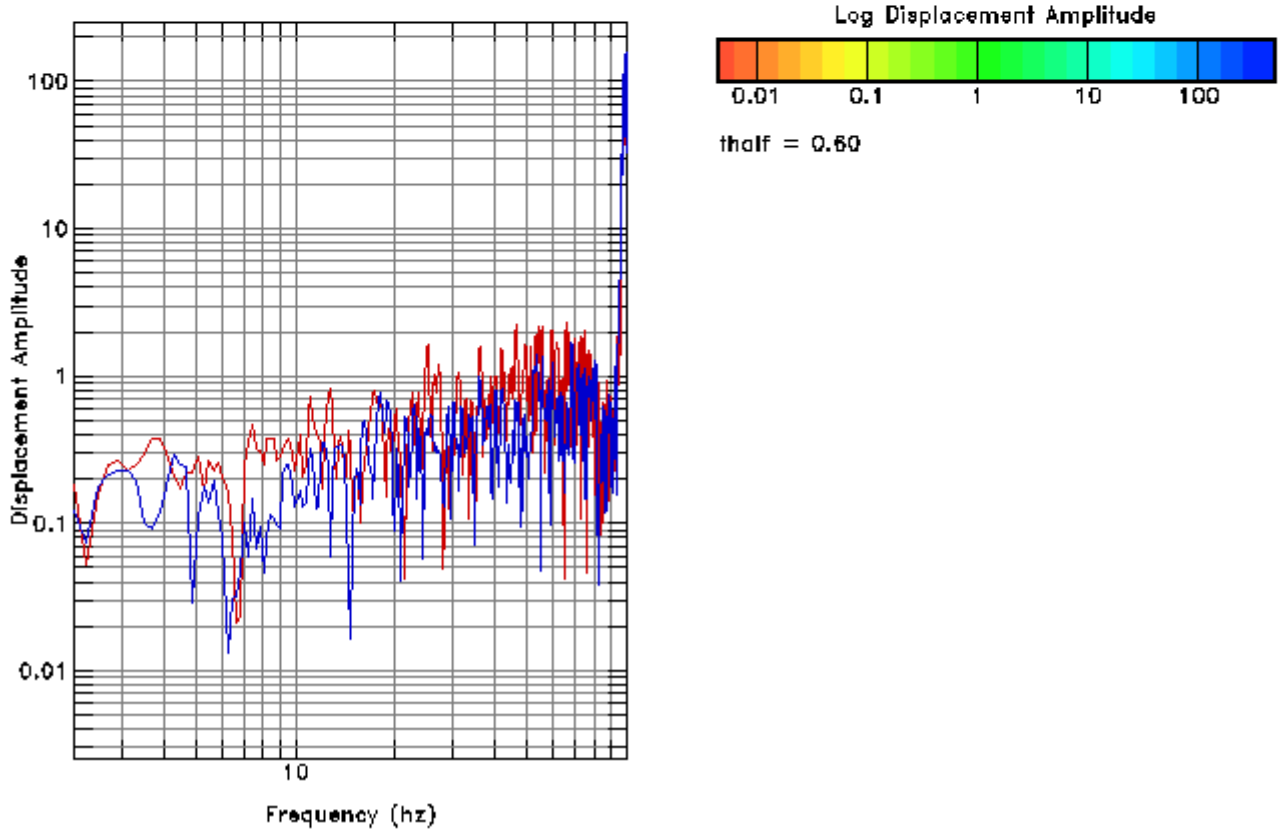

Instrument Correction: Episensor 200 Hz 10 Volt FS 2g/Quanterra 330 Linea

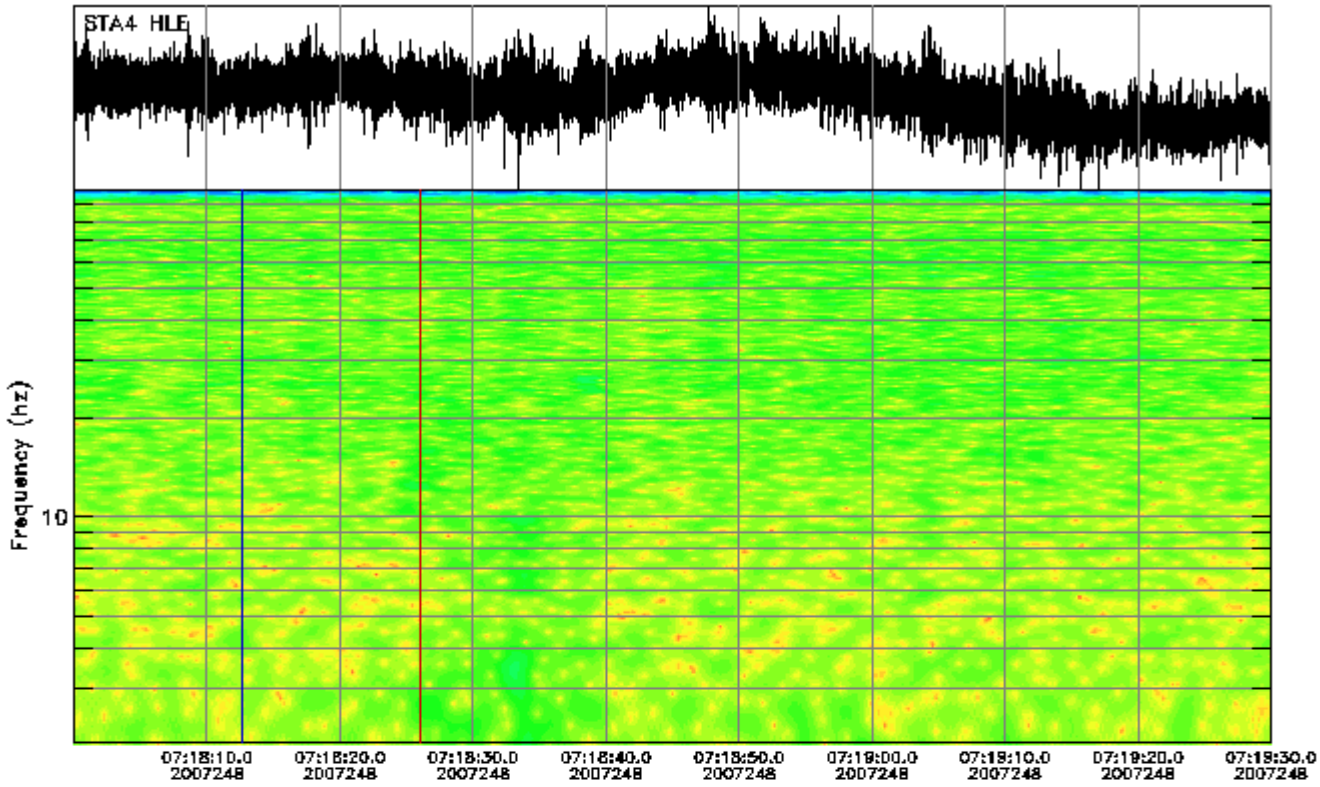

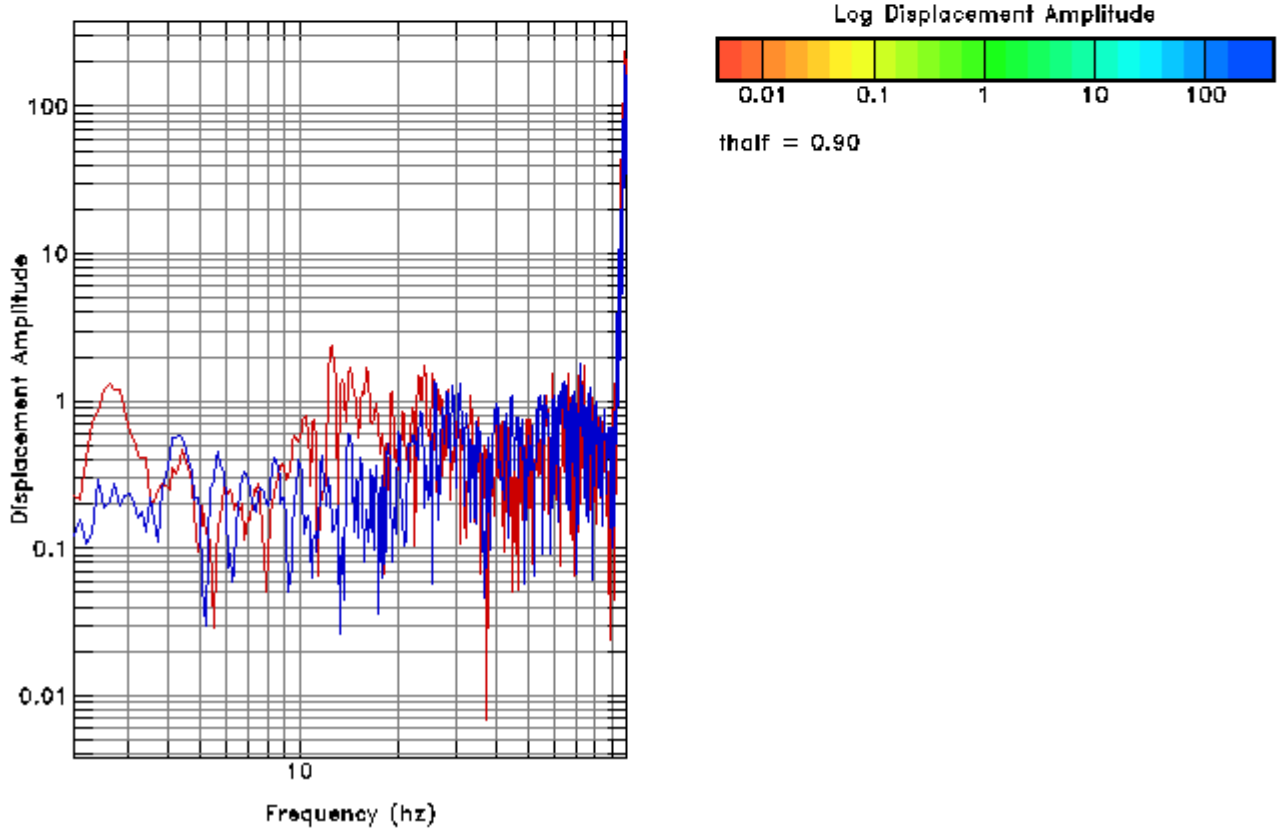

Instrument Correction: Episensor 200 Hz 10 Volt FS 2g/Quanterra 330 Linea

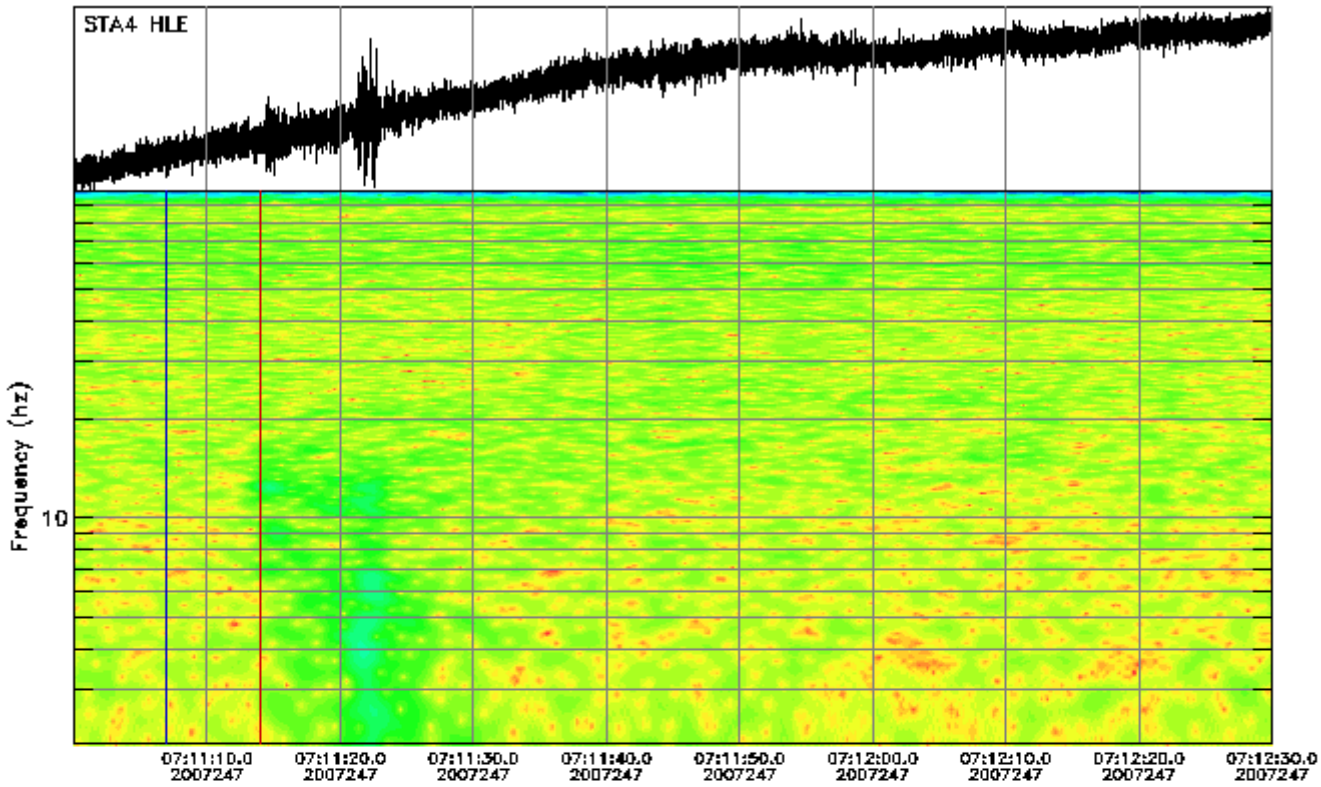

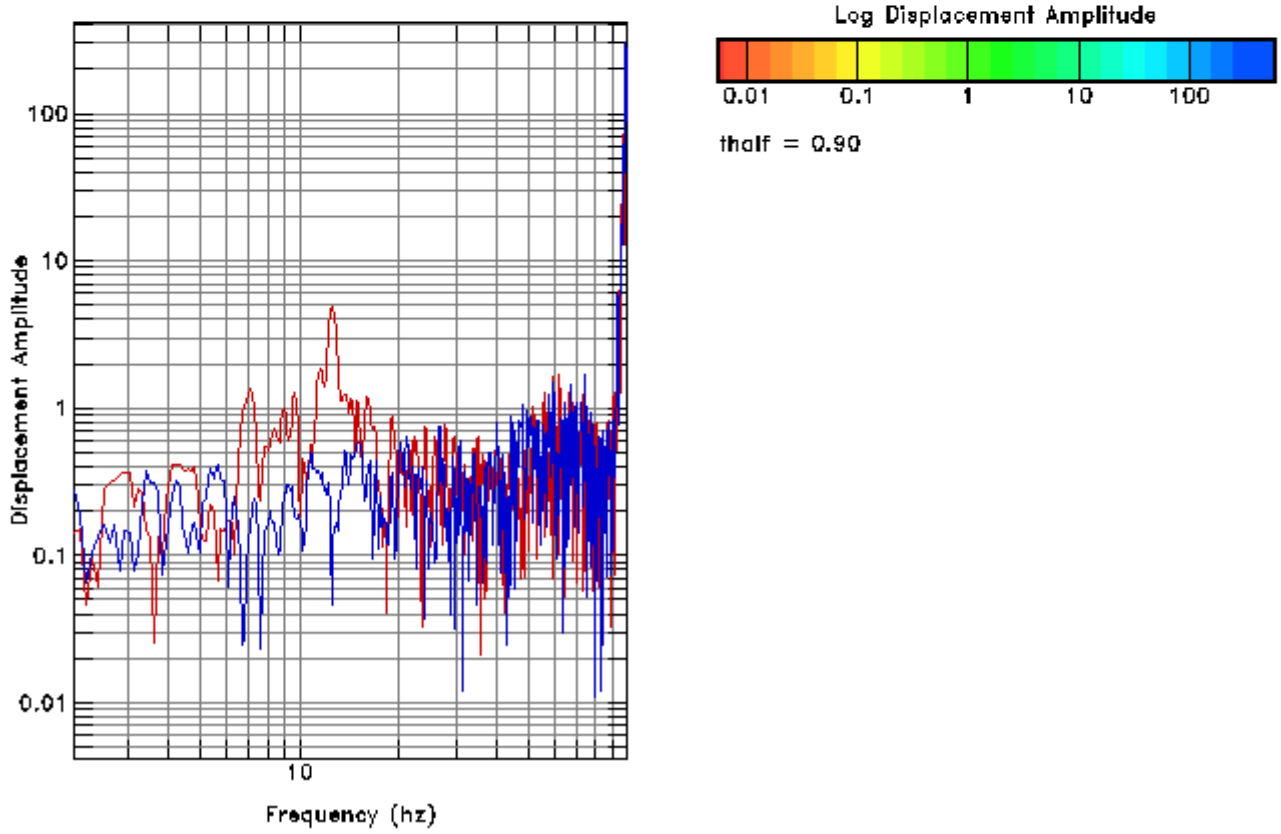

Instrument Correction: Episensor 200 Hz 10 Volt FS 2g/Quanterra 330 Linea

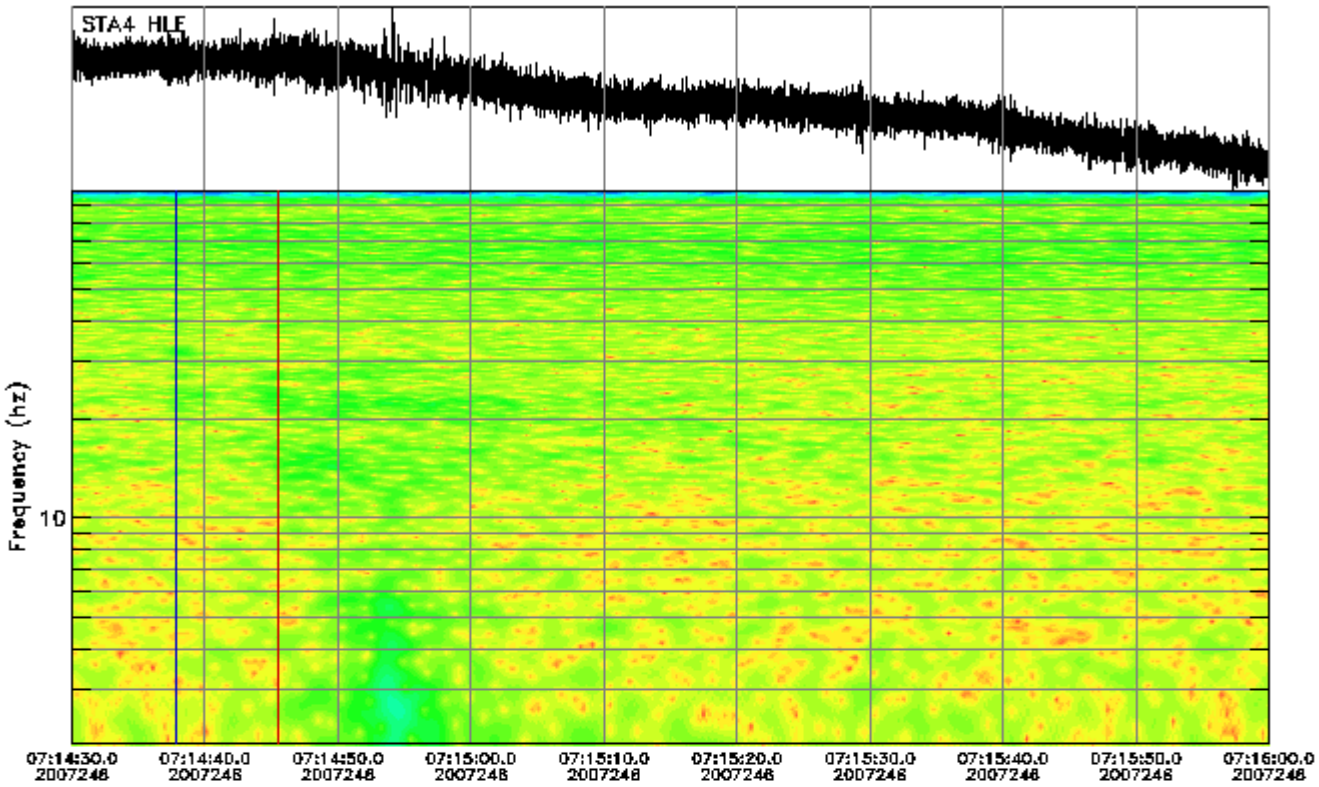

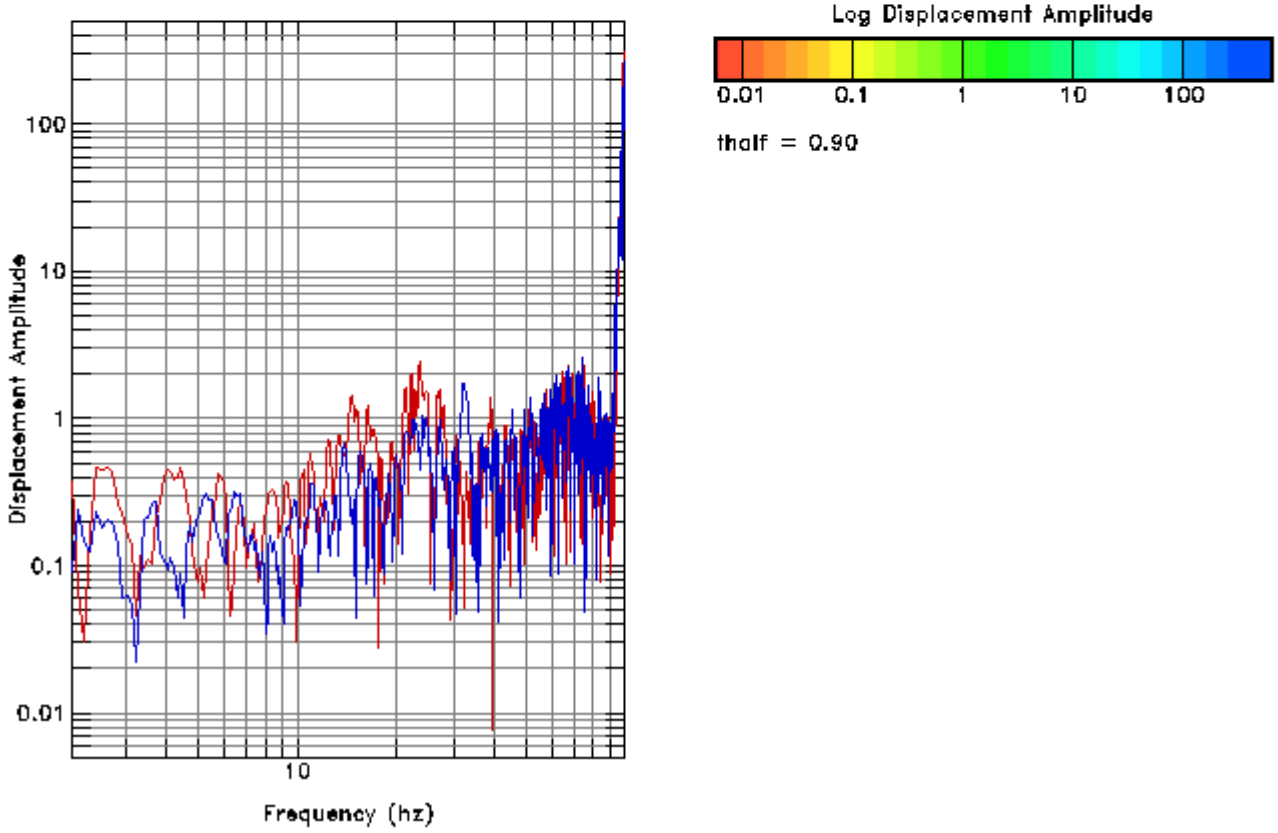

Instrument Correction: Episensor 200 Hz 10 Volt FS 2g/Quanterra 330 Linea

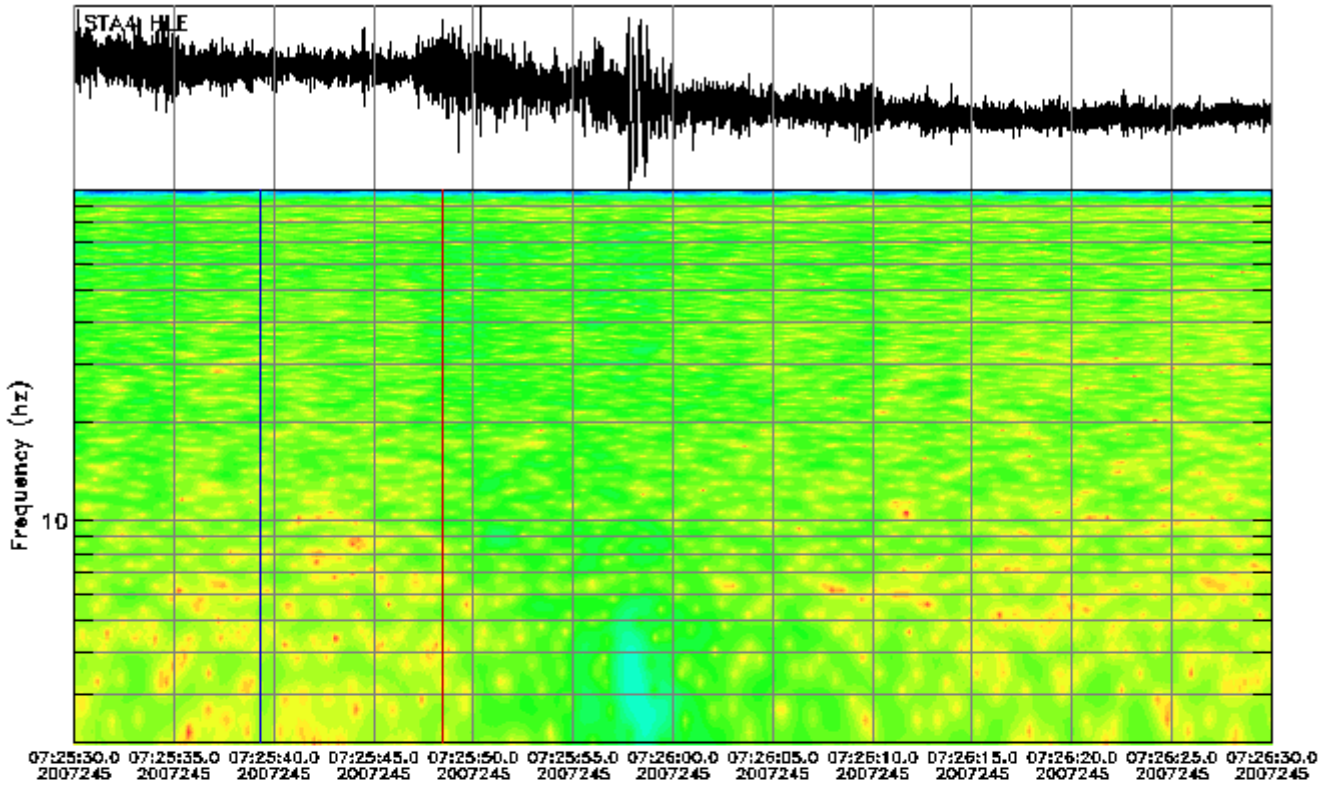

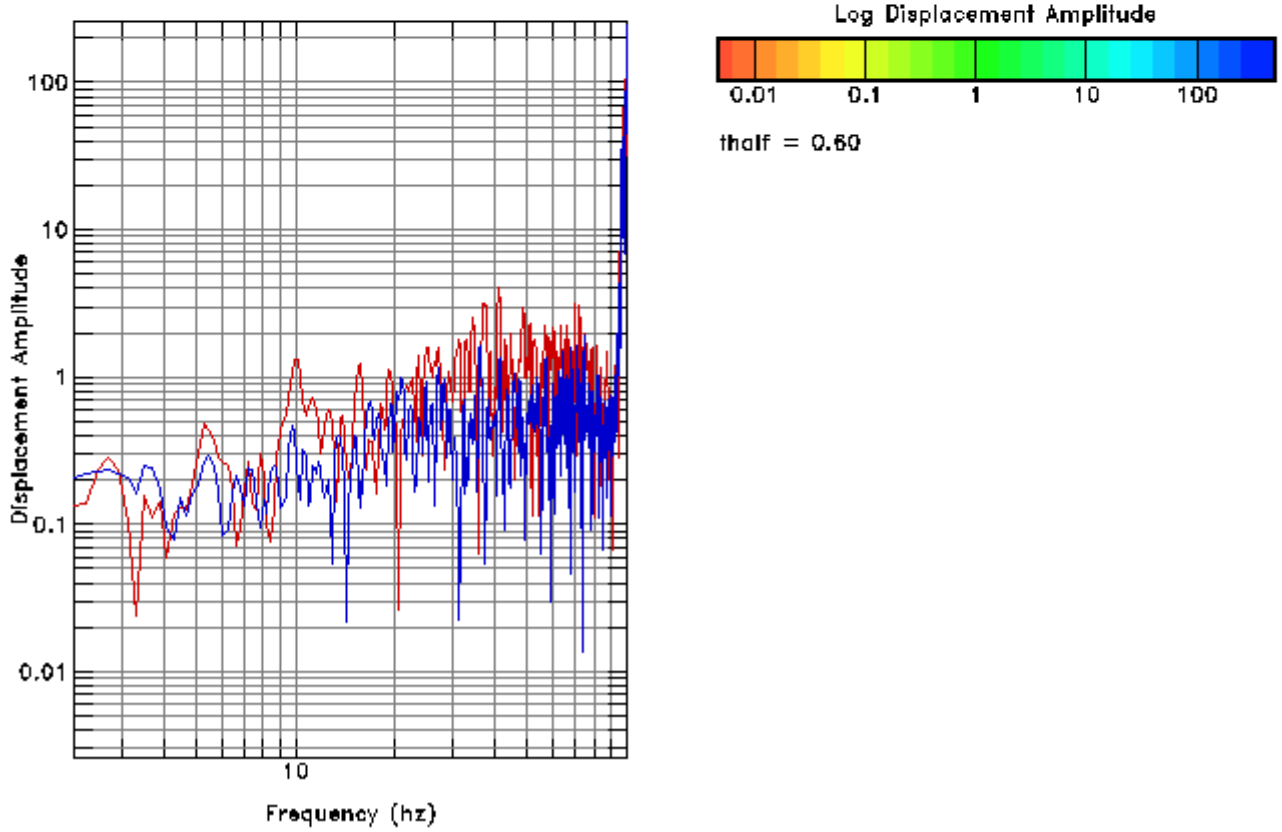

Instrument Correction: Episensor 200 Hz 10 Volt FS 2g/Quanterra 330 Linea

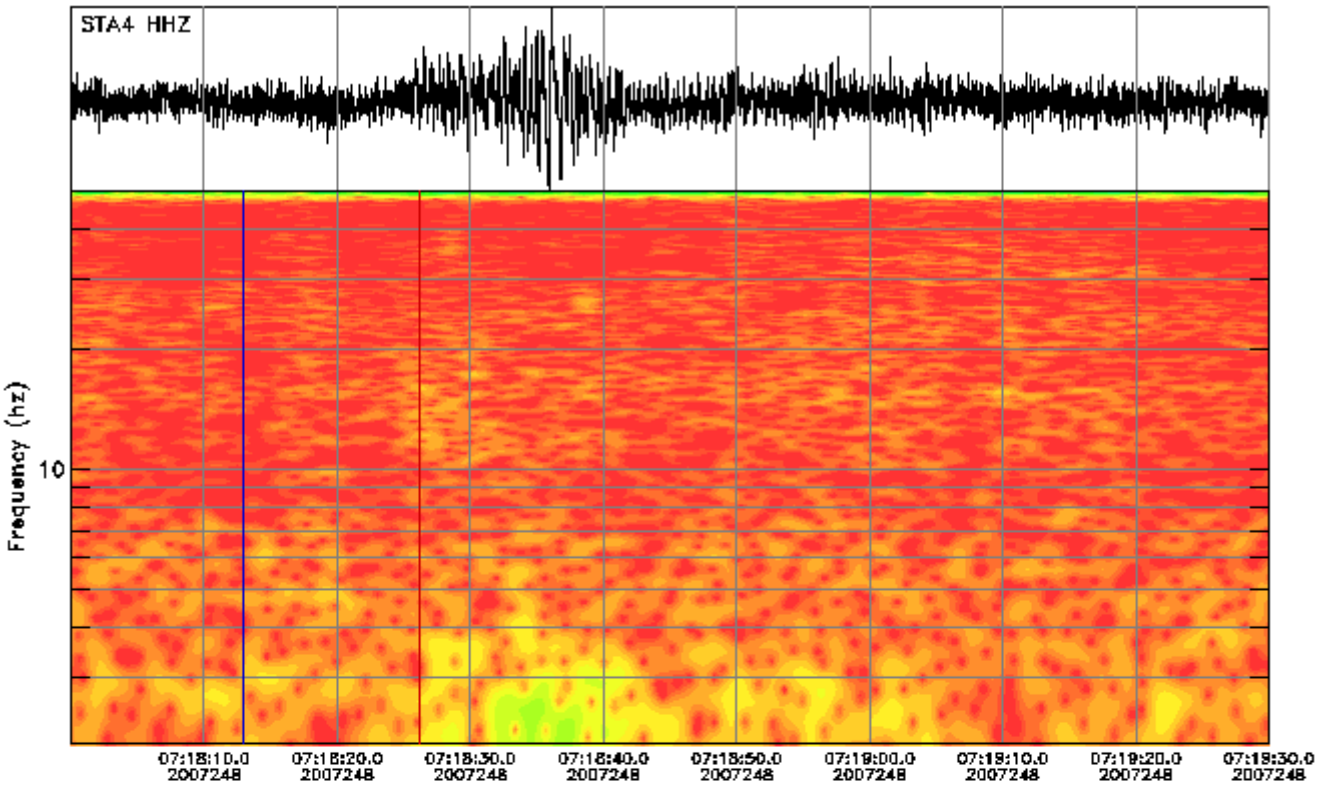

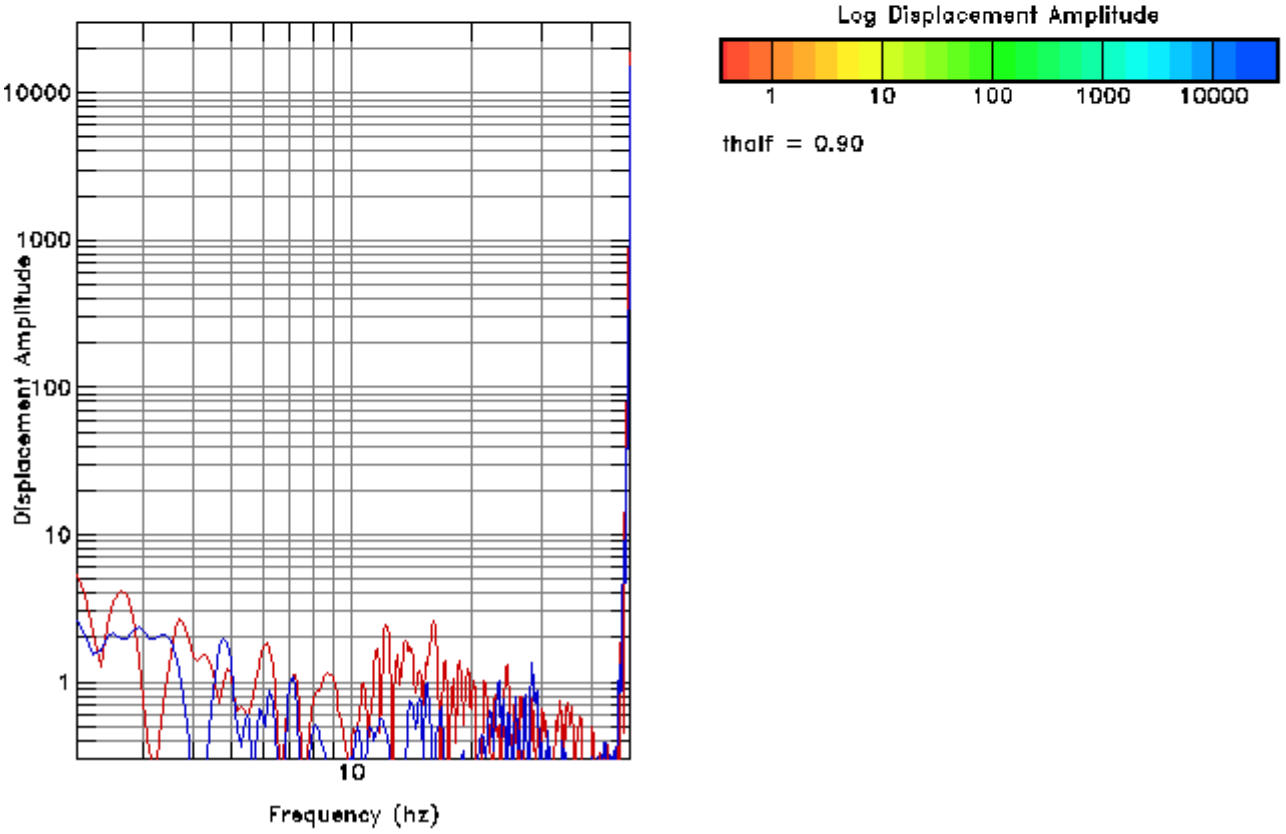

Instrument Correction: Ranger SS1/Quanterra 330 Linear Phase Composite

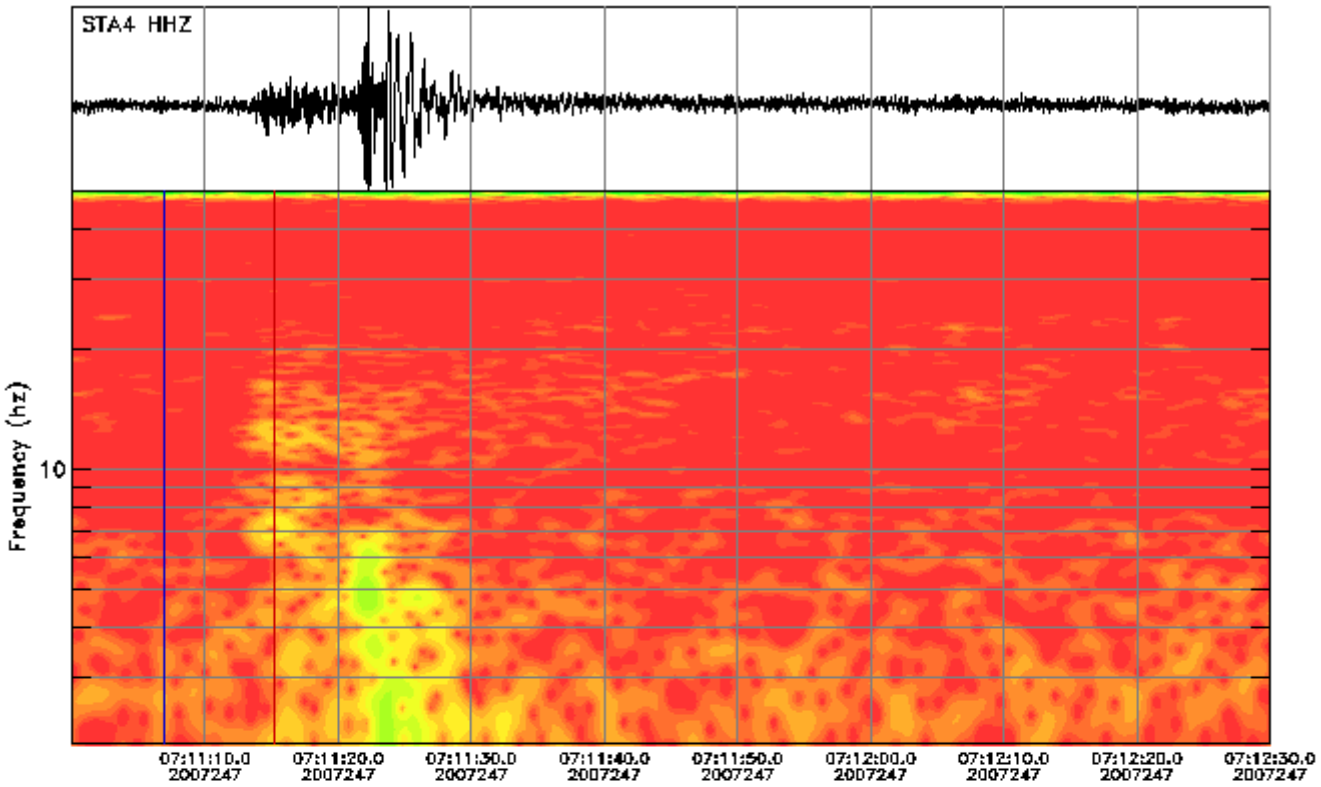

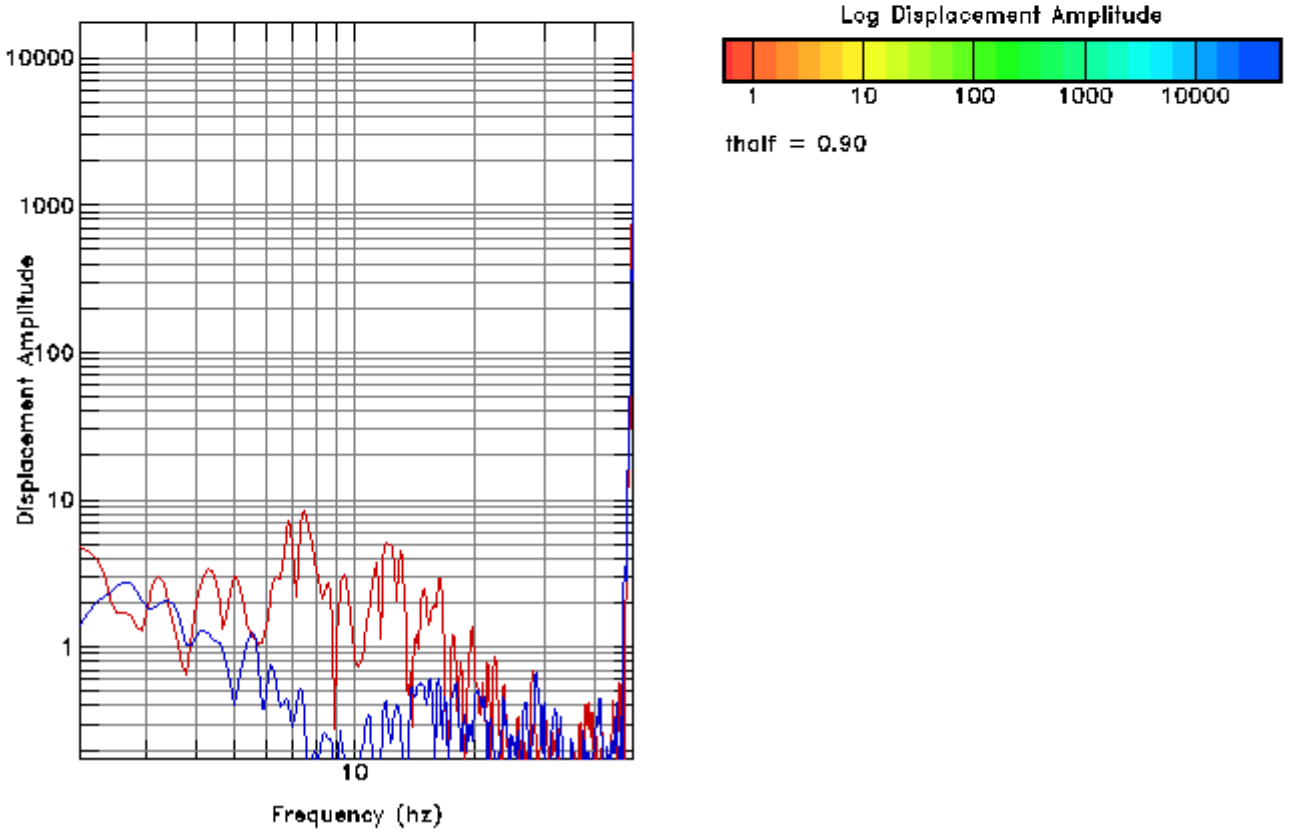

Instrument Correction: Ranger SS1/Quanterra 330 Linear Phase Composite

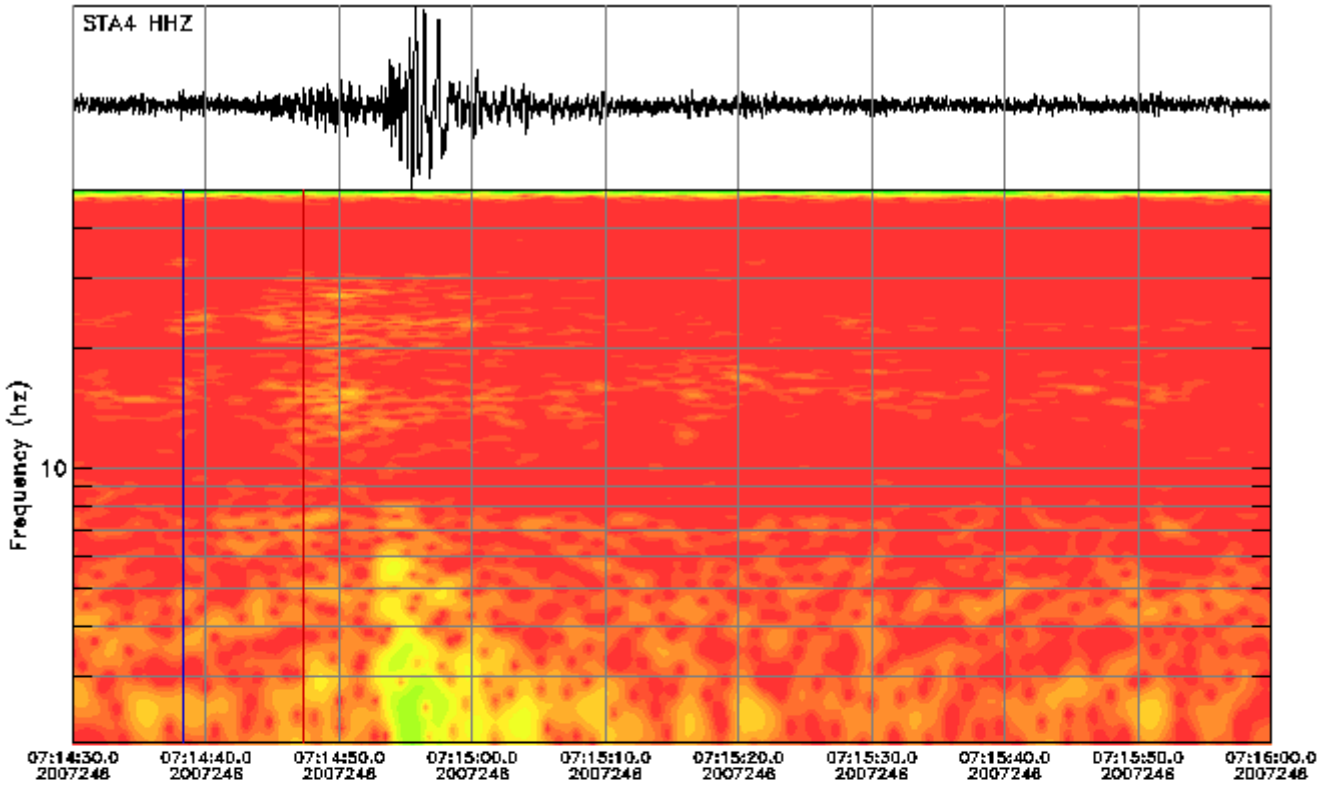

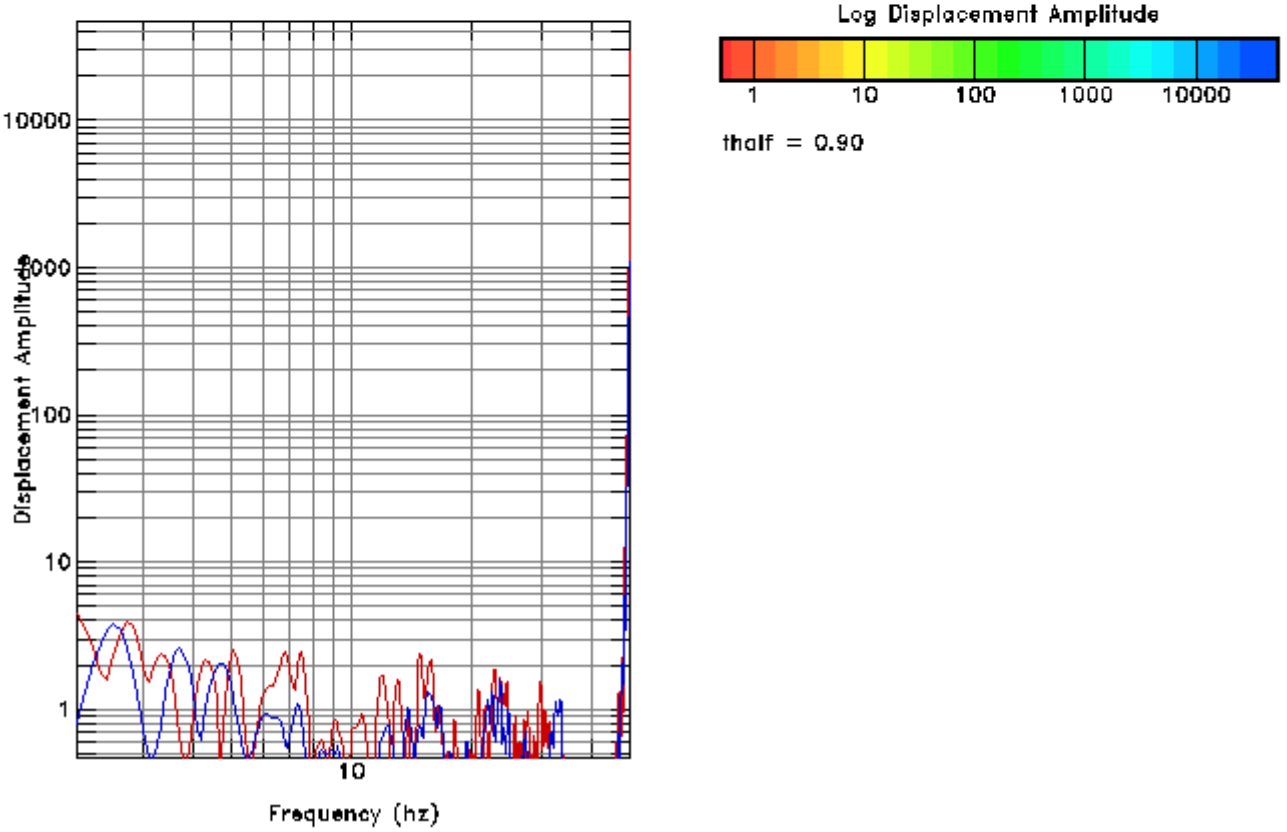

Instrument Correction: Ranger SS1/Quanterra 330 Linear Phase Composite

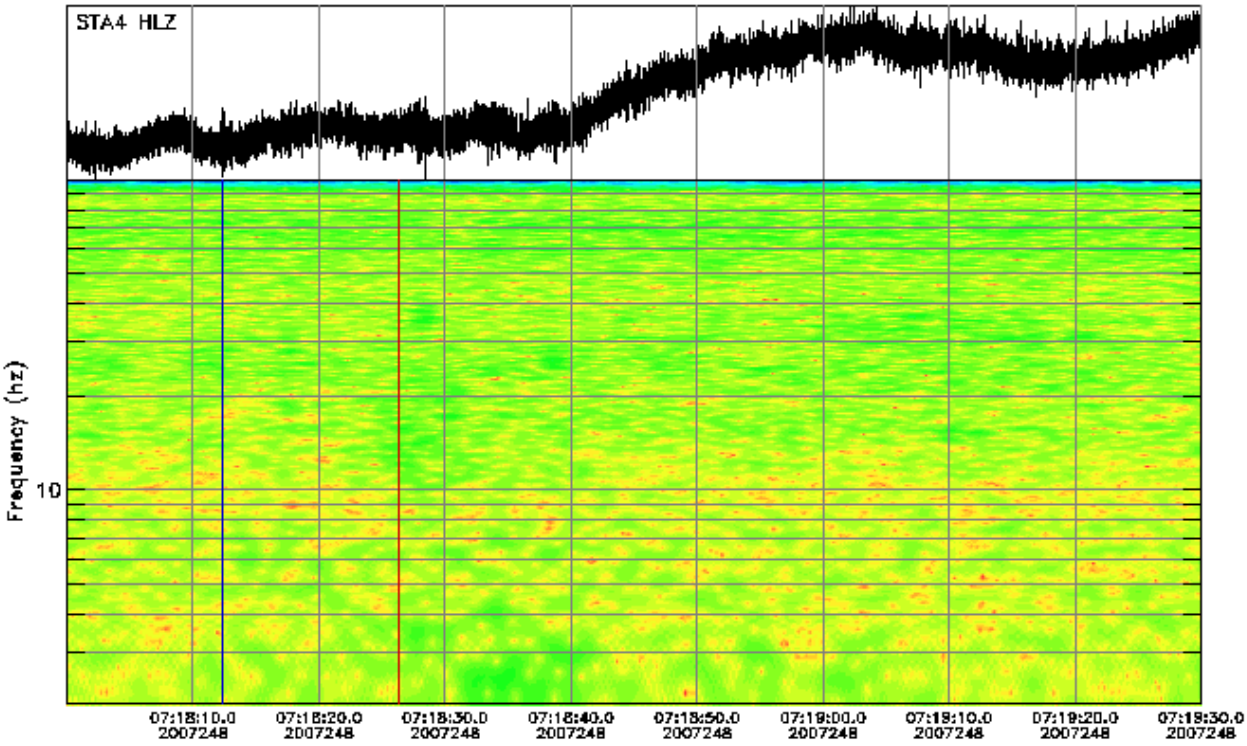

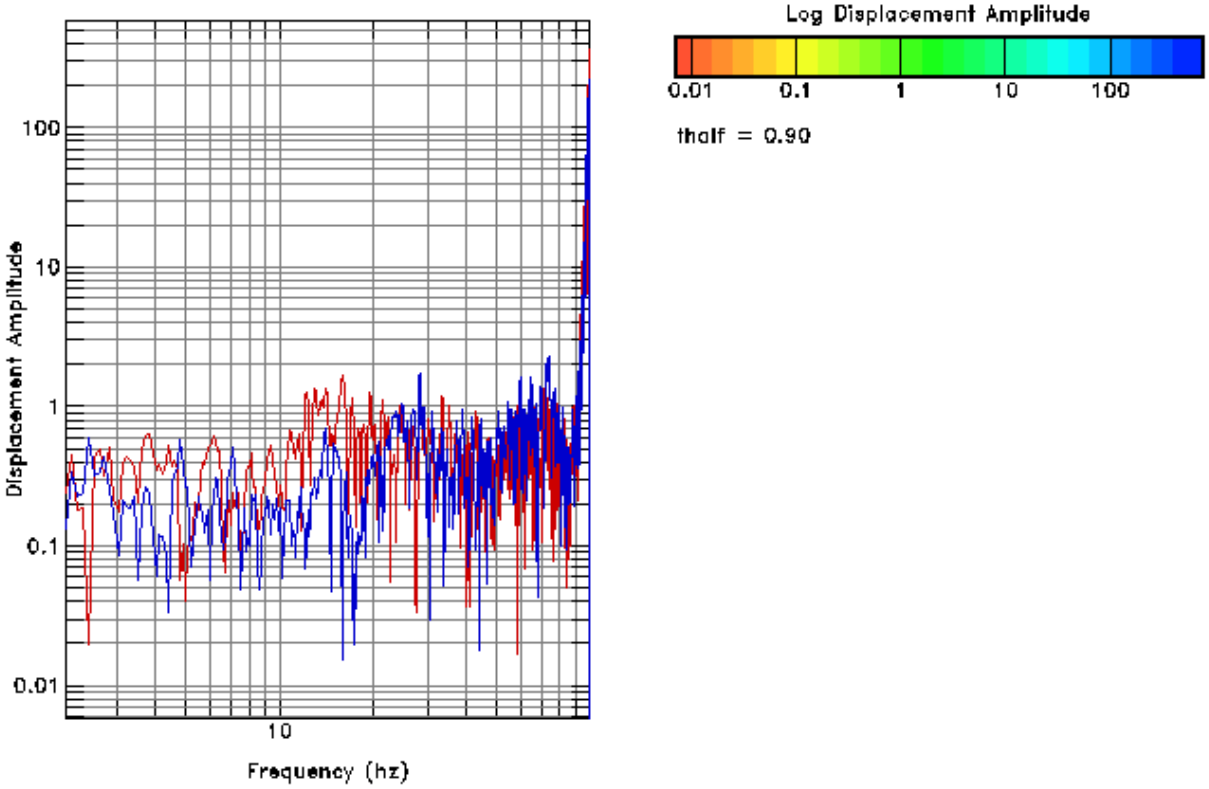

Instrument Correction: Episensor 200 Hz 10 Volt FS 2g/Quanterra 330 Linea

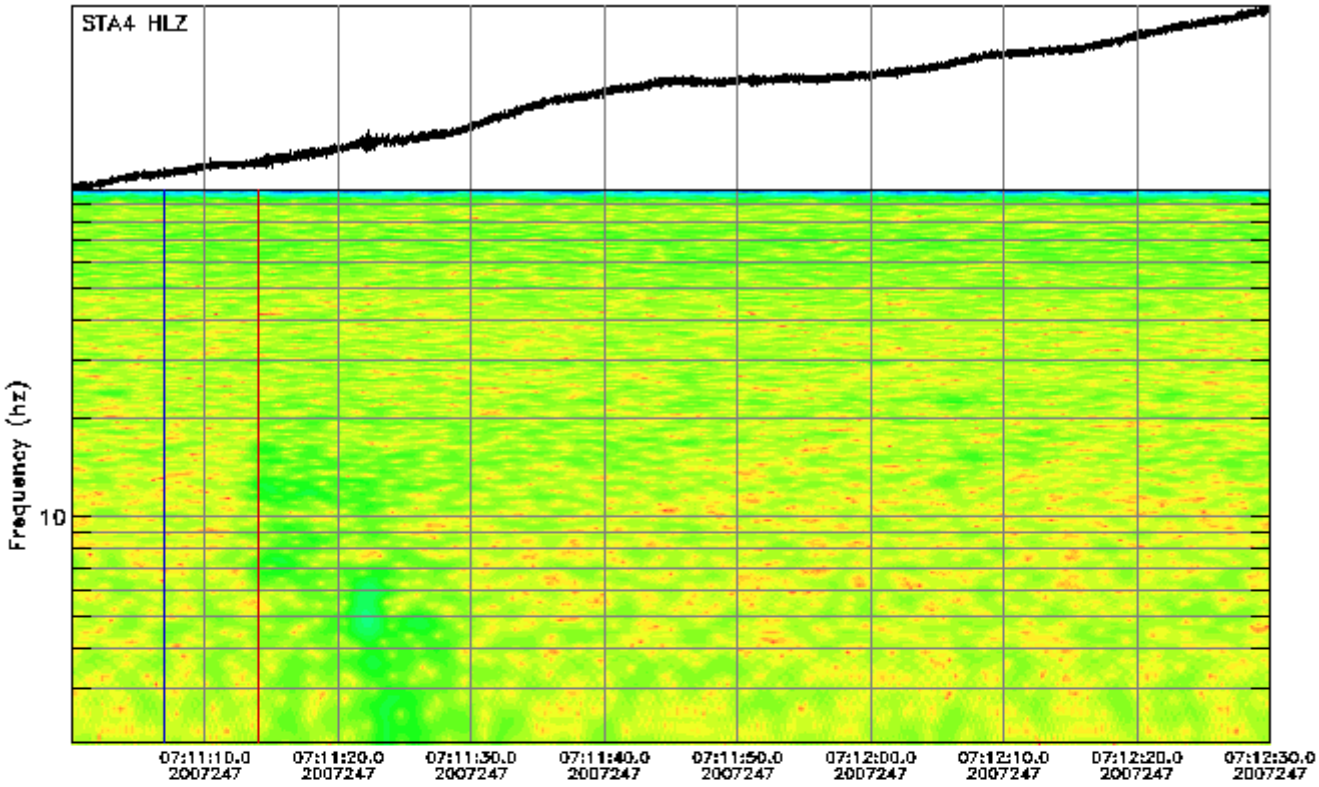

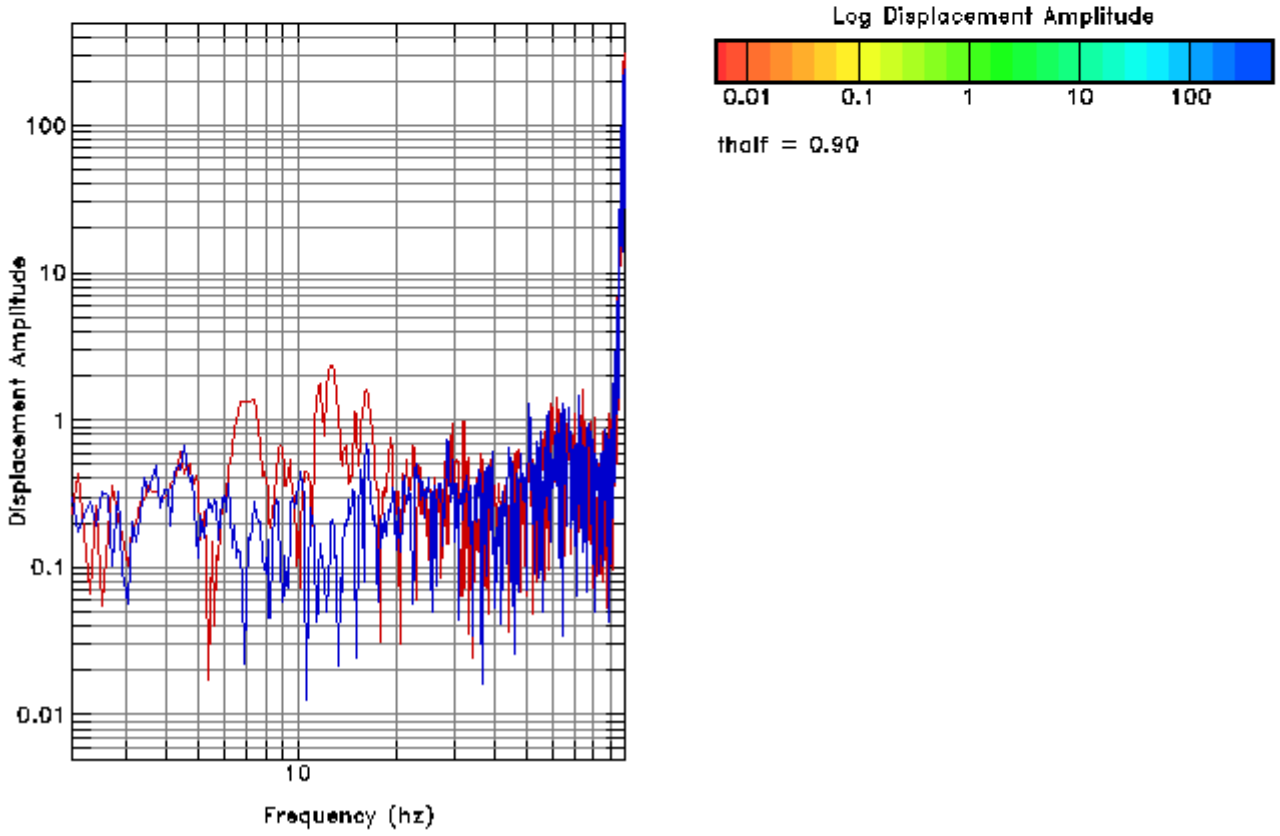

Instrument Correction: Episensor 200 Hz 10 Volt FS 2g/Quanterra 330 Linea

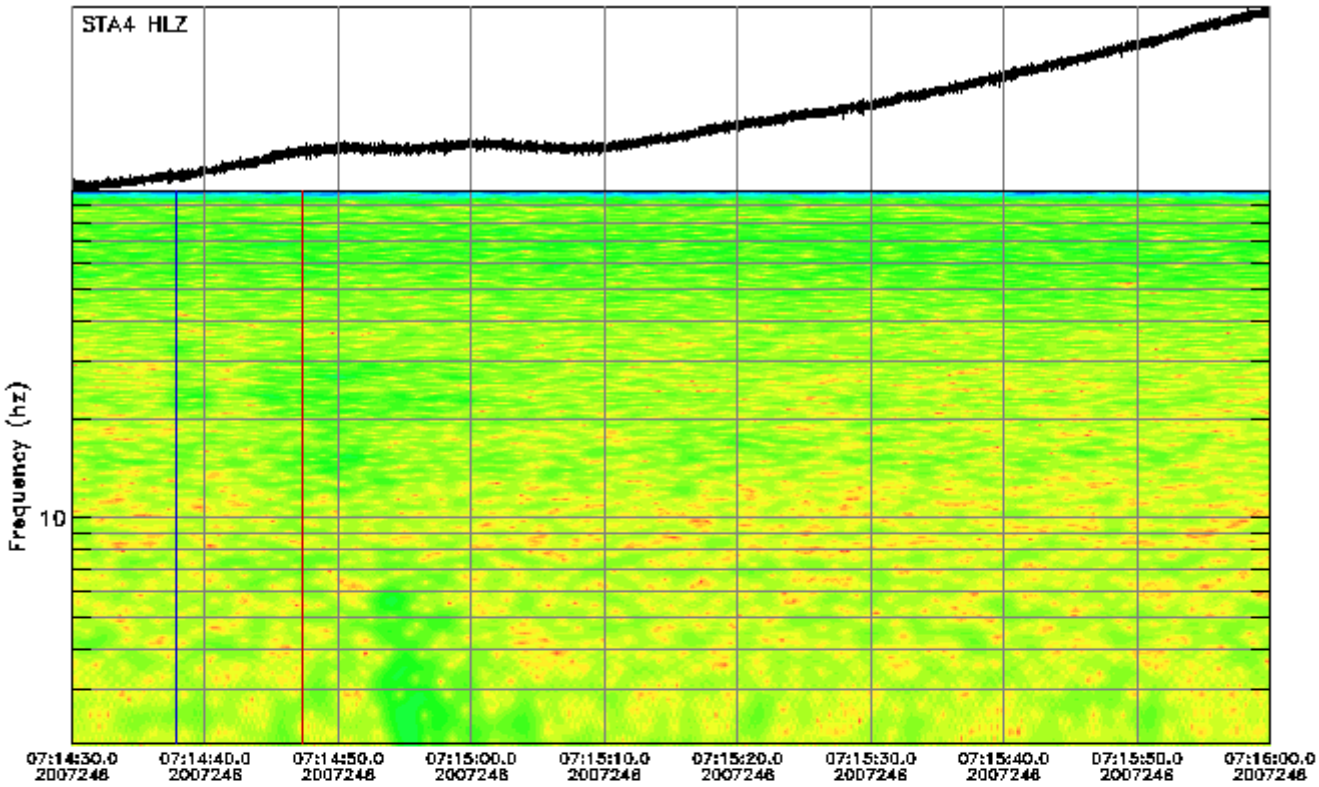

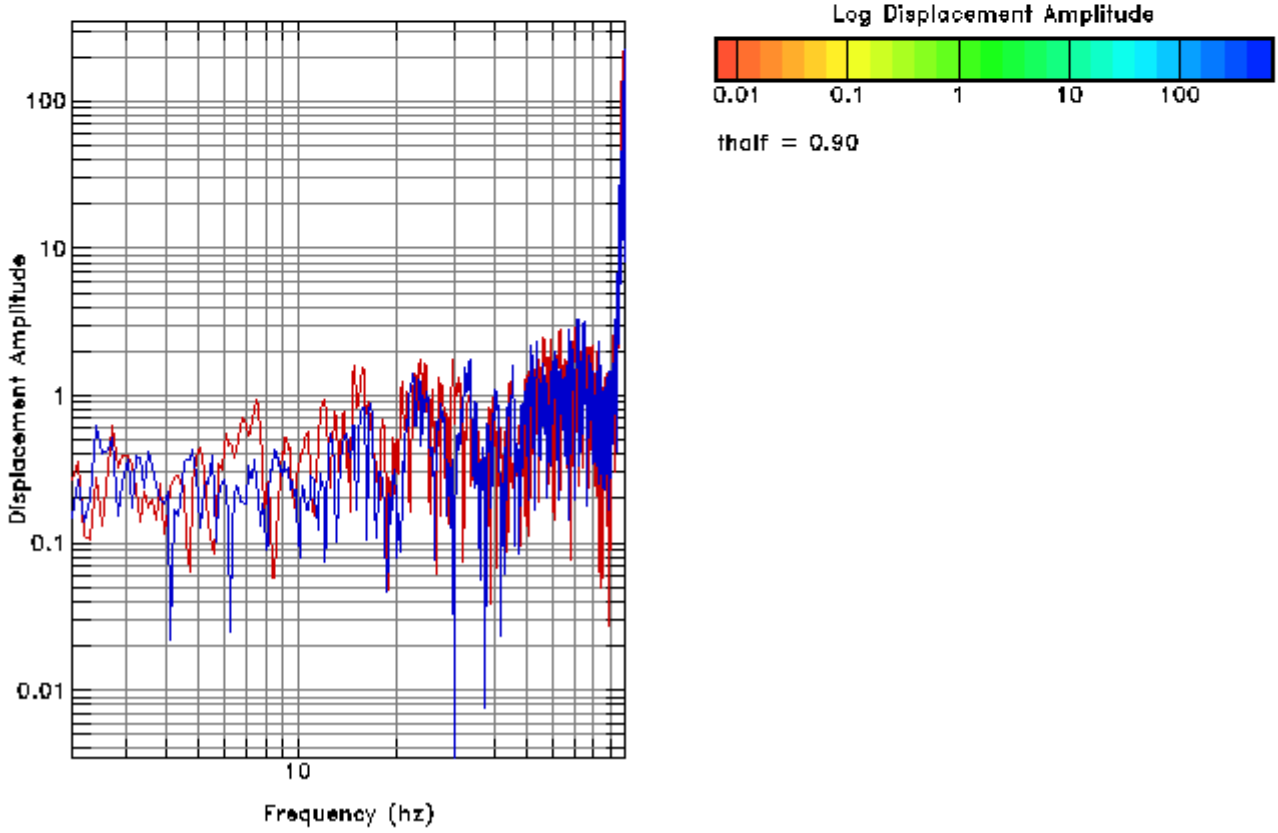

Instrument Correction: Episensor 200 Hz 10 Volt FS 2g/Quanterra 330 Linea

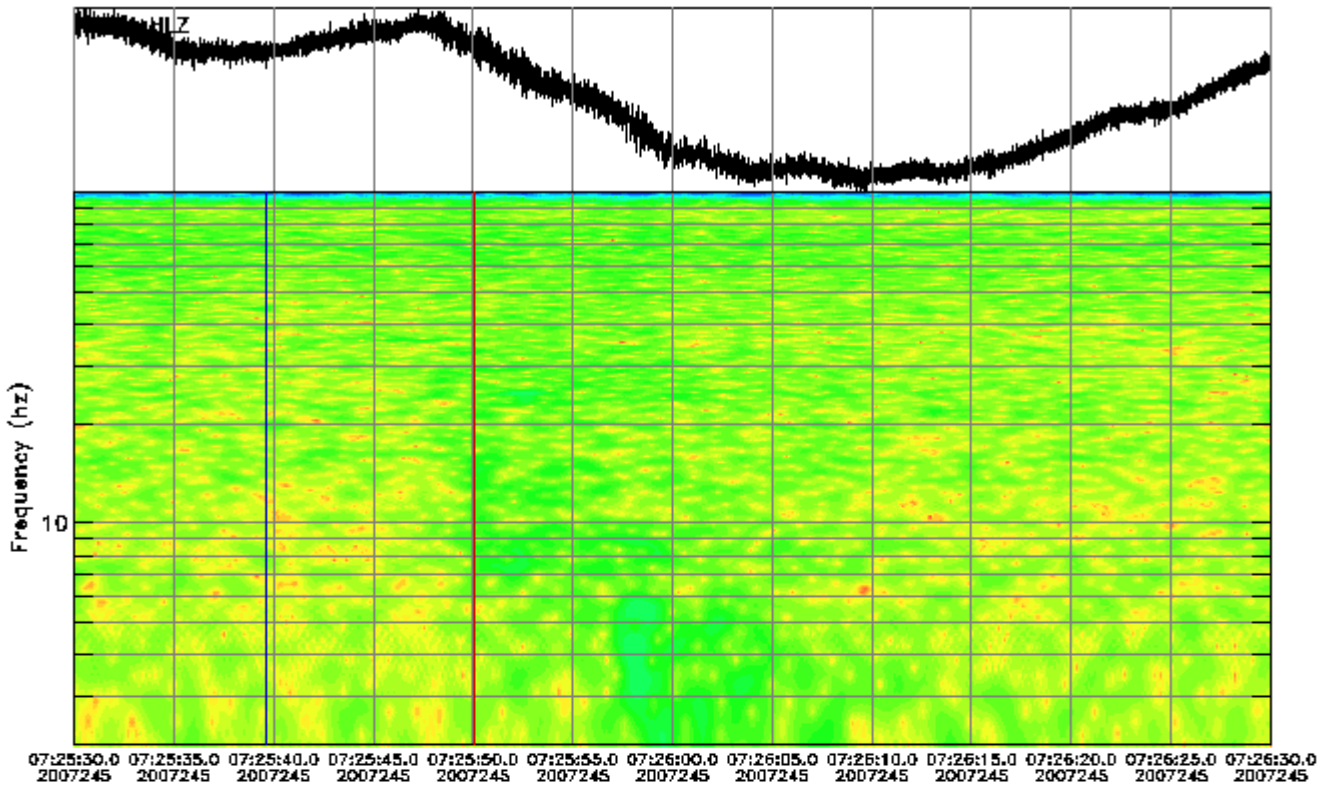

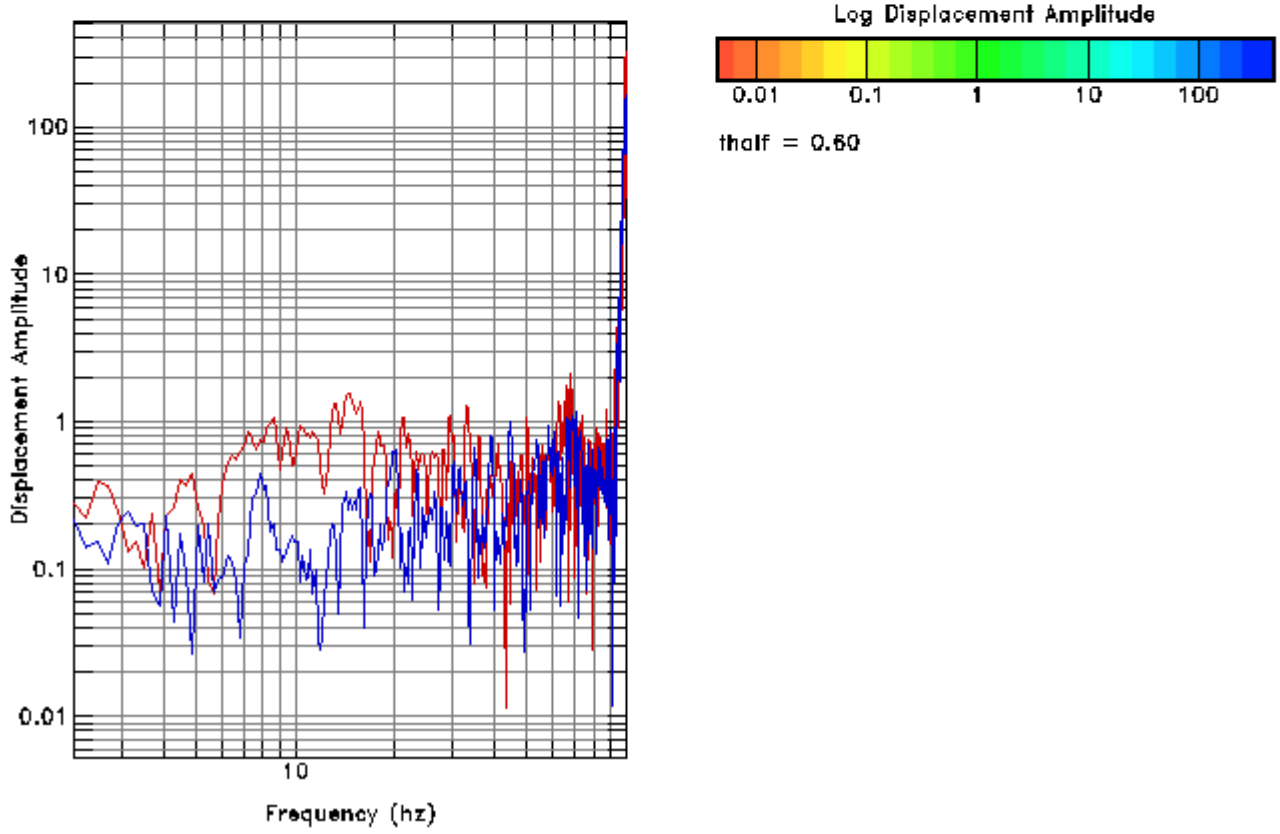

Instrument Correction: Episensor 200 Hz 10 Volt FS 2g/Quanterra 330 Linea

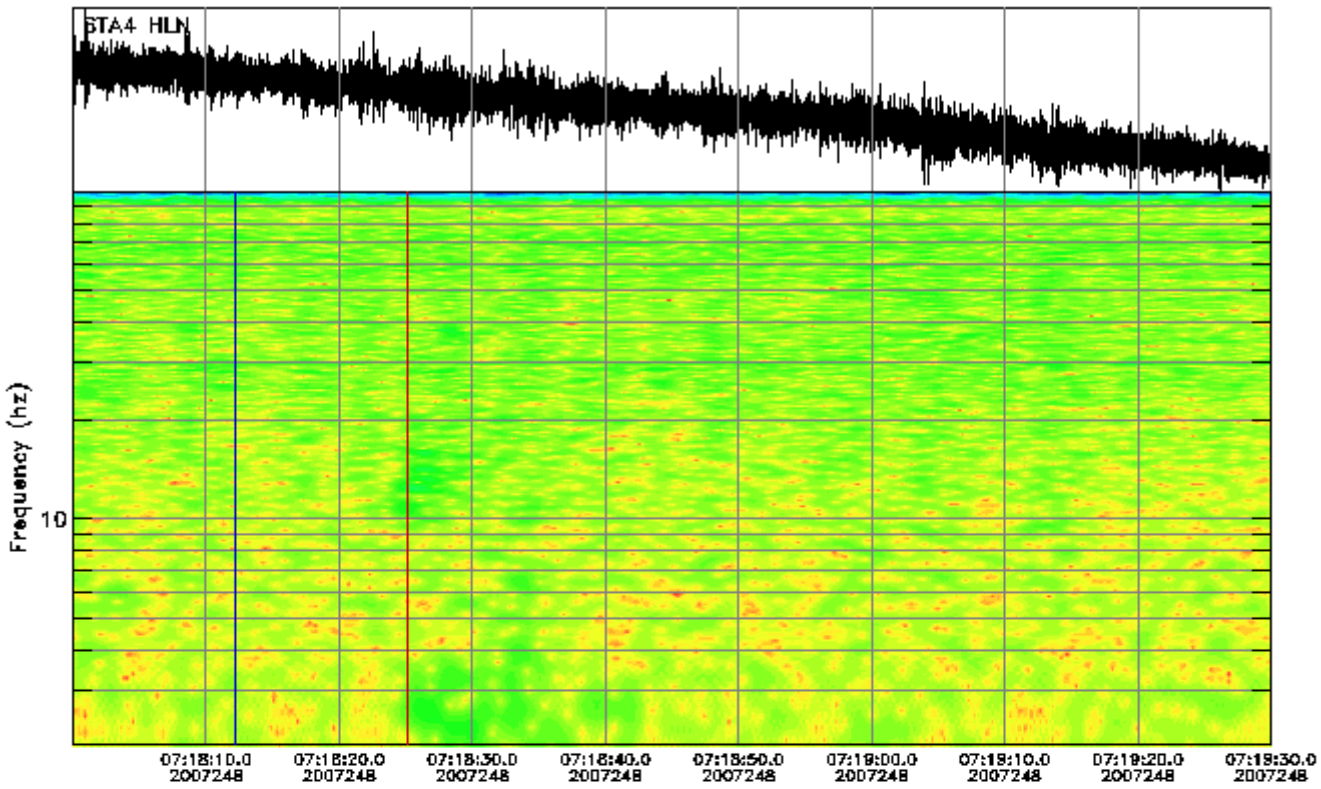

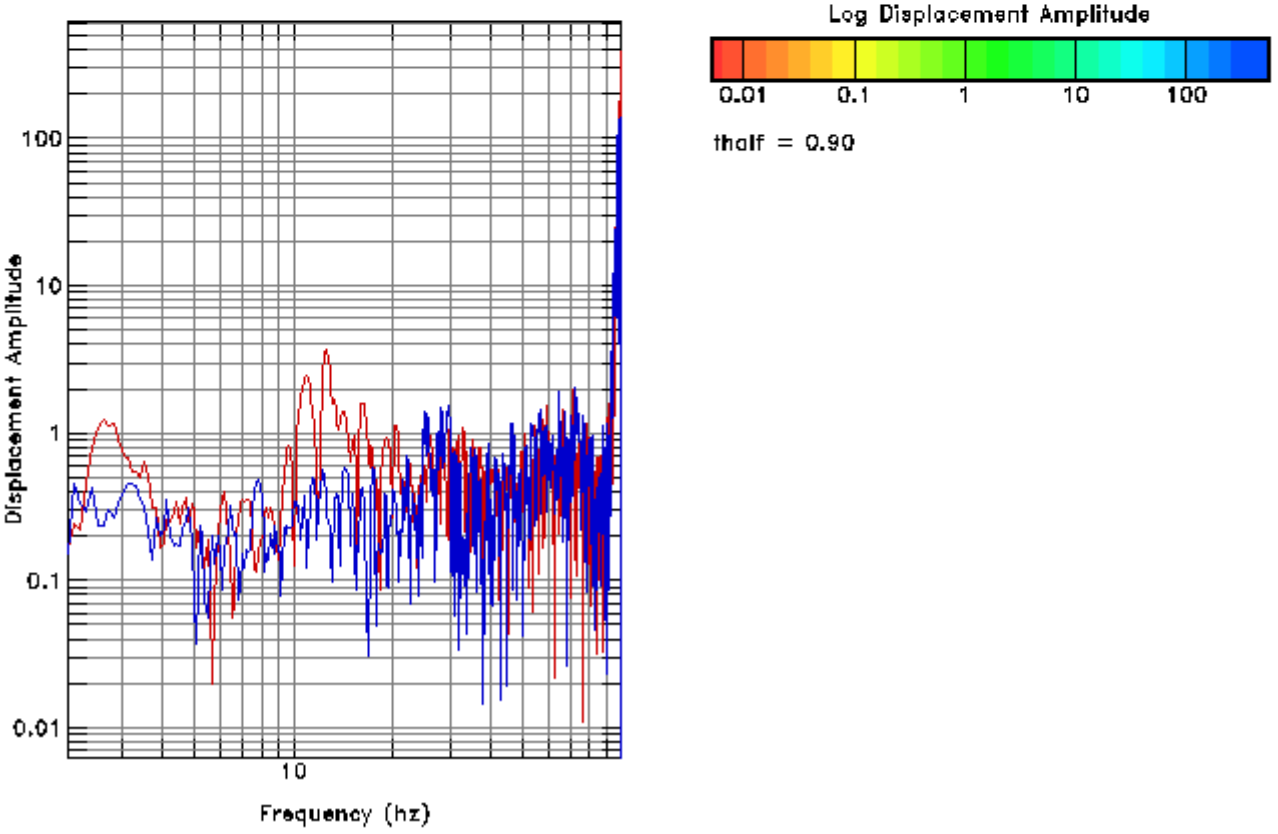

Instrument Correction: Episensor 200 Hz 10 Volt FS 2g/Quanterra 330 Linea

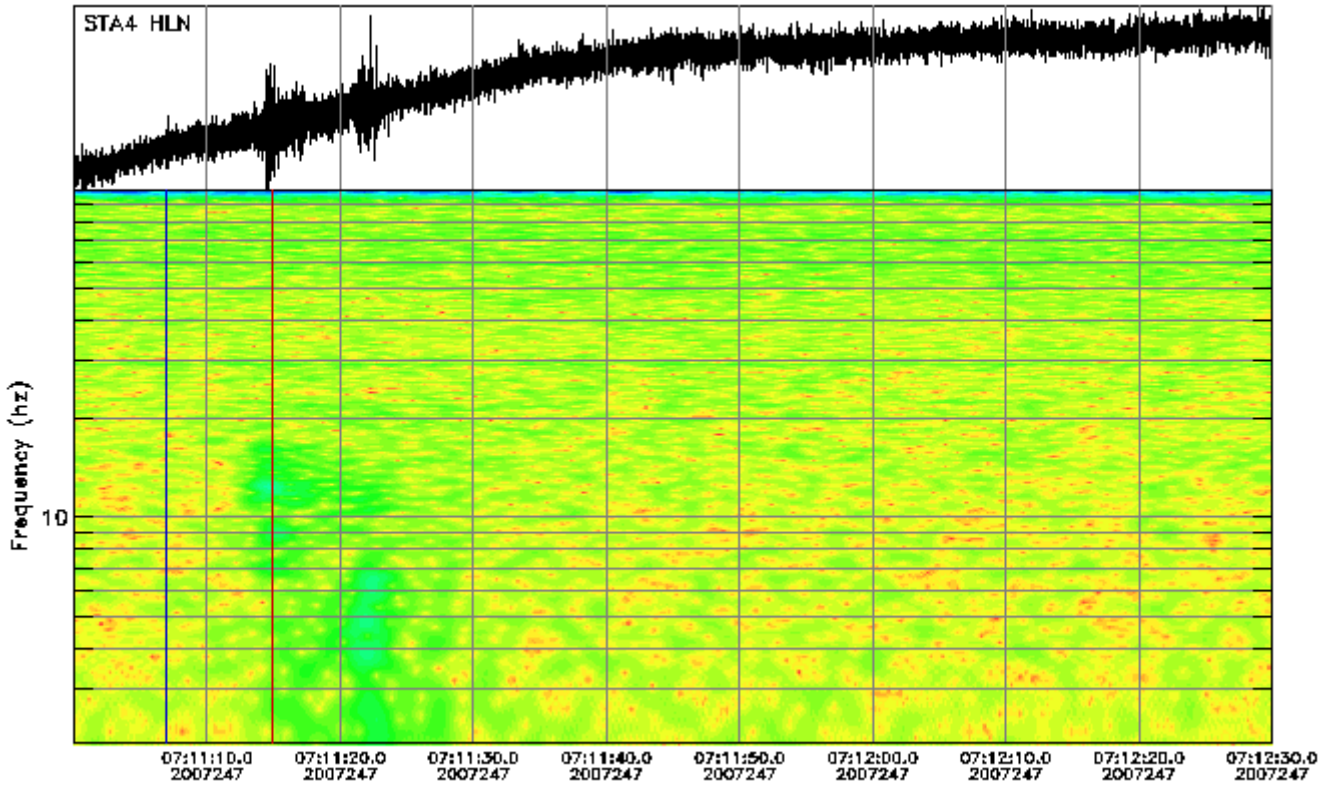

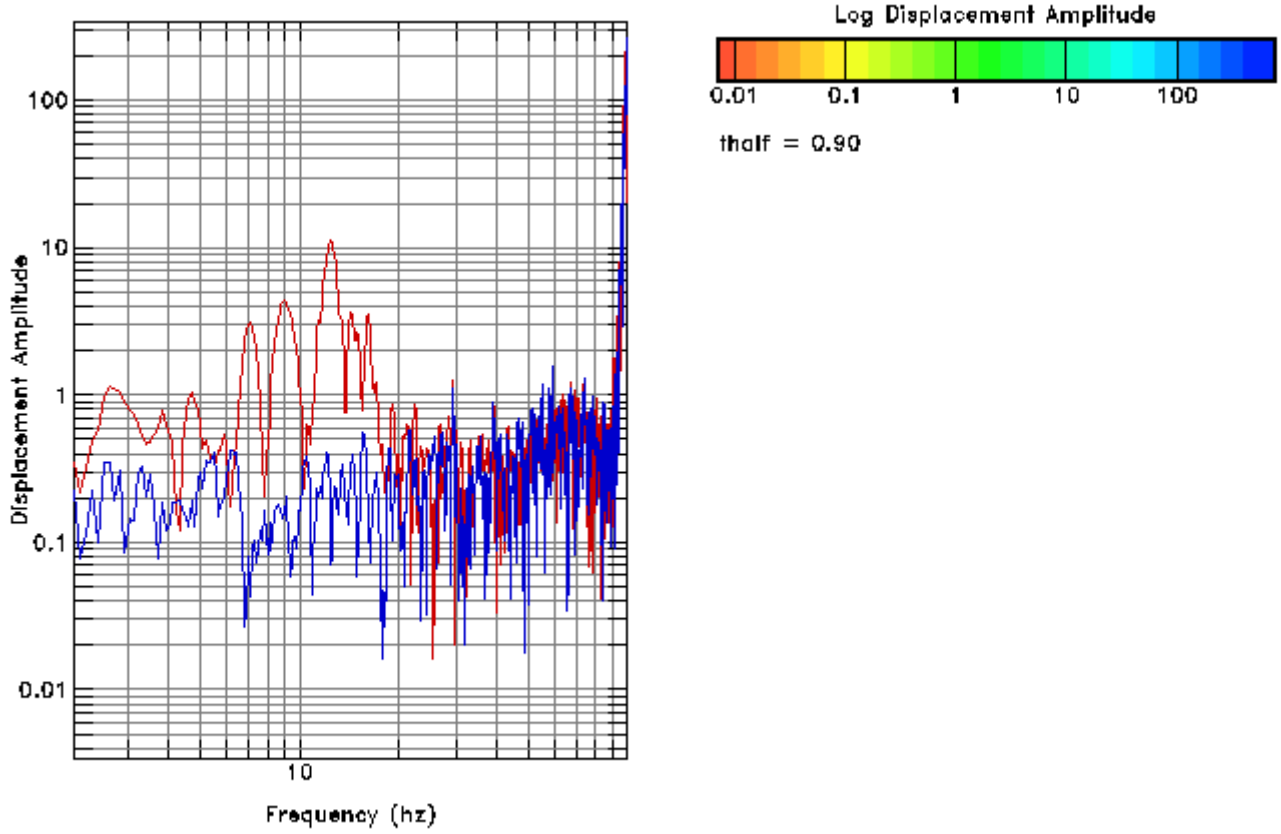

Instrument Correction: Episensor 200 Hz 10 Volt FS 2g/Quanterra 330 Linea

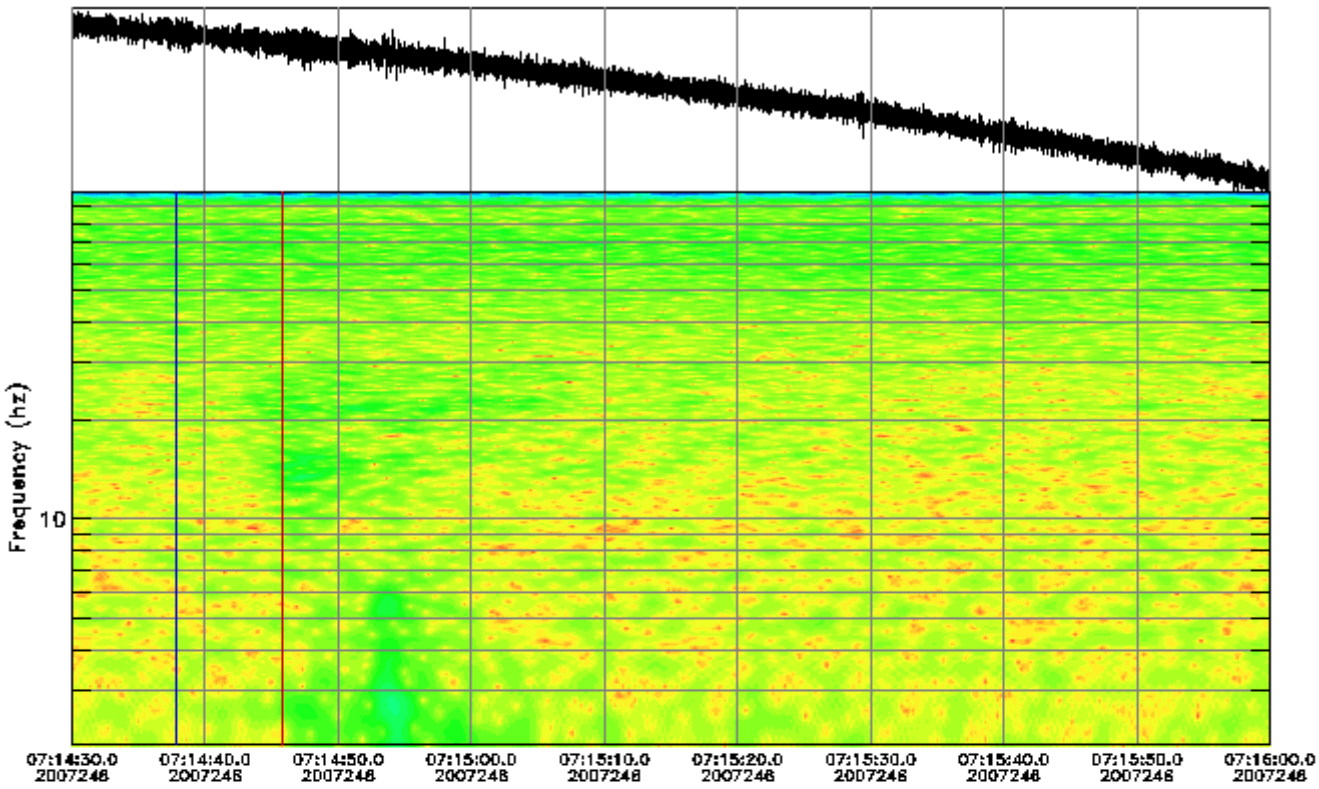

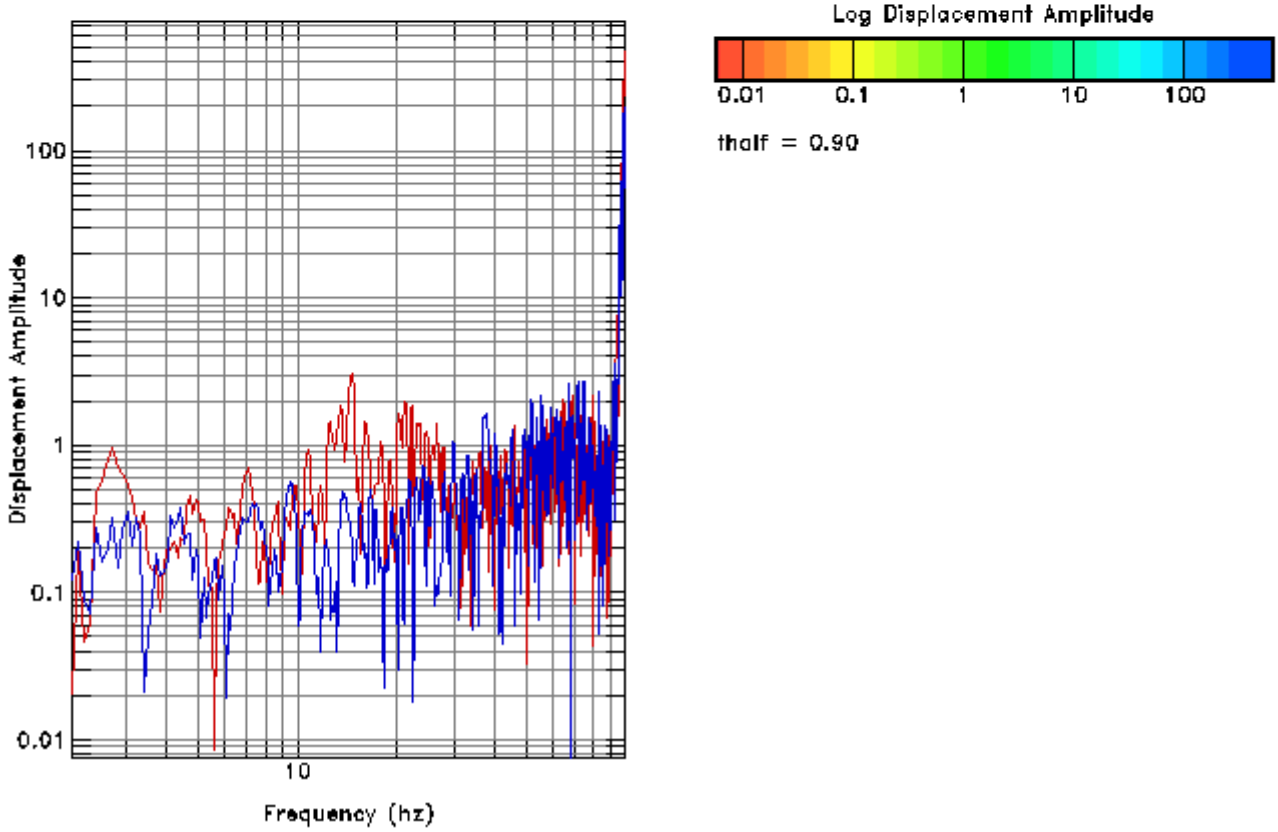

Instrument Correction: Episensor 200 Hz 10 Volt FS 2g/Quanterra 330 Linea

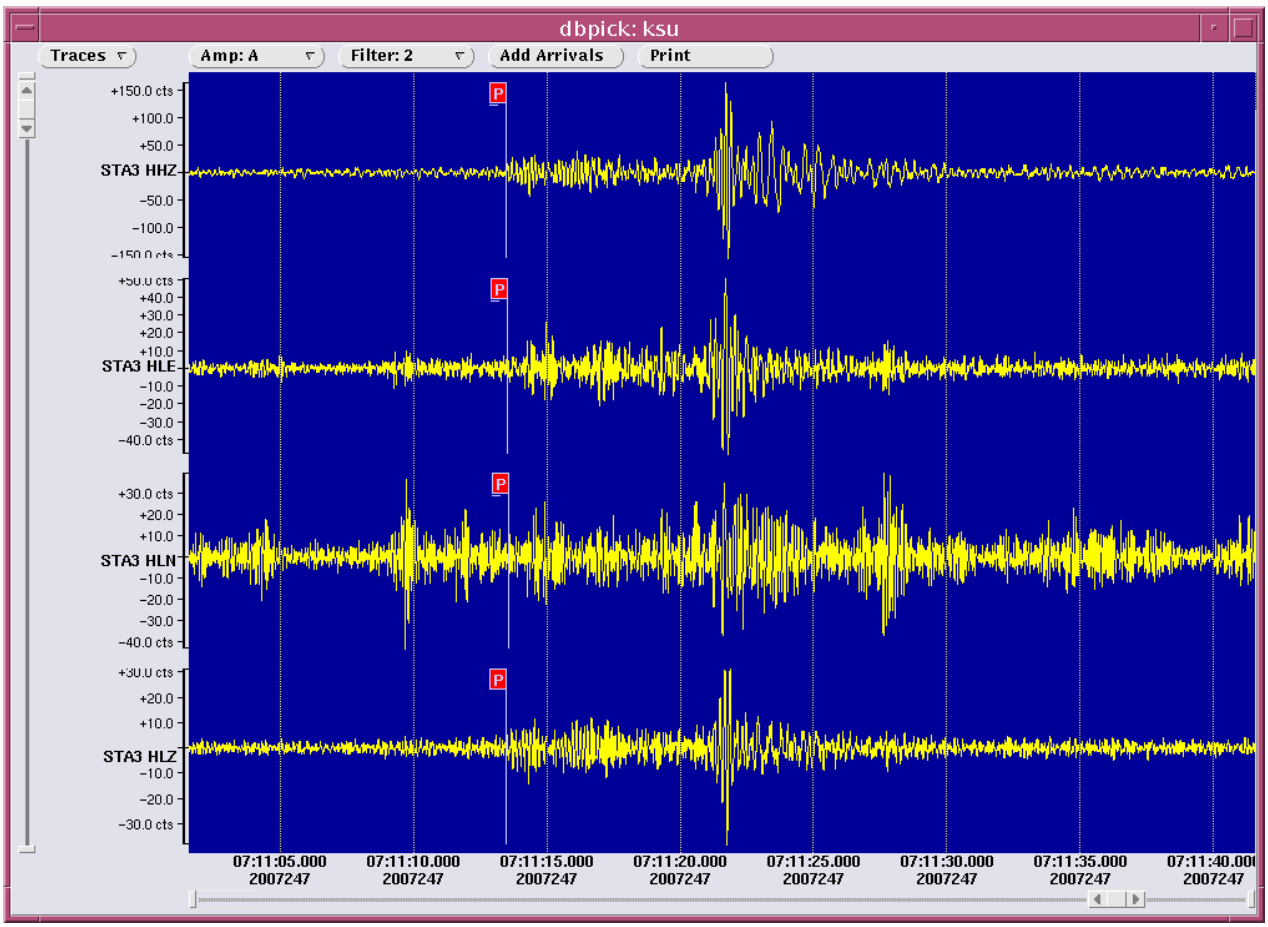
dbpick: ksu
Traces
Amp: A
Filter: 2
Add Arrivals
Print
+150.0 cts
+100.0
+50.0
STA3 HHZ
-50.0
-100.0
-150.0 cts
+50.0 cts
+40.0
+30.0
+20.0
+10.0
STA3 HLE
-10.0
-20.0
-30.0
-40.0 cts
+30.0 cts
+20.0
+10.0
STA3 HLN
-10.0
-20.0
-30.0
-40.0 cts
+30.0 cts
+20.0
+10.0
STA3 HLZ
-10.0
-20.0
-30.0 cts
P
07:11:05.000
2007247
07:11:10.000
2007247
07:11:15.000
2007247
07:11:20.000
2007247
07:11:25.000
2007247
07:11:30.000
2007247
07:11:35.000
2007247
07:11:40.000
2007247

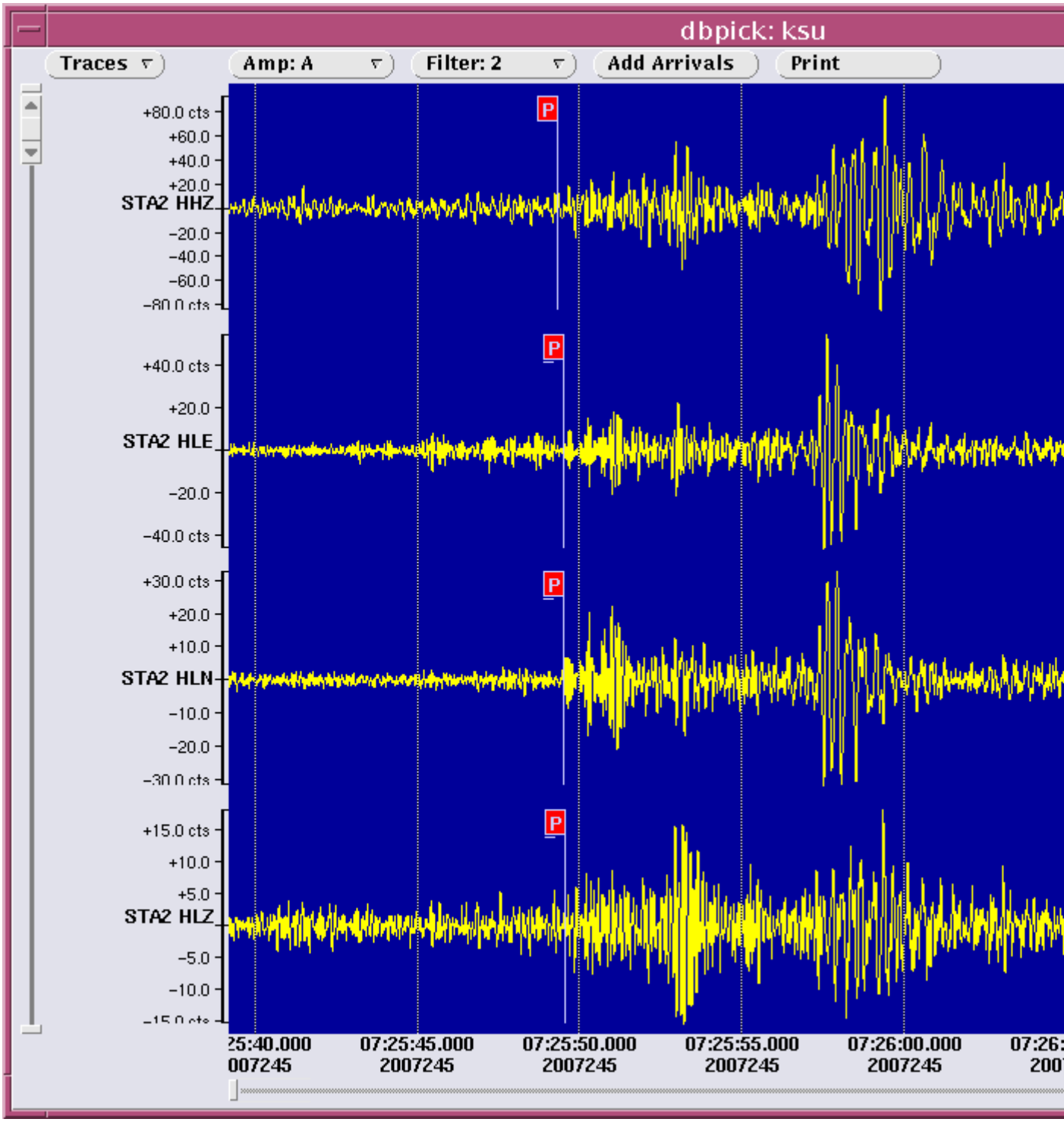
dbpick: ksu
Traces
Amp: A
Filter: 2
Add Arrivals
Print
+80.0 cts
+60.0
+40.0
+20.0
STA2 HHZ
-20.0
-40.0
-60.0
-80.0 cts
+40.0 cts
+20.0
STA2 HLE
-20.0
-40.0 cts
+30.0 cts
+20.0
+10.0
STA2 HLN
-10.0
-20.0
-30.0 cts
+15.0 cts
+10.0
+5.0
STA2 HLZ
-5.0
-10.0
-15.0 cts
P
25:40.000
007245
07:25:45.000
2007245
07:25:50.000
2007245
07:25:55.000
2007245
07:26:00.000
2007245

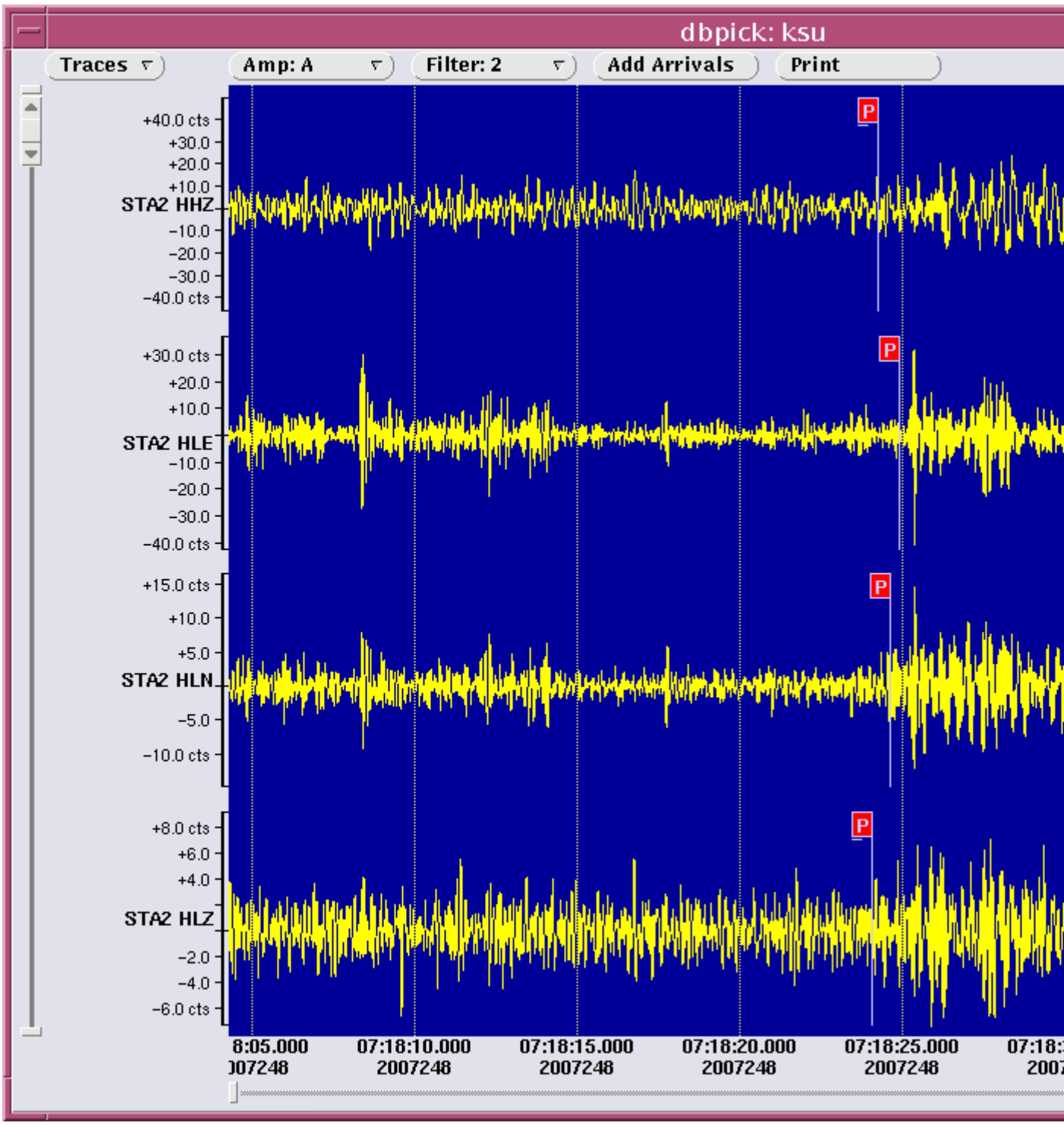
dbpick: ksu
Traces
Amp: A
Filter: 2
Add Arrivals
Print
+40.0 cts
+30.0
+20.0
+10.0
STA2 HHZ
-10.0
-20.0
-30.0
-40.0 cts
+30.0 cts
+20.0
+10.0
STA2 HLE
-10.0
-20.0
-30.0
-40.0 cts
+15.0 cts
+10.0
+5.0
STA2 HLN
-5.0
-10.0 cts
+8.0 cts
+6.0
+4.0
STA2 HLZ
-2.0
-4.0
-6.0 cts
P
8:05.000
)07248
07:18:10.000
2007248
07:18:15.000
2007248
07:18:20.000
2007248
07:18:25.000
2007248

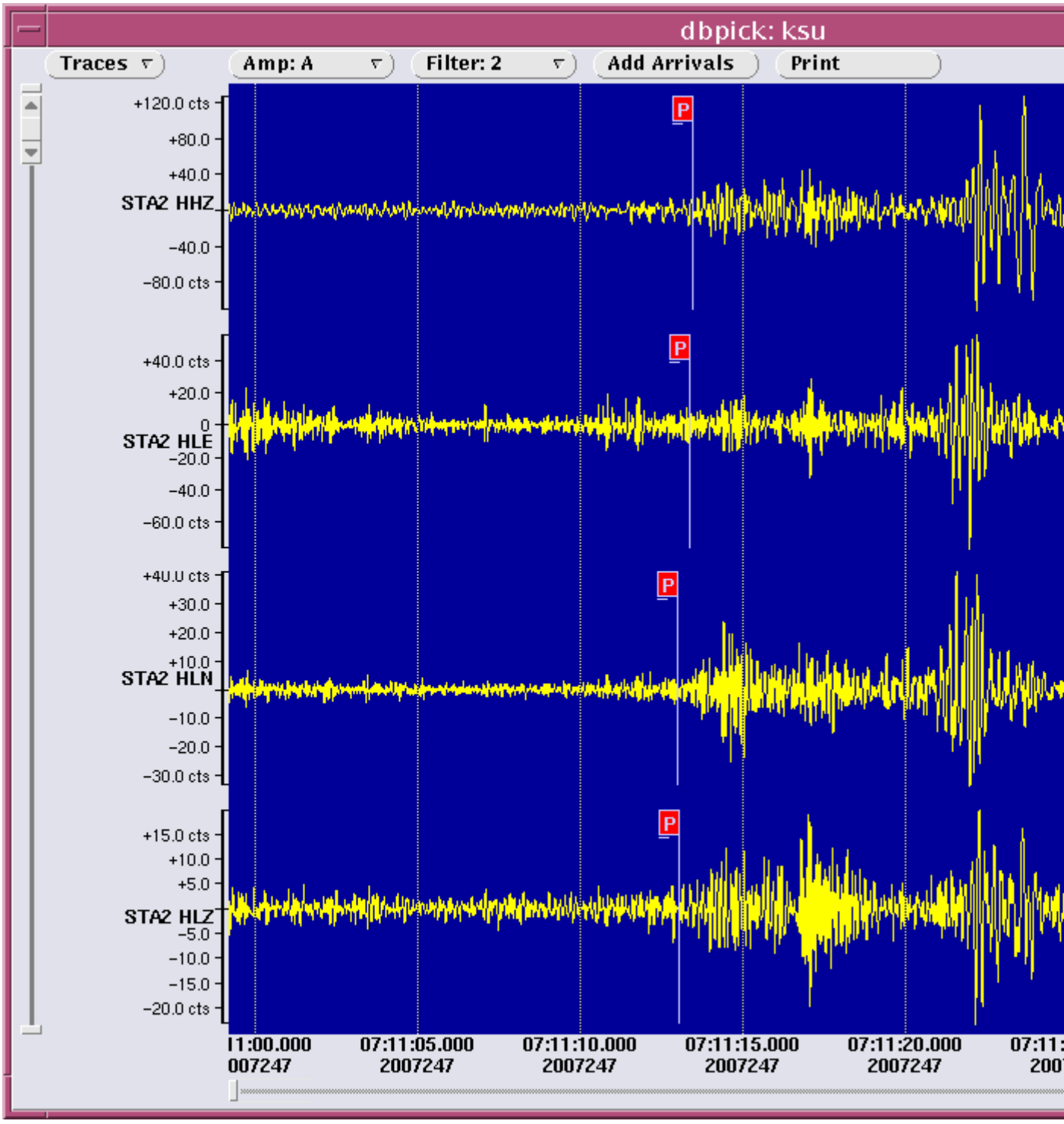
dbpick: ksu
Traces
Amp: A
Filter: 2
Add Arrivals
Print
+120.0 cts
+80.0
+40.0
STA2 HHZ
-40.0
-80.0 cts
P
+40.0 cts
+20.0
0
STA2 HLE
-20.0
-40.0
-60.0 cts
P
+40.0 cts
+30.0
+20.0
+10.0
STA2 HLN
-10.0
-20.0
-30.0 cts
P
+15.0 cts
+10.0
+5.0
STA2 HLZ
-5.0
-10.0
-15.0
-20.0 cts
P
11:00.000
007247
07:11:05.000
2007247
07:11:10.000
2007247
07:11:15.000
2007247
07:11:20.000
2007247

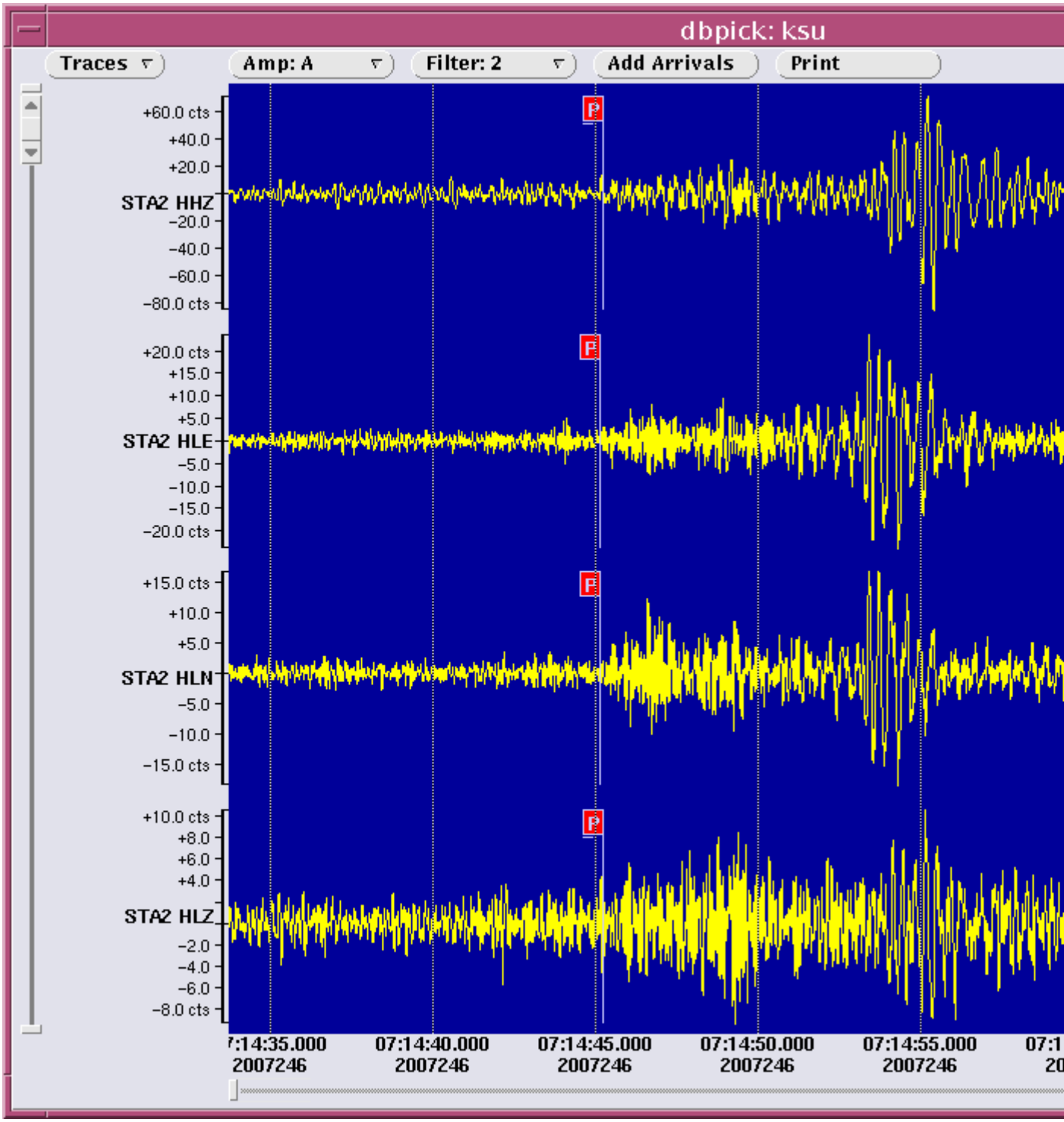
dbpick: ksu
Traces
Amp: A
Filter: 2
Add Arrivals
Print
+60.0 cts
+40.0
+20.0
STA2 HHZ
-20.0
-40.0
-60.0
-80.0 cts
+20.0 cts
+15.0
+10.0
+5.0
STA2 HLE
-5.0
-10.0
-15.0
-20.0 cts
+15.0 cts
+10.0
+5.0
STA2 HLN
-5.0
-10.0
-15.0 cts
+10.0 cts
+8.0
+6.0
+4.0
STA2 HLZ
-2.0
-4.0
-6.0
-8.0 cts
P
P
P
P
:14:35.000
2007246
07:14:40.000
2007246
07:14:45.000
2007246
07:14:50.000
2007246
07:14:55.000
2007246

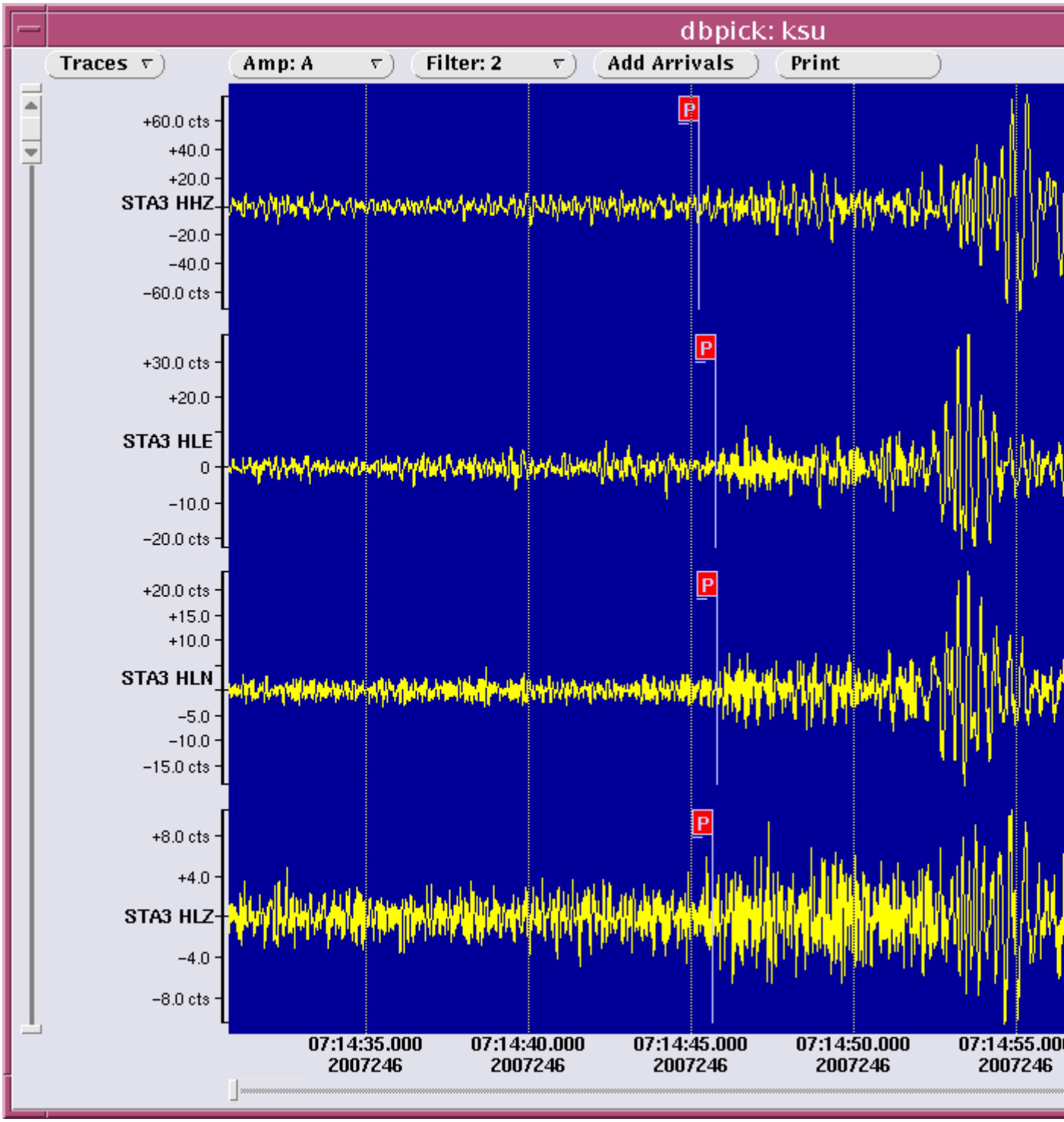
dbpick: ksu
Traces
Amp: A
Filter: 2
Add Arrivals
Print
+60.0 cts
+40.0
+20.0
STA3 HHZ
-20.0
-40.0
-60.0 cts
+30.0 cts
+20.0
STA3 HLE
0
-10.0
-20.0 cts
+20.0 cts
+15.0
+10.0
STA3 HLN
-5.0
-10.0
-15.0 cts
+8.0 cts
+4.0
STA3 HLZ
-4.0
-8.0 cts
P
07:14:35.000
2007246
07:14:40.000
2007246
07:14:45.000
2007246
07:14:50.000
2007246
07:14:55.000
2007246

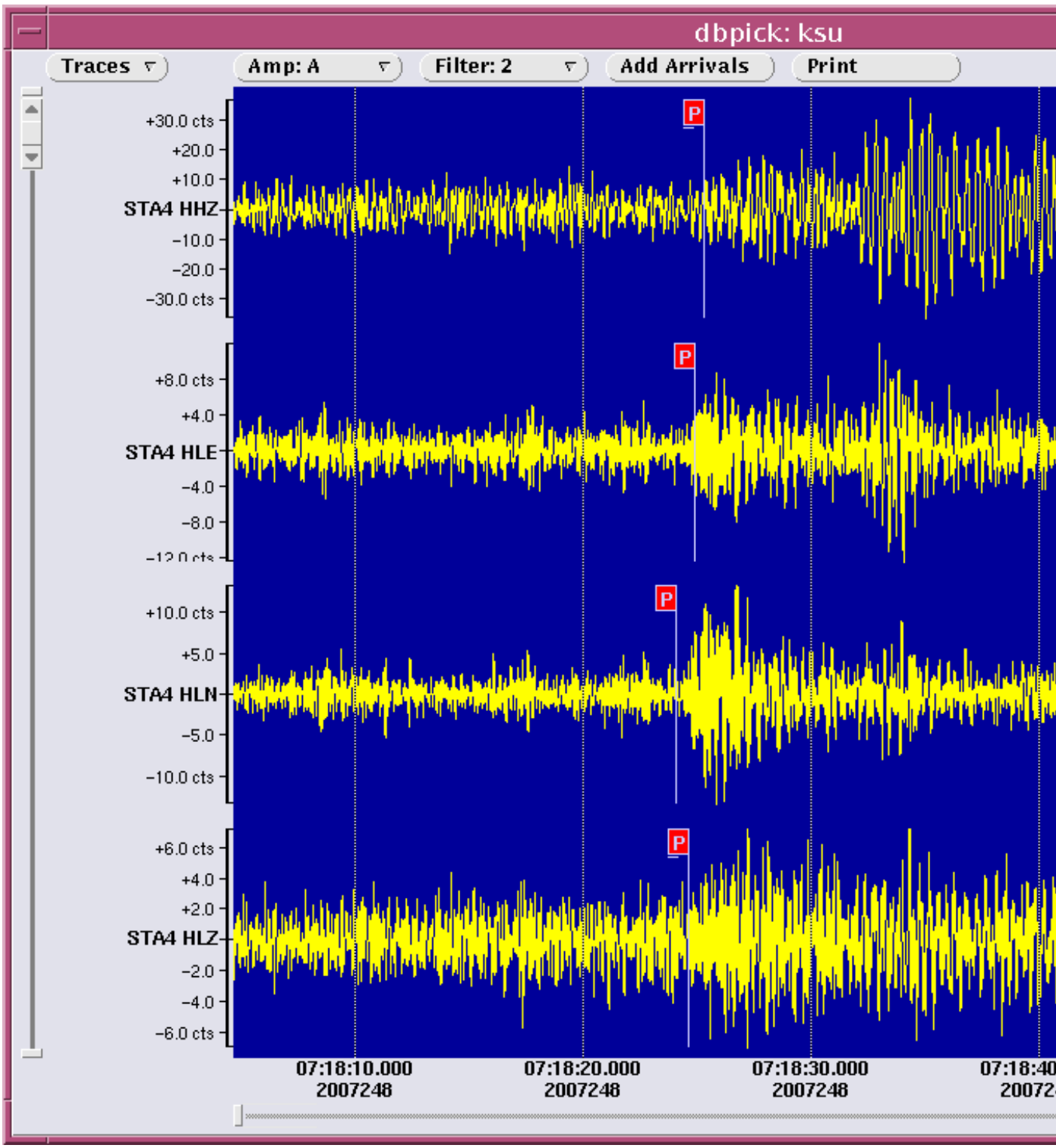
dbpick: ksu
Traces
Amp: A
Filter: 2
Add Arrivals
Print
+30.0 cts
+20.0
+10.0
STA4 HHZ
-10.0
-20.0
-30.0 cts
+8.0 cts
+4.0
STA4 HLE
-4.0
-8.0
+10.0 cts
+5.0
STA4 HLN
-5.0
-10.0 cts
+6.0 cts
+4.0
+2.0
STA4 HLZ
-2.0
-4.0
-6.0 cts
P
07:18:10.000
2007248
07:18:20.000
2007248
07:18:30.000
2007248

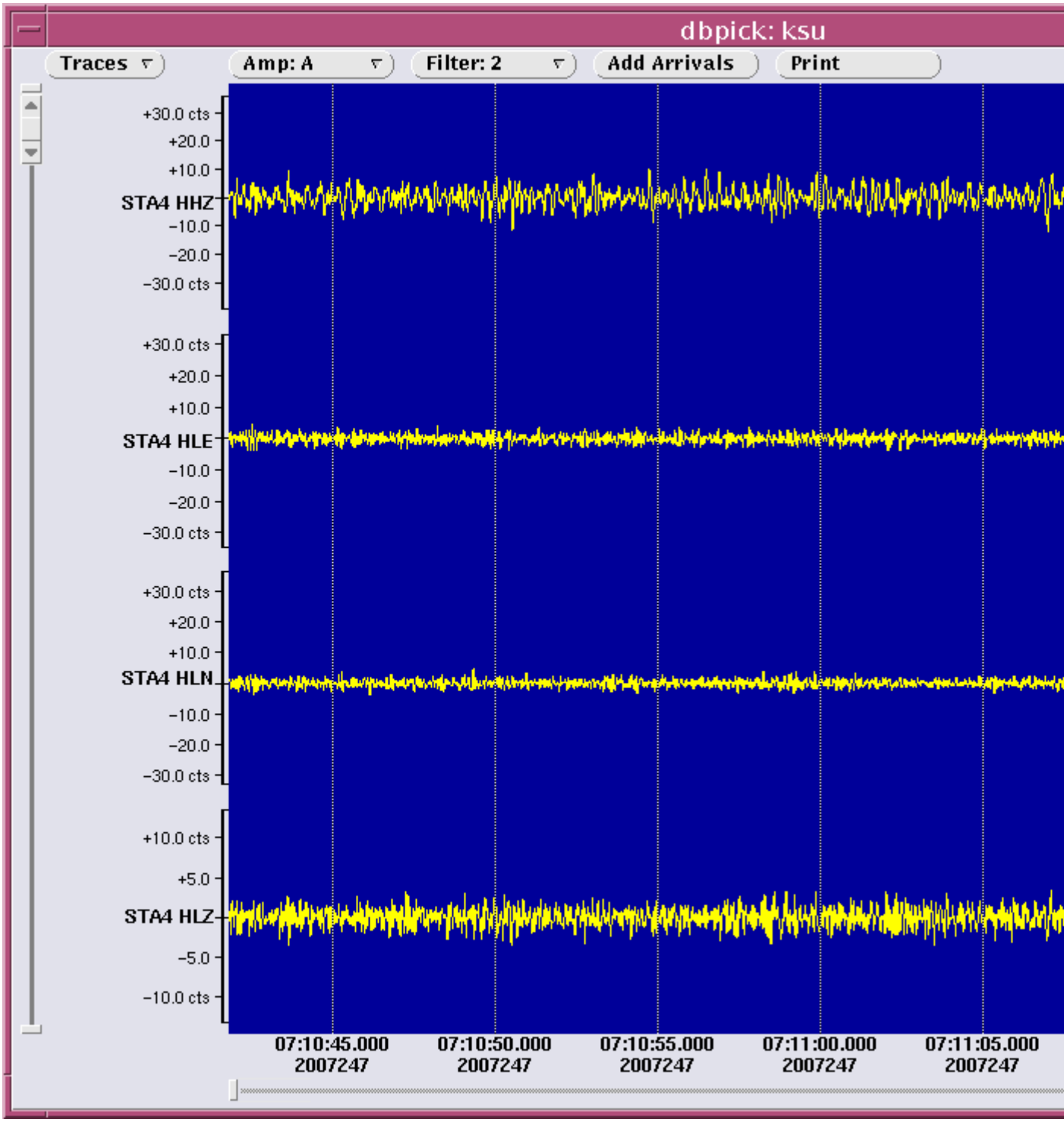
dbpick: ksu
Traces
Amp: A
Filter: 2
Add Arrivals
Print
+30.0 cts
+20.0
+10.0
STA4 HHZ
-10.0
-20.0
-30.0 cts
+30.0 cts
+20.0
+10.0
STA4 HLE
-10.0
-20.0
-30.0 cts
+30.0 cts
+20.0
+10.0
STA4 HLN
-10.0
-20.0
-30.0 cts
+10.0 cts
+5.0
STA4 HLZ
-5.0
-10.0 cts
07:10:45.000
2007247
07:10:50.000
2007247
07:10:55.000
2007247
07:11:00.000
2007247
07:11:05.000
2007247

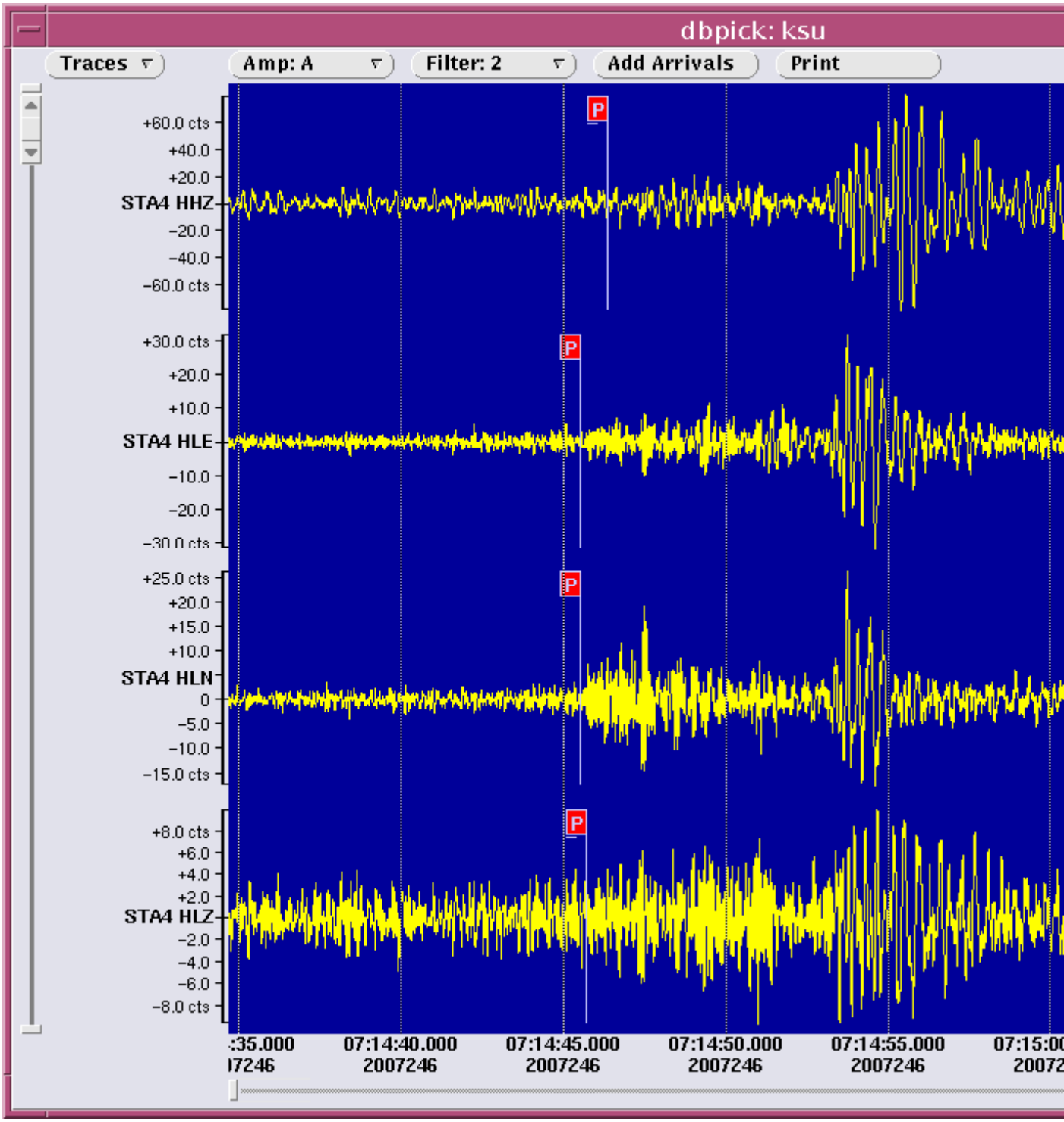
dbpick: ksu
Traces
Amp: A
Filter: 2
Add Arrivals
Print
+60.0 cts
+40.0
+20.0
STA4 HHZ
-20.0
-40.0
-60.0 cts
+30.0 cts
+20.0
+10.0
STA4 HLE
-10.0
-20.0
-30.0 cts
+25.0 cts
+20.0
+15.0
+10.0
STA4 HLN
0
-5.0
-10.0
-15.0 cts
+8.0 cts
+6.0
+4.0
+2.0
STA4 HLZ
-2.0
-4.0
-6.0
-8.0 cts
P
:35.000
07246
07:14:40.000
2007246
07:14:45.000
2007246
07:14:50.000
2007246
07:14:55.000
2007246
07:15:00
20072

Appendix IV

Spectral Amplitude Ratios for Five Explosions in Southern Riyadh.

9-1-2007 Sta1

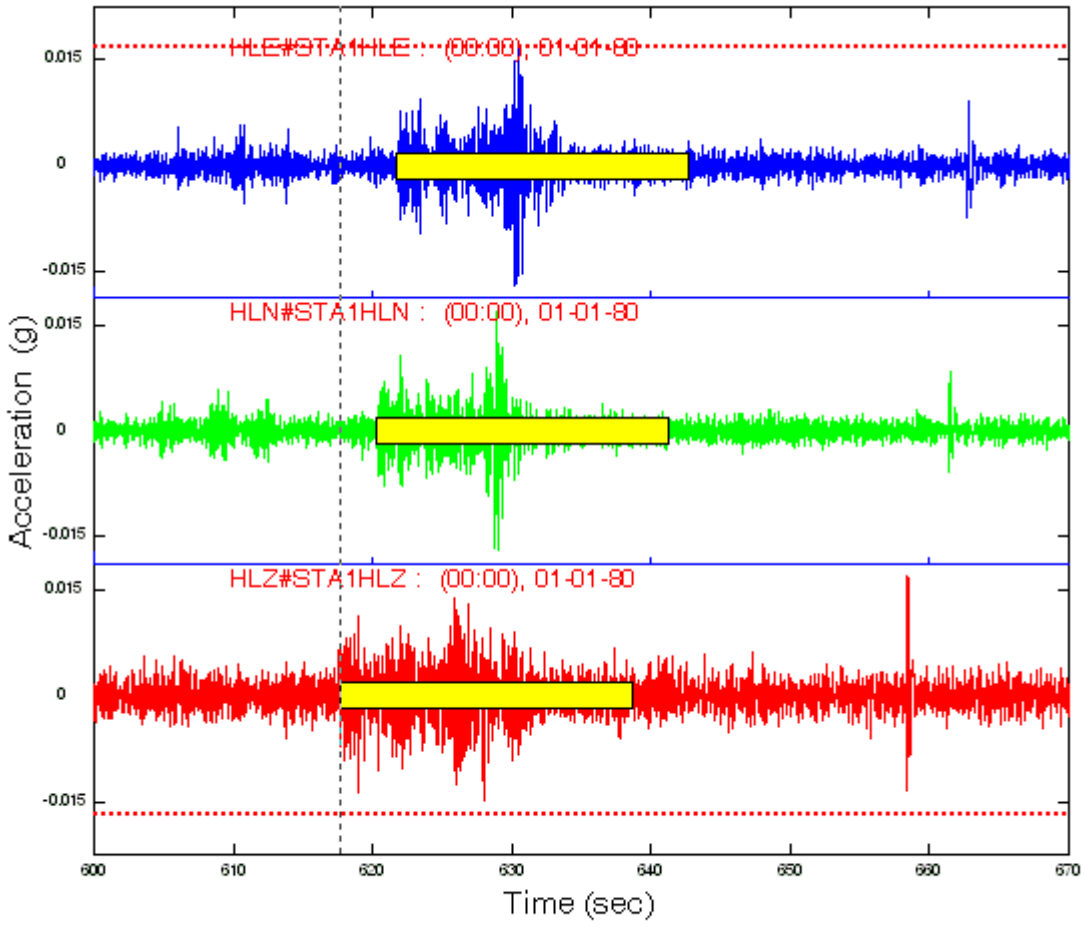

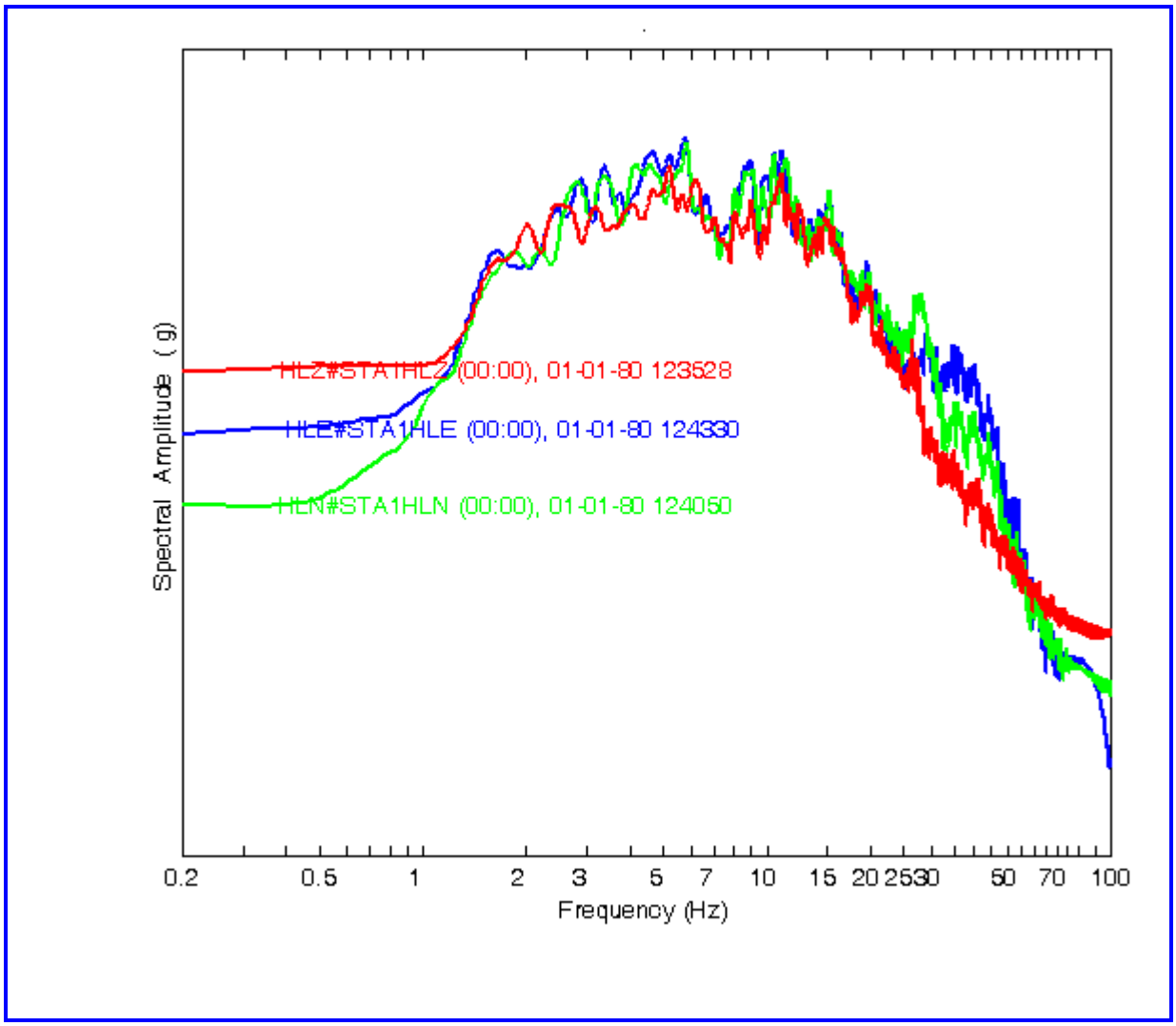
Spectral Amplitude (g)
HLZ#STA1HLZ (00:00), 01-01-80 123528
HLE#STA1HLE (00:00), 01-01-80 124330
HLN#STA1HLN (00:00), 01-01-80 124050
0.2
0.5
1
2
3
5
7
10
15
20
25
30
50
70
100
Frequency (Hz)

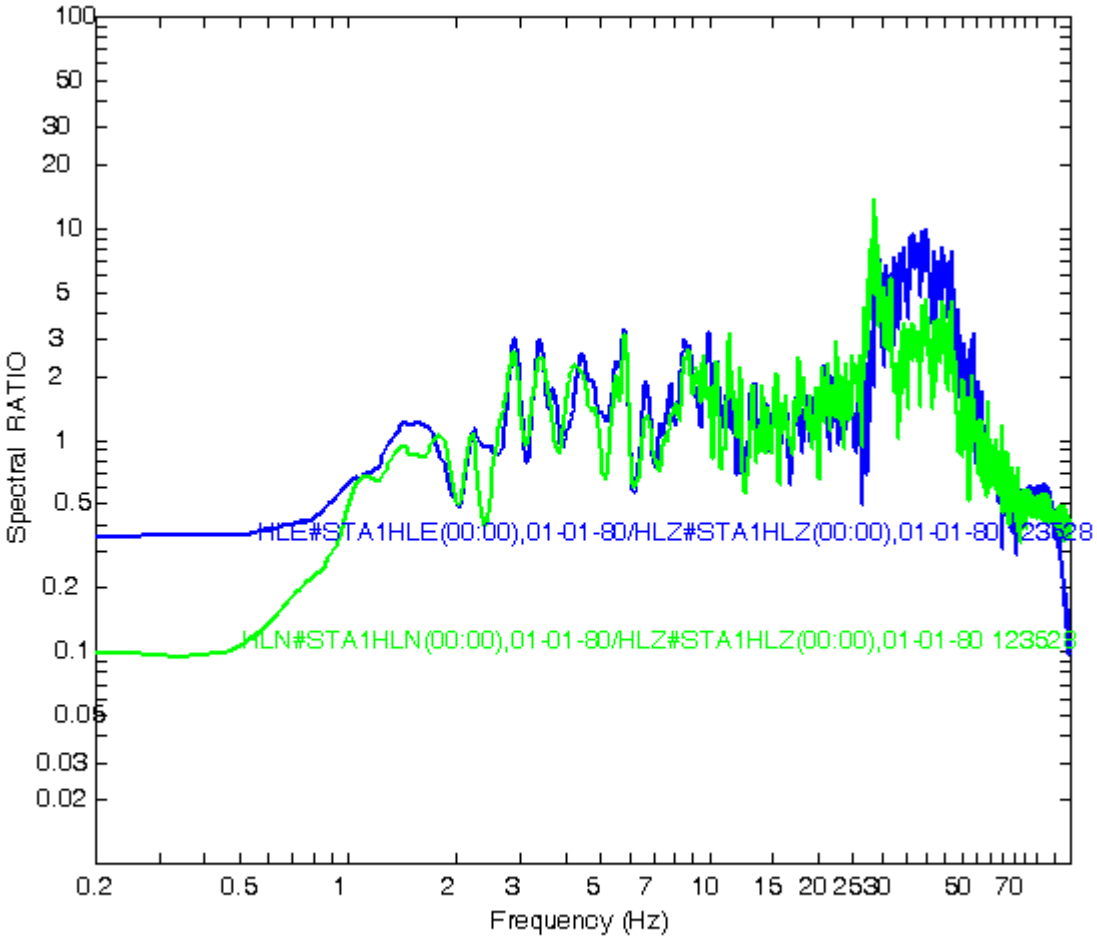
Spectral RATIO
100
50
30
20
10
5
3
2
1
0.5
0.2
0.1
0.05
0.03
0.02
0.2
0.5
1
2
3
5
7
10
15
20
25
30
50
70
Frequency (Hz)
HLE#STA1HLE(00:00),01-01-80/HLZ#STA1HLZ(00:00),01-01-80
HLN#STA1HLN(00:00),01-01-80/HLZ#STA1HLZ(00:00),01-01-80

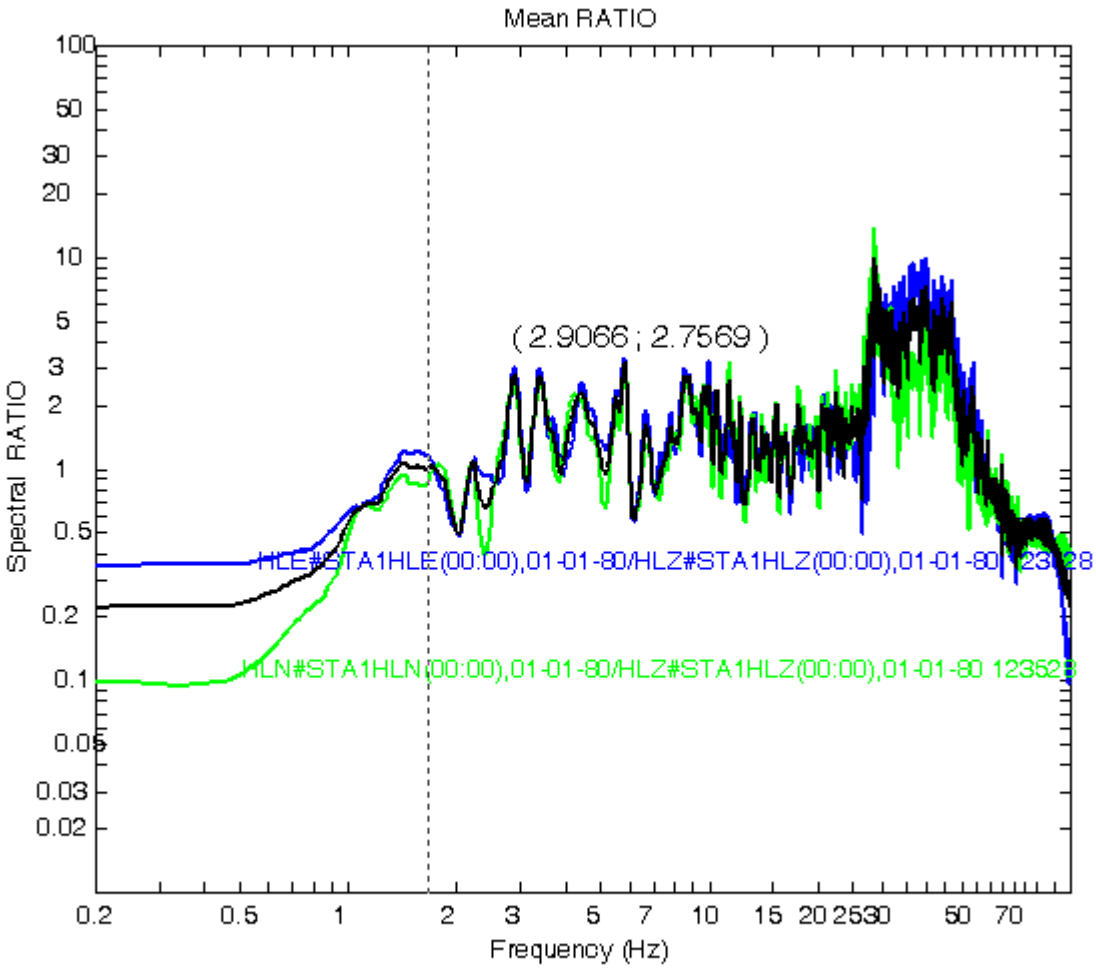
Mean RATIO
Spectral RATIO
100
50
30
20
10
5
3
2
1
0.5
0.2
0.1
0.05
0.03
0.02
(2.9066 ; 2.7569)
HLE#STA1HLE(00:00),01-01-80/HLZ#STA1HLZ(00:00),01-01-80
HLN#STA1HLN(00:00),01-01-80/HLZ#STA1HLZ(00:00),01-01-80
0.2
0.5
1
2
3
5
7
10
15
20
25
30
50
70
Frequency (Hz)

9-1-2007-sta2

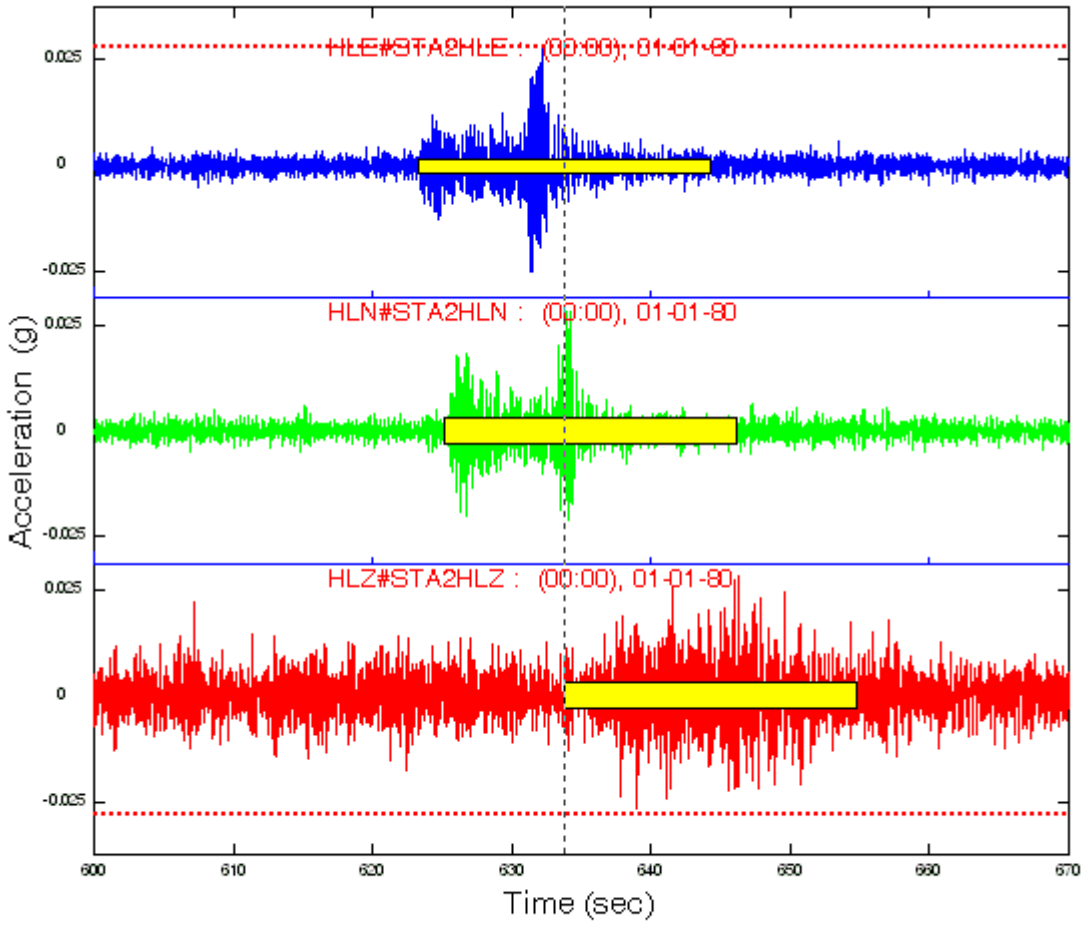
HLE#STA2HLE : (00:00), 01-01-80
HLN#STA2HLN : (00:00), 01-01-80
HLZ#STA2HLZ : (00:00), 01-01-80
Acceleration (g)
0.025
0
-0.025
600
610
620
630
640
650
660
670
Time (sec)

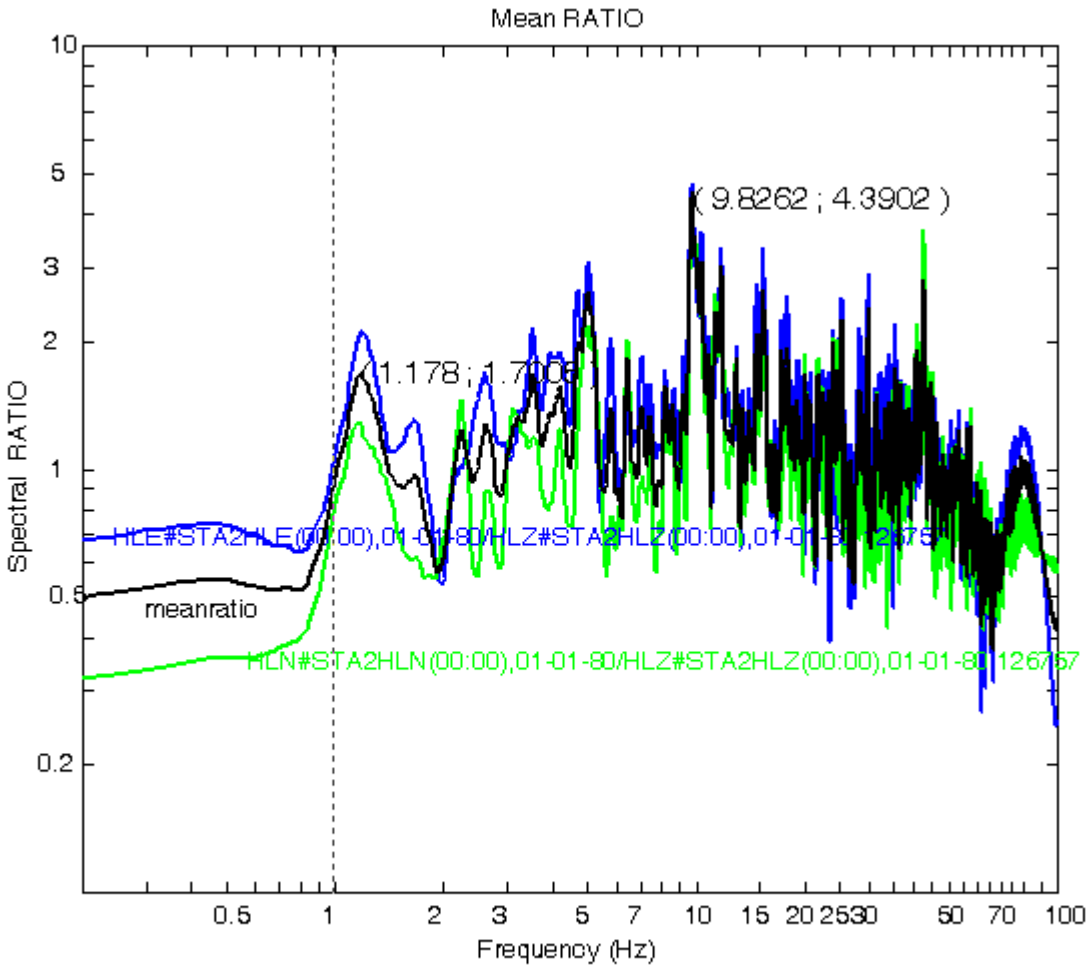
Mean RATIO
Spectral RATIO
Frequency (Hz)
(9.8262 ; 4.3902)
(1.178 ; 1.7006)
meanratio
10
5
3
2
1
0.5
0.2
0.5
1
2
3
5
7
10
15
20
25
30
50
70
100

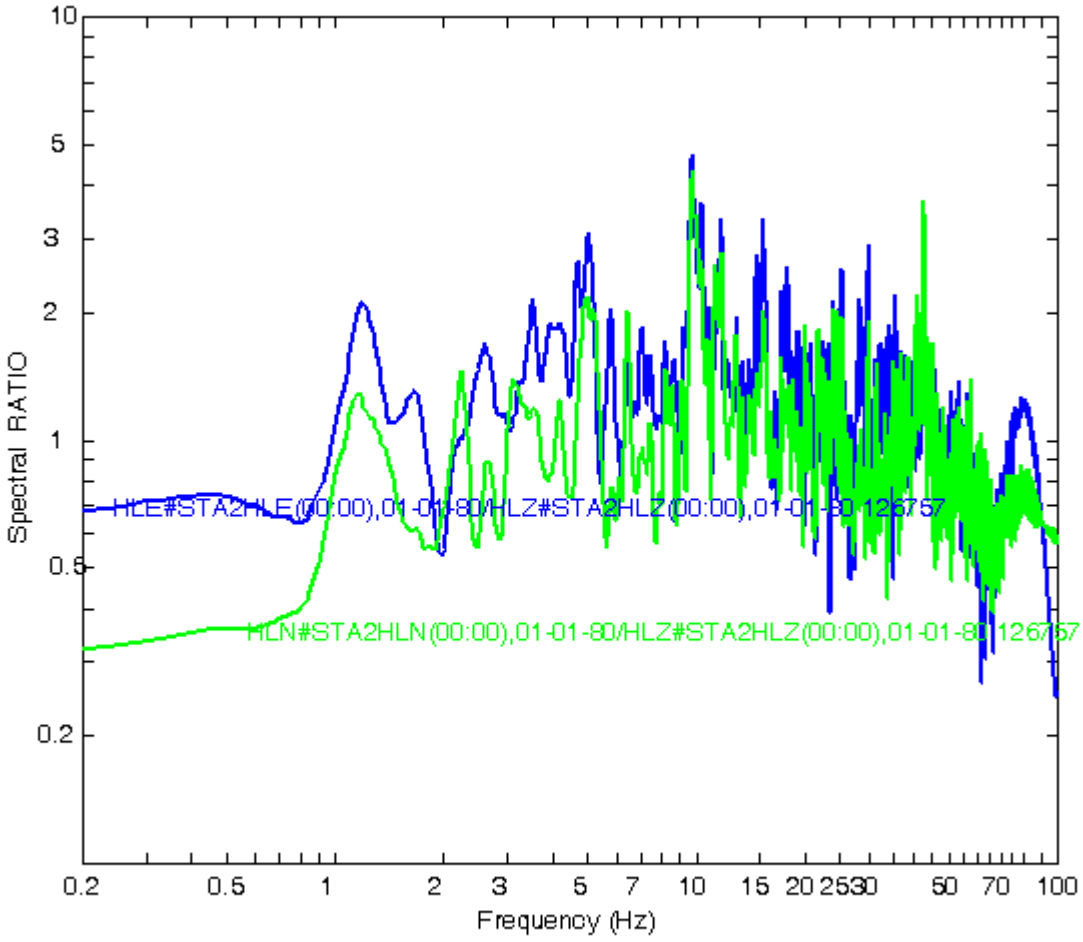
10
5
3
2
1
0.6
0.2
Spectral RATIO
HLE#STA2HLE(00:00),01-01-80/HLZ#STA2HLZ(00:00),01-01-80 126757
HLN#STA2HLN(00:00),01-01-80/HLZ#STA2HLZ(00:00),01-01-80 126757
0.2
0.5
1
2
3
5
7
10
15
20
25
30
50
70
100
Frequency (Hz)

9-2-2007-sta2

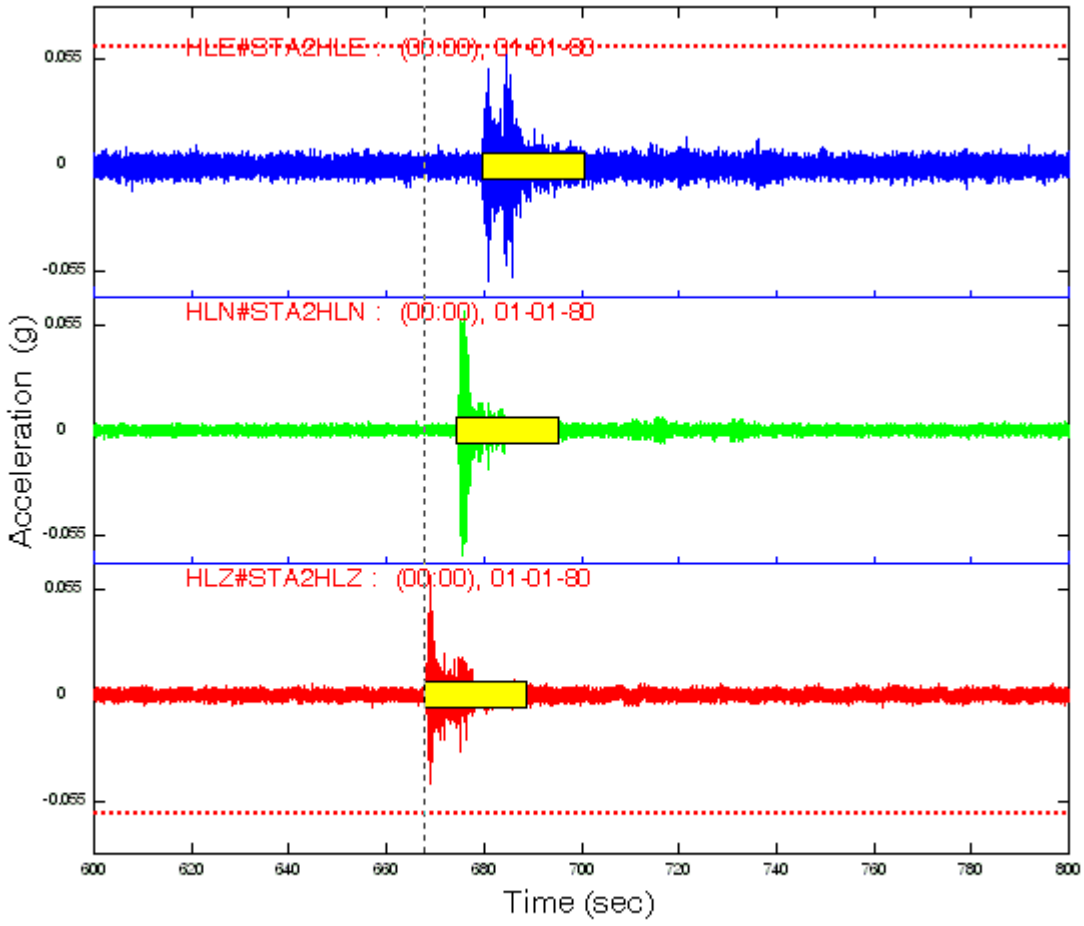
HLE#STA2HLE : (00:00), 01-01-80
HLN#STA2HLN : (00:00), 01-01-80
HLZ#STA2HLZ : (00:00), 01-01-80
0.055
0
-0.055
Acceleration (g)
600
620
640
660
680
700
720
740
760
780
800
Time (sec)

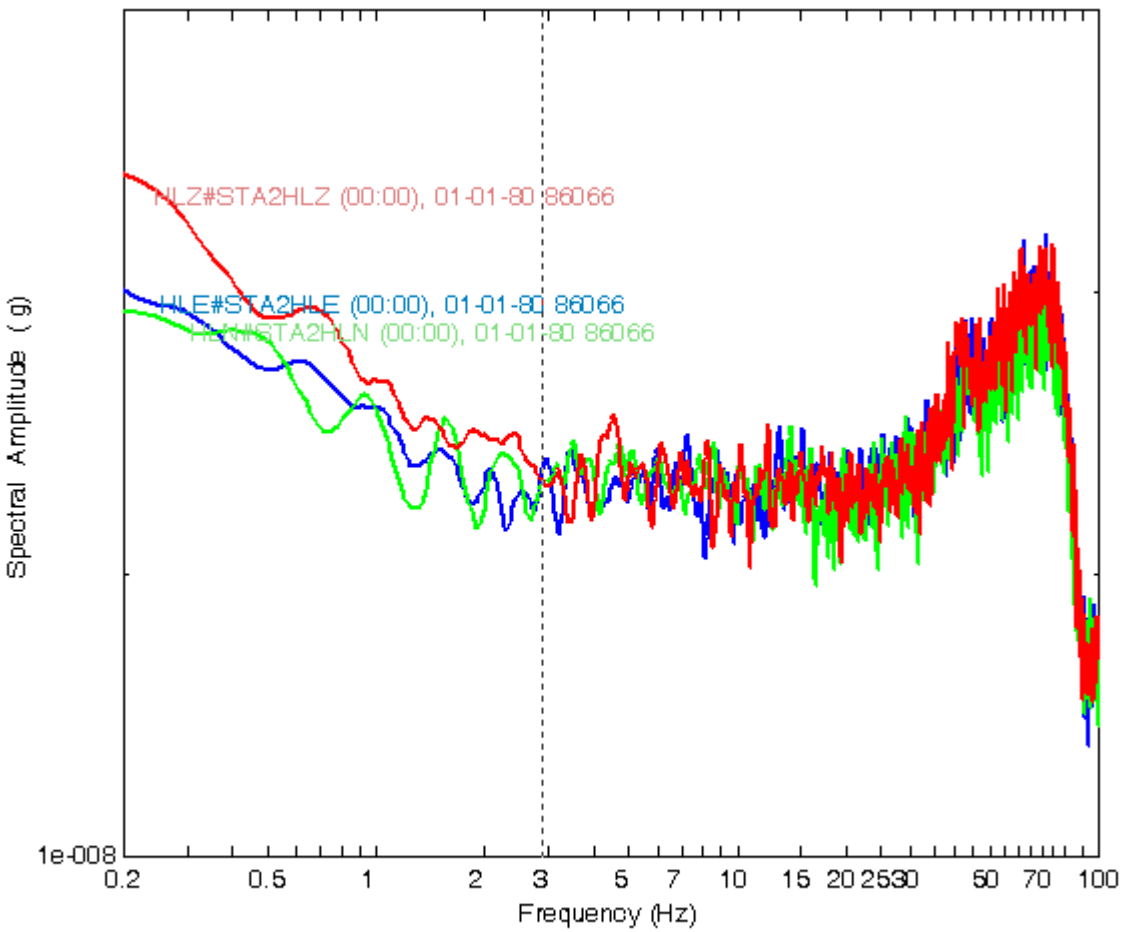
HLZ#STA2HLZ (00:00), 01-01-80 86066
HLE#STA2HLE (00:00), 01-01-80 86066
HLN#STA2HLN (00:00), 01-01-80 86066
Spectral Amplitude (g)
1e-008
0.2
0.5
1
2
3
5
7
10
15
20
25
30
50
70
100
Frequency (Hz)

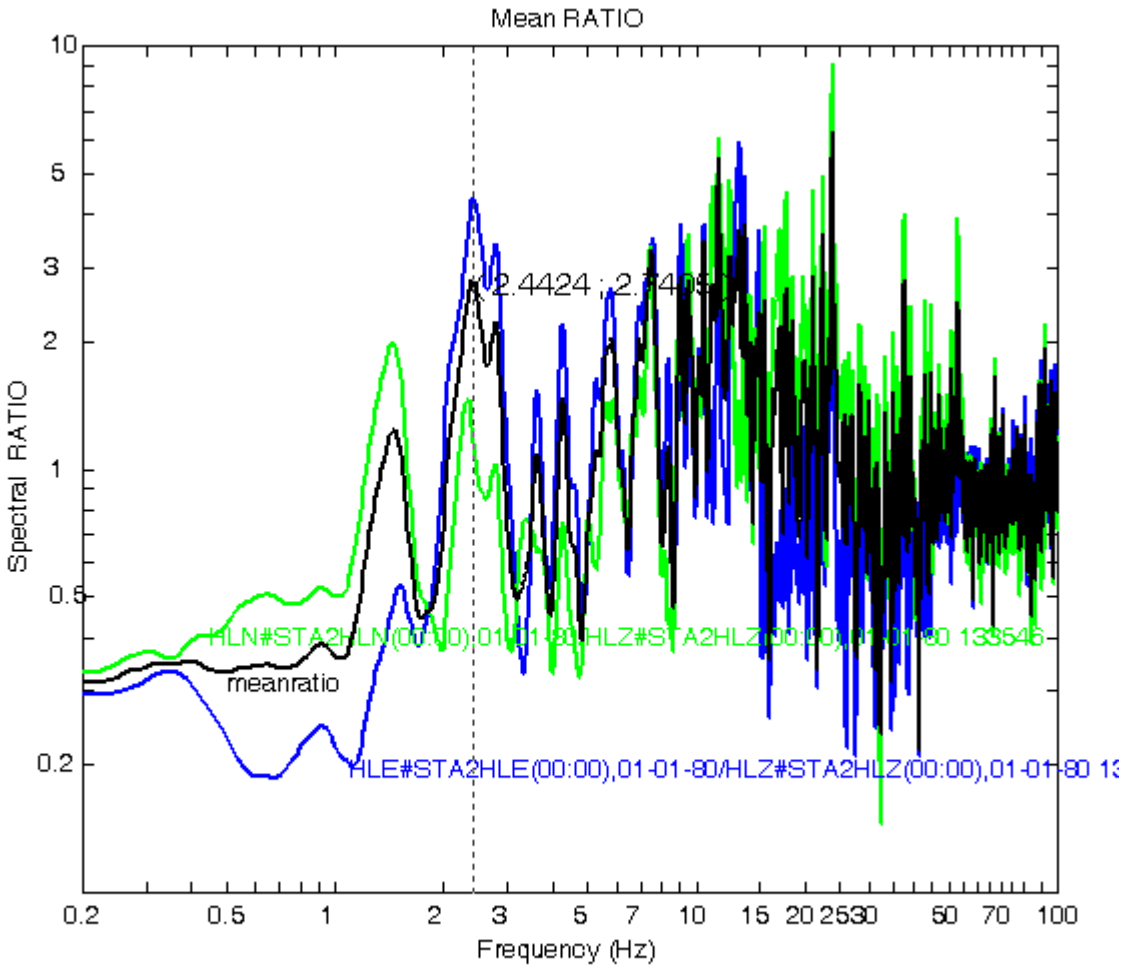
Mean RATIO
Spectral RATIO
Frequency (Hz)
meanratio
10
5
3
2
1
0.5
0.2
0.2
0.5
1
2
3
5
7
10
15
20
25
30
50
70
100

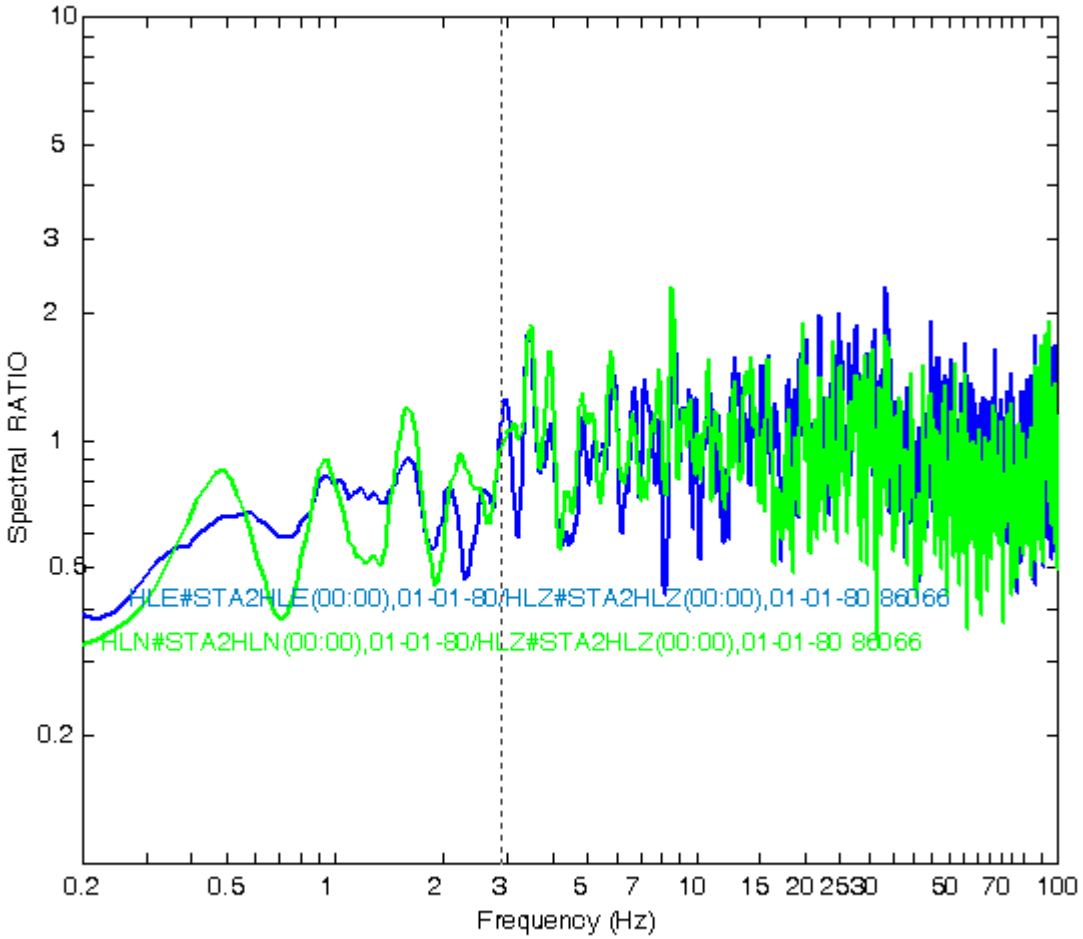
10
5
3
2
1
0.6
0.2
Spectral RATIO
HLE#STA2HLE(00:00),01-01-80/HLZ#STA2HLZ(00:00),01-01-80 86066
HLN#STA2HLN(00:00),01-01-80/HLZ#STA2HLZ(00:00),01-01-80 86066
0.2
0.5
1
2
3
5
7
10
15
20
25
30
50
70
100
Frequency (Hz)

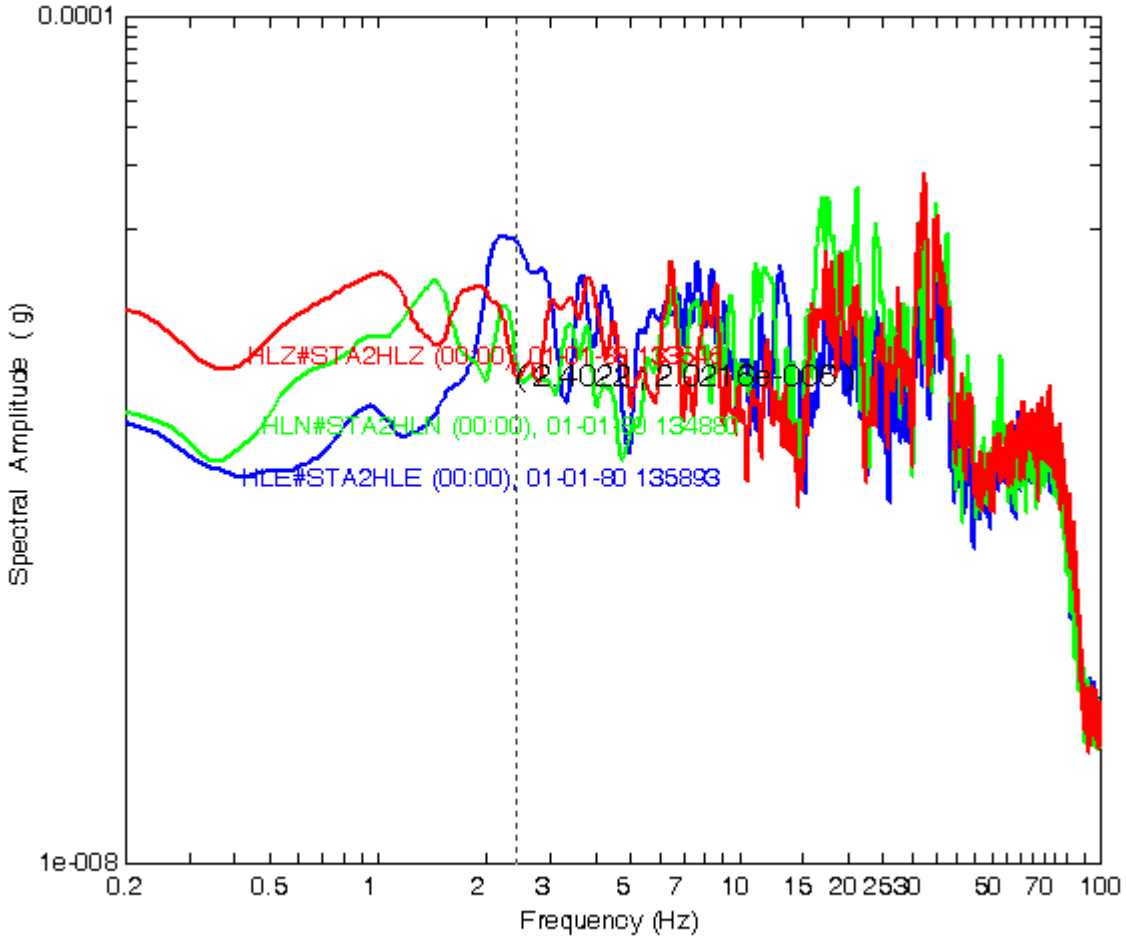
0.0001
1e-008
Spectral Amplitude (g)
0.2
0.5
1
2
3
5
7
10
15
20
25
30
50
70
100
Frequency (Hz)
HLZ#STA2HLZ (00:00), 01-01-80 135886
HLN#STA2HLN (00:00), 01-01-80 134880
HLE#STA2HLE (00:00), 01-01-80 135893

9-2-2007- sta3

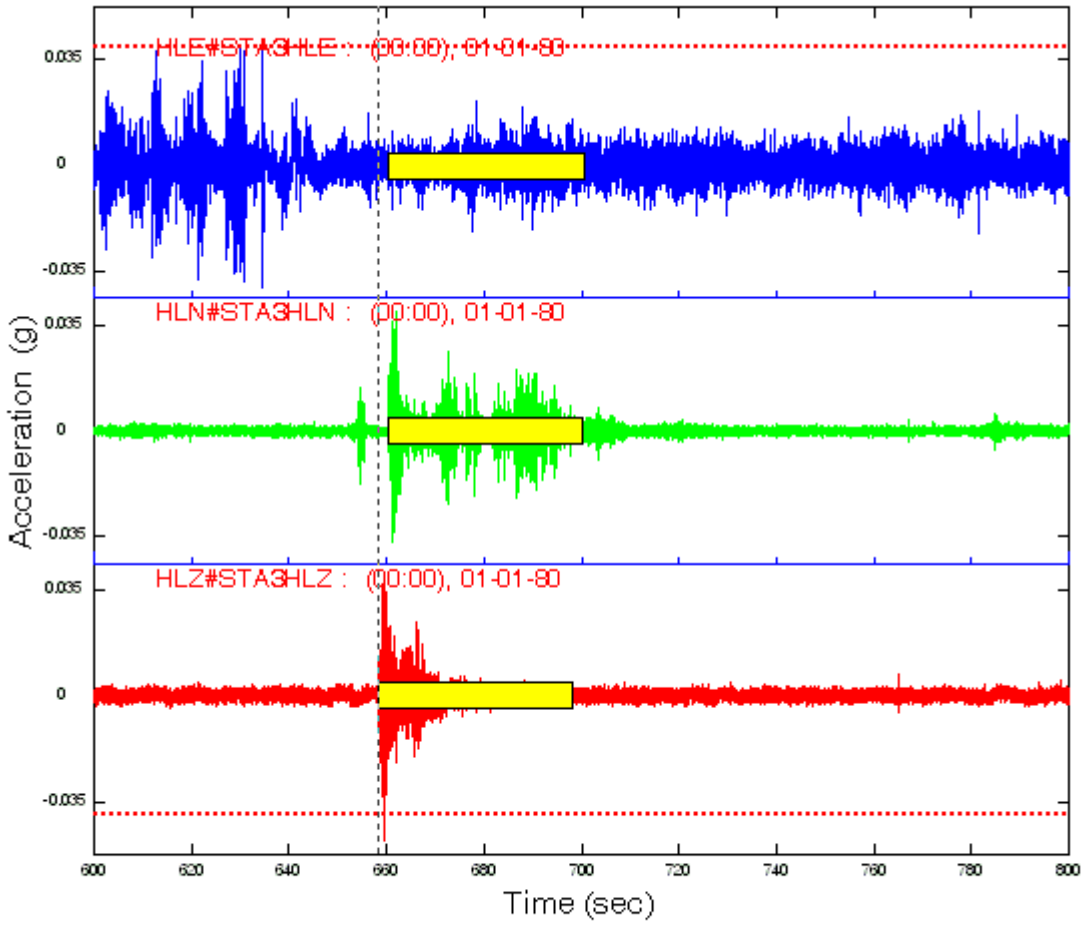
HLE#STA3HLE : (00:00), 01-01-80
HLN#STA3HLN : (00:00), 01-01-80
HLZ#STA3HLZ : (00:00), 01-01-80
0.035
0
-0.035
Acceleration (g)
600
620
640
660
680
700
720
740
760
780
800
Time (sec)

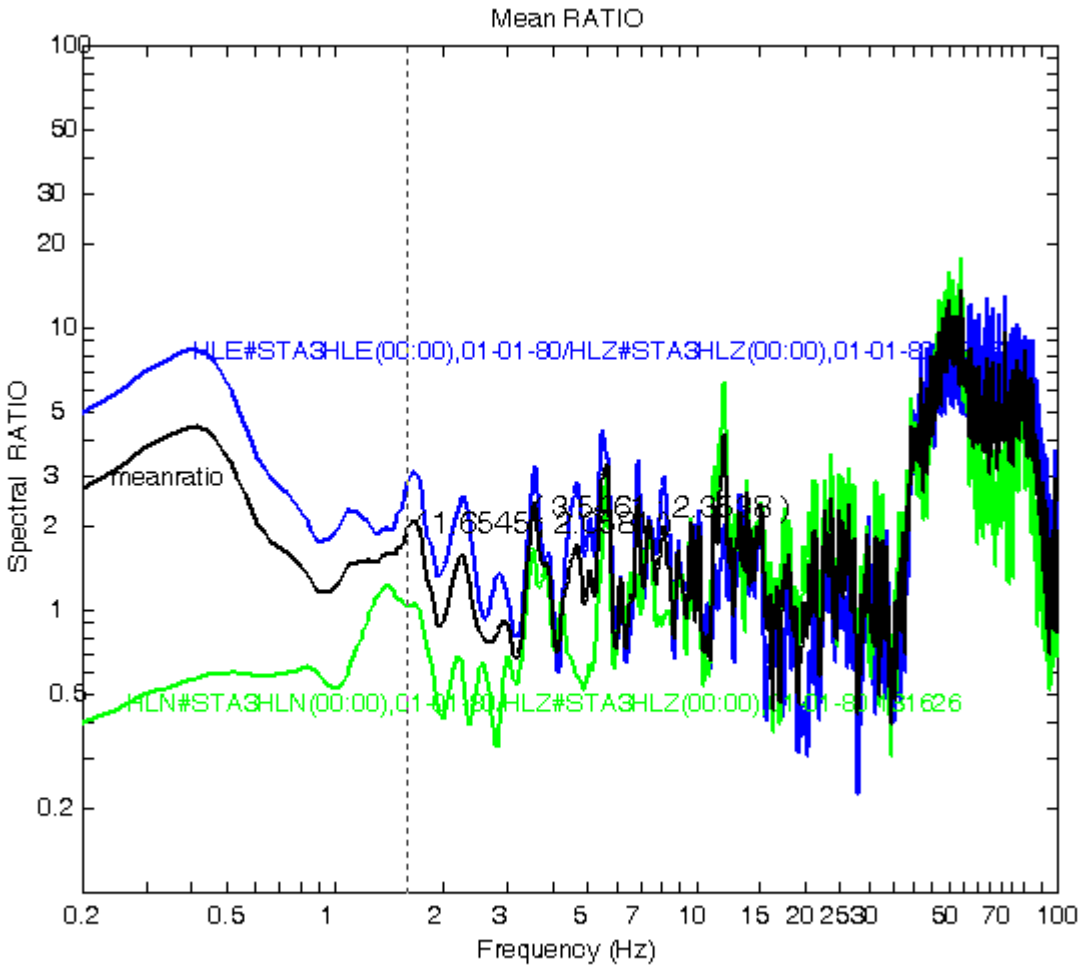
Mean RATIO
Spectral RATIO
Frequency (Hz)
meanratio
100
50
30
20
10
5
3
2
1
0.5
0.2
0.2
0.5
1
2
3
5
7
10
15
20
25
30
50
70
100

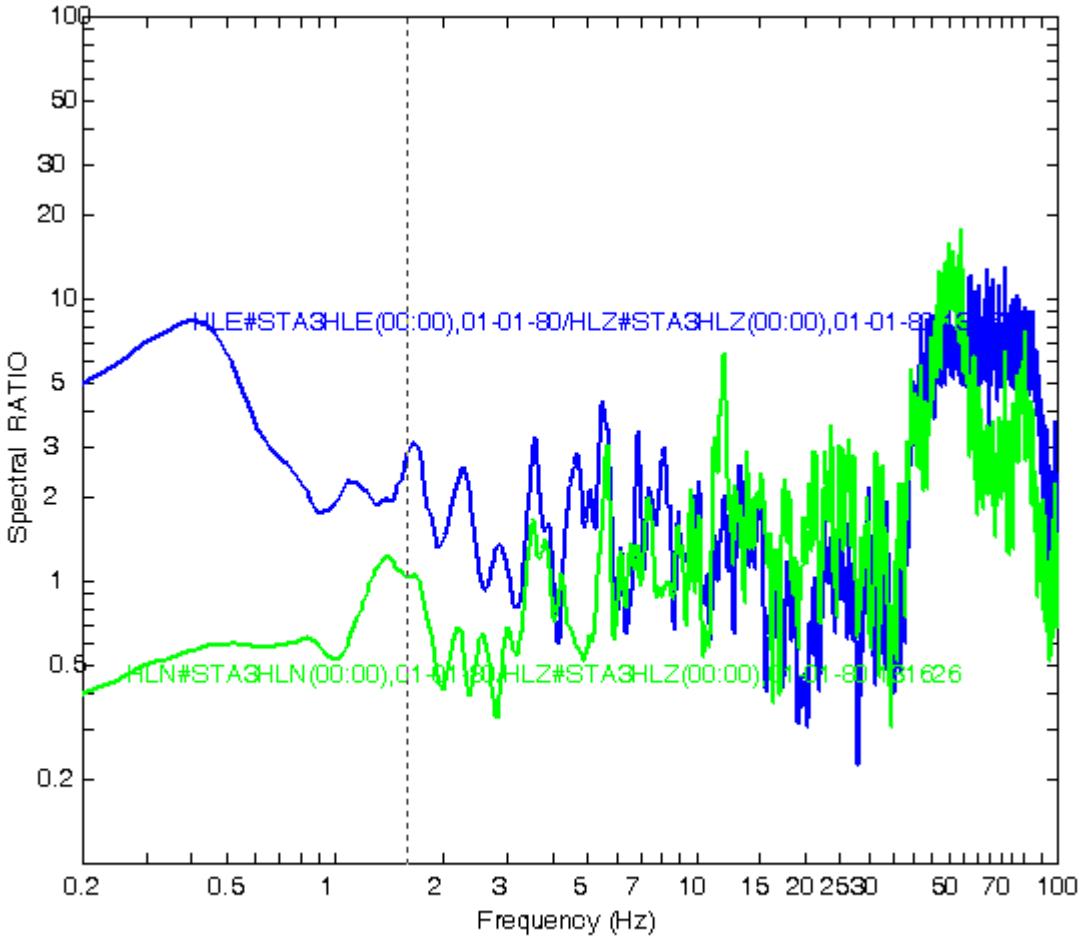
Spectral RATIO
Frequency (Hz)
100
50
30
20
10
5
3
2
1
0.5
0.2
0.2
0.5
1
2
3
5
7
10
15
20
25
30
50
70
100

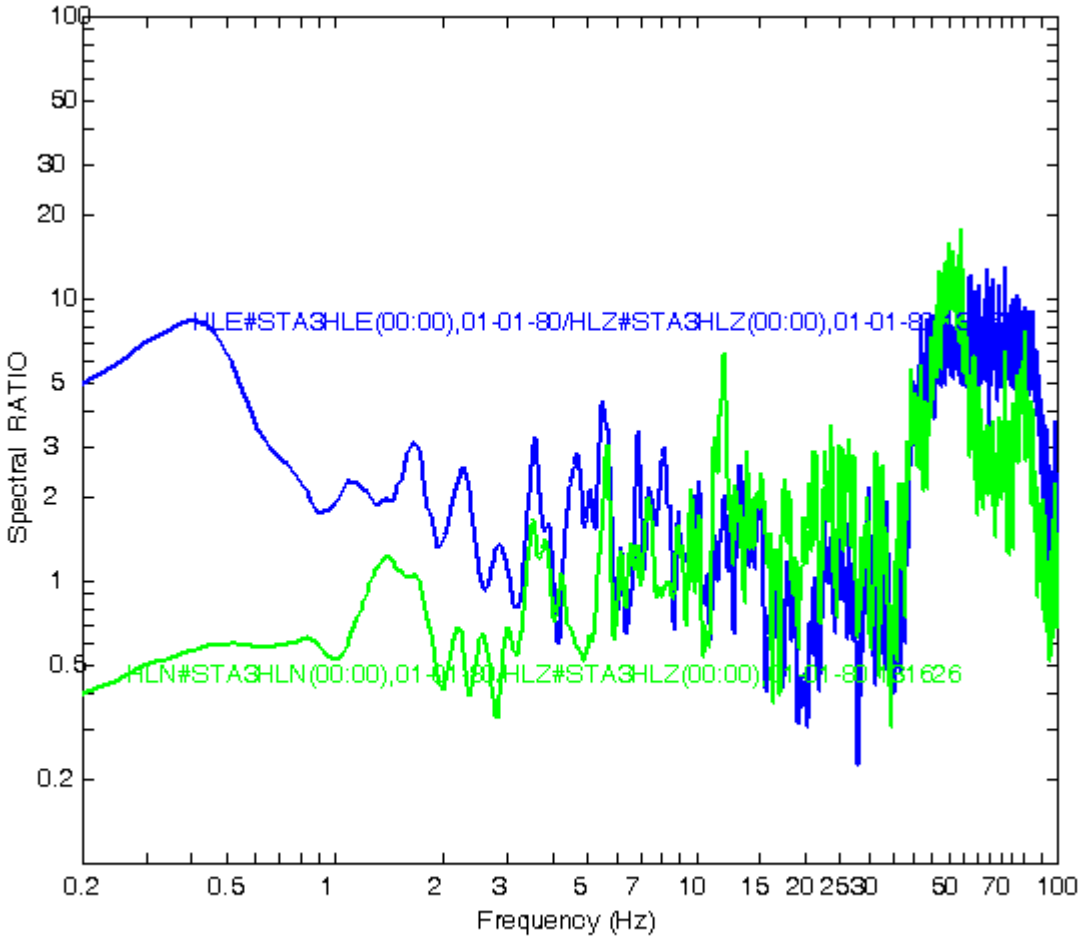
Spectral RATIO
Frequency (Hz)
100
50
30
20
10
5
3
2
1
0.5
0.2
0.2
0.5
1
2
3
5
7
10
15
20
25
30
50
70
100

9-2-2007-sta4

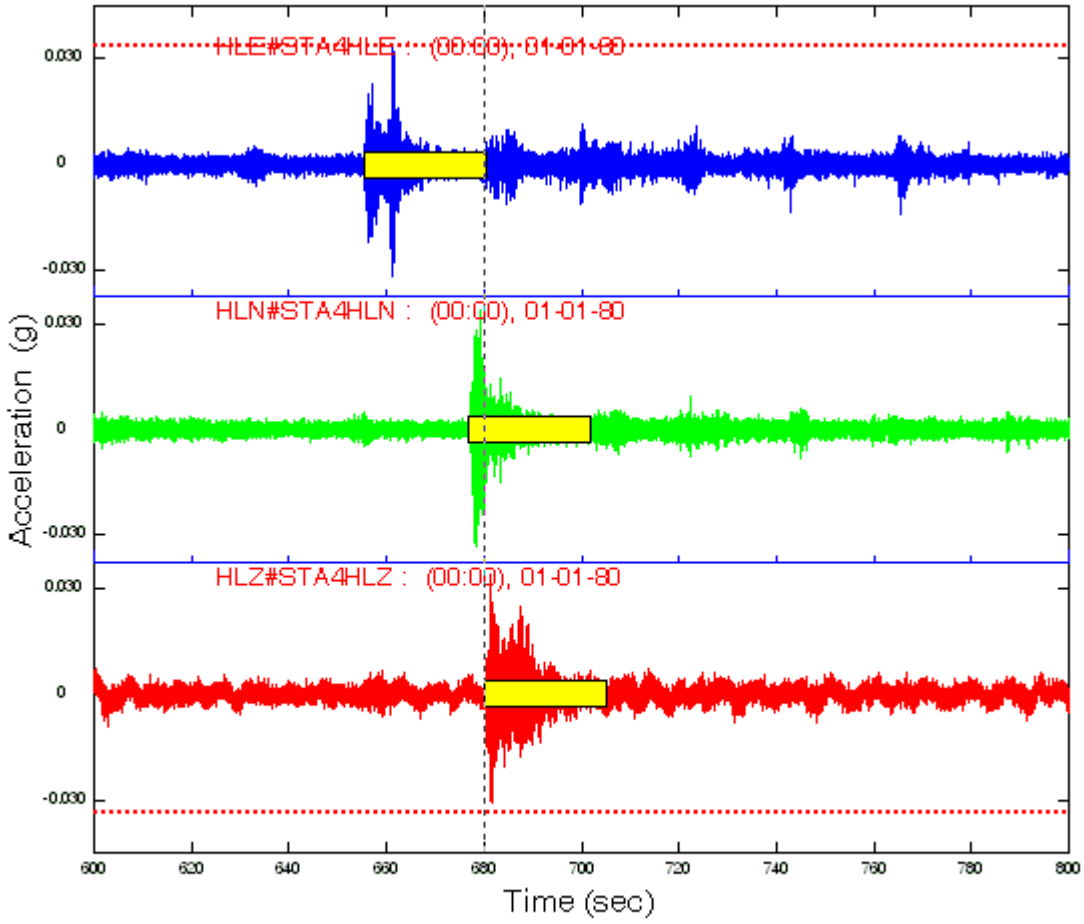
HLE#STA4HLE : (00:00), 01-01-80
HLN#STA4HLN : (00:00), 01-01-80
HLZ#STA4HLZ : (00:00), 01-01-80
0.030
0
-0.030
Acceleration (g)
600
620
640
660
680
700
720
740
760
780
800
Time (sec)

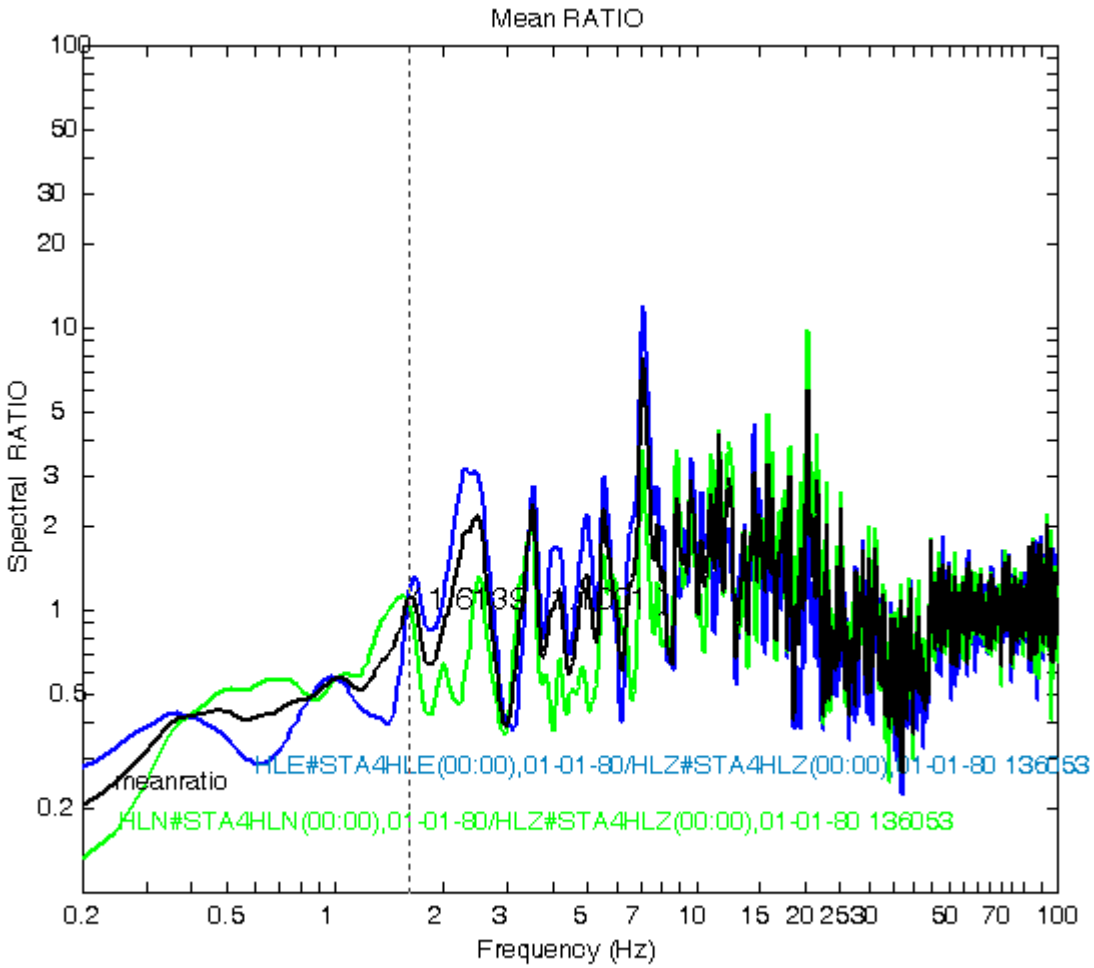
Mean RATIO
Spectral RATIO
100
50
30
20
10
5
3
2
1
0.5
0.2
meanratio
HLE#STA4HLE(00:00),01-01-80/HLZ#STA4HLZ(00:00),01-01-80 136053
HLN#STA4HLN(00:00),01-01-80/HLZ#STA4HLZ(00:00),01-01-80 136053
0.2
0.5
1
2
3
5
7
10
15
20
25
30
50
70
100
Frequency (Hz)

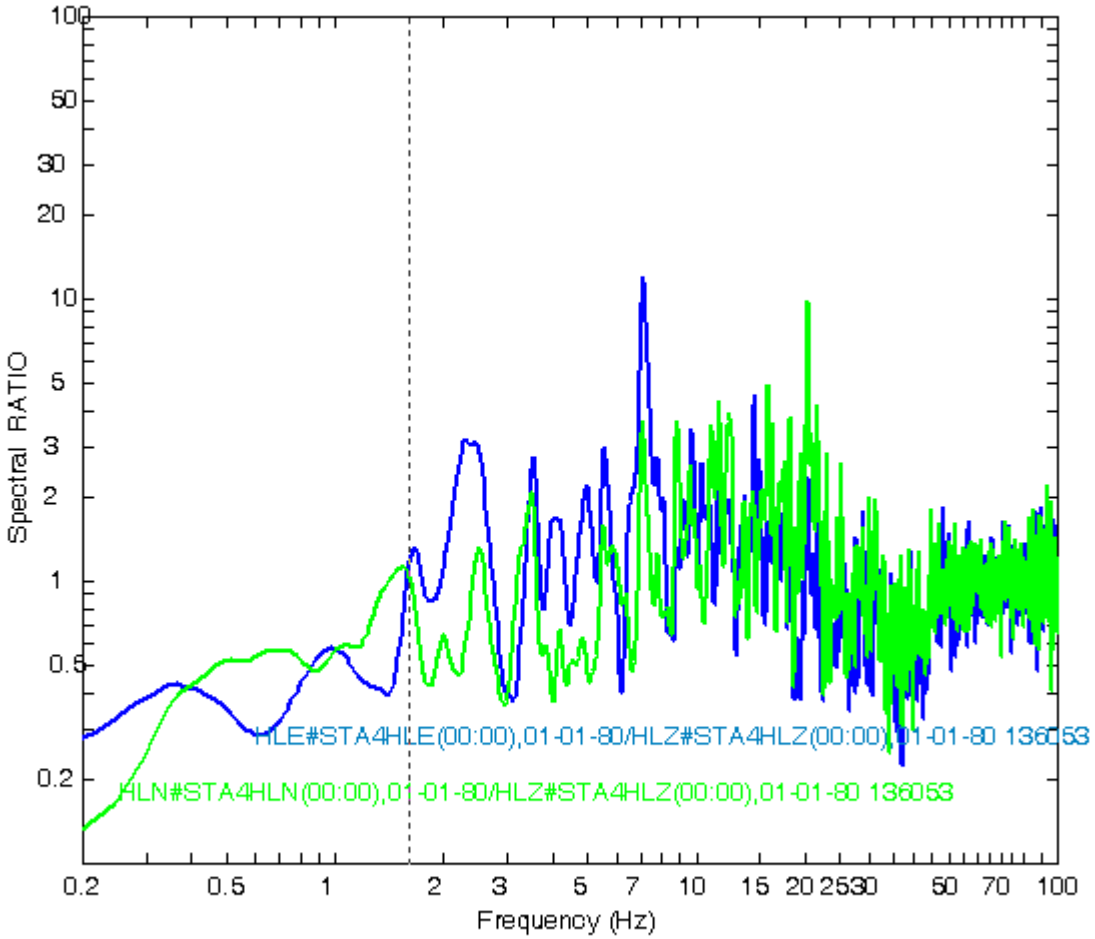
Spectral RATIO
100
50
30
20
10
5
3
2
1
0.5
0.2
0.2
0.5
1
2
3
5
7
10
15
20
25
30
50
70
100
Frequency (Hz)
HLE#STA4HLE(00:00),01-01-80/HLZ#STA4HLZ(00:00),01-01-80 136053
HLN#STA4HLN(00:00),01-01-80/HLZ#STA4HLZ(00:00),01-01-80 136053

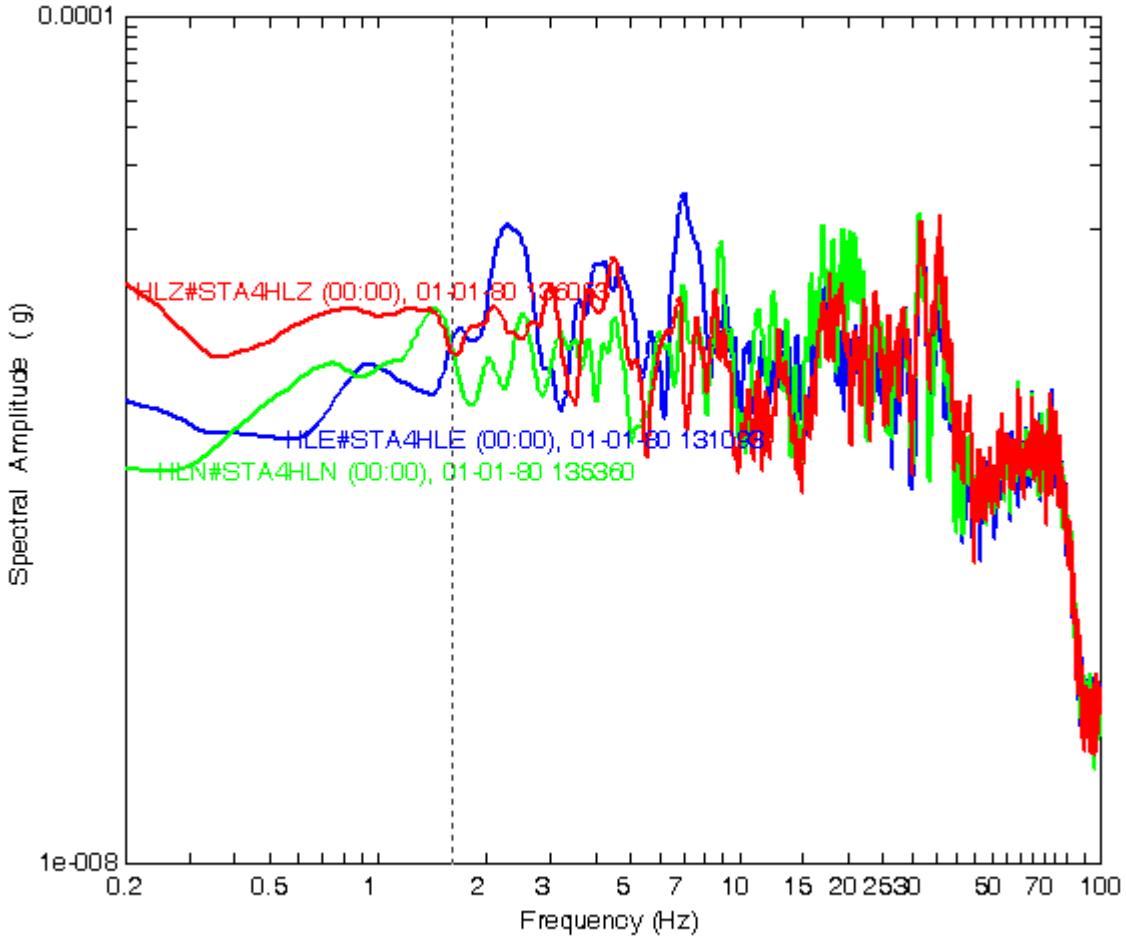
0.0001
1e-008
Spectral Amplitude (g)
HLZ#STA4HLZ (00:00), 01-01-80 135360
HLE#STA4HLE (00:00), 01-01-80 131008
HLN#STA4HLN (00:00), 01-01-80 135360
0.2
0.5
1
2
3
5
7
10
15
20
25
30
50
70
100
Frequency (Hz)